CFD modeling of biomass thermo-chemical conversion and its experimental study

Li, Xiyan

Publication date:
2020

Document Version
Publisher's PDF, also known as Version of record

CFD MODELING OF BIOMASS THERMO-CHEMICAL CONVERSION AND ITS EXPERIMENTAL STUDY

BY
XIYAN LI

DISSERTATION SUBMITTED 2020

AALBORG UNIVERSITY
DENMARK

CFD modeling of biomass thermo-chemical conversion and its experimental study

Ph.D. Dissertation

Xiyan Li

Dissertation submitted, 2020

Dissertation submitted: July, 2020

PhD supervisor: Professor Søren Knudsen Kær
Aalborg University

Assistant PhD supervisor: Associate Professor Thomas Joseph Condra
Aalborg University

PhD committee: Associate Professor Matthias Mandø (chairman)
Aalborg University

Professor Henrik Kofoed Nielsen
University of Agder

Professor Britt M.E. Moldestad
University of South-Eastern Norway

PhD Series: Faculty of Engineering and Science, Aalborg University

Department: Department of Energy Technology

ISSN (online): 2446-1636
ISBN (online): 978-87-7210-676-2

Published by:
Aalborg University Press
Kroghstræde 3
DK – 9220 Aalborg Ø
Phone: +45 99407140
aauf@forlag.aau.dk
forlag.aau.dk

Printed in Denmark by Rosendahls, 2020

Abstract

Understanding what is going on during biomass thermochemical conversion process is one of the technological hurdles in biomass thermal treatment. In this project, a reliable one-dimensional biomass pyrolysis/gasification/combustion model has been developed and programmed. The model developed is integrated into a finite volume based CFD code. A sequence of partial differential equations are discretized by central difference approximation spatially and an implicit method temporally, the discretized equations are solved by the tridiagonal matrix algorithm (TDMA). The model can reliably predict the temperature distribution, the pressure distribution, the species concentration, the size changes, spatially and temporally.

The project is divide into two parts. The first part is the development of a reliable one-dimensional single biomass pellet pyrolysis model. The model is verified using various experimental test cases. After that, the model is extended to a combustion model, by including more oxidation reactions. For both pyrolysis and combustion case, the experimental data for mass loss and temperature profile of a biomass particle under different conversion condition are collected from the literature for model validation. The second part of this project is designed to further investigate the combustion mechanism in more realistic operating conditions and in this part an experiment is done on a packed-bed biomass combustor in the laboratory of BEST - Bioenergy and Sustainable Technologies GmbH at Graz university of technology. A series of tests were performed to investigate the effect of the primary air flux on the in-bed biomass combustion behavior under normal air-firing condition (79% N_2 and 21% O_2 (vol)). Measurements include the mass loss of the bed, the temperatures in different bed locations, and the release of gas species O_2, CO, CO_2, NH_3, HCN, NO_x, SO_2, hydrocarbons by means of FTIR and FID. The experiment not only provided a physical understanding of the underlying conversion process and mechanisms under different operating conditions but also provided more detailed data for validating the model developed in the first part. For the smouldering combustion under 30 $l\,min^{-1}$, a comparison is made between the experimental results and the model simulation.

Resumé

At forstå, hvad der foregår under en termokemisk konverteringsproces, er en af de teknologiske hindringer i termisk behandling af biomasse. I dette projekt er en pålidelig, en-dimensionel model af -pyrolyse / forgasning / forbrænding af biomasse udviklet og programmeret. Modellen er udviklet ved hjælp af en finite volume metode i CFD. En sekvens af partielle differentialligninger diskretiseres rumligt ved hjælp af en central difference metode og tidsligt med en implicit metode. De diskretiserede ligninger løses ved hjælp af tridiagonal matrixalgoritme (TDMA). Modellen kan pålideligt forudsige hvordan temperaturfordelingen, trykfordelingen, gas specie koncentrationen og størrelsen ændrer sig rumligt og tidsligt.

Projektet er opdelt i to dele. Den første del fokuserer på udviklingen af den en-dimensionelle model af pyrolyse / forgasning / forbrænding af en enkelt biomassepartikel. Modellen er først verificeret ved forskellige pyrolysetesttilfælde. Derefter udvides modellen til en forbrændingsmodel ved at inkludere flere oxidationsreaktioner. Modellens resultater for både pyrolyse og forbrænding er valideret med eksperimentelle data fra litteraturen for massetab og temperaturprofil for en biomassepartikel. På grund af manglen på eksperimentelle data for gasartens udvikling under konvertering af en enkelt biomassepartikel i litteraturen udføres eksperimenter i projektets anden del.

I den anden del af dette projekt udføres eksperimenter på en biomasseforbrænder med packed bed i laboratoriet i BEST - Bioenergy and Sustainable Technologies GmbH at Graz university of technology. En række tests udføres for at undersøge indflydelsen af den primære luftstrøm (79 % vol N_2 og 21 % vol O_2) på forbrændingen af biomasse i packed bed. Målingerne inkluderer sengens massetab , temperaturer på forskellige placeringer i sengen og frigivelse af gasarter O_2, CO, CO_2, NH_3, HCN, NO_x, SO_2 og kulbrinter ved hjælp af FTIR og FID. Eksperimentet giver ikke kun en fysisk forståelse af den underliggende konverteringsproces og mekanismer under forskellige driftsbetingelser, men giver også mere detaljerede data til validering af modellen som blev udviklet i projektets første del. For den ulmende forbrænding under 30 $\mathrm{l\,min^{-1}}$ foretages en sammenligning mellem de eksperimentelle resul-

tater og modelsimuleringen.

Contents

Nomenclature

Physics Constants

A	Pre-exponent factor	s^{-1}
A_s	Surface area	m^2
b	Temperature order	$-$
C_{PB}	Specific heat capacity of Biomass	$J/(\mathrm{kgK})$
C_{PC}	Specific heat capacity of char	$J/(\mathrm{kgK})$
C_{mix}	Specific heat capacity of gas mixture	$J/(\mathrm{kgK})$
C_{Pg}	Specific heat capacity of gas	$J/(\mathrm{kgK})$
C_{PM}	Specific heat capacity of moisture	$J/(\mathrm{kgK})$
D_{AB}	Molecular diffusivity of gas A in B	m^2/s
D_{eff}	Effective diffusivity	m^2/s
$D_{j,m}$	Diffusivity of gas species j in the gas mixture	m^2/s
d_{pore}	Pore diameter	m
d_p	Particle diameter	m
E_k	Activation energy of reaction k	J/kmol
H	Bed height	m
h_M	Mass transfer coefficient	m/s
$h_{m,pore}$	Mass transfer coefficient of vapor in the pore	m/s
h_T	Heat transfer coefficient	$\mathrm{W}/\left(\mathrm{m}^2 \cdot \mathrm{K}\right)$
h_f^0	Enthalpy of formation	J/kg

h_f^s	Sensible enthalpy	J/kg
K	Permeability of biomass particle or bed	-
K_{eff}	Effective thermal conductivity	$\mathrm{W}/\left(\mathrm{m}\cdot\mathrm{K}\right)$
$K_{eff},0$	Effective thermal conductivity without flow	$\mathrm{W}/\left(\mathrm{m}\cdot\mathrm{K}\right)$
K_g	Thermal conductivity of gas	$\mathrm{W}/\left(\mathrm{m}\cdot\mathrm{K}\right)$
K_s	Thermal conductivity of solid	$\mathrm{W}/\left(\mathrm{m}\cdot\mathrm{K}\right)$
k_s	Thermal conductivity of solid	$\mathrm{W}/\left(\mathrm{m}\cdot\mathrm{K}\right)$
k_k	Arrhenius reaction rate of reaction k	s^{-1}
MW_j	Molecular weight of species j	$\mathrm{W}/\left(\mathrm{m}\cdot\mathrm{K}\right)$
n	order of reactions	-
Nu	Nusselt number	-
P	Pressure	Pa
P_{atm}	Atmospheric pressure	Pa
P_{in}	Initial gas pressure	Pa
P_{O_2}	Oxygen pressure in gas phase	Pa
Pr	Prandtl number	-
R_g	Universal gas constant	$KJ/(mol-K)$
r_k	Reaction rate of reaction k	$J/(mol-K)$
r_{H_2O}	Reaction rate of water evaporation	$J/(mol-K)$
Re	Reynolds number	-
R_p	Particle radius	m
Sc	Schmidt number	-
Sh	Sherwood number	-
$S_a,char$	Specific area of char	m^2/m^3
S_g	Source term in the continuity equation	$\mathrm{kg}/\left(\mathrm{m}^3\cdot\mathrm{s}\right)$
S_j	Source term in species transport equation	$\mathrm{kg}/\left(\mathrm{m}^3\cdot\mathrm{s}\right)$
S_T	Source term in the energy equation	$\mathrm{J}/\left(\mathrm{m}^3\mathrm{s}\right)$

t	time	s
T_c	Particle center temperature	K
T_{eve}	Evaporation temperature of liquid water	K
T_{ini}	Initial temperature	K
T_i	Local temperature of grid i	K
$T_{j,S}$	Particle surface temperature for species j	K
T_{ref}	Reference temperature in the ambient flow	K
T_S	Particle surface temperature	K
T_∞	The freeboard temperature	K
$\vec{u}$	Gas velocity	m/s
V	Particle volume	m^3
V_0	Initial particle volume	m^3
W	Weight of particle or bed	kg
X_C	Conversion rate of char	-
X_M	Conversion rate of moisture	-
X_V	Conversion rate of volatile	-
X_C	Conversion rate of char	-
Y_j	Mass fraction of species j	-
$Y_{j,S}$	Mass fraction of species j on the pellet surface	-
Y_{ref}	Mass fraction of gas mixture in the ambient flow	-
$Y_{j,\infty}$	Mass fraction of gas mixture of the carrier gas	-

Subscripts

Ash	Ash
B	Biomass
C	Char
f	Convection
g	Gas

i	Node i of meshing	
j	Species order	
k	Reaction order	
mix	Gas mixture	
rad	Radiation	
S	Surface	
v	Volatile	

Superscripts

$*$	Parameters that calculated from last iteration step	
0	Parameters that calculated from last time step	
∞	freeboard	

Greek letters

β	Drag force coefficient	-
$\mathcal{E}$	Porosity	-
η	Permeability of gas mixture	-
λ	Conductivity	$\mathrm{W}/\left(\mathrm{m}\cdot\mathrm{K}\right)$
μ	Dynamic viscosity	$\mathrm{kg}/\left(\mathrm{m}\cdot\mathrm{s}\right)$
ρ	Density	-
σ	Boltzmann radiation constant	$\mathrm{W}/\left(\mathrm{m}^2\cdot\mathrm{K}^4\right)$
τ	Tortuosity	-
ω	Emissivity	-

Abbreviations

CFD	Computational Fluid Dynamics
FVM	Finite volume method
LHS	Left hand solution
MVF	Minimum fluidization velocity
PAF	Primary air flow

PDE Partial Differential Equation

REA Association for Renewable Energy and Clean Technology

RHS Right hand solution

TDMA Tri Diagonal Matrix Algorithm

TGA Thermo Gravimetric Analysis

TIC Total organic carbon

TOC Thermo inorganic carbon

Operators

$\because$ Because

$\therefore$ Therefore

Preface

This work has been carried out at the Department of Energy Technology, Faculty of Science and Engineering, Aalborg University during the period of April 1^{th} 2016 to March 30^{th} 2020. The author got financial support from both China scholarship council and Department of Energy Technology. Conference to 13^{th} sdewes conference was granted from both Department of Energy Technology and Otto Mønsted Foundation. The study is supervised by Professor Søren Knudsen Kær and Assoc. Professor Thomas Joseph Condra from Aalborg University.

I would like to express great gratitude to my supervisors, Professor Søren Knudsen Kær and Assoc. Professor Thomas Joseph Condra for their constructive criticism and kind leading to my research and campus life. Many thanks to my former supervisor, Assoc. Professor Chungen Yin, for his guide and foresight for my study of CFD simulation. Henrik Sørensen, as my section leader, gives me great support in this department. Thanks to Claus Leth Bak, head of Energy Technology Ph. D. programme, gives me great support and guidance. I would also like to thank all the support from section 4 and doctoral school. I really appreciate the time we spent together for all the discussions with Anna Lyhne Jensen, Jakob Hærvig and Steffen Frensch.

I would like to thank my co-supervisor, Thomas Condra, for spending so much time proofreading my thesis. Great thanks to my former officemate Lennart Petersen and my great colleagues Ariya Schwooon, Rodical-Elisabeta stroe, Sobi Thomas, Samuel Simon Araya and Matje Novak.

Grateful acknowledge for the support from Graz University for letting me do the experiments and we had a great cooperation together. Thanks for the China Scholarship Council for supporting my Ph.D. financially.

In the memory of my Grandfather Shaoan Wang and my aunt Xiuchun Jiang, who have a significant impact on my childhood have passed away in the past four years.

Xiyan Li
Aalborg University, July 7, 2020

Part I

Summary

Chapter 1

Introduction

This chapter gives a brief introduction to the background of this study. It presents the state of the art for both the simulation of thermo-chemical conversion on a single biomass particle and a packed bed. It also presents an outline of the thesis and the main objectives of this work.

1.1 Introduction

Biomass gasification has received much attention, as a basis for a renewable source of energy and chemical feedstocks. In the biomass gasification process, pyrolysis is a key, initial sub-process which results in a complex system of intermediate products or product groups such as, gases, tars and char. Subsequently, the gases and tar vapors undergo further gas-phase reactions (e.g. cracking, reforming, shift) whilst the char takes part in heterogeneous reactions, yielding the final gasification products. Partly due to governmental regulations and partly due to unsolved technological hurdles, biomass gasification is still a technology under development despite over 30 years' research and development (R&D) and it has success only in a few niche markets [1]. Amongst the hurdles facing biomass gasification are: a lack of reliable modelling tools for biomass pyrolysis / gasification, lack of a proven design, fuel flexibility, efficiency, tar reduction, gas cleaning, scaling up. As a result of this, there has been a compelling need for reliable, cost-effective modelling tools for the design of biomass pyrolysis / gasification processes and components.

1.2 Background

With the population growth worldwide, the high consumption of fossil fuels is in public focus [2], and this motivates research efforts into finding and utilising more sustainable resources. Biomass is one of the most prominent renewable resources and it has significant potential.According to the Association for Renewable Energy and Clean Technology (REA),energy from biomass can result in significantly less greenhouse gas emissions compared to fossil fuels [3], as shown in Fig. 1.1. The United Nations environment programme has carried out a study of carbon sequestration, and this shows that the use of fossil fuel and industry in general are the main carbon emission sources [4]. Regulations have been enacted worldwide with the aim of limiting carbon emissions. Denmark,for example, has a stated aim of becoming independent of fossil fuels by 2050 [5], and in 2019 a new climate law was passed which requires a 70% reduction in CO_2 emissions by the end of 2030 [6].

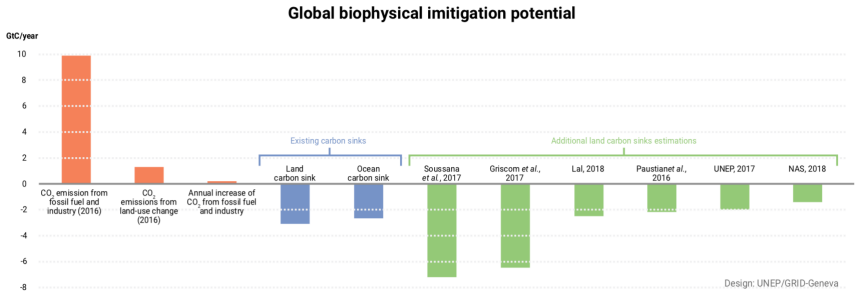

Fig. 1.1: Estimation of carbon emissions from fossil fuels and others [3]

Considering district heating in Denmark; according to the Danish energy model, the transformation from fossil fuel to biomass for combined heat and power plants has been done in the past and, for instance, over 50% of the district heating in 2015 was produced from biomass feedstock [7], as shown in Fig. 1.2.

In order to comply with the international agreements and ambitions, as well as to contribute to a more recyclable based world, the study of the use and treatment of biomass is necessary. Amongst all the biomass processing technologies, thermo-chemical treatment is probably the most effective due to the fast energy conversion under high temperature. The scope of this Ph.D. project was to contribute to an understanding of the thermal treatment of biomass through a study of the thermo-chemical conversion process of a single biomass pellet and a packed bed. The simulation results should support an understanding of biomass thermal conversion and aid the prediction of reliable results for the design of biomass pyrolysis/combustion plants.

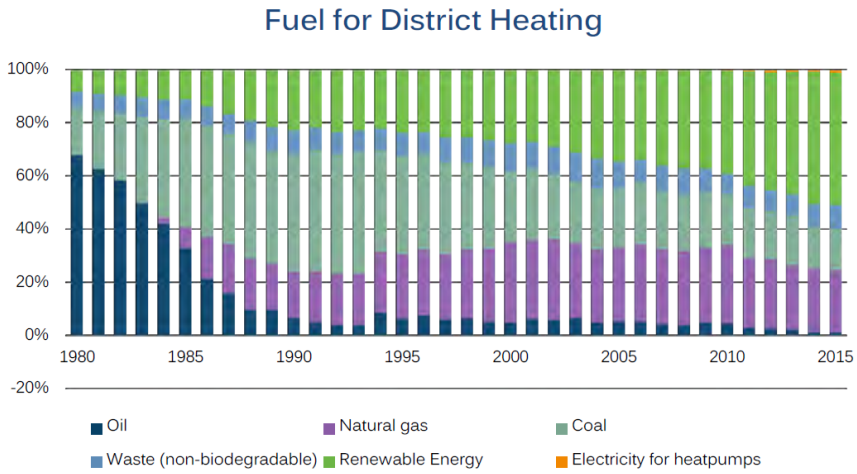

Fig. 1.2: Composition of fuels for district heating in Denmark in the past 35 years [7]

1.3 State of art

1.3.1 Single particle study

The basic concepts involved in the pyrolysis of a single biomass pellet are fairly straightforward and there is much research based on the single particle scale. However, considering the relatively high density within the particle, it is not easy to investigate what is actually occurring inside the pellet, though some details can be measured or ascertained through modelling.

The research into the processes occurring within a single biomass pellet has classically been based upon the research carried out on a single coal particle. Kobayashi et al. [8] studied the devolatilization of a coal particle under high temperature and this study produced some basic results; for example, the kinetic data over a temperature range of 1000 - 2000K. An empirical model for the coal decomposition is also introduced in their work. Two sets of kinetic data were published, based on the inter-competing reactions at different volatile yields, and this data is still used for modelling.

$$\text{Coal} \longrightarrow \text{Volatile}\,1 + \text{Residue}\,1 \tag{1.1}$$

$$\text{Coal} \longrightarrow \text{Volatile}\,2 + \text{Residue}\,2 \tag{1.2}$$

Pyle and Zaror [9] studied the heat transfer and kinetics during biomass pyrolysis at low temperature. In their work, the conversion rate and conversion time using four models were compared. These four models were: the

general distributed model (Bamford's model [10]), the uniform internal conditions model, the kinetic control model and the internal heat transfer control model (shrinking core model). These models are presented briefly here.

The Bamford's model was proposed by Bamford et al. [10] in 1946. The model assumes that the decomposition products and their properties are identical all over the wood pellet, without taking into consideration the diffusion of the species and under the assumption that the thermal decomposition rate is first-order. In Bamford's model, the internal temperature gradient is considered and perhaps as a result of this, Pyle and Zaror [9] reported good agreement with their experimental results. It is though, interesting to note that the modelling results fit the experimental results better without the use of the enthalpy of reaction. The main equation of Bamford's model is basically the partial differential equation of energy conservation equation, without considering convection or diffusion:

$$\frac{\partial C_p \rho T}{\partial t} = bK\frac{\partial^2 T}{\partial r^2} + \frac{\partial \rho}{\partial t} q \tag{1.3}$$

The uniform internal conditions model is the so-called external transfer control model and this implies that the internal temperature gradient is ignored [9], which means the Biot number is really small (Bi«1). The material that is studied by this kind of model is usually referred as thermally thin material. This kind of model is usually used for simple cases or for pulverized particles. The energy equation has, therefore, the following form:

$$C_p \rho \frac{\mathrm{d}T}{\mathrm{d}t} = \frac{b}{r}\left\{ h_c(T_f - T) + \sigma\epsilon(T_f^4 - T^4) + q\frac{\mathrm{d}\rho}{\mathrm{d}t} \right\} \tag{1.4}$$

The kinetic model applies to a condition that there is a fast heat transfer to and within a the biomass particle. In the end, the temperature of the particle temperature will reach the ambient temperature [9]. The kinetic model is a simplification of the uniform internal conditions model. The expression can be seen in equation 1.5.

$$\frac{\rho_t - \rho_\infty}{\rho_0 - \rho_\infty} = exp\left\{ -At\ exp(-\frac{E}{RT_f}) \right\} \tag{1.5}$$

The shrinking core model is the so-called diffusion-controlled model. It applies especially to the process during leaching where the solid is transformed into a porous media [9]. In such a situation the devolatilization rate is quite high and the internal temperature gradient is very large. To some extent, the shrinking core model is the pioneer of the so called layers model. The layout of the shrinking core model is shown in Fig. 1.3.

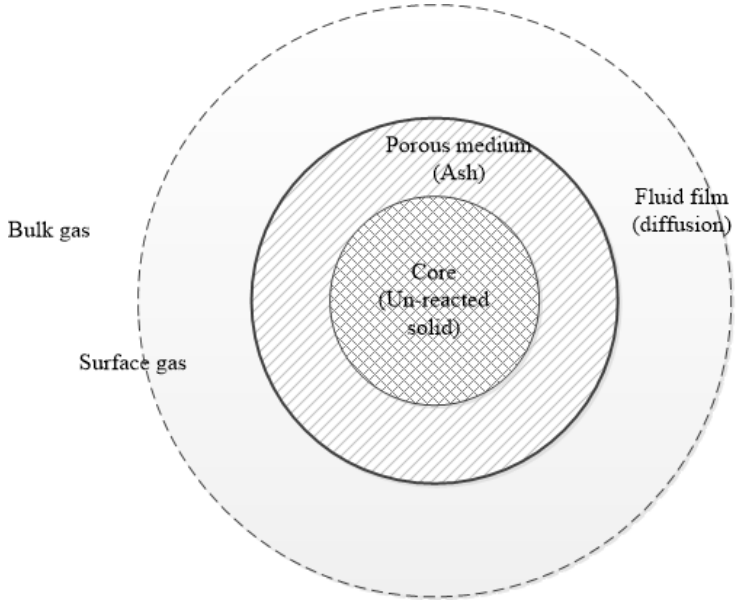

Fig. 1.3: The shrinking core model

The expression for diffusion controlled leaching can be solved by applying Fick's second law [11], as shown in equation 1.6. Fick's law describes the concentration changes of solute with respect to time and space.

$$\frac{\partial M}{\partial t} = D\frac{\partial^2 M}{\partial x^2} \tag{1.6}$$

where, M is the molecular mass of the leached substance, t the diffusion time, x the diffusion distance, D the diffusivity which changes with the concentration of the solute.

The reaction front of shrinking core model can be written as equation 1.7 [9].

$$\frac{\rho_0 - \rho_t}{\rho_0 - \rho_\infty} = 1 - \frac{r_c^b}{R_b} \tag{1.7}$$

In equation 1.7, ρ_0 represents the initial density, ρ_t the current time density and ρ_∞ the density of the surroundings. r_c is the position of the current reaction front, which is the characteristic dimension of the unreacted shrinking core and R_b is the characteristic dimension of the solid.

In the research by Pyle and Zaror [9], all these four models are compared. It was concluded that a simple model, such as Bamford's model, shows excellent agreement for a wide range of Biot number and pyrolysis number

($P_y = h/(k\rho C_p R)$). The kinetic model gives better results for smaller particles at low temperature with a limited Biot number range (not too large) and pyrolysis number. The shrinking core model applies to large Biot numbers ($Bi > 50$) and a small pyrolysis number. The kinetic model and the uniform internal conditions model apply to small Biot numbers ($Bi < 1$).

All the four models discussed above can predict, to a reasonable degree, the temperature and conversion rate under certain circumstances. However, the governing equations are not complete. For example, diffusion is not included in some models, and convection is not included in all the models. In order to include convection in the model, the velocity within the particle should also be incorporated.

Kansa et al. [12] added the momentum conservation equation to their one-dimensional mathematical model and that means that a relatively complete mathematical model was available. A temporal profile of mass loss rate, temperature and pressure is presented in their results. A spatial distribution of temperature, density, gas pressure, velocity, and pyrolysis rate at 150 seconds and 300 seconds are also given.

Chan et al. [13] describes another model for a large biomass particle. Compared to previous research, Chan et al. [13] emphasize more on the prediction of the devolatilization rate rather than the heat transfer rate and mass loss. In order to do this, a more complicated pyrolysis model was derived, which has been used by many researchers subsequently [14–17]. This model is the so-called two-stage pyrolysis model. A scheme of the two-stage pyrolysis model is shown in Fig. 1.4.

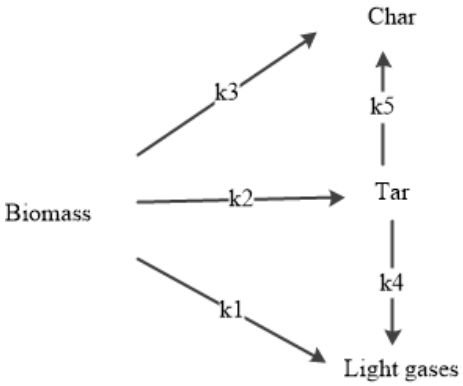

Fig. 1.4: Two-stage pyrolysis scheme

Apart from the pyrolysis mechanisms shown in Fig. 1.4, two other pyrolysis mechanisms are also popular and are often used in CFD simulations and reaction rate prediction, as concluded by Di Blasi [15]. The two models are: the one-step multi-reaction model and the one-step global model. The

one-step, multi-reaction model assumes that the devolatilization of biomass takes just one step to produce char, tar and light gases, but with three different reaction rates. The expression is shown in equation 1.8. The one-step global model assumes biomass decomposes into char and light gases, with the same reaction rate, as shown in equation 1.9.

$$\begin{aligned} &\text{Biomass} \rightarrow \text{Char} \\ &\text{Biomass} \rightarrow \text{Light gases} \\ &\text{Biomass} \rightarrow \text{Tar} \end{aligned} \tag{1.8}$$

$$\text{Biomass} \rightarrow \text{Char} + \text{Light gases} \tag{1.9}$$

It should be noted that all the detailed mathematical models are based on a thermally thick material, which means that there is a temperature gradient inside the solid. Di Blasi [18] developed a detailed mathematical model for the pyrolysis of Cellulose. She made some modifications to the previous model; for example, the energy equation is written in the form of enthalpy by ignoring the kinetic and potential energy; the velocity is calculated based on Darcy's law and continuity. These changes are still used in the more recent models [19–24].

By using the same model and some modifications afterwards, Di Blasi has done work on the simulation of the combustion process of charring and non-charring solid fuels [25], the numerical simulation of Cellulose pyrolysis [18], the heat, momentum and mass transport though a shrinking biomass particle [15], the kinetic and heat transfer control in the slow and flash pyrolysis of solids [26] , the influence of physical properties on biomass devolatilization characteristics [27], the multi-phase moisture transfer in the high temperature drying of wood particles [28], the comparison of semi-global mechanisms for primary pyrolysis of lignocellulosic fuels [29], the kinetics of primary product formation from wood pyrolysis [30], the Intra- and Extra-particle processes modeling of wood fast pyrolysis [31], the drying characteristics of wood cylinders for conditions pertinent to fixed-bed countercurrent gasification [32], the modeling of wood gasification in a countercurrent fixed-bed reactor [33], the modeling chemical and physical processes of wood and biomass pyrolysis [34] and the prediction of the combustion and gasification rate of lignocellulosic chars [35].

The multiple-use of Di Blasi's mathematical models shows the usefullness of numerical simulation in biomass thermo-chemical treatment. However, there is also room for the improvement of the numerical model.

Based on the efforts of previous research, especially the shrinking-core model and the measurement of the kinetic data, a commonly used mathematical model was developed. Thunman et al. [36] addresses the layer model

as, the moist layer, the devolatilizing fuel, the char core layer and the ash core layer. The idea is to assume the biomass particle as a mixture of all the four layers. As the pyrolysis process proceeds, the moisture layer propagates into the inner center, followed by the volatile layer and char layer. In the end, an ash layer is built outside the particle until all the layers disappear. The scheme of layer model is shown in Fig. 1.5 [37]. The layer model has been subsequently used by many researchers [38–43].

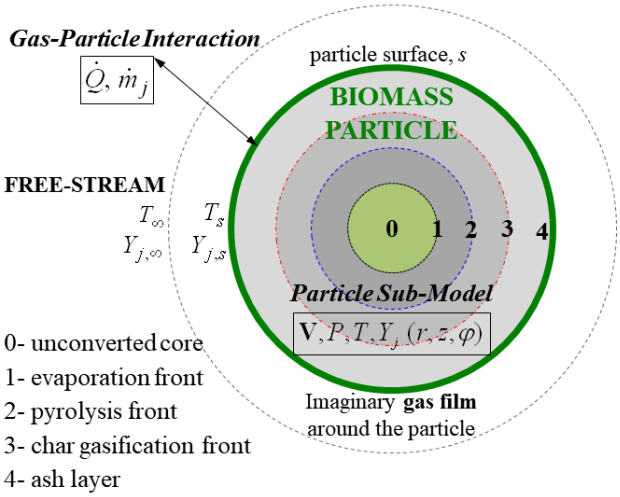

Fig. 1.5: Scheme of layer model

1.3.2 Packed bed gasification study

Biomass can participate in the Earth's biogeochemical cycle directly or indirectly, which makes biomass possibly the most important sustainable fuel in the world. Bridgwater [44] reviewed the feasibility of the biomass-to-electricity system in 1995. Even though there were quite a few technical barriers at that time, for example the gas cleaning system, the uncertainties in operation, the turbine fuel and engine fuel specifications are not identical in IGCC(Integrated gasification combined cycle) technology. Apart from IGCC technology, combustion and gasification are the more mature approach to the utilisation of biomass residues. Corella et al. [45] studied steam gasification of biomass waste in a fluidized bed. Due to the wide use of coal combustion, the technical barriers for biomass combustion/gasification is lower.

Considering the large cost of the design and construction of a new packed bed furnace, the availability of a good simulation modelling tool in advance

is vitally important. A correct prediction from a CFD simulation can improve the performance of the furnace, as well as estimate the production. It is necessary to emphasize here that a packed bed or fixed bed implies that the particles in the bed are not in motion - not fluidised.

Both the single biomass pellet and the packed bed are treated as porous media. A packed bed can be seen as a cuboid porous media. Therefore, the model that is applied to a single biomass pellet can be used on a packed bed by changing the boundary conditions and key parameters. For example, most of the transport equations, the reactions that take place, most of the algorithm and the solver that solves the partial differential equations, that are used on a single biomass pellet, are applicable to a packed bed simulation. The layer model that is used in single biomass pellet gasification can also be used in the packed bed combustion, as shown in Fig. 1.6 [46]. However, the differences are also obvious, such as the boundary conditions due to the shape change, the flow direction and the flow changes, the expressions for the properties due to shape change and flow changes, and so on.

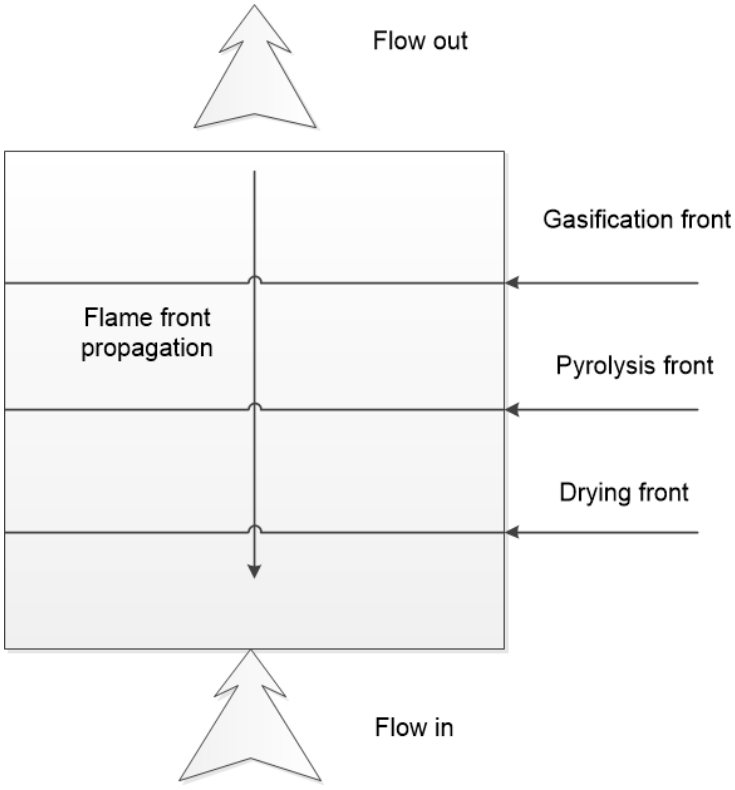

Fig. 1.6: Layer model for packed bed

The packed bed study on biomass gasification or combustion is based on the combustion theory of coal, owing to the similarities of the two materials. Hobbs et al.[47] simulated a counter-current fixed-bed commercial gasifier by using a one-dimensional model. Their model predicts the solid and gas temperature and the pressure loss, against experiments with eight coal types. The distribution of the void fraction in the bed was found to be essential for the correct prediction of the reaction rate. It should be mentioned that the convection and diffusion terms are not considered in all of their control equations. A similar one-dimensional fixed-bed model was also presented by Bryden and Ragland [48].

The transport equations for both a single biomass pellet and a packed bed are quite similar, but some of the properties can be different due to the diversity of the flow characteristics. In this work, the main differences are the effective conductivity and the diffusive number, and these will be presented separately here.

When dealing with the fluid in a packed bed, the velocity that goes through the bed, among the pellets, is significantly larger than the velocity within the pores of a single biomass pellet. Therefore, the non-linear term in the Navier-Stokes equation cannot be ignored. The momentum equation in a packed bed combustion simulation can be written as:

$$\frac{\partial\left(\phi\rho_g u\right)}{\partial t}+\frac{\partial\left(\rho_g uu\right)}{\partial x}=-\frac{\partial P}{\partial x}-\frac{\mu u}{K}-\beta\rho_g u^2 \tag{1.10}$$

Both the biomass pellet and the packed bed can be treated as a porous media and therefore the radiation from the void needs to be considered. The effective conductivity takes account of the conductivity within the particles and the radiation from the void, or the nearby particles [49], as shown in equation 1.11.

$$k_{\text{eff}}=k_{\text{cond}}+k_{\text{rad}} \tag{1.11}$$

where,k_{eff} denotes the effective conductivity [W/m K], k_{cond} denotes the conductivity of the sum the solid,liquid and gas and k_{rad} denotes the radiation effect from the intra-porous region.

The conductivity of the system can be written as:

$$k_{\text{cond}}=f\left(k_{\text{fiber}},k_{\text{bound,free water}},k_{\text{gas}},k_{\text{U}}\right) \tag{1.12}$$

Where k_{U} denotes the turbulent contributions of the fluid amongst the pellets [46].

The equivalent radiation heat transfer coefficient, k_{rad}, can be written as equation 1.13 for a single biomass pellet[14, 50].

$$K_{\text{rad}}=\frac{\varepsilon\sigma T^3 d_{\text{pore}}}{\omega} \tag{1.13}$$

Regarding the conductivity within the packed bed, the effects that can be considered can be much more sophisticated. For example, Hobbs et al. [47] considered fours effective radial conductivities: the static effective radial conductivity, the gas effective radial conductivity, the solid effective radial conductivity and the solid conductivity. Equations 1.14 to 1.17 shows the relationship amongst these four effective conductivities [51]. The original idea of the effective conductivity was mentioned by Kunii and Smith [52], who studied the effective conductivity considering a stagnant fluid in the void amongst the particles. In Kunii and Smith's model, the distance between the rock particles does not change in the fixed bed. However, in the case of biomass combustion in a fixed bed, the void changes along with the reaction process. Fjellerup and Henriksen [53] studied the heat transfer in a fixed bed where a void change is added, as shown in equations 1.18 to 1.20:

$$k_r^0 = k_g\epsilon\left(1+\frac{d_p h_{rv}}{k_g}\right)+\frac{k_s(1-\epsilon)}{\left(\frac{1}{\phi}+\frac{h_s d_p}{k_g}\right)^{-1}+\frac{2}{3_k}} \tag{1.14}$$

$$k_{rg} = k_g\left\{\epsilon\left(1+\frac{d_p h_{rv}}{k_g}\right)+0.14\mathrm{PrRe}/\left[1+46\left(\frac{d_p}{D}\right)^2\right]\right\} \tag{1.15}$$

$$k_{rs} = k_g(1-\epsilon)/\left[\left(\frac{1}{\phi}+\frac{h_{rs}d_p}{k_s}\right)^{-1}+\frac{2}{3\kappa}\right] \tag{1.16}$$

$$k_s = \left(\rho_s^t/4,511\right)^{3.5}\sqrt{T_s} \tag{1.17}$$

$$\frac{1-\eta}{1-\eta_0} = \frac{V_0}{V} = \left(\frac{\Delta l}{\Delta l_0}\right)^3 \tag{1.18}$$

$$\eta_0 = \frac{V_{\mathrm{tot}}-V_{\mathrm{cyl}}}{V_{\mathrm{tot}}} = \frac{6t^2\tan(\pi/6)L-\pi t^2 L}{6t^2\tan(\pi/6)L} = 1-\frac{\pi}{2\sqrt{3}} = 0.0931 \tag{1.19}$$

$$\Delta l = d_{\mathrm{p}}\left(\frac{1-0.0931}{1-\eta}\right)^{1/3} = 0.96795 d_{\mathrm{p}}(1-\eta)^{-1/3} \tag{1.20}$$

For the single biomass pellet gasification heat transfer a simplification is made, where the radiation from the voids is summarized into effective conductivity (equation 1.13). Therefore, the heat transfer in the energy equation

only includes the convective heat transfer from the ambient flow and the radiation heat transfer from the wall. Regarding the heat and mass transfer within the packed bed, more details need to be considered. Mehrabian et al. dealt with this issue by assuming a spherical control volume, which has one target particle surrounded by a few neighbouring particles [54]. In this way, the radiation problem amongst the particles can be transferred to the radiation problem amongst the control volumes, and the calculation is simplified. In the research by Yang et al. [46], the radiation amongst the particles within the bed are calculated into the effective conductivity of the bed.

Apart from the differences in heat transfer, the diffusion in the packed bed is also different. The effective diffusion coefficient for a single biomass pellet should be the diffusivity of the porous media.

$$D_{\text{eff}} = \frac{D\varepsilon\delta}{\tau} \tag{1.21}$$

where D is the diffusivity of the transported gas or liquid that fills the pores.

In the gasification case, all the species through the pores are considered as gases, which makes the effective diffusivity much more complex, as shown in equation 1.22. Due to the complexity of the diffusivity in the porous media, in most cases of single biomass pellet simulation, equation 1.21 is simplified as a constant number [40, 55] or polynomial [56] or by using the diffusivity of the solid [14, 57].

$$D_{i,j} = \frac{A \cdot T^{3/2}\sqrt{1/M_i + 1/M_j}}{p\sigma_{ij}^2\Omega} \tag{1.22}$$

Regarding the combustion/gasification in a fixed bed, the fluid field changes. Therefore, the simplification for the diffusivity of the single biomass pellet is not applicable to packed bed simulation. In the literature, many approaches are used to solve the effective diffusion coefficient based on the situation considered. Equation 1.22 would be too complex for a mixture of many gases for the simulation. An easy simplification would be to assume that each species diffuses into a mixture of gases. Under this simplification, equation 1.22 becomes equation 1.23.

$$D_{i,mix} = \frac{A \cdot T^{3/2}\sqrt{1/M_i + 1/M_{mix}}}{p\sigma_{i,mix}^2\Omega} \tag{1.23}$$

Moreover, after considering the turbulent contributions, the dispersion

coefficient is usually written as [46, 58, 59]:

$$D_{\mathrm{ig}} = \frac{\phi}{\tau} D_{ij} + 0.5 d_p \left| \mathbf{V}_{\mathrm{g}} \right| \tag{1.24}$$

1.4 Project objectives

It was the aim of this project to solve the following four key issues.

- Develop a detailed one-dimensional biomass gasification model. Predict the behaviour during the gasification process. Validate the simulation results with experimental data from the literature.
- Extend the gasification model of a single biomass pellet into a packed bed gasification model.
- Validate the packed bed gasification model with the experimental data in cooperation with BEST - Bioenergy and Sustainable Technologies GmbH at Graz University of Technology.
- Investigate the most influential factors in packed-bed gasification/combustion.

1.5 Thesis outline

This thesis dissertation comprises a summary section of six chapters and a collection of papers. An outline of the six chapters is as follows:

Chapter 1 gives a background of this work. It also defines the objectives and key aims to be solved in the project.

Chapter 2 explains the methodology of the mathematical model. The methodology includes two parts: thermochemistry and fluid mechanics. In the thermochemistry part, the reaction mechanisms, such as drying model, pyrolysis model and combustion model are explained. In the second part the algorithm that is used in the CFD model, the governing equations and the boundary conditions, are presented.

Chapter 3 presents the model validation for a single biomass particle. The chapter has two parts, the first part is about model validation of pyrolysis, the second part is about the model validation of combustion. In each part, the source term of the governing equations and the discretized equations of the partial differential equations are presented. The modeling results are also presented and discussed.

Chapter 4 presents the results of biomass packed bed combustion. It present the natural ignition of the packed bed under different primary flow.

This is followed by a presentation of the experimental data on the influence of the primary air flow on the combustion mechanism of the packed bed.

Chapter 5 draws conclusions on the Ph.D. project and gives recommendations for future work.

1.6 List of papers

In the period of this study, the following papers have been published or submitted under consideration for publication:

Journal papers:

- Paper A: A drying model for thermally large biomass particle pyrolysis **Xiyan Li**, Chungen Yin. Published in Energy Procedia 1294-1302 (2019)
- Paper B: A detailed pyrolysis model for a thermally large biomass. **Xiyan Li**, Chungen Yin, Søren Knudsen Kær, Thomas Condra. Fuel, 2020, Accepted
- Paper C: A detailed computational fluid dynamics model on biomass pellet smoldering combustion and its parametric study. **Xiyan Li**, Chungen Yin, Søren Knudsen Kær, Thomas Condra. Biomass & Bioenergy, 2020, submitted

Conference papers:

- Paper D: Description of a comprehensive mathematical model: Towards a comprehensive biomass particle gasification model. **Xiyan Li**, Chungen Yin. Proceedings of the 25th European Biomass Conference & Exhibition, EUBCE2017
- Paper E: Importance of the sub-processes in solid fuel particle gasification: heat conservation and reaction mechanism. **Xiyan Li**, Chungen Yin, Thomas Condra. Proceedings of the 13th Conference on Sustainable Development of Energy, Water, and Environment Systems, SDEWES2018.

Chapter 2

Model for the thermo-chemical conversion of biomass particles

This chapter presents the biomass gasification process. It explains the reactions that take place within different thermo-chemical conversion processes and presents the methodology for simulating the gasification process.

Biomass thermo-chemical conversion is normally considered as quite complex, not only because the water content in biomass is usually higher than conventional fossil fuels, but also because its complex reactions during thermo-chemical conversion. In this project, the study focuses on three key process paths during biomass thermo-chemical conversion: biomass drying, pyrolysis, and combustion/gasification. Drying is very important as water evaporation can delay the particles heating-up quite considerably [32]. As a result, sometimes a re-condensation is considered where there is high diffusion and convection rates [60]. During the biomass thermo-chemical conversion, the water content is usually in the form of capillary water, free water and bound water. Both capillary and free water are treated in the same manner in this project since they both exist in a liquid form within the pores. The bound water is generally considered as bound to the biomass fiber, and therefore a fiber saturation point (FSP) is taken into account in many studies. A free-water continuity point (45%) is used by S.S.Alves and J.L.Figueiredo [61].

For biomass pyrolysis, the main process is the decomposition of virgin biomass. After the volatiles are released from the biomass and decomposes into different kinds of light gases, reactions such as char gasification and ho-

mogeneous reactions need then to be considered. A typical thermo-chemical process for virgin biomass is shown in Fig.2.1.

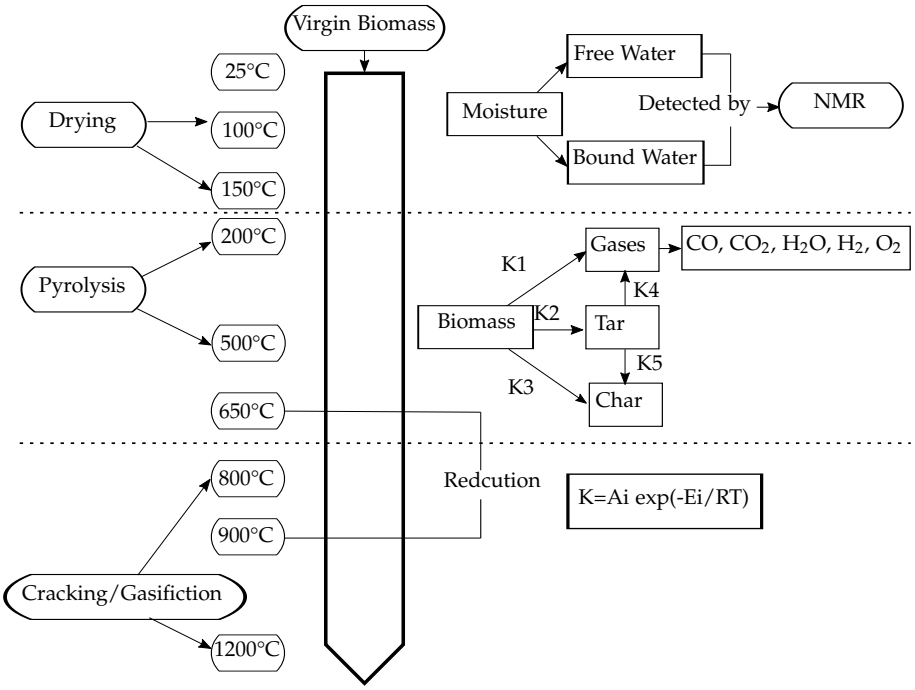

Fig. 2.1: Process of gasification

2.1 Drying model

As illustrated above, drying is the first step before any thermo-chemical treatment. The three different kinds of water in biomass, as mentioned above, are treated differently in the literature through different models.

Usually the capillary water evaporation is solved by using an equilibrium model, where the moisture content is assumed to be in dynamic equilibrium. If the saturation pressure is higher than the water vapour partial pressure, then the water changes from liquid form to gas form, and vice versa. The equilibrium model can be expressed as:

$$H_2O(l) \rightleftharpoons H_2O(g) \tag{2.1}$$

$$r_{H_2O} = S_a \frac{\rho_{fw}}{\rho^0_{fw}} \times h_{m,pore} \left(\rho^{sat}_{\nu} - \rho_g Y_{evap}\right) \tag{2.2}$$

where $h_{m,pore}$ represents the mass transfer coefficient of vapour within the pores. In previous studies, $h_{m,pore}$ is calculated using Fick's law to describe the moisture migration. A Sherwood number is introduced to calculate the mass transfer and this is normally written as:

$$Sh = h_{m,pore} \times L / d_{pore,hydraulic} \tag{2.3}$$

Under laminar flow conditions, the Sherwood number can be expressed in another form by using the Reynolds number and the Schmidt number, as shown in equation 2.4:

$$Sh = 2.0 + 0.6 Re^{1/2} Sc^{1/3} \tag{2.4}$$

It is assumed that the flow within the pore of a biomass pellet is laminar and according to [62], the Sherwood number for a laminar flow through a duct is:

$$Sh = 3.66 \tag{2.5}$$

Therefore, the mass transfer coefficient of the vapor within pores can be written as equation 2.6. This is also the equation used by Lu et al. [14] and Haberle et al. [55].

$$h_{m,pore} = 3.66 \times D_{eff,fw} / d_{pore,hydraulic} \tag{2.6}$$

The most commonly used free water evaporation model during thermo-chemical treatment is the so-called thermal model. Equation 2.7 applies to the situation when the temperature is above the evaporation temperature. In this model, the evaporation temperature is set to 100 °C.

$$r_{H_2O} = F_{heat} / (\delta h_{evap}) \tag{2.7}$$

$$F_{heat} = S_a (h_T (T_j - 373.15) + \epsilon \sigma ((T_j)^4 - 373.15^4)) \tag{2.8}$$

The bound water refers to the water that is bound in the biomass fiber or molecules through chemical bonds. In general, there are three kinds of bound water, compound water, vicinal water and multilayer water. In this model, they are unified as bound water and the reaction rate is expressed as an Arrhenius expression, as shown in equation 2.9.

$$k_{H_2O} = A_{evap} \exp(-E_{evap} / RT) \tag{2.9}$$

2.2 Pyrolysis model

To enable a CFD simulation of biomass pyrolyisis to be carried out, there is one more question that arises besides drying, and that is how to formulate the decomposition model. Much research has been done on the decomposition of biomass and one general approach is to treat biomass as a combination of solid volatile, ash, water and carbon [24, 59, 63–67]. In this way, the decomposition of biomass is treated as a one-step volatile release process, such as:

$$\text{Virgin biomass} \longrightarrow \text{Char} + \text{Ash} + \text{light gases} \tag{2.10}$$

More elaborate decomposition methods have also been discussed in Chapter 1. In this work, the one-step global model is used, because it avoids the instability of tar production in the simulation and avoids the measurement of cellulose, lignin and hemicellulose.

2.3 Combustion/gasification model

2.3.1 General combustion scheme for hydrocarbons

The hydrocarbon oxidation process can be very complex. The hydrocarbons can undergo complete or incomplete oxidation, depending on the oxygen flux. The hydrocarbon combustion mechanism can be classified into three categories based on the reaction schemes, namely, single-step, two-step and four-step reaction schemes.

The single-step reaction scheme: The single-step reaction scheme [68] assumes no intermediate products during the combustion. The oxygen is sufficient to support complete oxidative combustion. The reaction can be written as equation 2.11.

$$\text{Fuel} + \text{n}_1\,\text{O}_2 \longrightarrow \text{n}_2\,\text{CO}_2 + \text{n}_3\,\text{H}_2\text{O} \tag{2.11}$$

The rate expression of the single-step reaction scheme can be written as:

$$k_{\text{ov}} = AT^n \exp\left(-E_a/RT\right)[\ \text{Fuel}\ ]^a[\ \text{Oxidizer}\ ]^b \tag{2.12}$$

The two-step reaction scheme: The complete oxidation combustion process is very idealistic and gives no information of any intermediate components. This gives rise to the need for a multi-step scheme to describe the process. Therefore, a two-step combustion scheme that assumes one intermediate production during the combustion, as shown in equation 2.13 and equation 2.14,

can be used:

$$C_nH_n + \left(\frac{n}{2} + \frac{m}{4}\right) O_2 = nCO + \frac{m}{2}H_2O \tag{2.13}$$

$$CO + 1/2O_2 = CO_2 \tag{2.14}$$

Dryer and Westbrook [68] studied the single-step and two-step combustion schemes for hydrocarbons. The simplified hydrocarbon combustion scheme, discussed by Dryer and Westbrook [68], can correctly reproduce experimental flame speeds over a wide range of equivalence ratio and pressures. However, the model has only been applied to laminar flame propagation.

The four-step reaction scheme: Jones and Lindstedt [69] proposed a four-step global reaction schemes for alkane hydrocarbons up to butane. In their model, the intermediate products from hydrocarbon combustion are H_2 and CO. The reaction scheme is shown in equations 2.15 to 2.18.

$$C_nH_{2n+2} + n/2\, O_2 \longrightarrow nCO + (n+1)\, H_2 \tag{2.15}$$

$$C_nH_{2n+2} + n\, H_2O \longrightarrow nCO + (2n+1)\, H_2 \tag{2.16}$$

$$H_2 + 0.5\, O_2 \longleftrightarrow H_2O \tag{2.17}$$

$$H_2O + CO \longleftrightarrow H_2 + CO_2 \tag{2.18}$$

The four-step global hydrocarbon combustion mechanism gives excellent agreement with measured major species distribution. It also shows good agreement for the burning velocities for both lean and moderately rich mixtures. In addition, the four-step reaction mechanism also shows good agreement with counter-flow diffusion flames burning methane and propane at various rates of strain.

Considering all the good results shown by the four-step hydrocarbon reaction mechanism, it is also used in the model that is presented in this work. A parametric study is done with regards to the effect to the temperature profile for both the two-step and four-step combustion schemes.

2.3.2 Heterogeneous reaction model

The purpose of gasification is to make carbon react with CO_2, H_2O, H_2 to produce syngas. Usually this process takes place above 700 °C. The combustion process is where the carbon products and other combustible gases are oxidised in order to use the energy for heat and power. The two kinds of combustion reactions that occur within a porous media, homogeneous reactions and carbon oxidation reactions. There is complete oxidation and incomplete oxidation for carbon oxidation, as shown in equations 2.19 and 2.20. The products from incomplete oxidation can be further transformed into CO_2, as shown in equation 2.21. The combustion here only considers the carbon in biomass, whilst the trace elements are ignored.

$$2\,C + O_2 \longrightarrow 2\,CO \tag{2.19}$$

$$C + O_2 \longrightarrow CO_2 \tag{2.20}$$

Equations 2.19 and 2.20 can be unified into one reaction, as follows:

$$C + \alpha\,O_2 \longrightarrow 2\,(1-\alpha)CO + (2\,\alpha\text{-}1)\,CO_2 \tag{2.21}$$

A few more equations are added for gasification, mainly for carbon gasification. Equation 2.22 is also called the Boudouard reaction, equation 2.23 is called the water-gas reaction, and equation 2.24 is the methanation reaction.

$$C + CO_2 \longrightarrow 2\,CO \tag{2.22}$$

$$C + H_2O \longleftrightarrow CO + H_2 \tag{2.23}$$

$$C + 2\,H_2 \longleftrightarrow CH_4 \tag{2.24}$$

Table 2.1 shows all the reaction rates expressions in biomass combustion/gasification.

In this project, the reaction rates are calculated using an Arrhenius equation which has the form of equation 2.25. However, for the heterogeneous reactions, the Arrhenius equations has the form of equation 2.26.

$$k = Ae^{E_a/RT} \tag{2.25}$$

Table 2.1: Reaction rate

No.	Reaction	Reaction rate	Ref.
1	2.9	$r = \rho k_{H_2O}$	[58]
2	2.19	$r = \frac{\partial O_2}{\partial t} = S_{a,char} \frac{\rho_C}{\rho_C + \rho_B + \rho_A} k\varepsilon[O_2]$	[14]
3	2.20	$r = \frac{\partial O_2}{\partial t} = S_{a,char} \frac{\rho_C}{\rho_C + \rho_B + \rho_A} k\varepsilon[O_2]$	[14]
4	2.21	$r = \frac{\partial O_2}{\partial t} = S_{a,char} \frac{\rho_C}{\rho_C + \rho_B + \rho_A} k\varepsilon \frac{P_{O_2}}{1/k_r + 1/k_d}$	[58]
5	2.15	$r = \frac{\partial C_n H_{2n+2}}{\partial t} = k[C_n H_{2n+2}][O_2]^{n/2}$	[58]
6	2.14	$r = \frac{\partial CO}{\partial t} = k[CO][O_2]^{0.25}[H_2O]^{0.5}$	[70]
7	2.15	$r = \frac{\partial C_n H_{2n+2}}{\partial t} = k[C_n H_{2n+2}][O_2]^{n/2}$	[69, 70]
8	2.16	$r = \frac{\partial C_n H_{2n+2}}{\partial t} = k[C_n H_{2n+2}][H_2O]^n$	[58]
9	2.17	$r = \frac{\partial H_2}{\partial t} = k[H_2][CO_2]^{0.5}$	[70]
10	2.18	$r = \frac{\partial CO_2}{\partial t} = k[CO]^1[H_2O]^1$	[70]
11	2.22	$r = \frac{\partial CO_2}{\partial t} = S_{a,char} \frac{\rho_C}{\rho_C + \rho_B + \rho_A} k\varepsilon[CO_2]$	[14]
12	2.23	$r = \frac{\partial H_2O}{\partial t} = S_{a,char} \frac{\rho_C}{\rho_C + \rho_B + \rho_A} k\varepsilon[H_2O]$	[58]
13	2.24	$r = \frac{\partial H_2}{\partial t} = S_{a,char} \frac{\rho_C}{\rho_C + \rho_B + \rho_A} k\varepsilon[H_2]$	[36]

$$k = AT^b e^{E_a/RT} \tag{2.26}$$

The kinetic data for the Arrhenius equations are listed in Table 2.2.

Tables 2.1 and 2.2 show the basic reactions that occur in biomass thermochemical treatment. However, in reality the reaction rate adjustment is much more complex than that shown in the tables. An example of this is the combustion of carbon which is referred in the paragraph below.

There are usually two kinds of burning models for char combustion, the one-film model and the two-film model [71]. Both models assume that the char combustion is diffusion-controlled. The one-film model assumes that the burning process is quasi-steady, and that the highest temperature occurs on the surface of the char layer, without a flame. Therefore, the combustion front moves towards the pellet center in time. On the other hand, the two-film model assumes that homogeneous reactions occur in a flame sheet outside

Table 2.2: Kinetic data used in this model

Reaction equation	Pre-exponential factor (A) s^{-1}	Activation energy (E_a) [J/kmol]	Heat of reactions (δH)[kJ/kg]
2.9	5.13×10^{10}	8.8×10^{7}	-2440
2.19	$0.658(m/s/K)$	7.48×10^{6}	9212
2.20	-	-	-
2.21	$0.658(m/s/K)$	7.483×10^{7}	$9992.068\alpha - 1048.159$
2.15	2.119×10^{11}	2.027×10^{8}	$\frac{h_0+17383n+13433}{14n+2}$
2.14	2.39×10^{12}	2.39×10^{12}	10114.28
2.15	4.0×10^{11}	1.26×10^{8}	$\frac{h_0+3950n}{14n+2}$
2.16	3.0×10^{8}	1.26×10^{8}	$\frac{h_0-9483n}{14n+2}$
2.17	6.8×10^{15}	1.67×10^{8}	13435.94
2.18	2.75×10^{9}	8.4×10^{7}	-12879.38
2.22	3.42	1.297×10^{5}	-10933.33
2.23	3.42	1.297×10^{5}	-14383.33
2.24	3.42×10^{-3}	1.297×10^{5}	-1701.59

the char layer. The highest temperature is generated from the homogeneous reactions. Normally, the two-film model is assumed to be a refinement of the one-film model. But for single particle combustion, considering the existence of incandescence and no flame inside the pores, the one-film model is also used. Figure 2.2 shows the two models, where (B) is the one-film model, (C) is the two-film model, and (A) indicates the heterogeneous reactions that could happen during char combustion.

However, the following question arises: what if the reaction is not diffusion controlled? For the kinetic-controlled combustion model, the reaction rate is easily expressed with the Arrhenius law, and the particle diameter shrinks linearly with time. The reaction rate of carbon combustion is usually written in a circuit type equation, analogous to Ohm's law, in the form of equation 2.27.

$$\mathrm{r} = \frac{\mathrm{Y_{O_2,\infty}}}{\mathrm{R_{kin}} + \mathrm{R_{diff}}} \tag{2.27}$$

where R_{kin} denotes the kinetic reaction rate, which has a Arrhenius expression form as shown in equation 2.28 [71].

$$\mathrm{R_{kin}} = 1/\mathrm{K_{kin}} = \frac{\nu \mathrm{R_g T_s}}{4\pi \mathrm{r^2 MW_{mix} K_c P}} \tag{2.28}$$

where ν denotes the mass stoichiometric coefficient, MW_{mix} is the average

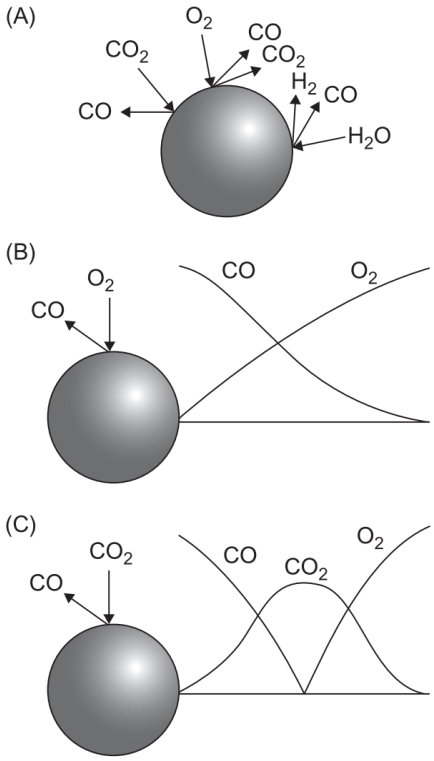

Fig. 2.2: Combustion models for char. [72]

molecular mass, K_c is the rate coefficient and R_g is the universal gas constant.

$$R_{diff} = \frac{(\nu + Y_{O_{2,s}})}{\rho D 4\pi r_s} \tag{2.29}$$

where R_{diff} denotes the diffusion rate, shown in equation 2.29.

The values of the two resistances in equation 2.27, R_{kin} and R_{diff}, depend on many parameters, such as the temperature, pellet size, pore size and so on: their values can vary greatly. If R_{diff} is much larger than R_{kin}, then the combustion is diffusionally controlled, otherwise it is kinetically controlled. The intermediate regime is when both resistances are about the same value. S. R. Turns [71] gives a summary of the reaction expressions in his book, as shown in Table 2.3.

Table 2.3: Combustion regimes

Regime	$R_{\mathbf{kin}}/R_{\mathbf{diff}}$	**Burning rate law**	**Conditions of occurrence**
Diffusion controlled	$<<1$	$\dot{m}_C = Y_{O_2,-}/R_{\text{diff}}$	r_s large T_s high P high
Intermediate	~ 1	$\dot{m}_C = Y_{O_2-}/(R_{\text{diff}} + R_{\text{kin}})$	$-$
Kinetically controlled	$>>1$	$\dot{m}_C = Y_{O_2-}/R_{\text{Lin}}$	r_s small T_s low P low

2.4 Numerical solutions

Due to the complexity of the model described above, the solution to the detailed gasification problem for a single pellet, or a fixed bed, can only really be solved using a numerical methods based approach. The finite volume method is used in this project. The clear advantage of using the finite volume method is that every term in the governing equations has its certain physical significance and that conservation of the governing equations is ensured and also makes it easier to explain the modeling results. The governing equations are integrated partial differential equations that are linearised and coupled together to solve the temperature, pressure and species [73].

The formulation of the model is based on a series of assumptions, which are published in paper D [74]. In this paper the algorithm for solving the key processes during gasification are given, as shown in Fig. 2.3. The assumptions are as follows:

- The biomass pellet shape is assumed as spherical in shape.
- The biomass particle is in local thermal equilibrium.
- The variables in the governing equations are under thermodynamic equilibrium.
- During the reaction, the biomass particle is considered as a porous structure media, and the gases generated inside the particle obey the ideal gas law.
- The specific surface area changes during the whole gasification process and thus shrinkage or swelling is also considered.
- The airflow inside the particle obeys Darcy's law.
- External forces are not considered.
- There is no fragmentation of the particle during the whole gasification process.

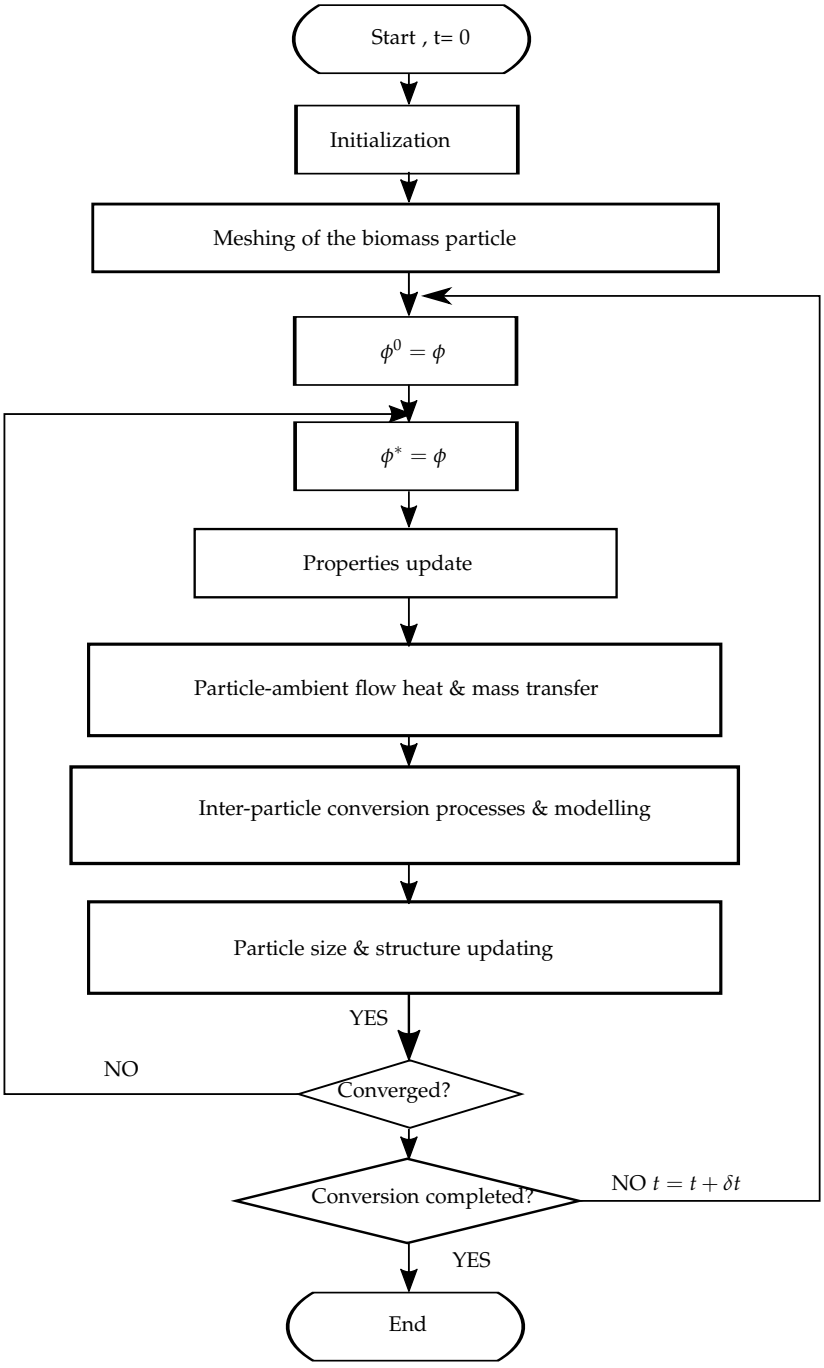

Fig. 2.3: Structure of algorithm

2.4.1 Transport equations

The same set of governing equations for both the single biomass pellet and the packed bed are applied and these are shown below. The discrete form of the transport equations are shown in Appendix II.

Energy conservation:

$$\frac{\partial\left(\rho_g C_{pg} T + \rho_s C_{ps} T + \rho_l C_{pl} T\right)}{\partial t} + \operatorname{div}\left(\varepsilon \rho_g u C_{pg} T_g\right) = \operatorname{div}\left(K_{eff} \nabla T\right) + S_T \tag{2.30}$$

$$S_T = -\sum_{k=1}^{N} \Delta h^0_{f,k} \dot{w}_k - \sum_{k=1}^{N} \Delta h_{f,k} \dot{w}_k \tag{2.31}$$

Gas species transportation:

$$\frac{\partial\left(\varepsilon \rho_g Y_{ig}\right)}{\partial t} + \operatorname{div}\left(\varepsilon \rho_g u Y_{ig}\right) = \operatorname{div}\left(D_{ig} \nabla\left(\varepsilon \rho_g Y_{ig}\right)\right) + S_{Y_{ig}} \tag{2.32}$$

Solid species:

$$\frac{\partial\left(\rho_i\right)}{\partial t} = S_i \tag{2.33}$$

Considering the low Mach number within the biomass pellet, the pressure and velocity within the control volume is calculated by Darcy's law and the continuity equation:

$$\frac{\partial\left(\partial \rho_g\right)}{\partial t} + \operatorname{div}\left(\varepsilon \rho_g u\right) = S_g \tag{2.34}$$

$$\vec{u} = -\frac{\eta}{u} \nabla P \tag{2.35}$$

2.4.2 Boundary conditions

Boundary conditions for a single biomass pellet

For the single biomass pellet simulation, the boundary conditions are set as follows:

At the pellet center:

$$\left.\frac{\partial \phi}{\partial x}\right|_{x=0} = 0 \quad \text{(symmetry)} \tag{2.36}$$

where ϕ represents $T4$, P, Y_j.

At the pellet surface:

$$k_{eff} A_s \left.\frac{\partial T}{\partial r}\right|_s = h_T A_s \left(T_\infty - T_s\right) + \varepsilon_{emis} \sigma A_s \left(T_{rad}^4 - T_s^4\right) \tag{2.37}$$

$$D A \frac{Y_B - Y_P}{\Delta x/2} = A h_M \left(Y_\infty - Y_B\right) \tag{2.38}$$

$$P|_{\mathrm{s}} = P_{\mathrm{atm}} \tag{2.39}$$

To linearize the radiation term, a Taylor series expansion is used for the linearization of the source term. Therefore, equation 2.37 can be written as:

$$k_{eff} A_s \frac{T_s - T_P}{\Delta r/2} = h_T A_s \left(T_\infty - T_s\right) + \varepsilon_{emis} \sigma A_s \underbrace{\left(T_{rad}^4 - \left(T_s^*\right)^4 - 4\left(T_s^*\right)^3 \left(T_s - T_s^*\right)\right)}_{\text{linearization}\left(T_{rad}^4 - T_s^4\right) \text{ using Taylor expansion}} \tag{2.40}$$

The selection of h_M and h_T is important in order to handle the boundary condition at the outer surface in a correct manner. To calculate h_M and h_T, a boundary layer outside spherical pellet is assumed. By applying Ohm's law and neglecting the Stefan flow effect, the heat and mass transfer coefficients can be calculated as [20]:

$$\mathrm{Nu}_0 \equiv \frac{h_{\mathrm{T}} d_{\mathrm{p}}}{\bar{k}_{\mathrm{g}}} = 2.0 + 0.64 \mathrm{Re}^{0.5} \overline{\mathrm{Pr}}^{0.33} \tag{2.41}$$

$$\mathrm{Sh}_0 \equiv \frac{h_{\mathrm{M}} d_{\mathrm{p}}}{\overline{D}_{\mathrm{g}}} = 2.0 + 0.64 \mathrm{Re}^{0.5} \overline{\mathrm{Sc}}^{0.33} \tag{2.42}$$

To calculate the average properties in equations 2.41 and 2.42, an average temperature and species concentration is assumed within the boundary layer. An empirical expression is applied here to calculate the average temperature and species concentration, the so-called one-third law [20, 24, 70].

$$T_{ref} = T_s + 1/3 \left(T_\infty - T_s\right) \tag{2.43}$$

$$Y_{j,ref} = Y_{j,s} + 1/3 \left(Y_{j,\infty} - Y_{j,s}\right) \tag{2.44}$$

Boundary conditions for a packed bed

At the bed bottom near the grate:

$$\begin{aligned} &\mathrm{u} = u_{\mathrm{in}}; \mathrm{P} \equiv P_{\mathrm{atm}} \\ &D_{\mathrm{g}} A \frac{\partial \mathrm{Yg}}{\partial x}\Big|_{\mathrm{s}} = A h_M \left(Y_\infty - Y_{\mathrm{g},s}\right) \\ &k_{\mathrm{eff}} A \frac{\partial T}{\partial x}\Big|_{\mathrm{s}} = A h_T \left(T_{\mathrm{in}} - T_S\right) + A\varepsilon\sigma \left(T_{\mathrm{in}}^4 - T_S^4\right) \end{aligned} \tag{2.45}$$

On the bed top close to the free board:

$$\begin{aligned} &\mathrm{u} = u_{N-1} \times \rho_{N-1}/\rho_{out}; \mathrm{P} \equiv P_{atm} \\ &D_g A \frac{\partial \mathrm{Y}_g}{\partial x}\Big|_{s} = A h_M \left(Y_\infty - Y_{g,s}\right) \\ &k_{cff} A \frac{\partial T}{\partial x}\Big|_{s} = A h_T \left(T_\infty - T_s\right) + A\varepsilon\sigma \left(T_{rad}^4 - T_s^4\right) \end{aligned} \tag{2.46}$$

2.4.3 Initial conditions

Initial conditions for the biomass pellet

$$\mathrm{u} = 0; \mathrm{P} \equiv P_{atm}; \mathrm{T} = T_{\mathrm{room}}; Y_{\mathrm{g}} = Y_{\mathrm{Inert}}; \tag{2.47}$$

Ambient flow conditions: For pyrolysis, the ambient flow conditions are shown in equation 2.48.

$$T_\infty = T_f; u_\infty = U_f; Y_{\mathrm{O_2},\infty} = 0.0; Y_{\mathrm{N_2},\infty} = 0.1; \rho_\infty = \rho_{\mathrm{f}} \tag{2.48}$$

For combustion, the ambient flow conditions are shown in equation 2.49.

$$T_\infty = T_f; u_\infty = U_f; Y_{\mathrm{O_2},\infty} = 0.23; Y_{\mathrm{N_2},\infty} = 0.77; \rho_\infty = \rho_{\mathrm{f}} \tag{2.49}$$

Initial conditions for the packed bed

$$\mathrm{u} = 0; \mathrm{P} \equiv P_{atm}; \mathrm{T} = T_{\mathrm{room}}; Y_{\mathrm{g}} = Y_{\mathrm{air}}; Y_s = Y_{s,\mathrm{in}}; \rho_{\mathrm{g}} = \rho_{\mathrm{air}}; \rho_s = \rho_{s,\mathrm{in}} \tag{2.50}$$

A spatial discretization of the transport equations is based on a central difference scheme in space and a fully implicit method is used for temporal discretization. The coefficients after solution using TDMA are presented in Appendix II.

Chapter 3

Model validation for single biomass particle conversion

This chapter presents the results of the simulation of a single biomass particle pyrolysis and combustion. The reactions used are also presented. The validation against the experimental data and detailed simulation results are presented in the papers attached.

The model was first based on a pyrolysis case of a single biomass pellet. After validating the pyrolysis case with experimental data from Lu et al. [14], the model was changed to a combustion model under atmospheric air. This chapter also presents the detailed form of the discretised partial differential equations and the main reactions that take place, both under nitrogen pyrolysis and air combustion.

3.1 Reactions on nitrogen pyrolysis of a single biomass pellet

The model validation is based on the experimental data from Lu et al. [14]. The biomass pellet is poplar wood, whose composition is shown in Table 3.1.

Table 3.1: Proximate analysis, ultimate analysis, heating value of poplar wood pellet

	Proximate analysis					Ultimate analysis				LHV
Sample	**C**	**H**	**O**	**N**	**S**	**FC**	**Vol**	**Ash**	**M**	$[kJ/kg]$
PW	47.4	8.8	43.7	<0.1	0.0	9.5	90	0.5	6.0	17050

No accurate heating value data is available in the original literature and therefore the lower heating value here is calculated based on the proximate analysis and ultimate analysis according to Basu's method [75]. The formation enthalpy is calculated as -157767 kJ kmol^{-1}, with a chemical formula of CH_xO_y and a relative molecular mass of 28.0 kg kmol^{-1}. The volatile is assumed as a solid form before devolatilization begins, and after devolatilization starts the volatile breaks into light gases. In this special case, after considering the heat and mass conservation, the light gases are taken as: C_3H_8, H_2, CO, CO_2. Therefore, the reactions that takes place in the pyrolysis can be written as listed in Table 3.2.

Table 3.2: Kinetic data used in this model

Reaction	Chemical reactions	References
2.10	r1 Virgin biomass $\longrightarrow$ Char + Ash + light gases	[58]
2.1	r2 $H_2O(l) \rightleftharpoons H_2O(g)$	[55]
2.1	r3 $H_2O(l) \rightleftharpoons H_2O(g)$	[14, 60]
2.22	r4 $C + CO_2 \longrightarrow 2\,CO$	[14]
2.23	r5 $C + H_2O \longleftrightarrow CO + H_2$	[14]
2.24	r6 $C + 2\,H_2 \longleftrightarrow CH_4$	[36]
2.16	r7 $C_3H_8 + 3\,H_2O \longrightarrow 3\,CO + 7\,H_2$	[69]
2.18	r8 $H_2O + CO \longleftrightarrow H_2 + CO_2$	[70]

r_i refers to the reaction rate
k_i refers to the rate constant in the Arrhenius equation of the current reaction.

3.2 Validation of pellet under N_2 pyrolysis and discussion

The pyrolysis model of a single biomass pellet is validated with the experimental data from Lu et al. [14] that is presented in section 3.1. Both the experimental data and the simulation data from Lu et al. [14] are compared with the simulation results from the model. The results are shown in Fig. 3.1.

Figure 3.1 plots the temperature at the pellet center and on the pellet surface. For the surface temperature, both the simulations from this model and from the model of Lu et al. [14] fit well with the experimental data. In this work, the surface temperature rises more rapidly than that from the experiments and from the model of Lu et al. [14] at the beginning, though within a reasonable range. At the pellet center, both simulation results show

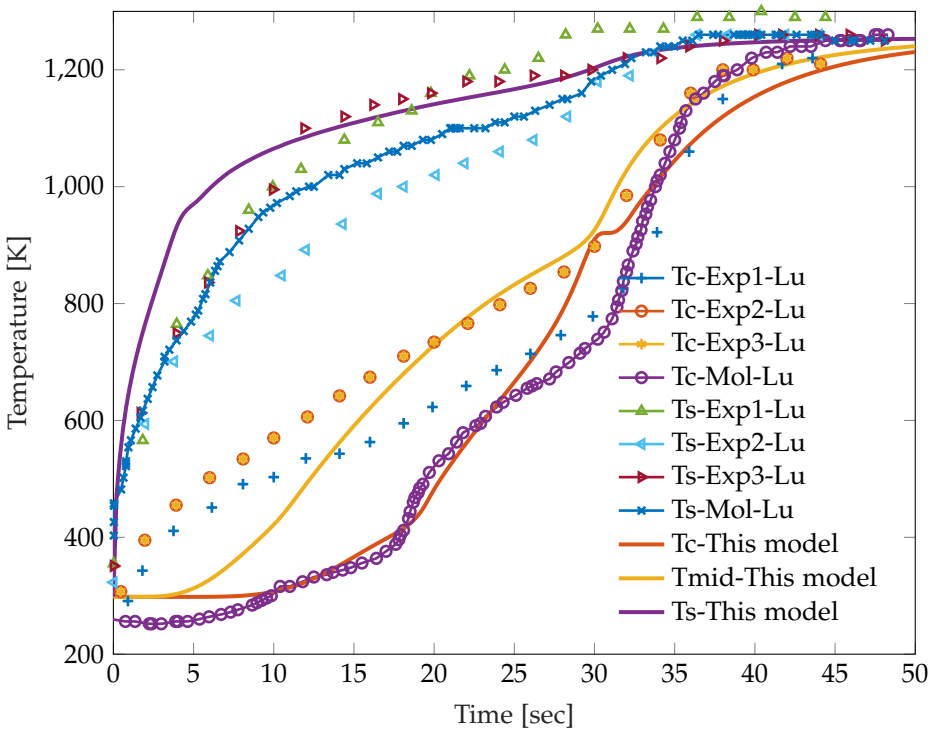

Fig. 3.1: Temperature validation for pyrolysis of a single biomass pellet

a much lower temperature than the experiments under the initial 20 seconds and this is because the water has evaporated by then. Before the water is totally consumed, the temperature of the water at a certain point within the pellet can not above the boiling point. To prove this claim, Fig. 3.2 is plotted.

Figure 3.2 shows the vapor concentration at seven different locations, which shows the distance from the calculation point to the pellet center. The vapor concentration reaches a peak immediately at the beginning, then slowly decreases. This means that the high temperature leads to the flash evaporation of moisture at the pellet surface, with the temperature rising within the pellet, layer by layer, and the vapor produced transported to the surface. The evaporation layer can be found in Fig. 3.2, which is the point when the vapor concentration begins to decrease.

Considering that the gas fraction within the pellet cannot be measured, and thus it cannot be validated, the gas fraction at the pellet surface is plotted in Fig. 3.3 instead. Vital information is shown in Fig. 3.3: the vapor reaches a peak immediately, the other gas species peak at 4 seconds and the devolatilization finishes at 33 seconds. That no gases are released after 33 seconds means that no reactions take place at the time, which also means the

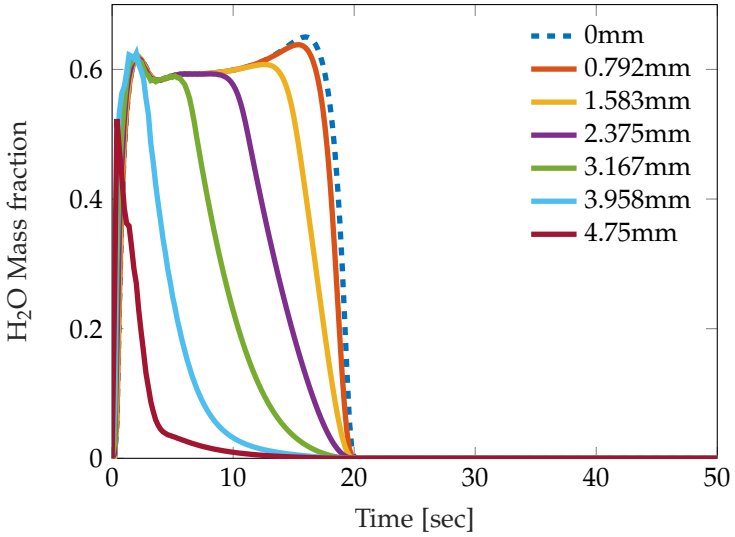

Fig. 3.2: Vapor fraction at seven different locations

temperature rise at the pellet center in Fig. 3.1 is because of the heat transfer from the environment to the pellet.

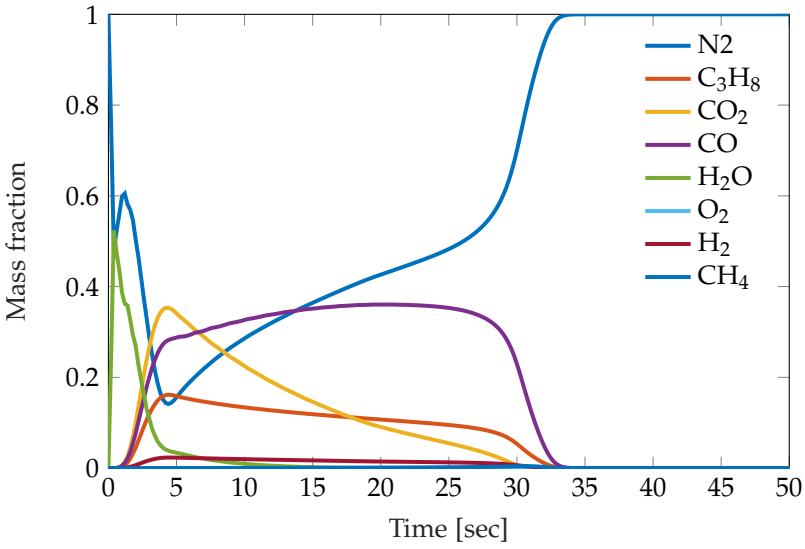

Fig. 3.3: Gas species fraction on the pellet surface

Further results that were produced from this pyrolysis model, together with an extended discussion, can be found in Paper B.

3.3 Reactions in air combustion of a single biomass pellet

Based on the same poplar wood sample, a combustion case was also studied in this work. The reactions that take place in an air combustion are quite different from those under nitrogen pyrolysis. Table 3.3 shows the air combustion reactions which are based on a four-step global reaction scheme for the hydrocarbons [69].

Table 3.3: Kinetic data used in this model

Reaction	Chemical reactions	References
2.10	r1 Virgin biomass $\longrightarrow$ Char + Ash + light gases	[58]
2.1	r2 $H_2O(l) \rightleftharpoons H_2O(g)$	[55]
2.1	r3 $H_2O(l) \rightleftharpoons H_2O(g)$	[14, 60]
2.21	r4 $C + \alpha\, O_2 \longrightarrow 2\,(1-\alpha)CO + (2\,\alpha\text{-}1)\,CO_2$	[58]
2.22	r5 $C + CO_2 \longrightarrow 2\,CO$	[14]
2.23	r6 $C + H_2O \longleftrightarrow CO + H_2$	[14]
2.17	r7 $H_2 + 0.5\,O_2 \longleftrightarrow H_2O$	[70]
2.14	r8 $CO + 0.5\,O_2 \longleftrightarrow CO_2$	[70]
2.16	r9 $C_3H_8 + 3\,H_2O \longrightarrow 3\,CO + 7\,H_2$	[69]
2.15	r10 $C_3H_8 + 1.5\,O_2 \longrightarrow 3\,CO + 4\,H_2$	[69]
2.18	r11 $H_2O + CO \longleftrightarrow H_2 + CO_2$	[70]

r_i refers to the reaction rate
k_i refers to the rate constant in the Arrhenius equation of the current reaction.

3.4 Validation of pellet under air combustion and discussion

The same kind of biomass pellet from pyrolysis analysis is also used in combustion under atmospheric air. Due to the carrier gas changes, the reactions that are used in the model are those shown in Table 3.3. The source terms of the transport equations are listed in Appendix II. Based on the discussion in Chapter 1, the four-step hydrocarbon reaction scheme is applied in this model.

Lu et al. [76] presents the combustion temperature of a single biomass pellet with 6% moisture. The validation is based on this case, and some results are presented below.

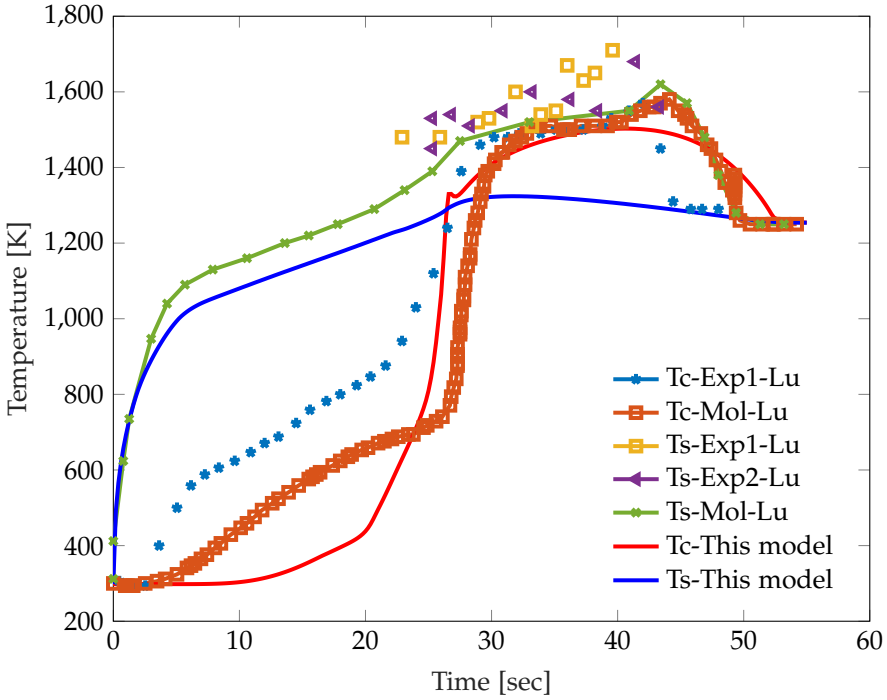

Fig. 3.4: Temperature validation for pyrolysis of a single biomass pellet

Figure 3.4 compares the temperature results from this model, Lu et al. [76] and the experimental data. The results show that the surface temperature from the simulation is lower than the surface temperature from Lu et al. [76] model and the experimental data. This is because the model from this work is for smoldering combustion, which means no flame is formed outside the pellet. Therefore, the pellet surface temperature remains identical to the environment temperature at the end of the process. Haberle et al. [49] simulated the same material for a combusting cylinder and a similar level of surface temperature was found in their model. The temperature at the pellet surface is still lower than the experimental data at the beginning of the combustion, which is similar to the pyrolysis case, caused by water evaporation.

To show a different perspective from section 3.1, the moisture is plotted in the combustion case. The evaporation front can also be found in Fig. 3.5. For example, the evaporation front is at the half-radius length of the pellet at 10 seconds. The moisture is fully evaporated after 20 seconds.

One of the important differences from combustion to pyrolysis is in the char combustion. Therefore, the char density and oxidation rate is plotted in

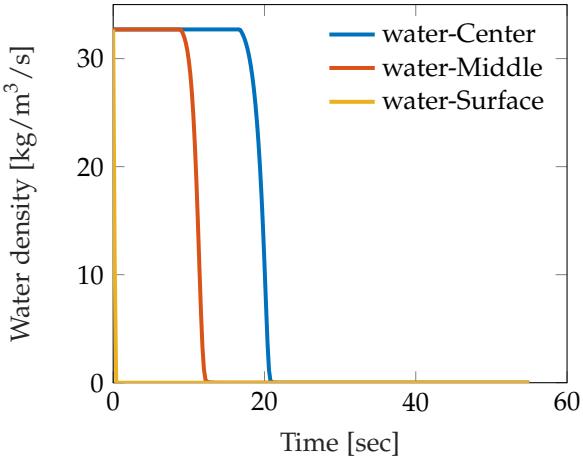

Fig. 3.5: Moisture profile at three locations of the pellet

Fig. 3.6 and Fig. 3.7.

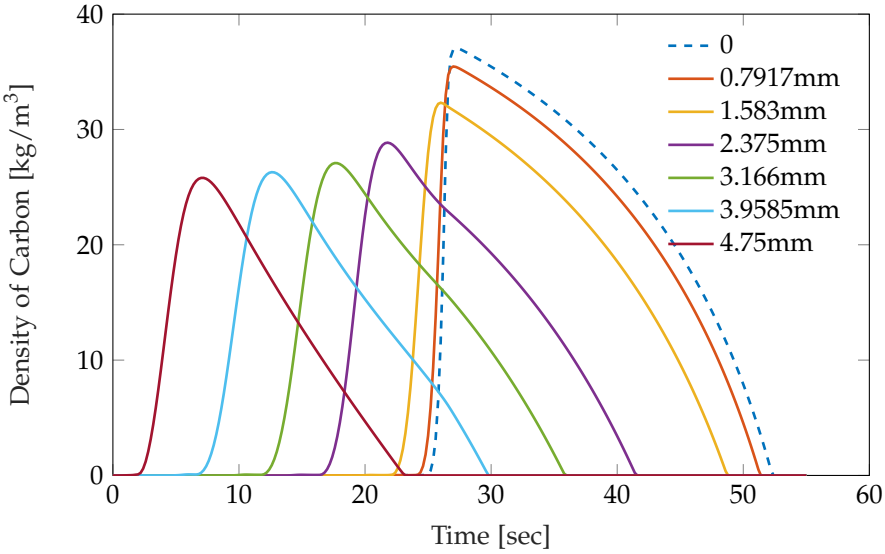

Fig. 3.6: Char density at different locations along the pellet radius

In Fig. 3.6, the char density in different control volumes is plotted. It shows that the char is produced layer by layer and then burnt layer by layer. The highest density of the surface layers is less that those close to the pellet center. This is because the char is generated and burnt at the same time in the control volume at, or near, the surface, due to the higher temperature,

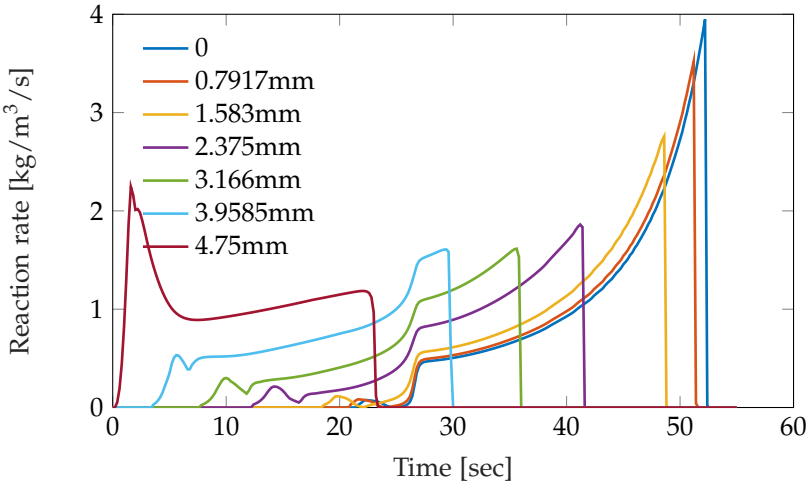

Fig. 3.7: Char combustion rate at the same locations to Fig.3.6

whilst at the pellet center, the char reaches the burning temperature when it is fully separated out from the biomass.

Figure 3.7 confirms this claim. At the location from 0 to 2.375 mm, the reaction rate of char combustion before 25 seconds is almost zero, which means the char is only produced but barely consumed at those locations before 25 seconds.

By comparing Fig. 3.6 and Fig. 3.7 with Fig. 3.4, it can be seen that the temperature increases rapidly after 25 seconds, which is also the same time as the char combustion rate at the pellet center begins to increases and the char density at the pellet center begins to decrease. To conclude, the char combustion at the pellet center contributes to the great temperature rise at the pellet center in Fig. 3.4.

More details on a single biomass combustion can be found in Paper B [77].

3.5 Parametric study on a single biomass combustion case

A parametric study of two parameters was investigated based on the single biomass combustion model. According to Yang et al. [58], the devolatilization rate can vary from slow to fast, and this might affect the duration of the devolatilization stage. Figure 3.8 shows three different devolatilization rates published in the literature. All these three rates were applied in this combustion model, and the results are plotted in Fig. 3.9.

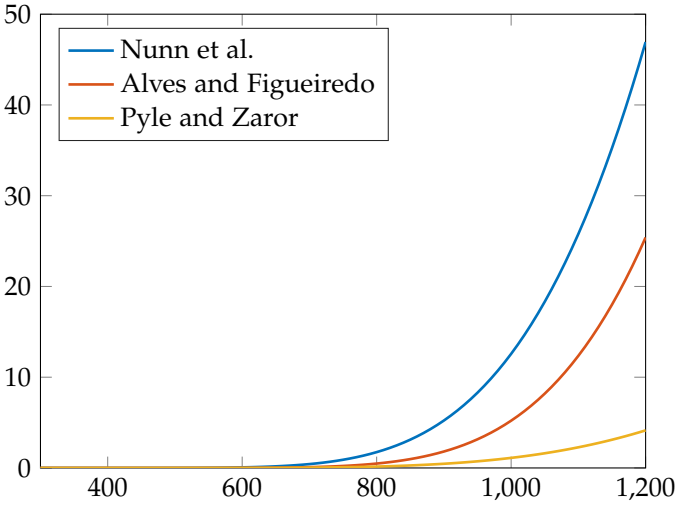

Fig. 3.8: Devolatilization rates parameters from slow to fast [9, 61, 78]

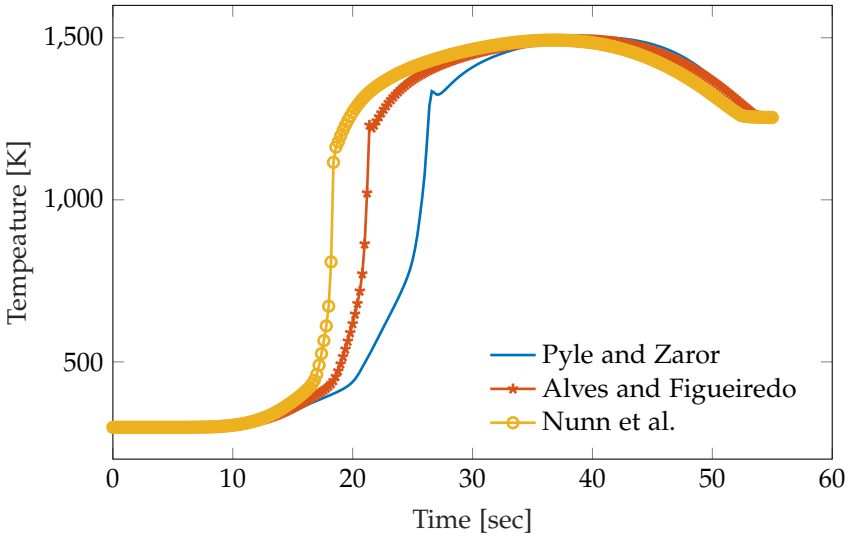

Fig. 3.9: Effect of devolatilization rate on the center temperature of the pellet

Figure 3.9 shows the temperature at the pellet center after applying the devolatilization rates in Fig. 3.8. The figure shows that the fast devolatilization rate leads to a shorter devolatilization stage duration. However, the temperature that the char combustion can reach is not affected.

Figure 3.10 plots the temperature on the pellet surface and at the pellet center after applying the two different hydrocarbon schemes that are men-

tioned in Chapter 2. The results show little discrepancy on the pellet surface between the two-step and the four-step combustion schemes. The temperature discrepancy at the pellet center is around 5% during the devolatilization stage, which is considered as acceptable. The reason for this discrepancy is probably due to gas species properties, as well as that the number of reactions and the composition of intermediate gases are slightly different.

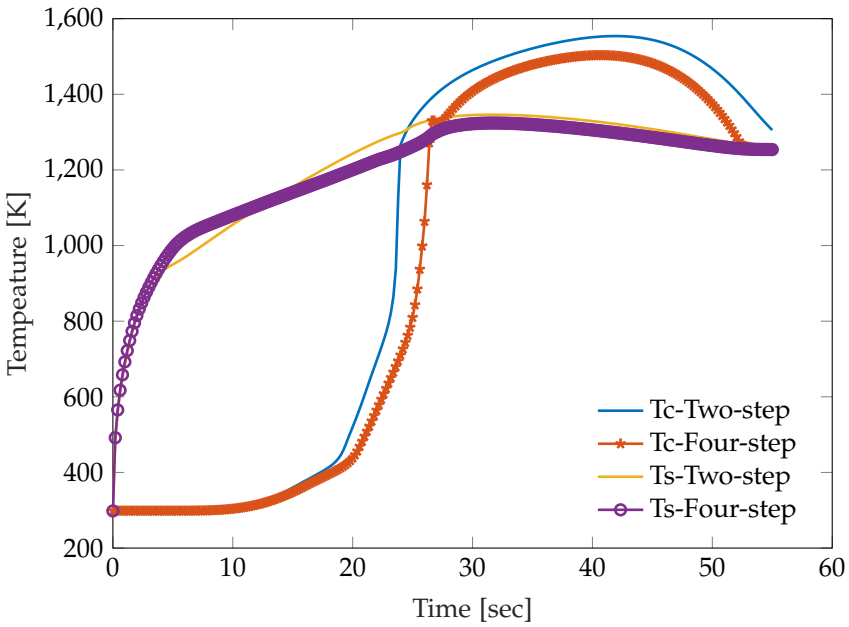

Fig. 3.10: Effect of different hydrocarbon combustion scheme on the simulation temperature

Chapter 4

Experimental study of biomass combustion in a packed bed

This chapter presents an experimental investigation, which was carried out at BEST-Bioenergy and Sustainable Technologies GmbH at Graz University of Technology, on the combustion phenomena in a packed bed. Research has shown that the air mass flow rate is the main operating parameter and distinguishes three stage of combustion: oxygen-limited, fuel limited and cooling by convection [79]. This knowledge was utilised in the experiments, which were carried out on the test rig in Graz, where the movement of the combustion front was investigated. The calculation of the minimum fluidization velocity (MFV), upon which the the experiments were based, is presented.

4.1 Determination of the primary air flow(PAF)

Since the experiments, carried out at BEST-Bioenergy and Sustainable Technologies GmbH, Graz University of Technology, were performed in a packed bed, a minimum fluidization velocity (MFV) was needed to be calculated. MFV is the superficial gas velocity at which the drag force of the upward moving gas becomes equal to the mass of the particles in the bed [80]. Above the value of the MFV, the packed bed becomes a fluidized bed.

Known conditions for the biomass pellet:

Density:

$$\rho_s = 1220 \text{ kg/m}^3 \qquad \rho_B = 291.66 \text{ kg/m}^3 \tag{4.1}$$

Geometry:

Pellet (Cylinder):
Diameter 6 mm, height: 18 mm.
Sample holder (Fig. 4.3):
Diameter: 86 mm, height: $L_m = 172\ mm$.

Calculation of the void fraction of the bed:

$$\begin{aligned} V_{bed} &= V_{fluid} + V_{solid} \\ W_{bed} &= W_{fluid} + W_{solid} \\ \rho_{bed} V_{bed} &= \rho_{fluid} V_{fluid} + \rho_{solid} V_{solid} \end{aligned} \tag{4.2}$$

$$\begin{aligned} &\because \quad \rho_{\text{solid}} V_{\text{solid}} > \rho_{\text{fluid}} V_{\text{fluid}} \\ &\therefore \quad \rho_{\text{bed}} V_{\text{bed}} \cong \rho_{\text{solid}} V_{\text{solid}} \end{aligned} \tag{4.3}$$

$$\varepsilon = \frac{V_{ed} - \frac{\rho_{bed} V_{bed}}{\rho_{solid}}}{V_{bed}} = 1 - \frac{\rho_{bed}}{\rho_{solid}} = 1 - \frac{291.66}{1220} \approx 0.75695 \tag{4.4}$$

Effective pellet diameter is a idealized diameter which calculated the diameter of a spherical pellet which has the equal volume of the original pellet. It can be calculated as:

$$\begin{aligned} \pi r^2 h &= \tfrac{\pi}{6} D_p^3 \\ D_p &= \sqrt[3]{6 r^2 h} = \sqrt[3]{6 \times 0.003^2 \times 0.018} = 0.0099058\ m \approx 10\ mm \end{aligned} \tag{4.5}$$

Sphericity:

$$\Phi_s = \frac{\text{Surface area of the sphere of same volume as the particle}}{\text{Surface area of particle}} \tag{4.6}$$

Volume of pellet:

$$V_S = \frac{1}{4}\pi d^2 h = 0.25 \times 3.14 \times 0.006^2 \times 0.018 = 5.0868 \times 10^{-7}\ m^3 \tag{4.7}$$

Radius of a sphere of volume V_S:

$$\frac{4}{3}\pi R^3 = V_S, \quad R = 7.25\ mm \tag{4.8}$$

Surface area of a sphere of the same volume as the pellet:

$$S_S = 4 \times \pi \times R^2 = 6.60185 \times 10^{-4}\ m^2 \tag{4.9}$$

Surface area of the pellet:

$$S_P = 2 \times \pi \left(\frac{d}{2}\right)^2 + \pi dh = 3.9564 \times 10^{-4}\ m^2 \tag{4.10}$$

Sphericity:

$$\phi_S = \frac{S_P}{S_S} = 0.5993 \tag{4.11}$$

For the unknown ε_{mf}, a correlation between ε_{mf} and Φ_s is given by Wen and Yu [81], as shown below:

$$\begin{aligned} &\because \Phi_s \varepsilon_{mf}^3 = \tfrac{1}{14} \\ &\therefore \varepsilon_{mf} = 0.4921 \end{aligned} \tag{4.12}$$

Minimum fluidization velocity can be calculated by Ergun equation [82, 83], which is shown in equation 4.13.

Pressure drop:

$$\Delta P = \frac{150 \mu u_{mf} L_{mf}}{\Phi_s^2 D_p^2} \frac{\left(1-\varepsilon_{mf}\right)^2}{\varepsilon_{mf}^3} + \frac{1.75 \rho u_{mf}^2 L_{mf}}{\Phi_s D_p} \frac{\left(1-\varepsilon_{mf}\right)}{\varepsilon_{mf}^3} \tag{4.13}$$

According to the height of the packed bed, the critical height of the fludized bed L_{mf} can be written as:

$$L_{mf} = \frac{M_{bed}}{\left(1-\varepsilon_{mf}\right) \times \rho_{bed} \times A} = 0.3795\ m \tag{4.14}$$

Total drag force by fluid on the particles = weight of solids in the bed, by assuming the cross-sectional area of the tube is A, equation 4.15 can be written:

$$\Delta P\ A = L_m (1-\varepsilon) \left(\rho_P - \rho_f\right) g A \tag{4.15}$$

By replacing ΔP with equation 4.13, gives equation 4.16:

$$\left(\rho_P - \rho_f\right) g = \frac{\rho_f u_{mf}^2}{\Phi_s D_p \varepsilon_{mf}^3} \left[\frac{150 \left(1-\varepsilon_{mf}\right) \mu}{\Phi_s D_p u_{mf} \rho_f} + 1.75\right] \tag{4.16}$$

Solving both sides separately gives:

LHS: Calculating the left hand of equation 4.16:

$$(1220 - 291.66) \times 9.81 = 8910.8154 \frac{kg}{m^2 s^2} \tag{4.17}$$

Calculating the two terms on the right hand of equation 4.16, separately. Each of the right hand terms are written as LHS1 and LHS2.

RHS1

$$\frac{1.75 \rho_f u_{mf}^2}{\Phi_s D_p \varepsilon_{mf}^3} = \frac{1.75 \times 291.66 \times u_{mf}^2}{0.5993 \times 0.01 \times 0.4921^3} = 714678.22 u_{mf}^2 \quad \frac{kg}{m^4} \tag{4.18}$$

RHS2

$$\begin{aligned} \frac{u_{mf}}{\varepsilon_{mf}^3} \frac{150\left(1-\varepsilon_{mf}\right)\mu}{\Phi_s^2 D_p^2} &= \frac{150 \times (1-0.4921) \times 1.849 \times 10^{-5} u_{mf}}{0.5993^2 \times 0.01^2 \times 0.4921^3} \\ &= \frac{0.0014087}{0.00000428} u_{mf} = 329.1355 u_{mf} \quad \left(\frac{kg}{m^3 s}\right) \end{aligned} \tag{4.19}$$

Finally

$$LHS = RHS1 + RHS2 \tag{4.20}$$

$$714678.22 u_{mf}^2 \frac{\mathrm{kg}}{m^4} + 329.1355 u_{mf} \left(\frac{kg}{m^3 s}\right) - 8910.8154 \left(\frac{kg}{m^2 s^2}\right) = 0 \tag{4.21}$$

Thus: $u_{mf} = 0.1114 \quad \mathrm{m\,s^{-1}}$

Anatharaman et al. [80] summarized the minimum fluidization velocities in the literature from different correlations with multiple particle sizes. A general tendency can be observed from the review that the minimum fluidization velocity not only decreases as the pressure increase but also decrease as the temperature increases. Furthermore, for the same particle size, the minimum fluidization velocity, calculated from different correlations, differs greatly. Therefore, the minimum fluidization velocity of the a packed bed has to be related to the operational and experimental conditions. In this work, a relaxation coefficient is added to the calculated velocity, it gives equation 4.22.

$$\mathrm{u_{out}} = 3\mathrm{u_{in}} = 0.3342 \quad \mathrm{m\,s^{-1}} \tag{4.22}$$

The mass flow rate per unit area, or mass flux G, can be calculated based on an inlet air density of 1.225 $\mathrm{kg/m^3}$ and the calculated value of u_{mf} as:

$$G = 0.3342 \times 1.225 = 0.41 \quad \mathrm{kg\,m^{-2}\,s^{-1}} \tag{4.23}$$

The volumetric flow rate can be calculated as:

$$v = 121.4\,\mathrm{l\,min^{-1}} \tag{4.24}$$

Table 4.1: Operational condition for the test rig

Name	Volumetric flow ($\mathrm{l\,min^{-1}}$)	Mass flux ($\mathrm{kg\,m^{-2}\,s^{-1}}$)
B-V/30	30	0.101
B-V/40	40	0.135
B-V/50	50	0.169
B-V/70	70	0.237
B-V/100	100	0.338
B-V/110	110	0.372

Therefore the MFV is approximately 121.4 $\mathrm{l\,min^{-1}}$ and the experimental flow rates are all smaller than this value. The experiments on the effect of PAFs was done at BEST-Bioenergy and Sustainable Technologies GmbH at Graz University of Technology. Experiments on five different PAFs were designed to investigate the most influential factors of air combustion; experiments on three different PAFs were designed to investigate the ignition on a packed bed without an ignitor and experiment on one PAF was designed to validate the CFD model. Six PAFs in total were used in these experiments and these are shown in Table 4.1.

4.2 Experimental setup

4.2.1 Equipment and measurement method

To perform these five experiment, the packed bed rig located in BEST-Bioenergy and Sustainable Technologies GmbH was used. The layout of the test rig is shown in Fig. 4.1. The test rig is made up of two main parts, a gas retort system and a product analysis system. The side view and the front view of the test rig can be seen in Fig. 4.2.

As is shown in Fig. 4.1, the gas retort is made of a mass measurement scale and a combustion furnace. The mass scale measures the mas loss during the experiment. A sample holder is inserted into the furnace and the

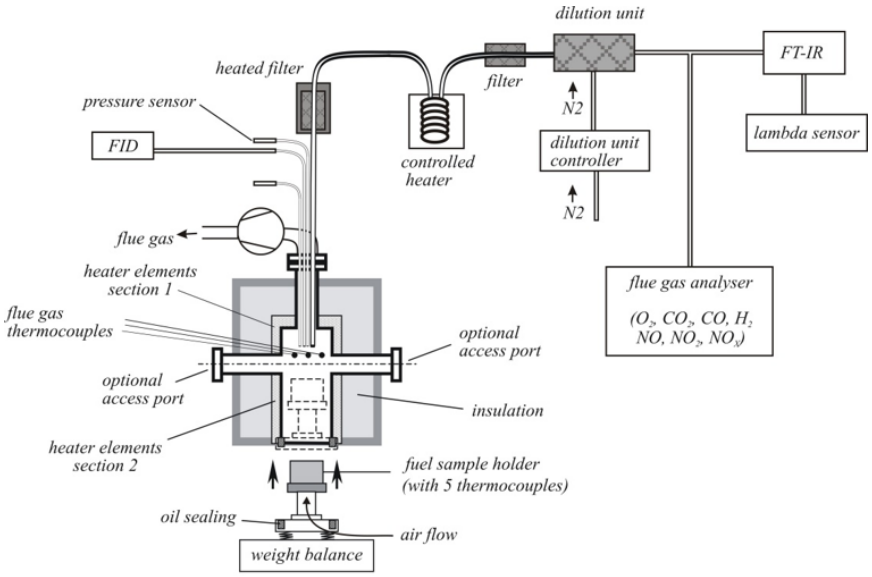

Fig. 4.1: Scheme of testing rig at BEST - Bioenergy and Sustainable Technologies GmbH

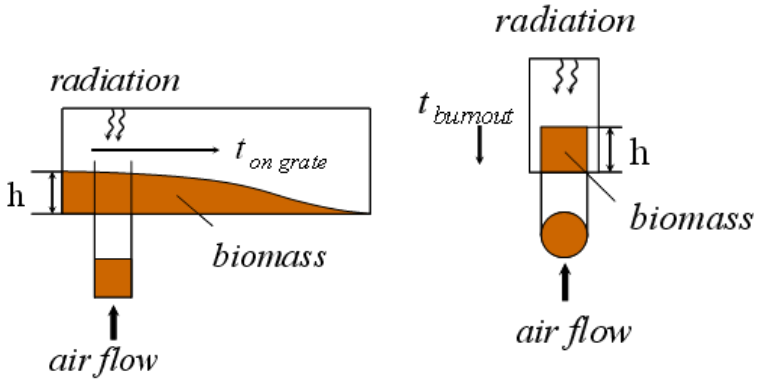

Fig. 4.2: Front view of furnace

whole furnace is sealed as a closed system. Five thermocouples (NiCr−Ni) are inserted from the bottom of the sample holder for the measurement of the temperature gradient along the diameter and the thickness of the reactor bed. The position of the thermocouples is shown in Fig. 4.3. An additional three thermocouples (NiCr−Ni) are placed on the top of the retort for the measurement of the gas temperature.

The product analysis system is made up of three parts. The ash remaining in the sample holder is collected for the measurement of organic carbon

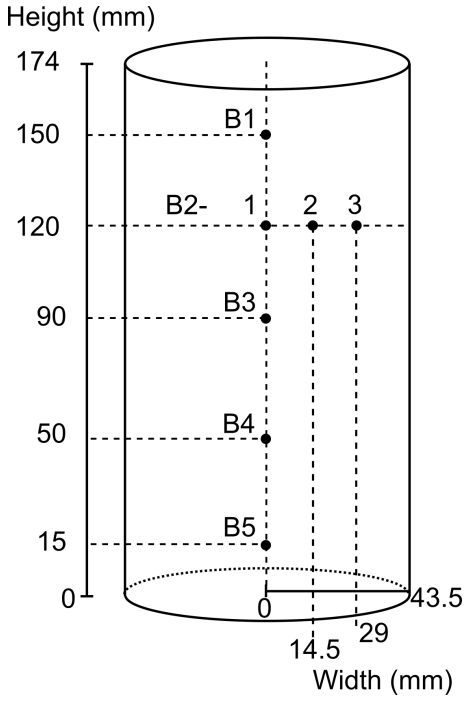

Fig. 4.3: Front view of sample holder

and inorganic carbon (TOC/TIC). The gases that come out of the retort divide into two paths. Some of the gases go to the flame ionization detector (FID (Messer Griesheim Austria Model VE7)), which detects organic compounds by ionization in a burning H_2 flame, for the measurement of total hydrocarbons (CxHy). The remaining gases go through a filter to a dilution unit before entering the multi-component Fourier transform infrared (FT-IR) spectroscope (Ansyo Series DX 4000). The FT-IR spectroscope then determines the basic hydrocarbons such as: $CO_2, CO, CH_4, NH_3, HCN, N_2O$ and H_2O. The concentration of CO_2, CO, CH_4, O_2, H_2 are then measured with a multi-component gas analyzer (ABB AO2020). The O_2 is detected through an electro-chemical cell, and the H_2 is detected through a thermal conductivity detector (TCD).

The operating conditions are shown in Table 4.2 :

4.2.2 Fuel properties

For the experiment, one kind of softwood pellet from Austria was chosen. The pellet was compressed to a diameter of 6 mm and a length of 18 mm - Fig. 4.4. The basic properties of the fuel, such as proximate analysis, ultimate

Table 4.2: Operation conditions for the test rig

Sample		**Reactor temperature**		**Air parameters**	
moisture content	Sample weight	Section1	Section2	Flow rate	Under Pressure
10%$w.b.$	610 g	750 °C	450 °C	30 – 110 $1\,min^{-1}$	30 Pa

analysis and heating value are shown in Table. 4.3. Table. 4.4 shows the content of the trace elements in the softwood pellets. The content of total inorganic carbon (TIC) in the raw material was also measured.

Fig. 4.4: Samples of softwood pellets

Table 4.3: Proximate analysis, ultimate analysis, heating value of softwood

	Proximate analysis					**Ultimate analysis**				**LHV**
Sample	C	H	O	N	S	**FC**	**Vol**	**Ash**	**M**	$[kJ/kg]$
SW	49.81	6.14	44.05	<0.1	0.0051	6.5	85.5	0.3	7.7	18680

Table 4.4: Trance elements content in softwood pellets $[mg/kg]$

Sample	Cl	Al	Ba	Ca	Cd	Cr	Cu	Fe	K	Mg
SW	28	11	13	865	<0.2	<0.5	<2	17	397	106
	Mn	Na	Ni	P	Pb	S	Si	Sr	Ti	Zn
	70	15	<1	55	<3	51	48	4	2	10
	As	Co	Mo	V	TIC					
	<3	<0.5	<1	< 0.5	67200					

4.3 Ignition experiment

The experiments were run with five PAF rates, with an ignitor and without an ignitor. The ignitor is a solid made of wax and pine tree fiber. A summary of the ignition status of the different test points is shown in Table 4.5. Fig. 4.5 shows the ignition with the ignitor before the sample holder enters the retort. Fig. 4.6 shows the ash and ignitor after combustion under a PAF of 30 $l\,min^{-1}$.

Table 4.5: Operational conditions for the test rig

Experiment	Ignition status
Without Ignition	
Ignition under air flow 30 $l\,min^{-1}$	Possible
Ignition under air flow 40 $l\,min^{-1}$	Impossible
Ignition under air flow 50 $l\,min^{-1}$	Impossible
Ignition under air flow 70 $l\,min^{-1}$	Impossible
Ignition under air flow above 70 $l\,min^{-1}$	Assumed impossible
With Ignitor	
Combustion under air flow 30 $l\,min^{-1}$	Possible
Combustion under air flow 50 $l\,min^{-1}$	Possible
Combustion under air flow 70 $l\,min^{-1}$	Possible
Combustion under air flow 100 $l\,min^{-1}$	Possible
Combustion under air flow 110 $l\,min^{-1}$	Possible
Pyrolysis (Abandoned)	
Pyrolysis under N_2 flow 30 $l\,min^{-1}$	Nearly not reacted
Pyrolysis under N_2 flow 5 $l\,min^{-1}$	For 2 h, less than 10% mass loss

Fig. 4.5: Ignition packed bed with an ignitor

A pyrolysis experiment was carried out with this test rig under an atmosphere

Fig. 4.6: Ashes after combustion under PF 30 $\mathrm{l\,min^{-1}}$

of pure nitrogen. Two kinds of primary flow of N_2 were chosen: 30 $\mathrm{l\,min^{-1}}$ and 5 $\mathrm{l\,min^{-1}}$. The original idea was to use 30 $\mathrm{l\,min^{-1}}$ to show the comparison between N_2 pyrolysis and air combustion under the same primary flow. However, the results were unfortunately not satisfactory. Fig. 4.7 shows the pyrolysis outcome under a nitrogen flow rate of 30 $\mathrm{l\,min^{-1}}$ for three hours. It can be observed that only the surface of the bed show signs of a slight reaction. Therefore, the primary flow of 30 $\mathrm{l\,min^{-1}}$ was assumed to be too large for N_2 pyrolysis. As a result, a primary flow of 5 $\mathrm{l\,min^{-1}}$ for N_2 pyrolysis was chosen. Fig. 4.8 shows the wood pellet after two hours pyrolysis under a N_2 flow of 5 $\mathrm{l\,min^{-1}}$. The scale shows only a 10% mass loss after two hours. Considering the long experimental period, the pyrolysis experiments were abandoned.

Fig. 4.7: The bed surface after two hours pyrolysis with N_2 at PF 30 $\mathrm{l\,min^{-1}}$

Zhou et al. [84] studied the ignition of cut straw and whole straw under air-flow, and they found that ignition can be obtained above an air flux of 0.4 $\mathrm{kg\,m^{-2}\,s^{-1}}$. However, the ignition could not be achieved with soft wood pellets on our test rig. As is shown in Table 4.5, for this test rig, the combustion

Fig. 4.8: The appearance of softwood pellet after two hours pyrolysis with N_2 at PF 5 $\mathrm{l\,min^{-1}}$

of the soft wood pellets could not happen without an ignitor once the PAF is above 40 $\mathrm{l\,min^{-1}}$ (0.137 $\mathrm{kg\,m^{-2}\,s^{-1}}$).

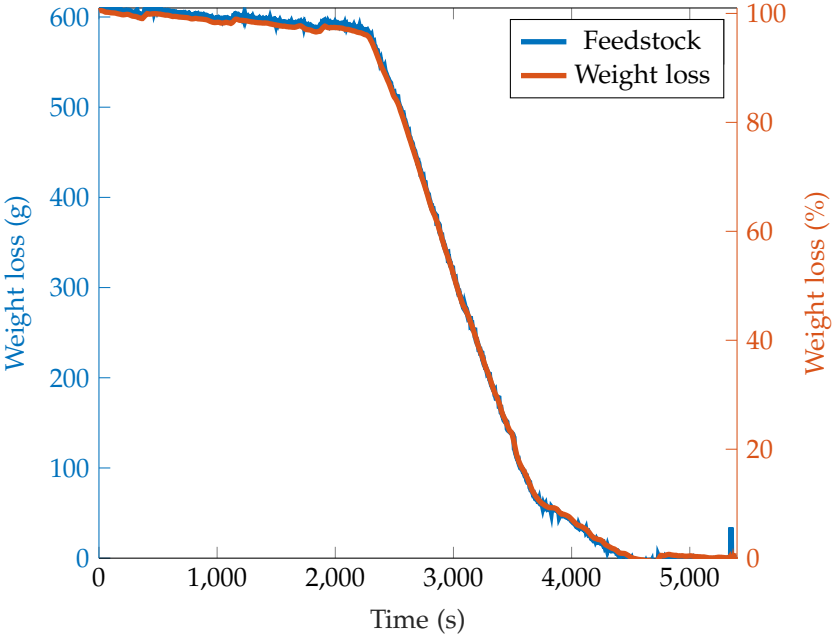

Fig. 4.9: Weight loss of smoldering combustion under primary airflow of 30 $\mathrm{l\,min^{-1}}$

Figure 4.9 shows the mass loss during the smoldering combustion. It can be seen that there is very little mass loss under the initial time period of 2200 s. The mass loss in this period might be attributed to the moisture evaporation (refer to Fig. 4.10 (b)). Between 2200 s and 4000 s is the most intense reaction area and where the maximum mass loss occurs.

Figure. 4.10 shows the main parameters during smoldering combustion without an ignitor. As shown in Fig. 4.10, both the temperature and the gas species concentration reach their own peaks. After 4700 s, the reactions finish. The temperature goes down and the atmosphere above the sample holder changes back to the atmospheric conditions.

It is observed that under a PAF of 30 $l\,min^{-1}$, that the ignition time is quite long (2200 s). The peak temperature at the bed bottom ($B5$) is higher than the peak temperature near the bed surface. Figure 4.10 (b) shows the possible reason. In Fig. 4.10 (b), the concentration of CO_2 and CO changes markedly at around 3500 s. At around 3800 s, the concentration of CO_2 increases, whilst the concentration of CO decreases. The possible reason could be that due to the high temperature and the relative abundance of O_2 close to the grate the char oxidation reaction is initiated.

4.3.1 How is the biomass ignited without an ignitor?

Whether the biomass ignites or not depends on a number of factors [72], such as energy input (ignitor in this study) and an elevated temperature (external heating source in this study). This experiment aimed at ignition without an ignitor.

The ignition characteristic is defined as the sudden temperature rise in the temperature profile, as it is marked (red cross) in Fig. 4.11. The next question is which part of the bed is ignited first: the free board with accumulated light gases or the biomass on the bed surface? Since it is difficult to verify whether the biomass is ignited or not, the research aimed at determining whether the evolved gases can be ignited at the same time as the bed is ignited. If one of the evolved gases reaches the ignition point before the bed is ignited, then the ignition of the bed is caused by the combustion of the evolved gas from the biomass devolatilization at the bed surface. Otherwise, the ignition of the bed is caused by the biomass combustion at the bed surface.

The ignition point of all the light gases and hydrocarbons that were measured in the experiment are given in Table 4.6.

Table 4.6: The ignition point of hydrocarbons in Fig. 4.10

C_2H_4	C_2H_6	C_3H_8	C_6H_6	$C_6H_5CH{=}CH_2$ CO	CH_4	H_2
542.8 °C	472 °C	470 °C	498 °C	490 °C	500 °C	537 °C

Figure 4.11 shows the temperature profile under two different PFs. According to the Fig. 4.11, the bed can be ignited under the PF of 30 $l\,min^{-1}$ with a ignition point of 476.8 °C. The bed could not be ignited under the PF of 40 $l\,min^{-1}$. This means, under the PF of 30 $l\,min^{-1}$, the bed could be ignited by the evolved gases if one of the detected gases in Table 4.6 has lower

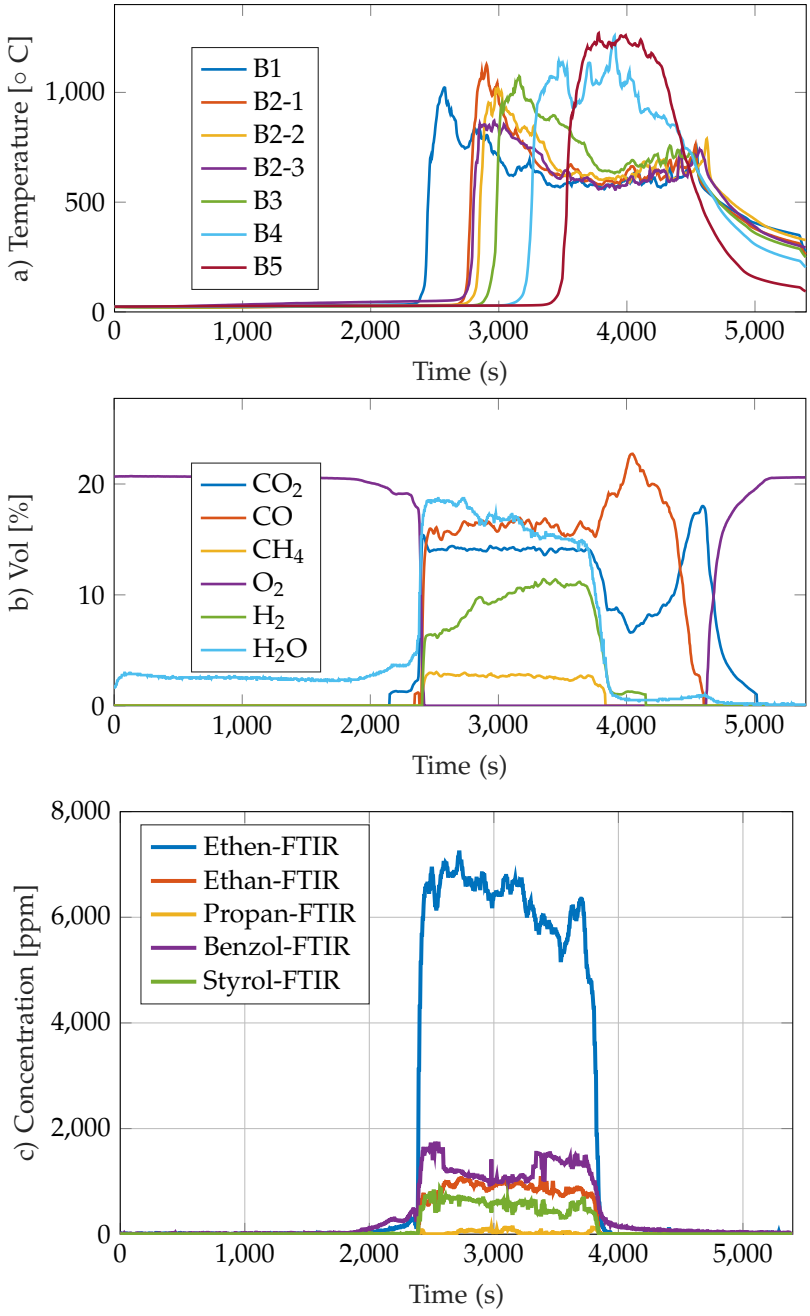

Fig. 4.10: Smoldering combustion under primary flow under 30 $l\,min^{-1}$

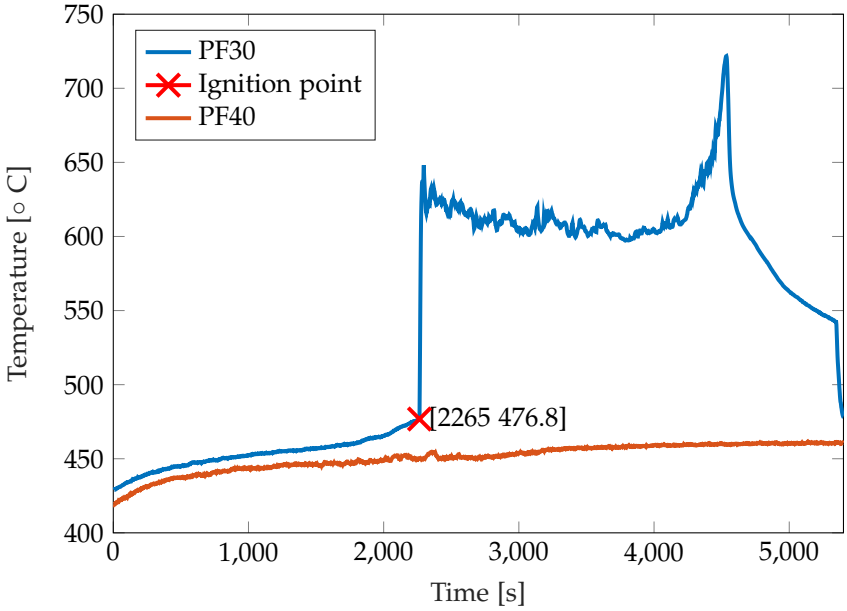

Fig. 4.11: Air temperature on the free board at two different primary flows

ignition point than 476.8 °C. Apparently C_2H_6 and C_3H_8 are the most likely gases.

To ignite the bed successfully, a certain amount of C_2H_6 and C_3H_8 has to be present. Figure 4.10 c) and 4.12 shows the concentration of detected hydrocarbons under the two values of PFs investigated. When the PF is 40 $l\,min^{-1}$, the concentration of C_2H_6 and C_3H_8 is around 50 times less than that under a PF of 30 $l\,min^{-1}$. Fig.4.10 c) clearly shows a sufficient gas concentration of C_2H_6 and C_3H_8.

To summarize, the experiments show that the bed can be ignited naturally when the PAF is 30 $l\,min^{-1}$, but the bed cannot be ignited naturally for the PAF of 40 $l\,min^{-1}$ and above. The external heat source can heat up the air temperature in the free board to the ignition temperature under a PF of 30 $l\,min^{-1}$, as is shown in Fig.4.11. For a PAF above 40 $l\,min^{-1}$, it is difficult to reach the lowest hydrocarbon ignition point. At the same time, the concentration of light hydrocarbons at a PAF 40 $l\,min^{-1}$ are fairly low (Fig. **??**) compared to the concentration of hydrocarbons at a PAF of 30 $l\,min^{-1}$.

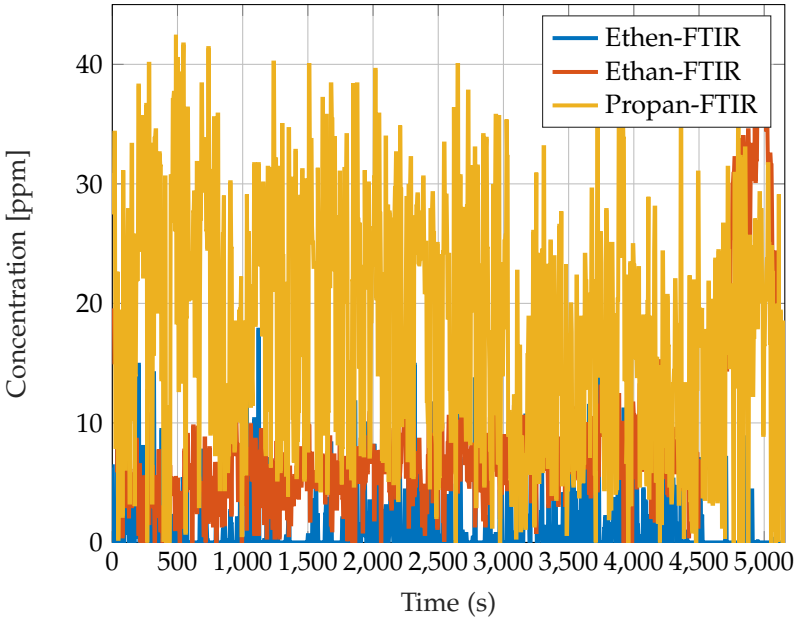

Fig. 4.12: Hydrocarbon concentration under primary flow under 40 $\mathrm{l\,min^{-1}}$

4.4 Change of PAF

Since it is difficult to ignite the bed with a high PAF, an ignitor made of pine tree fiber and wax was put on top of the sample holder to ignite the biomass. In order to make the experiments consistent with each other, the ignitor is also inserted when the PAF was 30 $\mathrm{l\,min^{-1}}$. Two main parameters are investigated here: the temperature at different bed locations and the light gas concentration.

Figure 4.13 shows the temperature profile and the gas concentration during gasification. Due to the effect of the ignitor, the combustion of the ignitor quickly consumes the O_2 and produces other gases. Therefore, the light gases released at the very beginning might come from the ignitor combustion. Since the bed is ignited from the bed surface, the heat from combustion should propagate from the surface to the grate. When the temperature reaches the ignition point, the biomass at that position is ignited and this is known as the ignition front. High levels of heat coming from the combustion of each ignition front contributes to a temperature peak, as shown in Fig. 4.13. The temperature at the height of 120 mm close to the bed center is higher than the temperature close to the wall. The possible reason for this is the sample holder temperature is lower than the combustion temperature of the biomass, the position closer to the sample holder is easier to lose heat

due to the temperature gradient from biomass to the wall.

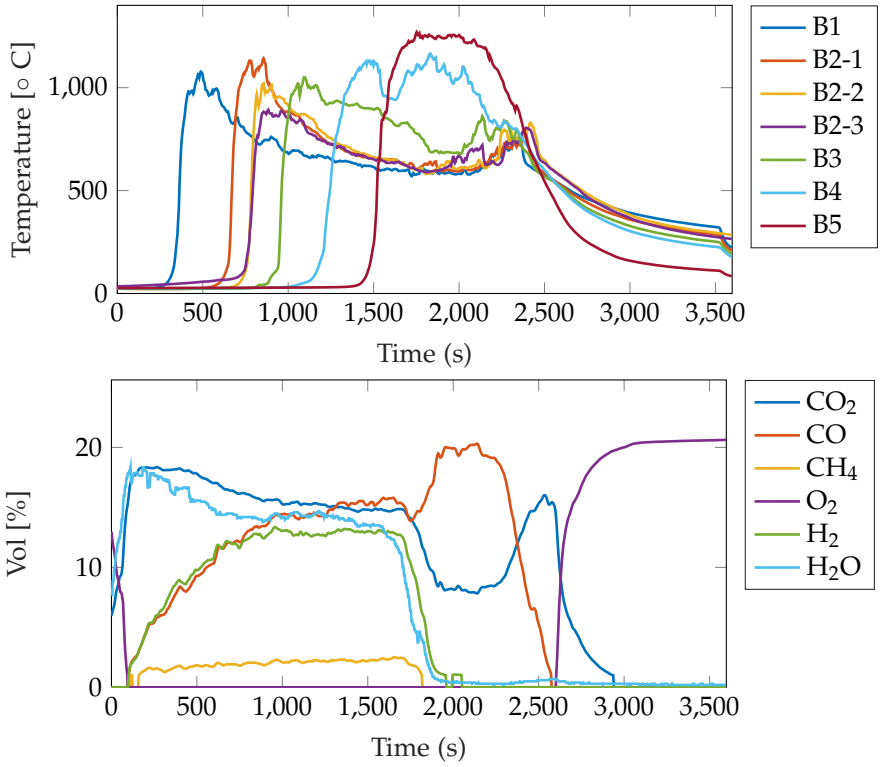

Fig. 4.13: Smoldering combustion under primary flow under 30 $l\,min^{-1}$

An important index to distinguish the combustion mechanism is the content of CO and CO_2. Depending on the concentration of oxygen, the production of CO and CO_2 is different. In Fig. 4.13, there is a sudden decrease of CO_2, and a sudden CO increase at 2000 s. This is where the temperature close to the grate reaches the highest peak temperature. Therefore, we can deduce that the char combustion starts at 2000 s under a PAF of 30 $l\,min^{-1}$ and is incomplete combustion (Oxygen-limited combustion) under these conditions.

Figures 4.14 to 4.17 show the temperature profile and the gas concentration for the smoldering combustion at PAF of 50 $l\,min^{-1}$, 70 $l\,min^{-1}$, 100 $l\,min^{-1}$ and 110 $l\,min^{-1}$, respectively. Due to the strong heat exchange under the high PAF, the difference amongst the temperature peaks is not obvious when the PAF is over 40 $l\,min^{-1}$. The temperature along the radial direction at three locations is very similar. Due to the high level of heat release from the strong oxidation at a high air flow, the time for reactions to complete gets less and less. When the PAF reaches 110 $l\,min^{-1}$, the combustion process takes a longer time to occur than when the process is under a PAF of 100

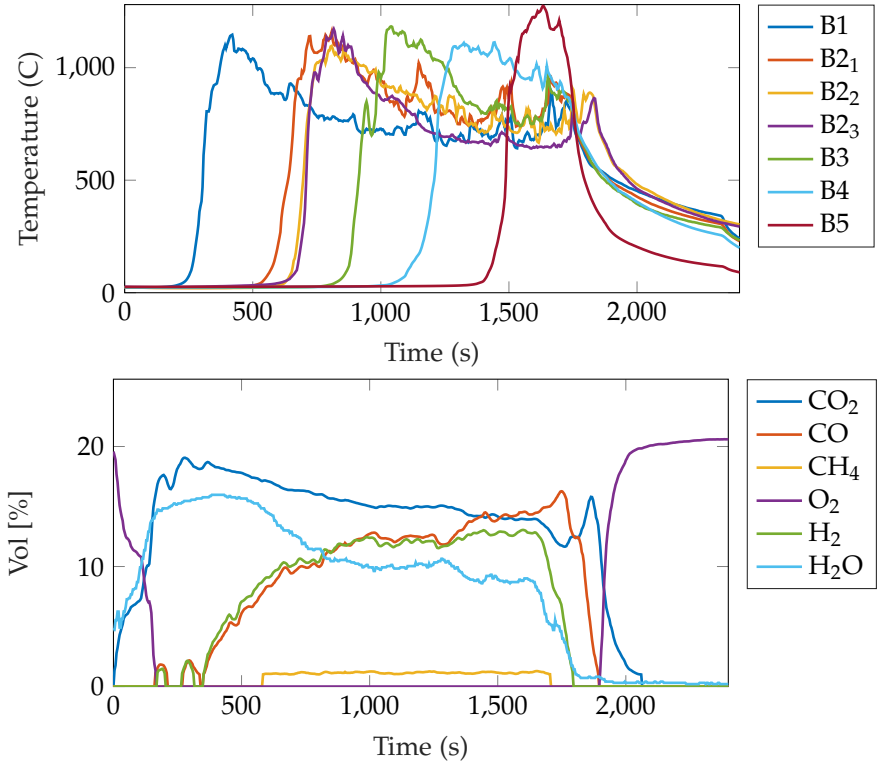

Fig. 4.14: Smoldering combustion under primary flow under 50 l min^{-1}

l min^{-1}, probably due to the strong convection where the combustion heat is carried away.

When the PAF increases from 50 l min^{-1} to 70 l min^{-1}, the concentration of CO_2 increases and the concentration of other species decreases. Specifically, the concentration of CH_4 disappears when the PAF exceeds 70 l min^{-1}.

At the same time, the distribution of each species gets more pronounced with the increase in air flow. When the PAF exceeds 100 l min^{-1}, almost only H_2O, O_2 and CO_2 are detected. The fact that there is no CO implies that the O_2 concentration is sufficient and that the char is completely burnt. O_2 can be detected all the way through the combustion process when the PAF is 110 l min^{-1}, which means that the combustion under this air flow has sufficient O_2.

In order to see the oxidation state at different air flows clearly, the CO/CO_2 is plotted, as shown in Fig. 4.18. It is clearly seen that the concentration of CO decreases with an increasing PAF. When the PAF is 110 l min^{-1}, no CO is detected.

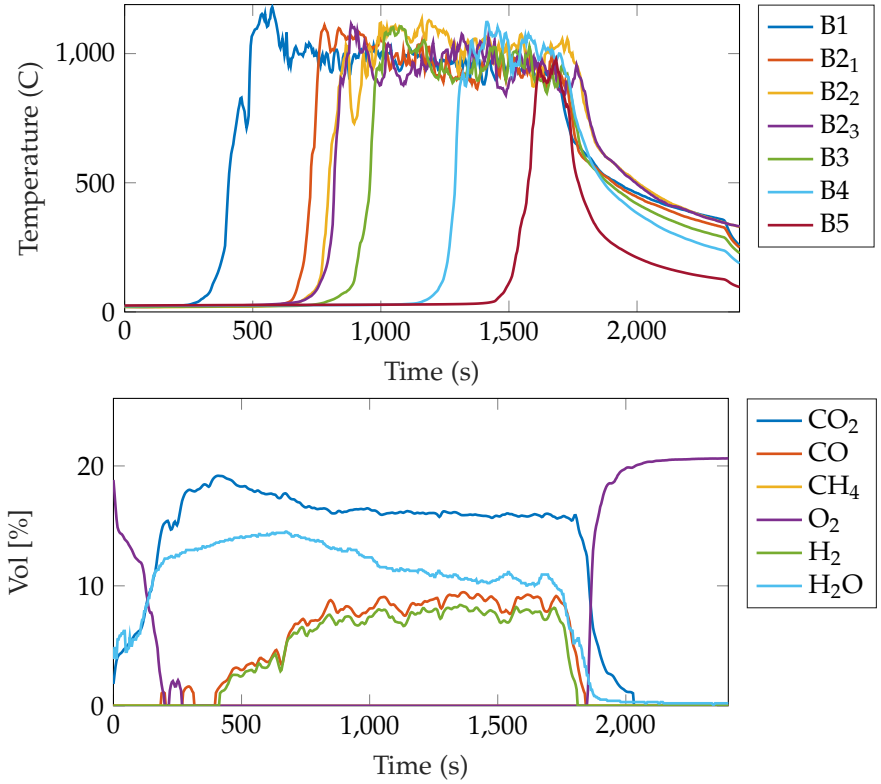

Fig. 4.15: Smoldering combustion under primary flow under 70 l min^{-1}

4.5 Ash analysis: Organic and inorganic carbon

In order to investigate the burning status under different PAFs, the organic carbon and inorganic carbon left in the ash was investigated. Two samples from the ash of each PAF were analyzed. Fig. 4.19 shows the results from the TIC/TOC analysis. It is observed that the content of organic carbon remaining in the ash is almost negligible (under 1g kg^{-1}). But regarding the inorganic carbon, it seems as if the higher the PAF increases, the higher content of inorganic carbon is left in the ash.

Fig. 4.16: Smoldering combustion under primary flow under 100 l min^{-1}

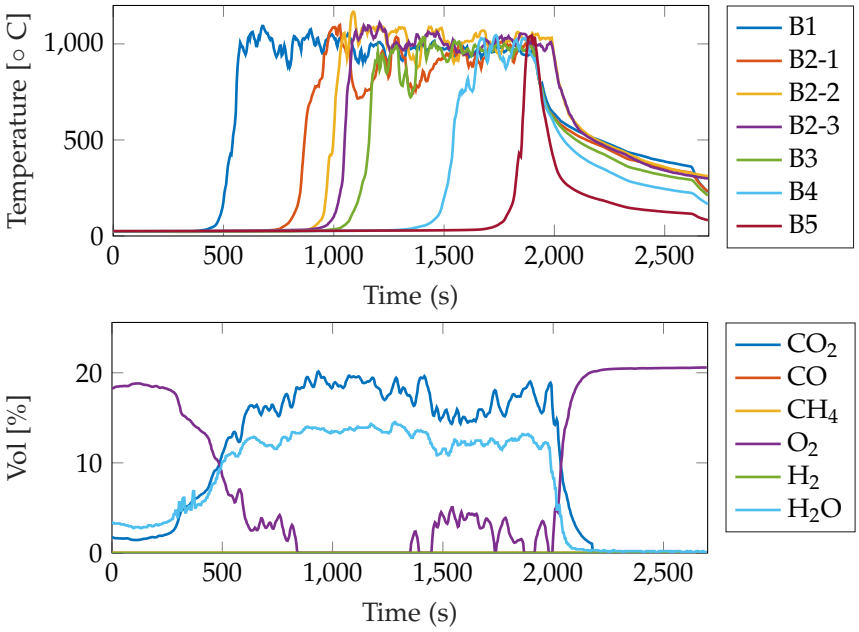

Fig. 4.17: Smoldering combustion under primary flow under 110 l min^{-1}

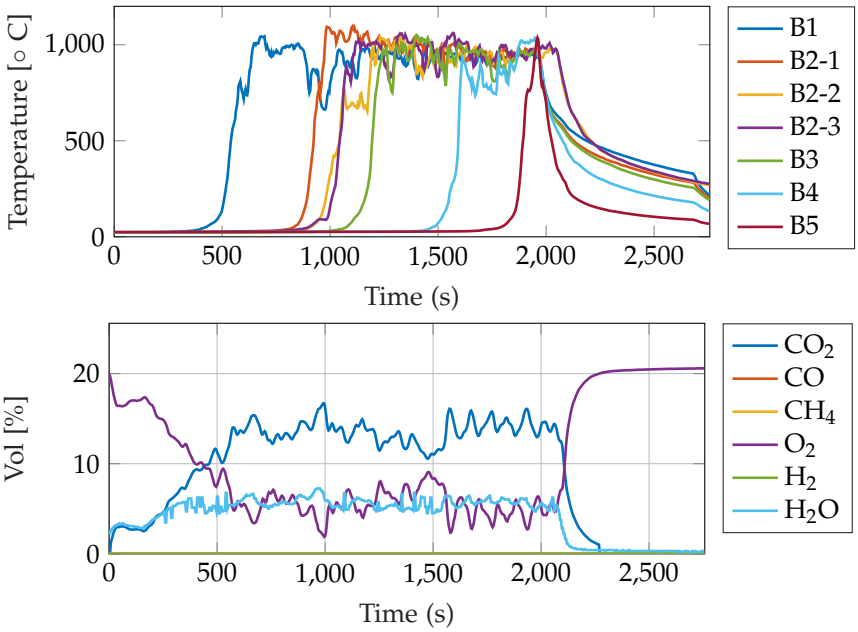

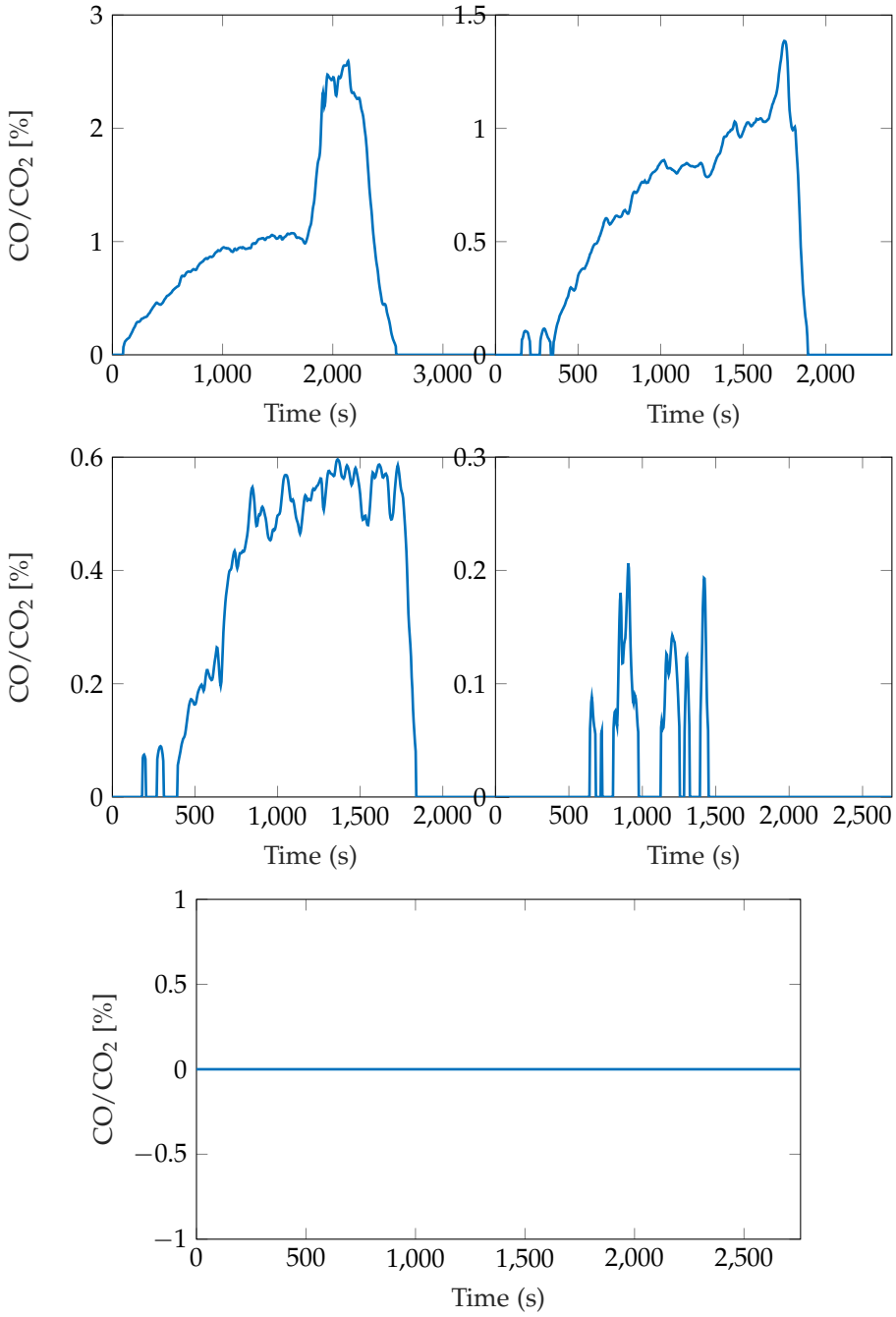

Fig. 4.18: CO/CO_2 ratio under different range of PAF of 30 $l\,min^{-1}$, 50 $l\,min^{-1}$, 70 $l\,min^{-1}$, 100 $l\,min^{-1}$, 110 $l\,min^{-1}$, respectively

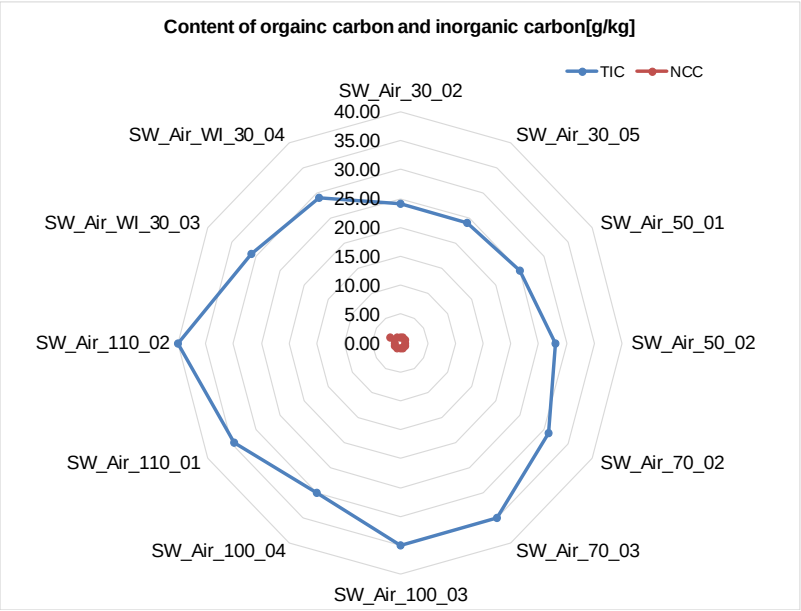

Fig. 4.19: The content of organic carbon and inorganic carbon left in ash after combustion under different PAF

Chapter 5

Conclusion

This chapter summarizes the main contributions of this dissertation. The future work is also recommended to improve or refine the research.

5.1 Final remarks

Thermo-chemical conversion has been one of the current interests of biomass conversion industry, due to the renewable characteristics and fast energy conversion of thermo-chemical treatment. The thermo-chemical conversion of biomass requires many different processes, such as fluid transport, heat and mass transfer, reaction mechanisms, and so on. To understand the intra-particle process during biomass thermo-chemical conversion, a CFD model for a single biomass particle thermo-chemical conversion was developed in this project. To analyse the inter-particle process during the biomass thermo-chemical conversion, a CFD model for a packed bed reactor was also developed. To verify the packed bed combustion, an experimental study was undertaken in collaboration with BEST-Bioenergy and Sustainable Technologies GmbH at Graz University of Technology, Austria.

For the single biomass particle thermo-chemical conversion, two different conditions were applied in the model: pyrolysis under nitrogen and smoldering combustion under air. The model reliably predicts the temperature profile both for the pyrolysis and combustion cases, which was confirmed by validation with experimental data from the literature. The model also predicts other profiles, such as pressure, velocity, gas species, and weight loss, etc. A parametric study was done in the smoldering combustion case where, two main parameters were studied, the devolatilization rate of biomass and the light gas combustion scheme. The results show that different devolatilization rates can affect the time of biomass degradation but cannot affect the

temperature of the combustion stage. Two different hydrocarbon combustion schemes were also compared in this work: a two-step hydrocarbon combustion scheme from Dryer and Westbrook [68] and a four-step hydrocarbon combustion scheme from Jones and Lindstedt [69]. The parametric study showed that both schemes can predict biomass smoldering combustion reliably. A maximum error of 5% was found between these two combustion schemes with the pellet temperature simulation.

I addition, a simulation was done to validate the smoldering combustion in a packed bed reactor under an air flow of 30 $\mathrm{l\,min^{-1}}$. The simulation results were then compared with temperature data from experiments and the gas species fraction at the bed surface location.

Apart from the validation, the experiment was also meant to study the effect of primary air flow on the packed bed smoldering combustion of biomass. To study that, a range of primary air flow rates of 30, 50, 70, 100, 110 $\mathrm{l\,min^{-1}}$ were applied. The bed could not be ignited for the primary air flow over 30 $\mathrm{l\,min^{-1}}$. By using the ignitor, the temperature profile at five different vertical locations and three horizontal locations were recorded under different primary air flows, as well as the gas distribution at the bed surface. The five different temperature profiles show the tendency of a biomass combustion mechanism from insufficient oxygen to sufficient oxygen, with PAF from low to high.

5.2 Contributions of this work

Four main contributions from this project can be highlighted:

- A one-dimensional CFD based model for the thermo-chemical conversion of a single biomass was developed.
- The effect of two important parameters under the combustion of a single biomass pellet was studied.
- A one-dimensional CFD based model for the thermo-chemical conversion in a packed bed was developed.
- The effects of the primary air flow on the performance of biomass combustion mechanisms was studied experimentally.

5.3 Future work

The effort of making a general thermo-chemical conversion model has been the aim of many researchers. From the author's point of view, a stable general thermo-chemical conversion model has two main requirements. Firstly,

it should predict results for a wide variety of biomass species. Secondly, it should be capable of predicting results from different thermo-chemical conversion conditions, for example, from laminar flow to turbulent flow. In order to achieve that, much work need to be done in the future. To mention some:

- Both models on a single biomass particle and the packed bed were on a one-dimensional approach. With the improvement of computer processing power and the development of different CFD solvers, a two-dimensional approach or a 3-D approach for the simulation could be used to investigate the process more thoroughly.
- Compare the results of this self-written code to the results generated from other CFD tools, such as *General Pyrolysis* or *OpenForm*. Refine the model by analysing the results from different tools.
- An object friendly user interface can be built based on this model.
- The models described in this research were done on the assumption that the mass transportation within the pores was in the laminar flow regime. However, in reality, many combustion cases are not laminar flow, such as combustion in fludized bed. Future study could explore the possibility of including turbulent flow in such models.

References

[1] Arjan F. Kirkels and G. P J Verbong. Biomass gasification: Still promising? A 30-year global overview. *Renewable and Sustainable Energy Reviews*, 15(1):471–481, 2011. ISSN 13640321. doi: 10.1016/j.rser.2010.09.046. URL http://dx.doi.org/10.1016/j.rser.2010.09.046.

[2] M. La Villetta, M. Costa, and N. Massarotti. Modelling approaches to biomass gasification: A review with emphasis on the stoichiometric method. *Renewable and Sustainable Energy Reviews*, 74(July):71–88, 2017. ISSN 18790690. doi: 10.1016/j.rser.2017.02.027. URL http://dx.doi.org/10.1016/j.rser.2017.02.027.

[3] REA. BIOMASS - REA, 2020. URL https://www.r-e-a.net/technologies/biomass/.

[4] United Nations Environment Programme. GRID - Resource details, 2020. URL https://unepgrid.ch/en/resource/29F4E814.

[5] Energy Danish Ministry of Climate and Utilities. Danish climate policies | Energistyrelsen. URL https://ens.dk/en/our-responsibilities/energy-climate-politics/danish-climate-policies?fbclid=IwAR2KV0itcFbYu-C6-XP80Pm{_}bibPpFPIUBnqLUMC3asKh60PzZRdHCefo5M.

[6] State of Green. Danish climate law, 2020. URL https://stateofgreen.com/en/partners/state-of-green/news/during-cop25-denmark-passes-climate-act-with-a-70-per-cent-reduction-targe

[7] Danish Energy Agency. The Danish Energy Model Innovative, efficient and sustainable. Technical report, The Danish Energy Agency, 2019. URL www.ens.dk/en.

[8] H. Kobayashi, J. B. Howard, and A. F. Sarofim. Coal devolatilization at high temperatures. *Symposium (International) on Combustion*, 16(1):411–425, 1977. ISSN 00820784. doi: 10.1016/S0082-0784(77)80341-X.

[9] D. L. Pyle and C. A. Zaror. Heat transfer and kinetics in the low temperature pyrolysis of solids. *Chemical Engineering Science*, 39(1):147–158, 1984. ISSN 00092509. doi: 10.1016/0009-2509(84)80140-2.

[10] C. H. Bamford, J Crank, D H Malan, and A. H. Wilson. The combustion of wood. Part I. *Mathematical Proceedings of the Cambridge Philosophical Society*, 42(02):166, 1946. ISSN 0305-0041. doi: 10.1017/S030500410002288X. URL http://www.journals.cambridge.org/abstract{_}S030500410002288X.

[11] Hamid Rezaei, C. Jim Lim, Anthony Lau, Xiaotao Bi, and Shahab Sokhansanj. Development of empirical drying correlations for ground wood chip and ground wood pellet particles. *Drying Technology*, 35(12): 1423–1432, 2017. ISSN 15322300. doi: 10.1080/07373937.2016.1198912. URL https://doi.org/10.1080/07373937.2016.1198912.

[12] Edward J Kansa, Henry E Perlee, and Robert F Chaiken. Mathematical model of wood pyrolysis including internal forced convection. *Combustion and Flame*, 29(C):311–324, 1977. ISSN 00102180. doi: 10.1016/0010-2180(77)90121-3.

[13] Wai Chun R Chan, Marcia Kelbon, and Barbara B Krieger. Modelling and experimental verification of physical and chemical processes during pyrolysis of a large biomass particle. *Fuel*, 64(11):1505–1513, 1985. ISSN 00162361. doi: 10.1016/0016-2361(85)90364-3.

[14] Hong Lu, Warren Robert, Gregory Peirce, Bryan Ripa, and Larry L. Baxter. Comprehensive study of biomass particle combustion. *Energy and Fuels*, 22(4):2826–2839, 2008. ISSN 08870624. doi: 10.1021/ef800006z.

[15] Colomba Di Blasi. Heat, momentum and mass transport through a shrinking biomass particle exposed to thermal radiation. *Chemical Engineering Science*, 51(7):1121–1132, 1996. ISSN 00092509. doi: 10.1016/S0009-2509(96)80011-X. URL http://linkinghub.elsevier.com/retrieve/pii/S000925099680011X.

[16] R. Font, A. Marcilla, J. Devesa, and E. Verdu. Kinetic study of the flash pyrolysis of almond shells in a fluidized bed reactor at high temperatures. *Journal of Analytical and Applied Pyrolysis*, 27(2):245–273, 1993. ISSN 01652370. doi: 10.1016/0165-2370(93)80012-O.

[17] Franz Thurner and Uzi Mann. Kinetic investigation of wood pyrolysis. *Industrial & Engineering Chemistry Process Design and Development*, 20:482–488, 1981. ISSN 0196-4305. doi: 10.1021/i200014a015. URL http://pubs.acs.org/doi/abs/10.1021/i200014a015.

[18] Colomba Di Blasi. Numerical simulation of cellulose pyrolysis. *Biomass and Bioenergy*, 7(1-6):87–98, 1994. ISSN 09619534. doi: 10.1016/0961-9534(94)00040-Z.

[19] Hesameddin Fatehi. *Numerical simulation of combustion and gasification of biomass particles*. 2014. ISBN 9789174739770.

[20] Maryam Momeni, Chungen Yin, Søren Knudsen Kær, and Søren Lovmand Hvid. Comprehensive study of ignition and combustion of single wooden particles. *Energy & Fuels*, 27:1061–1072, 2013.

[21] Andrés Anca-Couce, Nico Zobel, and Hugo Atle Jakobsen. Multi-scale modeling of fixed-bed thermo-chemical processes of biomass with the representative particle model: Application to pyrolysis. *Fuel*, 103:773–782, 2013. ISSN 00162361. doi: 10.1016/j.fuel.2012.05.063.

[22] Y. Haseli, J. A. van Oijen, and L. P H de Goey. Numerical study of the conversion time of single pyrolyzing biomass particles at high heating conditions. *Chemical Engineering Journal*, 169(1-3):299–312, 2011. ISSN 13858947. doi: 10.1016/j.cej.2011.02.073. URL `http://dx.doi.org/10.1016/j.cej.2011.02.073`.

[23] Andrés Anca-Couce and Nico Zobel. Numerical analysis of a biomass pyrolysis particle model: Solution method optimized for the coupling to reactor models. *Fuel*, 97:80–88, 2012. ISSN 00162361. doi: 10.1016/j.fuel.2012.02.033.

[24] Xiyan Li and Chungen Yin. A drying model for thermally large biomass particle pyrolysis. *Energy Procedia*, 158:1294–1302, 2019. ISSN 18766102. doi: 10.1016/j.egypro.2019.01.322.

[25] Colomba Di Blasi. Modeling and simulation of combustion processes of charring and non-charring solid fuels. *Progress in Energy and Combustion Science*, 19:71–104, 1993. ISSN 03601285. doi: 10.1016/0360-1285(93)90022-7.

[26] Colomba Di Blasi. Kinetic and heat transfer control in the slow and flash pyrolysis of solids. *Industrial & Engineering Chemistry Research*, 35 (1):37–46, 1996. ISSN 0888-5885. doi: 10.1021/ie950243d. URL `http://pubs.acs.org/doi/abs/10.1021/ie950243d`.

[27] Colomba Di Blasi. Influences of physical properties on biomass devolatilization characteristics. *Fuel*, 76(10):957–964, 1997. ISSN 00162361. doi: 10.1016/S0016-2361(97)00096-3.

[28] Colomba Di Blasi. Multi-phase moisture transfer in the high temperature drying of wood particles. *Chemical Engineering Science*, 53(2):353–366,

1998. ISSN 00092509. doi: 10.1016/S0009-2509(97)00197-8. URL http://linkinghub.elsevier.com/retrieve/pii/S0009250997001978.

[29] Colomba Di Blasi. Comparison of semi-global mechanisms for primary pyrolysis of lignocellulosic fuels. *Journal of Analytical and Applied Pyrolysis*, 47(1):43–64, 1998. ISSN 01652370. doi: 10.1016/S0165-2370(98)00079-5. URL http://linkinghub.elsevier.com/retrieve/pii/S0165237098000795.

[30] Colomba Di Blasi and Carmen Branca. Kinetics of Primary Product Formation from Wood Pyrolysis. *Industrial & Engineering Chemistry Research*, 40(23):5547–5556, 2001. ISSN 0888-5885. doi: 10.1021/ie000997e. URL http://pubs.acs.org/doi/abs/10.1021/ie000997e.

[31] Colomba Di Blasi. Modeling intra- and extra-particle processes of wood fast pyrolysis. *AIChE Journal*, 48(10):2386–2397, 2002. ISSN 00011541. doi: 10.1002/aic.690481028.

[32] Colomba Di Blasi, Carmen Branca, Silvio Sparano, and Barbara La Mantia. Drying characteristics of wood cylinders for conditions pertinent to fixed-bed countercurrent gasification. *Biomass and Bioenergy*, 25:45–58, 2003.

[33] Colomba Di Blasi. Modeling wood gasification in a countercurrent fixed-bed reactor. *AIChE Journal*, 50(9):2306–2319, 2004. ISSN 00011541. doi: 10.1002/aic.10189.

[34] Colomba Di Blasi. Modeling chemical and physical processes of wood and biomass pyrolysis. *Progress in Energy and Combustion Science*, 34(1):47–90, 2008. ISSN 03601285. doi: 10.1016/j.pecs.2006.12.001.

[35] Colomba Di Blasi. Combustion and gasification rates of lignocellulosic chars. *Progress in Energy and Combustion Science*, 35(2):121–140, 2009. ISSN 03601285. doi: 10.1016/j.pecs.2008.08.001. URL http://dx.doi.org/10.1016/j.pecs.2008.08.001.

[36] H Thunman, B Leckner, F Niklasson, and F Johnsson. Combustion of wood particles - A particle model for Eulerian calculations. *Combustion and Flame*, 129:30–46, 2002. ISSN 00102180. doi: 10.1016/S0010-2180(01)00371-6.

[37] Xiyan Li and Chungen Yin. Description of a comprehensive mathematical model Towards a comprehensive biomass particle gasification model. In *Proceedings of the 25th European Biomass Conference & Exhibition, EUBCE2017*, pages 853–859, Stockholm, 2017. doi: 10.5071/25thEUBCE2017-2CV.3.49.

[38] Ramin Mehrabian, Selma Zahirovic, Robert Scharler, Ingwald Obernberger, Stefan Kleditzsch, Siegmar Wirtz, Viktor Scherer, Hong Lu, and Larry L Baxter. A CFD model for thermal conversion of thermally thick biomass particles. *Fuel Processing Technology*, 95:96–108, 2012. ISSN 03783820. doi: 10.1016/j.fuproc.2011.11.021. URL `http://dx.doi.org/10.1016/j.fuproc.2011.11.021`.

[39] Ai Jun Xue, Ji Hong Pan, Mao Cheng Tian, Guan Min Zhang, and Xue Li Leng. Pyrolysis model of single biomass particle in stratified downdraft gasifier. *Transactions of Tianjing University*, 22:174–181, 2016. ISSN 02532417. doi: 10.3969/j.issn.0253-2417.2016.01.002.

[40] Amit Kumar Biswas and Kentaro Umeki. Simplification of devolatilization models for thermally-thick particles: Differences between wood logs and pellets. *Chemical Engineering Journal*, 274:181–191, 2015. ISSN 13858947. doi: 10.1016/j.cej.2015.03.131.

[41] F. Tabet, V. Fichet, and P. Plion. A comprehensive CFD based model for domestic biomass heating systems. *Journal of the Energy Institute*, 89: 199–214, 2016. ISSN 17460220. doi: 10.1016/j.joei.2015.02.003.

[42] B V Babu and A S Chaurasia. Heat transfer and kinetics in the pyrolysis of shrinking biomass particle. *Chemical Engineering Science*, 59:1999–2012, 2004. ISSN 00092509. doi: 10.1016/j.ces.2004.01.050.

[43] Nelson Sousa and João L.T. Azevedo. Model simplifications on biomass particle combustion. *Fuel*, 184:948–956, 2016. ISSN 00162361. doi: 10.1016/j.fuel.2016.03.106.

[44] A V Bridgwater. The technical and economic feasibility of biomass gasification for power generation. *Fuel*, 74(5):631–653, 1995. ISSN 00162361. doi: 10.1016/0016-2361(95)00001-L. URL `http://www.sciencedirect.com/science/article/pii/001623619500001L`.

[45] José Corella, María P. Aznar, Jesús Delgado, and Elena Aldea. Steam Gasification of Cellulosic Wastes in a Fluidized Bed with Downstream Vessels. *Industrial and Engineering Chemistry Research*, 30(10):2252–2262, 1991. ISSN 15205045. doi: 10.1021/ie00058a003.

[46] Yao Bin Yang, Changkook Ryu, Adela Khor, Vida N Sharifi, and Jim Swithenbank. Fuel size effect on pinewood combustion in a packed bed. *Fuel*, 84(16):2026–2038, 2005. ISSN 00162361. doi: 10.1016/j.fuel.2005.04.022.

[47] M L Hobbs, P T Radulovic, and L D Smoot. Modeling fixed-bed coal gasifiers. *AIChE Journal*, 38(5):681–702, 1992. ISSN 00011541. doi: 10.1002/aic.690380506.

[48] Kenneth M. Bryden and Kenneth W. Ragland. Numerical modeling of a deep, fixed bed combustor. *Energy & Fuels*, pages 269–275, 1996.

[49] Inge Haberle, Øyvind Skreiberg, Joanna Łazar, and Nils Erland L Haugen. Numerical models for thermochemical degradation of thermally thick woody biomass, and their application in domestic wood heating appliances and grate furnaces. *Progress in Energy and Combustion Science*, 63:204–252, 2017. ISSN 03601285. doi: 10.1016/j.pecs.2017.07.004.

[50] J. Collazo, J. Porteiro, D. Patiño, and E. Granada. Numerical modeling of the combustion of densified wood under fixed-bed conditions. *Fuel*, 93:149–159, 2012. ISSN 00162361. doi: 10.1016/j.fuel.2011.09.044.

[51] Gilbert F. Froment and Kenneth B. Bischoff. *Chemical reactor analysis and design*. John Wiley & Sons. Inc., 1979. ISBN 0-471-02447-3.

[52] Daizo Kunii and J. M. Smith. Heat transfer characteristics of porous rocks. *AIChE Journal*, 6(1):71–78, 1960.

[53] Jan Fjellerup and Ulrik Henriksen. Heat transfer in a fixed bed of straw char. *Energy and Fuels*, 17(5):1251–1258, 2003. ISSN 08870624. doi: 10.1021/ef030036n.

[54] Ramin Mehrabian, Ali Shiehnejadhesar, Robert Scharler, and Ingwald Obernberger. Multi-physics modelling of packed bed biomass combustion. *Fuel*, 122:164–178, 2014. ISSN 00162361. doi: 10.1016/j.fuel.2014.01.027.

[55] Inge Haberle, Nils Erland L. Haugen, and Øyvind Skreiberg. Drying of thermally thick wood particles: A study of the numerical efficiency, accuracy, and stability of common drying models. *Energy & Fuels*, 31:13743–13760, 2017. ISSN 0887-0624. doi: 10.1021/acs.energyfuels.7b02771.

[56] Abraham Teklay, Chungen Yin, Lasse Rosendahl, and Martin Bøjer. Calcination of kaolinite clay particles for cenment production: A modeling study. *Cement and Concrete Research*, 61-62:11–19, 2014. ISSN 0008-8846. doi: 10.1016/j.cemconres.2014.04.002.

[57] Bernhard Peters and Christian Bruch. Drying and pyrolysis of wood particles: experiments and simulation. *Journal of Analytical and Applied Pyrolysis*, 70:233–250, 2003. ISSN 01406701. doi: 10.1016/S0140-6701(04)93143-8.

[58] Y. B. Yang, H. Yamauchi, V. Nasserzadeh, and J. Swithenbank. Effects of fuel devolatilisation on the combustion of wood chips and incineration of simulated municipal solid wastes in a packed bed. *Fuel*, 82(18):2205–2221, 2003. ISSN 00162361. doi: 10.1016/S0016-2361(03)00145-5.

[59] Tianbao Gu, Chungen Yin, Wenchao Ma, and Guanyi Chen. Municipal solid waste incineration in a packed bed: A comprehensive modeling study with experimental validation. *Applied Energy*, 247(January):127–139, 2019. ISSN 03062619. doi: 10.1016/j.apenergy.2019.04.014. URL `https://doi.org/10.1016/j.apenergy.2019.04.014`.

[60] Kenneth M Bryden and Mathew J Hagge. Modeling the combined impact of moisture and char shrinkage on the pyrolysis of a biomass particle. *Fuel*, 82(13):1633–1644, 2003. ISSN 00162361. doi: 10.1016/S0016-2361(03)00108-X.

[61] S S Alves and J L Figueiredo. A model for pyrolysis of wet wood. *Chemical Engineering Science*, 44(12):2861–2869, 1989. ISSN 00092509. doi: 10.1117/12.533183. URL `http://www.sciencedirect.com/science/article/pii/0009250989850961`.

[62] F P Incropera, D P Dewitt, T L Bergman, and A S Lavine. *Fundamentals of heat and mass transfer*. John Wiley & Sons, 6th editio edition, 1993. ISBN *9780471457282. doi: 10.1109/TKDE.2004.30.

[63] Liang Yu, Jing Lu, Xiangping Zhang, Suojiang Zhang, and Xiaoling Wang. Two fluid model using kinetic theory for modeling of one-step hydrogen production gasifier. *Particle therory and fluidization*, 54(11):2833–2851, 2008. ISSN 12350621. doi: 10.1002/aic.

[64] Yao B Yang, Vida N Sharifi, Jim Swithenbank, Lin Ma, Leilani I, Jenny M Jones, Mohamed Pourkashanian, Alan Williams, and Leilani I Darvell. Combustion of a single particle of biomass. *Energy*, 22(1):306–316, 2008. ISSN 0887-0624. doi: 10.1021/ef700305r.

[65] Yao Bin Yang, Lynne Sliwinski, Vida Sharifi, and Jim Swithenbank. Dynamic behaviour of sewage sludge incineration in a large-scale bubbling fluidised bed in relation to feeding-rate variations. *Fuel*, 87(8-9):1552–1563, 2008. ISSN 00162361. doi: 10.1016/j.fuel.2007.08.004.

[66] Yao Bin Yang, Robert Newman, Vida Sharifi, Jim Swithenbank, and John Ariss. Mathematical modelling of straw combustion in a 38 MWe power plant furnace and effect of operating conditions. *Fuel*, 86:129–142, 2007. ISSN 00162361. doi: 10.1016/j.fuel.2006.06.023.

[67] Yao Bin Yang, Vida N. Sharifi, and Jim Swithenbank. Converting moving-grate incineration from combustion to gasification - Numerical simulation of the burning characteristics. *Waste Management*, 27(5):645–655, 2007. ISSN 0956053X. doi: 10.1016/j.wasman.2006.03.014.

[68] Frederick L Dryer and Charles K Westbrook. Simplified reaction mechanisms for the oxidation of hydrocarbon fuels in flames. *Combustion Science and Technology*, 27(1-2):31–43, 1981. ISSN 1563521X. doi: 10.1080/00102208108946970.

[69] W P Jones and R P Lindstedt. Global reaction schemes for hydrocarbon combustion. *Combustion and Flame*, 73:233–249, 1988. ISSN 00102180. doi: 10.1016/0010-2180(88)90021-1.

[70] Chungen Yin, Søren K. Kær, Lasse Rosendahl, and Søren L. Hvid. Co-firing straw with coal in a swirl-stabilized dual-feed burner: Modelling and experimental validation. *Bioresource Technology*, 101:4169–4178, 2010. ISSN 09608524. doi: 10.1016/j.biortech.2010.01.018. URL `http://dx.doi.org/10.1016/j.biortech.2010.01.018`.

[71] Stephen R. Turns. *An introduction to combustion-concepts and applications*. Raghothaman Srinivasan, 3rd edicti edition, 2012. ISBN 9780073380193. doi: http://dx.doi.org/10.2139/ssrn.2257783.

[72] Russell A Ogle. *Dust Explosion Dynamics*. Joe Hayton, 2017. ISBN 9780128037713. doi: 10.1016/c2014-0-03833-6.

[73] H. K. Versteeg and Malalasekera W. *An introduction to Computational Fluid Dynamics*. Pearson Education Limited, second edition, 2016. ISBN 9780131274983. doi: 10.1002/9781119369189.

[74] Jun Li, Manosh C. Paul, Paul L. Younger, Ian Watson, Mamdud Hossain, and Stephen Welch. Prediction of high-temperature rapid combustion behaviour of woody biomass particles. *Fuel*, 165:205–214, 2016. ISSN 00162361. doi: 10.1016/j.fuel.2015.10.061.

[75] Prabir Basu. *Biomass gasification and pyrolysis: Practical design and theory*. Elsevier, first edit edition, 2010. ISBN 9780123749888. doi: 10.1017/CBO9781107415324.004.

[76] Hong Lu. *Experimental and Modeling Investigations of Biomass Particle Combustion*. PhD thesis, Brigham Young University, 2006.

[77] Xiyan Li, Chungen Yin, Søren Knudsen Kær, and Thomas Condra. A detailed pyrolysis model for a thermally large biomass particle. *Fuel*, 278:118397, 2020. ISSN 0016-2361. doi: 10.1016/j.fuel.2020.118397. URL `https://doi.org/10.1016/j.fuel.2020.118397`.

[78] Theodore R. Nunn, Jack B. Howard, John P. Longwell, and William A. Peters. Product compositions and kinetics in the rapid pyrolysis of milled wood lignin. *Industrial and Engineering Chemistry Process Design and Development*, 24(3):844–852, 1985. ISSN 01964305. doi: 10.1021/i200030a054.

[79] J Porteiro, D Patiño, J Collazo, E Granada, J Moran, and J L Miguez. Experimental analysis of the ignition front propagation of several biomass fuels in a fixed-bed combustor. *Fuel*, 89:26–35, 2010. ISSN 00162361. doi: 10.1016/j.fuel.2009.01.024.

[80] Aditya Anantharaman, Ray A. Cocco, and Jia Wei Chew. Evaluation of correlations for minimum fluidization velocity (Umf) in gas-solid fluidization. *Powder Technology*, 323:454–485, 2018. ISSN 1873328X. doi: 10.1016/j.powtec.2017.10.016.

[81] C. Y. Wen and Y. H. Yu. A generalized method for predicting the minimum fluidization velocity. *AIChE Journal*, 12(3):610–612, 1966. ISSN 15475905. doi: 10.1002/aic.690120343.

[82] Sabri Ergun. Che Eng Pro48, 89.pdf. *Chemical enfineering progress*, 48(2): 89–94, 1952.

[83] Antoni Lucas, Josep Arnaldos, Joaqulm Casal, and Lluis Pulgjaner. Improved Equation for the Calculation of Minimum Fluidization Velocity. *Industrial and Engineering Chemistry Process Design and Development*, 25 (2):426–429, 1986. ISSN 01964305. doi: 10.1021/i200033a013.

[84] H Zhou, A D Jensen, P Glarborg, P A Jensen, and A Kavaliauskas. Numerical modeling of straw combustion in a fixed bed. *Fuel*, 84:389–403, 2005. ISSN 00162361. doi: 10.1016/j.fuel.2004.09.020.

Part II

Appendices

Appendix A: Discretization

This part of Appendix shows the discretized partial differential equations that are presented in Chapter 2. The domain of a single biomass pellet is shown in Fig. 1. The linearised equations based on the underlying partial differential equations are solved using the TDMA equation solver.

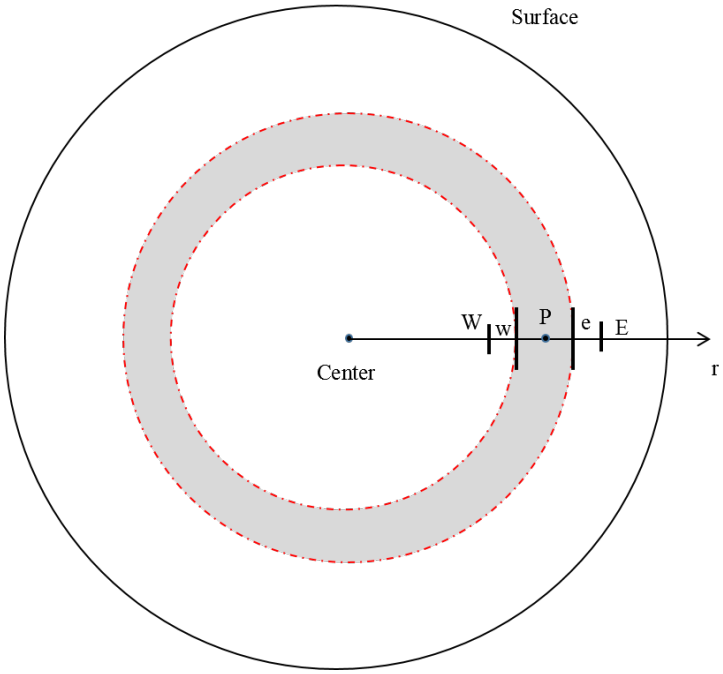

Fig. 1: Caption

A standard discretised transport equation can be written as:

$$a_p \phi_p = a_W \phi_W + a_E \phi_E + b \tag{1}$$

According to the geometry in Fig. 1, the solutions to the discretized partial differential equations of a single biomass pellets can be written as shown in the following.

There is no convection and diffusion for the solid and liquid matter in this model, therefore the densities of these matter are calculated with equation 2 to equation 5

Biomass

$$\rho_B = \rho_{B0} + S_B \Delta t \tag{2}$$

Carbon

$$\rho_c = \rho_{c0} + S_c \Delta t \tag{3}$$

Ash

$$\rho_{ash} = \rho_{ash0} \tag{4}$$

Moisture

$$\rho_m = \rho_{m0} + S_c \tag{5}$$

Gas species

$$\begin{aligned} b &= S\Delta V + \varepsilon_P^0 \rho_P^0 Y_P^0 \Delta V^0 / \Delta t Y_0 \\ a_W &= \frac{\varepsilon \rho_w A_w u_w}{2} + \varepsilon D_w \rho_W A_w / \Delta x \\ a_E &= -\frac{\varepsilon \rho_e A_e u_e}{2} + \varepsilon D_e \rho_E A_e / \Delta x \\ a_P &= a_E + a_W + \frac{\varepsilon_P \rho_P \Delta V}{\Delta t} \end{aligned} \tag{6}$$

At the pellet center:

$$\begin{aligned} b &= S\Delta V + \frac{\varepsilon_P^0 \rho_P^0 Y_P^0 \Delta V}{\Delta t} Y_0 \\ a_W &= 0 \\ a_E &= -\frac{\varepsilon \rho_e A_e u_e}{2} + \varepsilon D_e \rho_e A_e / \Delta x \\ a_P &= a_E + a_W + \frac{\varepsilon_P \rho_P \Delta V}{\Delta t} \end{aligned} \tag{7}$$

On the pellet surface:

$$\begin{aligned} b &= S\Delta V + \frac{\varepsilon_P^0 \rho_P^0 Y_P^0 \Delta V}{\Delta t} Y_0 \\ a_W &= \frac{\varepsilon \rho_w A_w u_w}{2} + \varepsilon D_w \rho_W A_w / \Delta x \\ a_E &= -\rho_B u_B A_S + 2 D_B A_S \varepsilon_B \rho_B / \Delta x \\ a_p &= a_w + 2 D_B \cdot \frac{\varepsilon_P \rho_P}{\Delta x} + \frac{\varepsilon_P \rho_P \Delta V}{\Delta t} \end{aligned} \tag{8}$$

$$\begin{aligned} a_W &= 2 D_{N-1} \\ a_E &= 0 \\ a_P &= 2 D_B + h_s \Delta x \\ b &= h_S Y_\infty \Delta x \end{aligned} \tag{9}$$

Temperature

$F = \varepsilon \rho_g C_{p,g} \mathbf{U} A \quad D = \frac{k_{eff} A}{\Delta x}$

$$
\begin{aligned}
b &= S\Delta V + \left(\varepsilon_P^{g0} \rho_P^{g0} C_P^{g0} + \rho_P^{s0} C_P^{s0}\right) \frac{\Delta V}{\Delta t} T0 \\
a_W &= F_w/2 + D_w \\
a_E &= -F_e/2 + D_e \\
a_P &= a_W + a_E + F_e - F_w + \left(\varepsilon_p \rho_P^g C_P^g + \rho_S^g C_S^g\right) \frac{\Delta V}{\Delta t}
\end{aligned}
\tag{10}
$$

At the pellet center:
$T_0 = T_1$

On the pellet surface:

$$
\begin{aligned}
a_P^0 &= \left(\varepsilon_P^{g0} \rho_P^{g0} C_P^{g0} + \rho_P^{s0} C_P^{s0}\right) \frac{\Delta x}{\Delta t} \\
a_W &= F_w C_w^g/2 + k_w/\Delta x \\
a_E &= -\rho_B u_B C_B^g + 2k_B/\Delta x \\
a_P &= -\frac{F_w}{2} + D_w + \frac{2k_B}{\Delta x} + \left(\varepsilon_P \rho_P^g C_P^g + \rho_P^g C_P^g\right) \frac{\Delta x}{\Delta t} \\
b &= a_P^0 T_P^0 + S \cdot \Delta V
\end{aligned}
\tag{11}
$$

$$
\begin{aligned}
a_W &= 2k_B \\
a_E &= 0 \\
a_P &= 2k_B + h_s \Delta x + 4\varepsilon\sigma T_B^{*3} \Delta x \\
b &= h_s T_\infty \Delta x + \varepsilon\sigma \left(T_\infty^{*4} + 3T_B^{*4}\right) \Delta x
\end{aligned}
\tag{12}
$$

Continuity equation

$$
\begin{aligned}
a_W &= \rho_{g,w} A_w \frac{\eta}{\mu \Delta x} \\
a_E &= \rho_{g,e} A_e \frac{\eta}{\mu \Delta x} \\
a_P &= a_E + a_W \\
b &= \frac{\nabla V s_g}{\varepsilon} - \left(\rho_{g,P} - \rho_{g,P}^0\right) \frac{\nabla V}{\nabla t} - \rho_{g,e} A_e u_e^* + \rho_{g,w} A_w u_w^*
\end{aligned}
\tag{13}
$$

At the pellet center $P_0' = P_1'$

On the pellet surface:

$$
\begin{aligned}
a_W &= \rho_{g,w} A_w \frac{\eta}{\mu \Delta x} \\
a_E &= \rho_{g,s} A_s \frac{\eta}{\mu \Delta x} \\
a_P &= a_E + a_W \\
b &= \frac{\nabla V * S_g}{\varepsilon} - \left(\rho_{g,P} - \rho^0_{g,P}\right) \frac{\sigma V}{\nabla t} - \rho_{g,e} A_e u^*_{e(i+1)} + \rho_{g,w} A_w u^*_{e(i)} \\
P'_{\text{surf}} &= 0
\end{aligned}
\tag{14}
$$

Appendix B: Source terms for the transport equations

According to the reactions in Table 3.2, the source term of different species can be written as:

Biomass:

$$S_B = -\left(k_1\right)\rho_B \tag{15}$$

Carbon:

$$S_C = k_1\rho_s - S_{a,char}\frac{\rho_C}{\rho_C+\rho_B+\rho_{ash}}\left(\varepsilon k_4\rho_{CO_2}\frac{2M_C}{M_{CO_2}} + \varepsilon k_5\rho_{H_2O}\frac{2M_C}{M_{H_2O}} + \varepsilon k_6\rho_{H_2}\frac{M_C}{2M_{H_2}}\right) \tag{16}$$

Moisture:

$$S_w = -\left(k_{2,3}\right)\rho_{H_2o} \tag{17}$$

Carbon monoxide:

$$S_{CO} = \alpha_{CO}k_1\rho_B + S_{a,char}\frac{\rho_C}{\rho_C+\rho_B+\rho_{ash}}\left(\varepsilon k_4\rho_{CO_2}\frac{2M_{CO}}{M_{CO_2}} + \varepsilon k_5\rho_{H_2O}\frac{M_{CO}}{M_{H_2O}}\right) - 3k_7\rho_{C_3H_8}\rho_{H_2O}\frac{3M_{CO}}{M_{C_3H_8}} - k_8\rho_{CO} \tag{18}$$

Carbon dioxide:

$$S_{CO_2} = \alpha_{CO_2}k_1\rho_B - S_{a,char}\frac{\rho_C}{\rho_C+\rho_B+\rho_{ash}}\varepsilon k_4\rho_{CO_2} + k_8\rho_{CO}\rho_{H_2O}\frac{M_{CO_2}}{M_{CO}} \tag{19}$$

Hydrogen:

$$S_{H_2} = \alpha_{H_2}k_1\rho_B + S_{a,char}\frac{\rho_C}{\rho_C+\rho_B+\rho_{ash}}\left(\varepsilon k_5\rho_{H_2O}\frac{M_{H_2}}{M_{H_2O}} - \varepsilon k_6\rho_{H_2}\right) + 7k_7\rho_{C_3H_8}\rho_{H_2O}\frac{7M_{H_2}}{M_{C_3H_8}} + k_8\rho_{CO}\rho_{H_2}\frac{M_{H_2}}{M_{CO}} \tag{20}$$

Vapor:

$$S_{H_2O} = \alpha_{H_2O}k_1\rho_B - S_{a,char}\frac{\rho_C}{\rho_C+\rho_B+\rho_{ash}}\varepsilon k_5\rho_{H_2O} - 3k_7\rho_{C_3H_8}\rho_{H_2O}\frac{7M_{H_2O}}{M_{C_3H_8}} + k_8\rho_{CO}\rho_{H_2}\frac{M_{H_2O}}{M_{CO}}$$

(21)

Nitrogen:

$$S_{N_2} = 0 \tag{22}$$

C_3H_8:

$$S_{C_3H_8} = \alpha_{C_3H_8} k_1 \rho_B - k_7 \rho_{C_3H_8} \rho_{H_2O} \tag{23}$$

For the continuity equation, the source term can be written as:

$$S_C = k_1 \rho_s + (k_{2,3})\, \rho_{H_2 o} + S_{a,char} \frac{\rho_C}{\rho_C + \rho_B + \rho_{ash}} \left(\varepsilon k_4 \rho_{CO_2} \frac{2M_C}{M_{CO_2}} + \varepsilon k_5 \rho_{H_2O} \frac{2M_C}{M_{H_2O}} + \varepsilon k_6 \rho_{H_2} \frac{M_C}{2M_{H_2}} \right) \tag{24}$$

For the reaction under biomass combustion, such as the reactions in Table 3.3, the source terms for the transport equations are: Biomass:

$$S_B = -\left(k_1\right)\rho_B \tag{25}$$

Carbon:

$$S_C = k_1\rho_s - S_{a,char}\frac{\rho_C}{\rho_C+\rho_B+\rho_{ash}}\left(\varepsilon k_4\rho_C + \varepsilon k_5\rho_{CO_2}\frac{2M_C}{M_{CO_2}} + \varepsilon k_6\rho_{H_2O}\frac{2M_C}{M_{H_2O}}\right) \tag{26}$$

Moisture:

$$S_w = -\left(k_{2,3}\right)\rho_{H_2O} \tag{27}$$

Carbon monoxide:

$$\begin{aligned} S_{CO} = {} & \alpha_{CO}k_1\rho_B \\ & + S_{a,char}\frac{\rho_C}{\rho_C+\rho_B+\rho_{ash}}\left(\varepsilon k_4\rho_{CO_2}\frac{2M_{CO}}{M_{CO_2}} + \varepsilon k_5\rho_{CO_2}\frac{2M_{CO}}{M_{CO_2}} + \varepsilon k_6\rho_{H_2O}\frac{M_{CO}}{M_{H_2O}}\right) \\ & - k_8\rho_{CO}{\rho_{O_2}}^{0.25} + k_9\rho_{C_3H_8}\rho_{H_2O}\frac{3M_{CO}}{M_{C_3H_8}} \\ & + k_{10}{\rho_{CO}}^{0.5}{\rho_{O_2}}^{1.25}\frac{3M_{CO}}{M_{C_3H_8}} - k_{11}\rho_{CO}\rho_{H_2O} \end{aligned} \tag{28}$$

Carbon dioxide:

$$\begin{aligned} S_{CO_2} = {} & \alpha_{CO_2}k_1\rho_B \\ & - S_{a,char}\frac{\rho_C}{\rho_C+\rho_B+\rho_{ash}}\left(\varepsilon k_4\rho_{CO_2}\frac{2M_C}{M_{CO_2}} + \varepsilon k_5\rho_{CO_2}\right) \\ & + k_8\rho_{CO}{\rho_{O_2}}^{0.25} + k_{11}\rho_{CO}\rho_{H_2O}\frac{M_{CO_2}}{M_{CO}} \end{aligned} \tag{29}$$

Hydrogen:

$$\begin{aligned} S_{H_2} = {} & \alpha_{H_2}k_1\rho_B + S_{a,char}\frac{\rho_C}{\rho_C+\rho_B+\rho_{ash}}\varepsilon k_6\rho_{H_2O}\frac{M_{H_2}}{M_{H_2O}} - K_7{\rho_{H_2}}^{0.25}{\rho_{O_2}}^{1.5} \\ & + k_9\rho_{C_3H_8}\rho_{H_2O}\frac{M_{H_2}}{M_{C_3H_8}} + k_{10}{\rho_{CO}}^{0.5}{\rho_{O_2}}^{1.25}\frac{4M_{H_2}}{M_{C_3H_8}} + k_{11}\rho_{CO}\rho_{H_2O}\frac{M_{H_2}}{M_{CO}} \end{aligned} \tag{30}$$

Vapor:

$$S_{H_2O} = \alpha_{H_2O} k_1 \rho_B - S_{a,char} \frac{\rho_C}{\rho_C + \rho_B + \rho_{ash}} \varepsilon k_6 \rho_{H_2O} + K_7 {\rho_{H_2}}^{0.25} {\rho_{O_2}}^{1.5} \frac{M_{H_2O}}{M_{H_2}} - k_9 \rho_{CO} \rho_{H_2} \frac{M_{H_2O}}{M_{CO}} \tag{31}$$

Oxygen:

$$S_{O_2} = S_{a,char} \frac{\rho_C}{\rho_C + \rho_B + \rho_{ash}} \varepsilon k_4 \rho_C \frac{\alpha M_{O_2}}{M_C} - K_7 {\rho_{H_2}}^{0.25} {\rho_{O_2}}^{1.5} \frac{0.5 M_{O_2}}{M_{H_2}} - k_8 \rho_{CO} {\rho_{O_2}}^{0.25} \frac{0.5 M_{O_2}}{M_{CO}} - k_{10} {\rho_{CO}}^{0}.5 {\rho_{O_2}}^{1.25} \frac{1.5 M_{O_2}}{M_{C_3H_8}} \tag{32}$$

C_3H_8:

$$S_{C_3H_8} = \alpha_{C_3H_8} k_1 \rho_B - k_9 \rho_{C_3H_8} \rho_{H_2O} - k_{10} {\rho_{CO}}^{0.5} {\rho_{O_2}}^{1.25} \tag{33}$$

Based on Table 3.3, the source terms for different species can be written as following:

Biomass:

$$S_B = -\left(k_1\right)\rho_B \tag{34}$$

Carbon:

$$S_C = k_1\rho_s - S_{a,char}\frac{\rho_C}{\rho_C+\rho_B+\rho_{ash}}\left(\varepsilon k_4\rho_C + \varepsilon k_5\rho_{CO_2}\frac{2M_C}{M_{CO_2}} + \varepsilon k_6\rho_{H_2O}\frac{2M_C}{M_{H_2O}}\right) \tag{35}$$

Moisture:

$$S_w = -\left(k_{2,3}\right)\rho_{H_2O} \tag{36}$$

Carbon monoxide:

$$\begin{aligned} S_{CO} = {} & \alpha_{CO}k_1\rho_B \\ & + S_{a,char}\frac{\rho_C}{\rho_C+\rho_B+\rho_{ash}}\left(\varepsilon k_4\rho_{CO_2}\frac{2M_{CO}}{M_{CO_2}} + \varepsilon k_5\rho_{CO_2}\frac{2M_{CO}}{M_{CO_2}} + \varepsilon k_6\rho_{H_2O}\frac{M_{CO}}{M_{H_2O}}\right) \\ & - k_8\rho_{CO}{\rho_{O_2}}^{0.25} + k_9\rho_{C_3H_8}\rho_{H_2O}\frac{3M_{CO}}{M_{C_3H_8}} \\ & + k_{10}{\rho_{CO}}^{0.5}{\rho_{O_2}}^{1.25}\frac{3M_{CO}}{M_{C_3H_8}} - k_{11}\rho_{CO}\rho_{H_2O} \\ & + k_{12}{\rho_{CO}}^{0.5}{\rho_{O_2}}^{1.25}\frac{2M_{CO}}{M_{CH_4}} + k_{13}\rho_{CH_4}\rho_{H_2O}\frac{M_{CO}}{M_{CH_4}} \end{aligned} \tag{37}$$

Carbon dioxide:

$$\begin{aligned} S_{CO_2} = {} & \alpha_{CO_2}k_1\rho_B - S_{a,char}\frac{\rho_C}{\rho_C+\rho_B+\rho_{ash}}\left(\varepsilon k_4\rho_{CO_2}\frac{2M_C}{M_{CO_2}} + \varepsilon k_5\rho_{CO_2}\right) \\ & + k_8\rho_{CO}{\rho_{O_2}}^{0.25} + k_{11}\rho_{CO}\rho_{H_2O}\frac{M_{CO_2}}{M_{CO}} \end{aligned} \tag{38}$$

Hydrogen:

$$\begin{aligned} S_{H_2} = {} & \alpha_{H_2}k_1\rho_B + S_{a,char}\frac{\rho_C}{\rho_C+\rho_B+\rho_{ash}}\varepsilon k_6\rho_{H_2O}\frac{M_{H_2}}{M_{H_2O}} - K_7{\rho_{H_2}}^{0.25}{\rho_{O_2}}^{1.5} \\ & + k_9\rho_{C_3H_8}\rho_{H_2O}\frac{M_{H_2}}{M_{C_3H_8}} + k_{10}{\rho_{CO}}^{0}.5{\rho_{O_2}}^{1.25}\frac{4M_{H_2}}{M_{C_3H_8}} + k_{11}\rho_{CO}\rho_{H_2O}\frac{M_{H_2}}{M_{CO}} \\ & + k_{12}{\rho_{CH_4}}^{0.5}{\rho_{O_2}}^{1.25}\frac{4M_{H_2}}{M_{CH_4}} + k_{13}\rho_{CH_4}\rho_{H_2O}\frac{3M_{H_2}}{M_{CH_4}} \end{aligned}$$

(39)

Vapor:

$$S_{H_2O} = \alpha_{H_2O} k_1 \rho_B - S_{a,char} \frac{\rho_C}{\rho_C + \rho_B + \rho_{ash}} \varepsilon k_6 \rho_{H_2O} + K_7 {\rho_{H_2}}^{0.25} {\rho_{O_2}}^{1.5} \frac{M_{H_2O}}{M_{H_2}} - k_9 \rho_{CO} \rho_{H_2} \frac{M_{H_2O}}{M_{CO}} - k_{13} \rho_{CH_4} \rho_{H_2O} \frac{M_{H_2O}}{M_{CH_4}} \tag{40}$$

Oxygen:

$$S_{O_2} = S_{a,char} \frac{\rho_C}{\rho_C + \rho_B + \rho_{ash}} \varepsilon k_4 \rho_C \frac{\alpha M_{O_2}}{M_C} - K_7 {\rho_{H_2}}^{0.25} {\rho_{O_2}}^{1.5} \frac{0.5 M_{O_2}}{M_{H_2}} - k_8 \rho_{CO} {\rho_{O_2}}^{0.25} \frac{0.5 M_{O_2}}{M_{CO}} - k_{10} {\rho_{CO}}^{0.5} {\rho_{O_2}}^{1.25} \frac{1.5 M_{O_2}}{M_{C_3H_8}} - k_{12} {\rho_{CH_4}}^{0.5} {\rho_{O_2}}^{1.25} \frac{1.5 M_{O_2}}{M_{CH_4}} \tag{41}$$

C_3H_8:

$$S_{C_3H_8} = \alpha_{C_3H_8} k_1 \rho_B - k_9 \rho_{C_3H_8} \rho_{H_2O} - k_{10} {\rho_{CO}}^{0.5} {\rho_{O_2}}^{1.25} \tag{42}$$

Part III

Papers

Paper A

A drying model for thermally large biomass particle pyrolysis

Xiyan Li, Chungen Yin

The paper has been published in the
Energy Procedia Vol. 158, pp. 1294-1302, 2019.

The layout has been revised.

Available online at www.sciencedirect.com

ScienceDirect

Energy Procedia 158 (2019) 1294–1302

Energy Procedia

www.elsevier.com/locate/procedia

10th International Conference on Applied Energy (ICAE2018), 22-25 August 2018, Hong Kong, China

A drying model for thermally large biomass particle pyrolysis

Xiyan Li*, Chungen Yin

Department of Energy Technology, Aalborg University, Aalborg, 9200, Denmark

Abstract

Biomass drying has always been a big issue in biomass thermal treatment. Especially in pyrolysis, combustion and gasification, water evaporation is a necessary step before other reactions can take place. This paper presents a detailed drying for single poplar particle pyrolysis under nitrogen. In this model, the transport equations are numerically solved using finite volume method to obtain the pressure, temperature and species fractions. Two different water contents found from literature are applied to test the model. The result shows that this numerical model can predict water behavior during biomass drying process of pyrolysis.

Keywords: Pyrolysis; Biomass; FVM; Drying;

Nomenclature

A	The surface area [m^2]
A_{evp}	Pre-exponential factor of water evaporation [s^{-1}]
$C_{P,S}$	Specific heat [J/(kg · K)]
E_{evp}	Activation energy of water evaporation, [J/Kmol]
$D_{eff,fw}$	Free water effective mass diffusivity [m^2/s]
F_{heat}	Assumed as the sum of radiation heat and convection heat transfer [W/m^3]
h_T	Heat transfer coefficient [$W/(m^2 \cdot K)$]
h_M	Mass transfer coefficient [m/s]

* Corresponding author. Tel.: 45 20703591; fax: 45 99403820
E-mail address: xli@et.aau.dk

1876-6102
10.1016/j.egypro.2019.01.322

$h_{m,pore}$	The mass transfer coefficient of vapor in the pore [m/s]
K_B	The thermal conductivity [W/(m · K)]
k_{H_2O}	Reaction rate constant [s^{-1}]
Nu	Nusselt number
Pr	Prandtl number
R_g	Universal gas constant [J/(mol · K)]
r_i	Reaction rate [kg/(m^3 · s)]
r_{H_2O}	The volumetric vaporization rate [kg/(m^3 · s)]
Sc	Schmidt number
Sh	Sherwood number
S_T	Source term in energy equation [W/m^3]
S_a	The specific area of the wood particle [m^2/m^3]
T_{ini}	Initial temperature [K]
T_∞	Ambient gas temperature [K]
T_S	Particle surface temperature [K]
$T_{j,S}$	Particle surface temperature for species j [K]
T_C	Particle centre temperature [K]
T_{evap}	Defined as evaporation point of liquid water [K]
Y_{vap}	The percentage of vapor within all the species
$Y_{j,ref}$	Reference mass fraction of species *j* in the gas film around the particle
$Y_{j,s}$	Mass fraction of species *j* at particle surface
$Y_{j,\infty}$	Mass fraction of species *j* in the ambient gas
ρ_g	Gas density [kg/m^3]
ρ_g^{sat}	The saturated vapor density [kg/m^3]
ρ_{fw}^0	The initial free water density [kg/m^3]
ρ_{fw}	The free water density at the present time [kg/m^3]
$\dot{w}_k$	Reaction rate
λ	The average conductivity of all the gases in the film [W/(m · K)]
ε	Porosity
μ	Dynamic viscosity [kg/(m · s)]
σ	Boltzmann radiation constant, 5.86×10^{-8} (W/m^2K^4)
g	Gas
l	Liquid
s	Solid

1. Introduction

Drying, as the first step of biomass gasification and pyrolysis, plays an important role in the whole process, not only for preheating, but also for the stability of industrial production. Many researchers have studied the drying technology for biomass, from lab-scale to industrial scale [1][2][3][4]. The particle size studied in literature can be as small as a pulverized particles, as well as a large piece of wood, usually around 1mm to 10 mm in diameter [5]. The drying media can be superheated steam or flue gas from biomass residues or even air or nitrogen [6]. A raw material as received usually has water content up to 40% to 50%. After drying, the water content can be 6% to 8%, which is suitable for industrial use [7].

The moisture exists in biomass in three forms: in pore and capillary as vapor or as liquid water and in fiber as bound water [3]. Normally, there is a circumscription known as Fiber saturation point (FSP) that defines the bound water and the free water. The FSP describes the ability that cellulose molecule can absorb bound water. Babiak and Kudela [8] studied the definition of FSP. FSP can be 30% of dry biomass weight [9].

There are three commonly used drying models in literature, the thermal model, the kinetic rate drying model and the equilibrium model. The equilibrium model is usually used in low temperature drying, and is numerically unstable for high temperature drying [3]. The thermal model is the most commonly used model, and has been used in literature

both in particle pyrolysis [10] and packed be pyrolysis [5][11]. The kinetic rate model is commonly used for bound water evaporation [12][13]. Below is a description of these three models.

Equilibrium model has the following expression. For thermal model, the expression is shown as eq. (4). For the kinetic rate model, the water evaporation is treated as a chemical reaction; hence, Arrhenius expression can be used to describe the behavior of reaction rate. The expression is shown in eq. (5).

$$H_2O(l) \xrightarrow{yields} H_2O(g) \tag{1}$$

$$r_{H_2O} = s_a(\rho_{fw}/\rho_{fw}^0)h_{m,pore}(\rho_\vartheta^{sat} - \rho_g Y_{vap}) \tag{2}$$

$$h_{m,pore} = 3.66\frac{D_{eff,fw}}{d_{pore,hydraulic}} \tag{3}$$

$$r_{H_2O} = \begin{cases} 0, & T < T_{evap} \\ \frac{F_{heat}}{\Delta h_{evap}}, & T > T_{evap} \end{cases} \tag{4}$$

$$F_{heat} = s_a\left(h_T\left(T_j - T_{ini}\right) + \varepsilon\sigma\left(T_j^4 - T_{ini}^4\right)\right) \tag{5}$$

$$r_{H_2O} = A_{evp}exp\left(-\frac{E_{evp}}{RT}\right) \tag{6}$$

Haberle et al [3] summarize the kinetic data from literature, as shown in Table1 .

Table 1 Kinetic data for water evaporation

Pre-exponential factor (s-1)	Activation energy (J Kmol-1)	Ref.
5.13×10^{10}	8.8×10^7	[12][14]
5.13×10^6	$24/120 \times 10^6$	[15]
5.60×10^8	8.8×10^7	[16]
5.13×10^6	8.8×10^7	[17]

Table 2 Proximate and ultimate analysis

Fixed carbon	9.5%
Moisture	6% and 40%
Ash	0.5%
Volatile	90%
C(DB)	48.1%
H(DB)	5.77%
O(DB)	45.53%
Others	
LHV(6% moisture)	17.05 MJ/kg
density	540kg/m3

In this work, all the three models are tested. After each time step, the local temperature will be updated at the locations where the thermal model for free water and kinetic model for bound water is active or being used. To make a comparison, a thermal model is also used for bound water and a kinetic model is used for free water, too. The equilibrium model is only used for free water under 100 ℃[18]. The result shows choosing a thermal model or choosing a kinetic model does not affect the whole pyrolysis process, although a kinetic model is preferred for bound water.

2. Model description

In order to study the drying issue of a single biomass pellet. A poplar tree particle sample is chosen from the literature [12][19] to study here, partly because the experimental data is easy to find in the literature to do model validation, partly because different water content of poplar wood particle under pyrolysis can be found in the literature. The poplar wood particle properties can be found in Table 2. The moisture here is treated as 6% and 40% the mass fraction of dry biomass. The reaction is operated under nitrogen pyrolysis and with the wall temperature of 1273K and gas flow temperature of 1050K.

A CFD code based on C++ has been generated for this model, where a finite volume method was used to solve the transport equations numerically. The convective terms are discretized by central differencing scheme, and the time step is set to 0.01s, the temporal scheme used here is implicit scheme. The meshing is along the radial direction, in which 60 grids were made. The proximate analysis and ultimate analysis, as well as density and lower heating value

is given in Table 2, which is also used for validation of Lu et al's model [12] by Mehrabian et al [19]. The model assumes that the biomass particle is isotropic and near-sphere.

For wood pyrolysis, there are many kinetic models. The most commonly used ones assume a set of heat of reactions for different reactions. After that the heat of reactions are used in temperature calculations. In this work, a lower heating value (LHV) or a higher heating value (HHV) is found for the specific wood used in the pyrolysis. Therefore, the formation enthalpy of volatile can be calculated. In this work, the molecular formula of the volatile is calculated as $CH_{2.1348}O_{0.9851}$, with a molecular weight of 30.13 kg/Kmol and the formation enthalpy of $-7926\mathrm{kJ/kg}$. Assuming volatile will crack into real species: CO, CO2, H2, CH4, with a molar fraction of 0.442, 0.200, 0.358 and 0.2695.

Energy equation is expressed as eq. (7), while the source term can be found in eq. (6).

$$\frac{\partial(\varepsilon\rho_g C_{pg}T+\rho_s C_{ps}T+\rho_l C_{pl}T)}{\partial t} + div(\varepsilon\rho_g u C_{pg}T_g) = div\left(k_{eff}\nabla T\right) + S_T \quad (7)$$

$$S_T = -\sum_{k=1}^{N}\Delta h_{f,k}^0 \dot{w}_k - \sum_{k=1}^{N}\Delta h_{f,k}\dot{w}_k \quad (8)$$

S_T is the source term of energy equation and consists of a sum of formation enthalpy of each species and a sum of sensible enthalpy of each species. In this paper, whenever the source term model for water is changed, the corresponding source term in the energy equation is also replaced. For the boundary condition of temperature, the gradient is treated as 0 at center point. For the surface, due to the existence of radiation and convection, the boundary condition can be written as eq.(9). To calculate the heat transfer coefficient, a gas film surrounding the particle is assumed. The temperature used for gas properties in the gas film is treated as reference temperature, as defined by one-third law [20].

$$k_B A\frac{T_B-T_P}{\Delta r/2} = Ah_T\left(T_\infty - T_B\right) + A\varepsilon\sigma(T_\infty^4 - T_B^4) \quad (9)$$

$$T_{ref} = T_s + 1/3\left(T_\infty - T_s\right) \quad (10)$$

$$h_T = \frac{Nu\lambda}{d_p} \quad (11)$$

Nu denote Nusselt number, here it uses the Nusselt number from Lu et al[12] for a sphere particle, with the expression:

$$Nu \equiv \frac{h_T L_c}{k_g} = 1.05 + 0.6Re^{0.65}Pr^{0.33} \quad (12)$$

The pressure is solved by Darcy law, together with continuity equation as follows:

$$\vec{u} = -\frac{\eta}{\mu}\nabla P \quad (13)$$

$$\frac{\partial(\varepsilon\rho_g)}{\partial t} + div(\varepsilon\rho_g u) = S_g \quad (14)$$

The boundary condition for pressure in the center point is treated with a zero-gradient, and a mass flow conservation is used for the surface boundary condition.

For the gaseous species, a transport equation is expressed as eq. (15). Similar to the energy equation, the boundary condition of the gaseous species at center point is to set the gradients to zero. For the surface, the reference species of gas film is calculated by one-third law, as shown in eq. (16) (17), $S_{Y_{ig}}$ denotes the source term of each gas species, h_M denotes the mass transfer coefficient, and can be calculated by the following correlation. While the solid terms have the simple expression of eq. (19), ρ_i denotes the density of water, remaining volatile in solid by time t, ash and carbon, and s_i denotes their source term.

$$\frac{\partial(\varepsilon\rho_g Y_{ig})}{\partial t} + div(\varepsilon\rho_g u Y_{ig}) = div\left(D_{ig}\nabla(\varepsilon\rho_g Y_{ig})\right) + S_{Y_{ig}} \quad (15)$$

$$Y_{j,ref} = Y_{j,s} + 1/3\left(Y_{j,\infty} - Y_{j,s}\right) \quad (16)$$

$$DA\frac{Y_B-Y_P}{\Delta x/2} = Ah_M(Y_\infty - Y_B) \quad (17)$$

$$Sh \equiv \frac{h_M L_c}{D_g} = 2.0 + 0.6Re^{1/2}Sc^{1/3} \quad (18)$$

$$\frac{\partial(\rho_i)}{\partial t} = s_i \quad (19)$$

All the reactions used in this model are listed in Table 3. A one-step global biomass decomposition model is used in this work. Thermal model and kinetic model used for moisture evaporation have already been stated in Equ. (2) to (6), the results will be discussed later in this paper. All the kinetics data used in Table 3 is shown in Table 4.

Table 3: Chemical reactions and reaction rate

Reaction index	Chemical reactions	Rate expression	Ref
1	Biomass → Volatile + Char	$r_1 = \partial\rho_{Vol}/\partial t = k_1\rho_{vol}$	[21]
2	H2O (free)→ H2O (g)	Equation (2-6)	
3	H2O(bound)→H2O (g)	Equation (2-6)	
4	C+1/2O2→CO	$r_4 = \partial C_{O_2}/\partial t = s_{a,char}[\rho_C/(\rho_C+\rho_B+\rho_A)]k_4 C_{O_2}$	[12]
5	C+CO2→2CO	$r_5 = \partial C_{CO_2}/\partial t = s_{a,char}[\rho_C/(\rho_C+\rho_B+\rho_A)]k_5 C_{CO_2}$	[12]
6	C+H2O→H2 + CO	$r_6 = \partial C_{H_2O}/\partial t = s_{a,char}[\rho_C/(\rho_C+\rho_B+\rho_A)]k_6 C_{H_2O}$	[12]
7	C+2H2→ CH4	$r_7 = \partial C_{H_2}/\partial t = s_{a,char}[\rho_C/(\rho_C+\rho_B+\rho_A)]k_7 C_{H_2}$	[22]
8	H2+1/2O2→H2O	$r_8 = \partial H_2/\partial t = k_8 C_{H_2} C_{O_2}^{0.5}$	[23]
9	CO+1/2O2→CO2	$r_9 = \partial C_{CO}/\partial t = k_9 C_{CO} C_{O_2}^{0.25} C_{H_2O}^{0.5}$	[12]
10	CH4+H2O→CO+3H2	$r_{10} = \partial C_{CH_4}/\partial t = k_{10} C_{CH_4}^{1.0} C_{H_2O}^{1.0}$	[24]
11	CH4+0.5O2→CO+2H2	$r_{11} = \partial C_{CH_4}/\partial t = k_{11} C_{CH_4}^{0.7} C_{H_2O}^{0.8}$	[24]
12	CO+H2O→CO2+H2	$r_{12} = \partial C_{CO}/\partial t = k_{12} C_{CO}^{1} C_{H_2O}^{1}$	[24]

Table 4: Kinetic data used in this model

Reaction index	Pre-exponential factor(s^{-1})	Activation energy(J/Kmol)	Heat of reactions (KJ/kg)
1	3.4×10^4	6.9×10^7	-1376.09
2	-	-	-
3	5.13×10^{10}	8.8×10^7	-2440
4	0.658a	7.4831×10^7	3950
5	3.42a	1.297×10^5	-14383.33
6	3.42a	1.297×10^5	-10933.33
7	2083a	115137	1701.59
7	$10^{12.71}$	1.71×10^5	13435.94
8	2.39×10^{12}	1.702×10^8	10114.28
9	3.0×10^8	1.26×10^8	-12879,38
10	5.012×10^{11}	2.0×10^8	2233.13
11	2.75×10^9	8.4×10^7	1480

a Those units are m/s-1k-1

3. Model validation and discussion

A grid independence check is made in Fig.1 A). The simulation results are based on 6% moisture content under nitrogen pyrolysis. As mentioned in introduction, 6% moisture content is far away from FSP, the reaction mechanism used in Fig1 is kinetic model. 60, 80, 100 grids along the radius were meshed, respectively. The grid independence check shows that the results from this model are independent of the meshing. Fig. 1 A) also shows three obvious pyrolysis stage as shown by arrows. It can be seen that the water vanishes around 6^{th} or 7^{th} second. The devolatilization stage stops after 32 seconds. The first stage is called drying stage, it stops after 6 seconds. During this stage, the bound water release. The biomass is significantly heated up. The second stage is the devolatilization stage, the pre-pyrolysis takes place from 400K to 700K with the release of light gases. The weight loss loses quickly in this stage (will be discussed in extended version), which is also a sign of gases releasing. Once the devolatilization reaction is finished, the temperature of the poplar particle goes up immediately, the pyrolysis comes to the final stage, in this stage the large molecules crack into char or non-condensable gases (will be discussed in extended version). The light gases take reactions or leave the pellet quickly. More information to show the three stages and the comparison of the mass fraction will be discussed later.

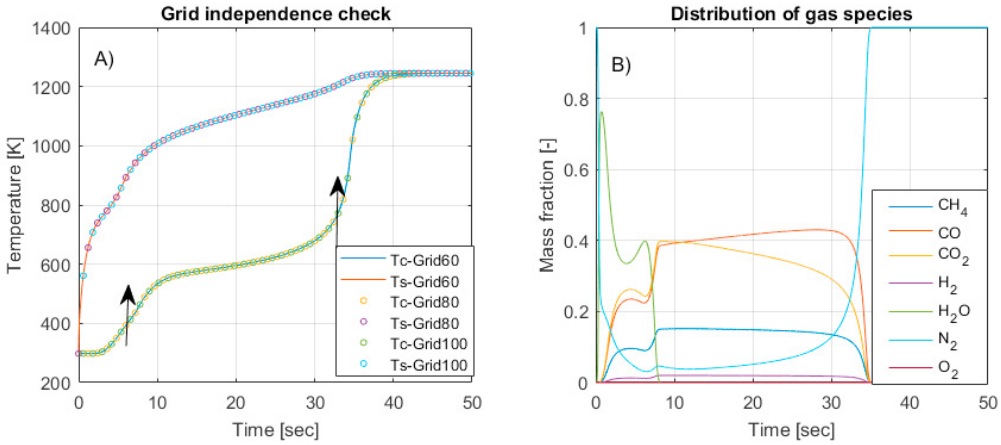

Fig 1A) Grid independence check. B) Gas species release with respect to time

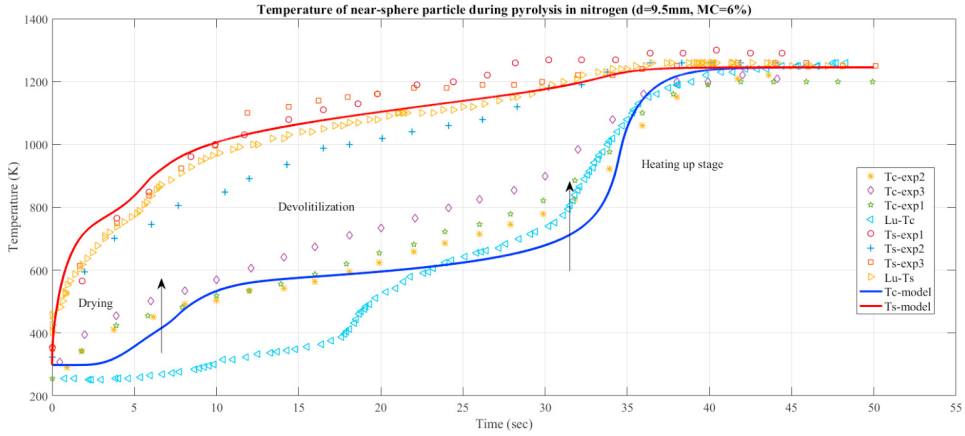

Fig. 2 Temperature profile from model and lu et al's results

Figure 1 B) shows the light gases released from the pyrolysis process at the center point of biomass pellet. It uses the same amount of moisture content as in Fig.1 A). The green line is water vapor release curve. Obviously, there are two peeks in this curve. The first one is because the fast release of free water. With the decomposition of biomass starts, the other small molecular-weight gases, like H_2, CO, CO_2, CH_4, the mass fraction of water vapor decreases. This stage is called initial stage by Basu [25], around temperature 100℃ to 300℃. The mass fraction of water goes down because the mass fraction of other gas species come out. Another vapor peak is caused by the intermediate stage (200℃ to 600℃) [25], where the primary pyrolysis starts. This stage finished until 35th second. During pyrolysis, there is not many homogeneous reactions happening after devolitilization stage. Fig. 1A) shows the devolitilization stops around 32 seconds, after that, as shown in Fig.1 B), the mass fraction of small molecules gas species decreases and comes to zero after 35 seconds. After that, there is no other gas coming out. As a result, the third stage is mainly heating up stage caused by the heat transfer from the surrounding environment.

The model has been validated using H. Lu et al's [12] experimental results and Rath et al's results[26], separately. In both validation, the modelling results shows a nice agreement with the experiments that Lu et al and Rath et al made. In experiment that Lu et al did, a poplar biomass particle is exposed to a furnace of 1276K with the flow temperature of 1050K. The gas media is nitrogen, the water content is set to 6% for sphere pellet and 40% for cylinder pellet. Since this work focuses on simulation of a sphere pellet, 6% moisture content from Lu et al's experimental work is used for comparison here. Simulation of 40% moisture content biomass pellet under nitrogen pyrolysis will be discussed, too. The validation against experimental results from Lu et al is shown in Fig. 2.

In Fig. 2, the solid blue line is temperature for center point from simulation result that authors made, the solid red line is the temperature for surface point using the simulation that authors made. It also shows the three experimental data from Lu et al and the simulation results from Lu et al. As shown in Fig. 2, the simulation agrees with experiment data better than the modelling results that H. Lu et al show. A one-step global devolatilization model for biomass decomposition is used here. Depending on the kinetic data that is chosen, the time interval of plateau in Fig.2 between the two arrows can be different. The devolatilization model affects the devolatilization rate, as discussed by Yang et al [18]. Here a 'fast' one-step devolatilization rate by Nunn[27] and defined by Yang et al[18] is used in this model, because it shows a better simulation result for poplar wood used by Lu et al [12] and Mehrabian et al [19]. The plot of center point temperature shows clearly three stage of devolatilization, drying and heating up stage after reactions are finished.

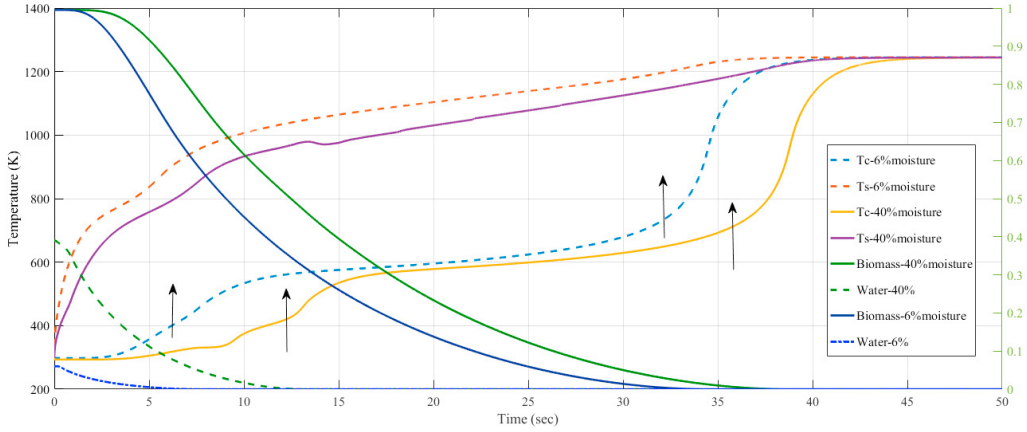

Fig. 3 Temperature profile of biomass pyrolysis with 40% moisture content and 6% moisture content and mass fraction of biomass (DB) and mass fraction of 40% moisture content

Figure 3 shows the temperature from the biomass pellet center and from the biomass pellet surface with 6% moisture content and 40% moisture content, respectively. The solid lines are temperature for 40% moisture content, and the dash lines are temperature for 6% moisture content. The solid green line is the mass fraction of dry biomass with respect to time during the condition of 40% moisture, and the dash green line is the mass fraction of 40% moisture content with respect to time. Fig. 6 also shows the same data of 6% moisture of dry biomass and water evolution, as show in solid deep blue line and dash deep blue line. Two arrows are made on the light blue dash line to show three different pyrolysis stages. Compared with 6% moisture content, the drying process of 40% moisture content takes longer time. To further investigate the moisture behavior and the relationship of water behavior and temperature, the mass fraction of moisture content and biomass is added in Fig.6. If the mass fraction of moisture or biomass does not exist at the center point anymore, it means all the mass is consumed and the reaction is finished. The solid green line is the mass fraction of biomass (DB) with respect of time, and the dash green line is the mass fraction of water with respect of time. The process of drying stage stops when the moisture evaporate totally, while the devolatilization stage finishes when the biomass is totally consumed. As it is shown in Fig.6 by arrows of 40% moisture content biomass pyrolysis, the drying process stops after 12 seconds, while the devolatilization stage stops after 40 seconds. It can also

be found that the time when the drying stage stops is also the time when the center temperature of the biomass pellet reaches above 100℃, and the time devolatilization stage stops is the time center temperature of the pellet start to go up quickly after a plateau.

Conclusion

A CFD model based on finite volume method was used to study the drying of a poplar particle during pyrolysis process. The model uses one-step global biomass decomposition reactions to describe the pressure, temperature and species behavior of the drying process. A validation using literature data shows good agreement with experimental results. In extended version, water behavior from using two different kind of water evaporation models has been discussed. The results show using thermal model can cause longer time of drying stage and therefore delay the following up reactions. To better balance the thermal model and kinetic model, it is suggested here when the moisture content is over FSP, both thermal and kinetic water evaporation models should be considered in the biomass pyrolysis process.

Acknowledgements

Xiyan Li is grateful to the help from department of energy technology of Aalborg University and support from Chinese scholarship council.

References

[1] Messai S, Sghaier J, Lecomte D, Belghith A. Drying kinetics of a porous spherical particle and the inversion temperature. Dry Technol 2008;26:157–67. doi:10.1080/07373930701831127.

[2] Mezhericher M, Levy A, Borde I. The influence of thermal radiation on drying of single droplet/wet particle. Dry Technol 2008;26:78–89. doi:10.1080/07373930701781686.

[3] Haberle I, Haugen NEL, Skreiberg Ø. Drying of thermally thick wood particles: A study of the numerical efficiency, accuracy, and stability of common drying models. Energy & Fuels 2017:acs.energyfuels.7b02771. doi:10.1021/acs.energyfuels.7b02771.

[4] Rezaei H, Lim CJ, Lau A, Bi X, Sokhansanj S. Development of empirical drying correlations for ground wood chip and ground wood pellet particles. Dry Technol 2017;35:1423–32. doi:10.1080/07373937.2016.1198912.

[5] Yang YB, Sharifi VN, Swithenbank J. Effect of air flow rate and fuel moisture on the burning behaviours of biomass and simulated municipal solid wastes in packed beds. Fuel 2004;83:1553–62. doi:10.1016/j.fuel.2004.01.016.

[6] Ståhl M, Granström K, Berghel J, Renström R. Industrial processes for biomass drying and their effects on the quality properties of wood pellets. Biomass and Bioenergy 2004;27:621–8. doi:10.1016/j.biombioe.2003.08.019.

[7] Di Blasi C, Hernandez EG, Santoro A. Radiative pyrolysis of single moist wood particles. Ind Eng Chem Res 2000;39:873–82. doi:10.1021/ie990720i.

[8] Babiak M, Kúdela J. A contribution to the definition of the fiber saturation point. Wood Sci Technol 1995;29:217–26. doi:10.1007/BF00204589.

[9] Di Blasi C. Multi-phase moisture transfer in the high-temperature drying of wood particles. Chem Eng Sci 1998;53:353–66. doi:10.1016/S0009-2509(97)00197-8.

[10] Yang YB, Sharifi VN, Swithenbank J, Ma L, I L, Jones JM, et al. Combustion of a single particle of biomass. Energy 2008:306–16. doi:10.1021/ef700305r.

[11] Yang YB, Lim CN, Goodfellow J, Sharifi VN, Swithenbank J. A diffusion model for particle mixing in a packed bed of burning solids. Fuel 2005;84:213–25. doi:10.1016/j.fuel.2004.09.002.

[12] Lu H, Robert W, Peirce G, Ripa B, Baxter LL. Comprehensive study of biomass particle combustion. Energy and Fuels 2008;22:2826–39. doi:10.1021/ef800006z.

[13] Bryden KM, Hagge MJ. Modeling the combined impact of moisture and char shrinkage on the pyrolysis of a biomass particle. Fuel 2003;82:1633–44. doi:10.1016/S0016-2361(03)00108-X.

[14] Fatehi H, Bai XS. A comprehensive mathematical model for biomass combustion. Combust Sci Technol 2014;186:574–93. doi:10.1080/00102202.2014.883255.

[15] Peters B, Bruch C. Drying and pyrolysis of wood particles: experiments and simulation. Fuel Energy Abstr 2004;45:100. doi:10.1016/S0140-6701(04)93143-8.

[16] Blasi C Di, Branca C, Sparano S, Mantia B La. Drying characteristics of wood cylinders for conditions pertinent to ÿxed-bed countercurrent gasiÿcation 2003;25:45–58.

[17] Chan WCR, Kelbon M, Krieger BB. Modelling and experimental verification of physical and chemical processes during pyrolysis of a large biomass particle. Fuel 1985;64:1505–13. doi:10.1016/0016-2361(85)90364-3.

[18] Yang YB, Yamauchi H, Nasserzadeh V, Swithenbank J. Effects of fuel devolatilisation on the combustion of wood chips and incineration of simulated municipal solid wastes in a packed bed. Fuel 2003;82:2205–21. doi:10.1016/S0016-2361(03)00145-5.

[19] Mehrabian R, Zahirovic S, Scharler R, Obernberger I, Kleditzsch S, Wirtz S, et al. A CFD model for thermal conversion of thermally thick biomass particles. Fuel Process Technol 2012;95:96–108. doi:10.1016/j.fuproc.2011.11.021.

[20] Yin C. Modelling of heating and evaporation of n-Heptane droplets: Towards a generic model for fuel droplet/particle conversion. Fuel 2015;141:64–73. doi:10.1016/j.fuel.2014.10.031.

[21] Yang YB, Yamauchi H, Nasserzadeh V, Swithenbank J. Effects of fuel devolatilisation on the combustion of wood chips and incineration of simulated municipal solid wastes in a packed bed. Fuel 2003;82:2205–21. doi:10.1016/S0016-2361(03)00145-5.

[22] Klose E, Köpsel R. Mathematical model for the gasification of coal under pressure. Fuel 1978;72:714. doi:10.1016/0016-2361(93)90662-L.

[23] Zhou H, Jensen AD, Glarborg P, Jensen PA, Kavaliauskas A. Numerical modeling of straw combustion in a fixed bed. Fuel 2005;84:389–403. doi:10.1016/j.fuel.2004.09.020.

[24] Yin C, Kær SK, Rosendahl L, Hvid SL. Co-firing straw with coal in a swirl-stabilized dual-feed burner: Modelling and experimental validation. Bioresour Technol 2010;101:4169–78. doi:10.1016/j.biortech.2010.01.018.

[25] Basu P. Biomass Gasification and Pyrolysis: Practical Design. vol. 28. 2010. doi:10.1017/CBO9781107415324.004.

[26] Rath J, Steiner G, Wolfinger MG, Staudinger G. Tar cracking from fast pyrolysis of large beech wood particles. J Anal Appl Pyrolysis 2002;62:83–92. doi:10.1016/S0165-2370(00)00215-1.

[27] Nunn TR, Howard JB, Longwell JP, Peters WA. Product compositions and kinetics in the rapid pyrolysis of milled wood lignin. Ind Eng Chem Process Des Dev 1985;24:844–52. doi:10.1021/i200030a054.

Paper B

A detailed pyrolysis model for a thermally large biomass particle

Xiyan Li, Chungen Yin, Søren Knudsen Kær,Thomas Condra

Fuel, 2020.

The layout has been revised.

Fuel 278 (2020) 118397

Contents lists available at ScienceDirect

Fuel

journal homepage: www.elsevier.com/locate/fuel

Full Length Article

A detailed pyrolysis model for a thermally large biomass particle

Xiyan Li*, Chungen Yin, Søren Knudsen Kær, Thomas Condra

Department of Energy Technology, Aalborg University, Pontoppidanstræde 111, Aalborg Øst, Aalborg, Denmark

ARTICLE INFO

Keywords:
Biomass
CFD
Finite volume method
Pyrolysis

ABSTRACT

Pyrolysis of a single biomass pellet involves multiple processes, such as evaporation, decomposition, flow field changes, shrinking or swelling. These processes can be simulated by consolidating pyrolysis theories and computational fluid dynamics. In this paper, a one-dimensional transient model is formulated in a C++ code to simulate the process of pyrolysis of a single biomass pellet. Experimental data from the literature is used to validate this model. This paper presents detailed modelling results for a single biomass pellet under pyrolysis in nitrogen. The model can determine the temperature distribution at different locations at any certain time, and the temperature distribution, at the same location, over time. In this paper, the focus is on how different parameters develop with time within the biomass pellet.

1. Introduction

Pyrolysis occurs when biomass goes through a thermal decomposition in an inert atmosphere which is usually, though not limited to, nitrogen and is converted to smaller volatile molecules. The volatile components are the main products of pyrolysis, as well as bio-char. In terms of the temperature, the heating rate and the residence time during biomass decomposition, biomass pyrolysis is usually classified as either fast pyrolysis, slow pyrolysis or conventional pyrolysis, with the distinction based on the quantity of light gas production [1].

Slow pyrolysis aims to obtain bio-char; whilst fast pyrolysis aims at obtaining bio-oil. On the other hand the conventional pyrolysis process, normally considered as a clean energy processing technology, is very popular for treating biomass residues and producing syngas, i.e. CO, CH_4, H_2 and hydrocarbons [2]. There are many uncertainties during the process of biomass pyrolysis, such as the conversion rate and time, the temperature distribution, the mass loss, the pressure and intra-particle velocity and the changes in pellet size. A CFD model for the pyrolysis process is useful not only for the pilot scale packed bed but also can be scaled up for use in an industrial grate fired boiler.

Research into biomass pyrolysis is approximately 40 years. Many studies have been done on cellulose pyrolysis, probably because cellulose is the main component of most biomass fuels [3–6]. There was also some research into lignin and hemicellulose [7,8]. Thermogravimetric analysis (TGA) was widely used at that time and as a result, much kinetic data about biomass thermal degradation were published and used for numerical modelling [9–11]. Ranzi's et al. [22] published a kinetic model with a few multistep kinetic schemes based on three main compositions of biomass, cellulose, lignin and hemicellulose, with the rate kinetics of the reactions derived from TGA experiments. Ranzi's model can give good results with regard to temperature and residues, but gives results in considerable error for the prediction of the gas fraction.

Much work has been done on the kinetics of biomass pyrolysis, such as Bio-FLASHCHAIN model, Bio-FG DVC model and Bio-CPD model, who were originally used for coal chemistry research. These models use simplified chemistry and network statistics to describe the generation of the tar precursor. However, there are many differences in the molecular lattice geometry, broken bridges and crosslinking chemistry, pyrolysis products, mass transfer hypotheses and statistical methods.

The Bio-FLASHCHAIN model applies the flash distillation mechanism to a distributed-energy array model to predict the monomer production, without considering the functional group, hydrogen extraction, reaction available for hydrogen and mass transfer resistance [12,13].

The Bio-FG DVC model combines the functional group (FG) model with the depolymerization-vaporization-cross-linking (DVC) algorithm to predict the composition of biomass pyrolysis yields. Contradictory to the Bio-FLASHCHIAN model, the Bio-FG DVC model assumes that the decomposition of a functional group can produce small molecule gases, the breaking of the bridge bond is limited by active hydrogen and therefore controls the decomposition of the macromolecular lattice and the release of tar is controlled by mass transfer [12,14]. The Bio-CPD model uses chemical structural parameters to describe the biomass structure. The generation of tar precursors is described by the penetration statistics method, according to the number of unstable bridges

* Corresponding author.
E-mail address: xli@et.aau.dk (X. Li).

https://doi.org/10.1016/j.fuel.2020.118397
Received 28 December 2019; Received in revised form 25 May 2020; Accepted 11 June 2020

Nomenclature

A	Surface area [m^2]
A_{evp}	Water evaporation pre-exponential factor [s^{-1}]
E_{evp}	Water evaporation activation energy [J/kmol].
$C_{P,S}$	Specific heat [J/(kg·K)]
d_{pore}	Pore hydraulic diameter [m]
D_{eff}	Free water effective mass diffusivity [m^2/s]
F_{heat}	Sum of radiation heat and convection heat transfer [$J/(m^2 \bullet s)$]
h_T	Heat transfer coefficient [W/(m^2·K)]
h_M	Mass transfer coefficient [m/s]
$h_{m,pore}$	Mass transfer coefficient of vapor in the pore [m/s]
h_f^0	Enthalpy of formation [J/kg]
h_f^s	Sensible enthalpy [J/kg]
K	Permeability [m^2]
K_B	Thermal conductivity [W/(m·K)]
k_{H_2O}	Reaction rate constant [s^{-1}]
Nu	Nusselt number
Pr	Prandtl number
R_g	Universal gas constant [J/(mol·K)]
r_i	Reaction rate of reaction i [kg/(m^3·s)]
r_{H_2O}	Volumetric vaporization rate [kg/(m^3·s)]
Sc	Schmidt number
Sh	Sherwood number
S_T	Source term in energy equation [W/m^3]
S_a	Specific area of the wood particle [m^2/m^3]
$S_{a,char}$	Specific area of char [m^2/m^3]
T_{ini}	Initial temperature [K]
T_∞	Ambient gas temperature [K]
T_S	Particle surface temperature [K]
T_i	Particle temperature at grid i [K]
$T_{j,S}$	Particle surface temperature for species j [K]
T_C	Particle center temperature [K]
T_{evap}	Evaporation temperature of liquid water [K]
V	Current particle volume [m^3]
V_0	Initial particle volume [m^3]
X_C	Conversion ratio of char
X_M	Conversion ratio of moisture
X_V	Conversion ratio of volatile
Y_{vap}	Percentage of vapor of all the species
$Y_{j,ref}$	Reference mass fraction of species j in the gas film around the particle
$Y_{j,s}$	Mass fraction of species j at particle surface
$Y_{j,\infty}$	Mass fraction of species j in the ambient gas
ρ_g	Gas density [kg/m^3]
ρ_g^{sat}	Saturated vapor density [kg/m^3]
ρ_{fw}^0	Initial free water density [kg/m^3]
ρ_{fw}	Free water density at the present time [kg/m^3]
$\dot{w}_j$	Reaction rate of species j [kg/(m^3·s)]
β	Drag force coefficient
λ	Average conductivity of all the gases in the film [W/(m·K)]
ε	Porosity [m^3/m^3]
μ	Dynamic viscosity [kg/(m·s)]
σ	Boltzmann radiation constant,$5.86 \times 10^{-8}[W/m^2K^4]$
τ	Tortuosity
ω	Emissivity
g	Gas
k	Number of reactions
l	Liquid
s	Solid

broken in the infinite biomass lattice [12,15].

All the three models mentioned above attempt to determine the exact composition of the decomposition products and their molecular formula, especially for the tar composition.

However, it is not always necessary to know the molecular form for pyrolysis process simulation. When the research aim is focused on the thermal chemical conversion instead of the kinetics or the composition of pyrolysis, some other more simplified pyrolysis models are often used [16–19]. In many studies, a semi-global mechanisms for pyrolysis is used for the decomposition of biomass [8,20,21]. In the semi-global mechanisms assumption, tar is a necessary intermediate product. However, due to the instability of tar, the yield and composition of tar is not always the same, based on different heating rates and other experimental conditions. Therefore, the input parameters for the model under one experimental condition, for one specific kind of biomass, cannot be used on another condition. In 1981, Thurner and Mann [15] studied the wood kinetics of pyrolysis. With a modified tube pyrolysis reactor, they presented results for the gas composition in the temperature range of 300–400 °C by using three parallel first-order primary reactions, with each reaction producing gas, tar and char, respectively. The one-step global devolatilization model is also widely used [22–25]. By assuming the devolatilization reaction is first-order, the complexity of the devolatilization is simplified. Thus, the CFD model presented in this paper, focusses on the heat and mass transfer within the porous medium.

The advantage of using a CFD model is that a model can rapidly predict the possible results before the real investment in an industrial application. For example, such a model can be used to investigate the ignition mechanism [26], the pyrolysis kinetics, and heat transfer [27], physical or chemical behavior [10], and so on. In addition, as the minimum composition unit of the packed bed, studies on the single biomass pellet thermal conversion behavior can help to understand more of the details during the thermo-chemical conversion process on a larger scale. Therefore, in this paper, a more detailed mathematical model is developed, and as mentioned above, the main processes during biomass pyrolysis, the exchange of heat and mass, the mass loss, the gas concentration changes, the swelling and shrinking, are discussed.

Considering the complexity of the biomass pyrolysis process, some assumptions are needed. The layer model is one of them. This is where each control volume passes four processes: the drying layer, pyrolysis layer, char layer and the ash layer, which refers to the moist wood, the dry wood, the char residue, and the ash, respectively [28]. The layer model assumes there is a mass and heat transfer front moving from the outer layer to the inner core until a thermal equilibrium, between the solid pellet and the heating environment, is reached. As shown in Fig. 1 [29], the evaporation front starts from the pellet surface and moves

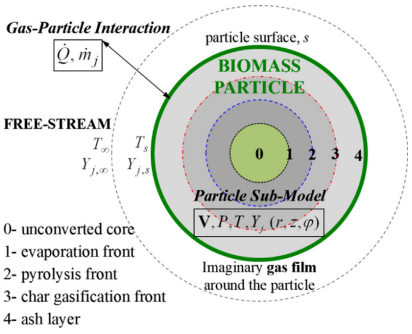

Fig. 1. Layer model scheme.

towards the center core, followed by the pyrolysis and the char gasification fronts. After all the reactions are completed, an ash layer is built from the pellet surface all the way to the pellet center. The layer model can predict many results that fit well with experimental results [30,28,31,32], even though some reports show, that there might be a temperature discontinuity near the center temperature curves [32]. In the layer model, the pellet is usually assumed to be isotropic when it is compressed [31,33] and anisotropic when it is a wood log [34–36]. The detailed sub-model will be discussed under the model description.

The model presented in this paper aims at providing a solution to the general pyrolysis problem for a single biomass pellet. By incorporating the research that has been published hitherto, a general CFD model is formulated and written in C + +. In this paper, a full map of a single biomass pellet pyrolysis is given.

2. Model description

The process of biomass pyrolysis is a complex thermal chemical conversion process. It includes not only the physical and chemical conversion process, such as water evaporation, volatile devolatilization, char gasification, but also the physical dynamical process, such as fluid flow changes, temperature and process changes etc. Referring to Case 1 which is presented later in this paper as an example. In this case, a single biomass pellet has a steady temperature of room temperature of 25 °C. Then the biomass pellet is placed in a high temperature isothermal system (around 1200 K). In this system, the temperature of the biomass pellet will ultimately reach the system temperature. Under the heating process, changes will occur within the biomass pellet. At the beginning, the biomass pellet will heat up and assuming that the biomass pellet is thermally thick (high Biot number), the temperature of the whole particle cannot be uniform for quite some time. Therefore, the reactions that take place within the pellet will follow the local temperature change. There are three separate stages, divided according to the temperature. A rough temperature range for these three stages are [37]: drying process (water evaporation) for temperature under 100 °C (or slightly over 100 °C for bound water), the devolatilization process (release of volatiles) for temperatures between 380 °C to 500 °C and finally the gasification process reactions for temperature above 500 °C [38]. The temperature of the biomass pellet can be higher or lower than the environment temperature depending on the heat absorbed or released during these three processes.

In this project, a CFD model was developed for such a thermochemical conversion process. The key assumptions are:

1. The biomass pellet is a spherical porous media with a constant porosity.
2. The biomass pellet is thermally thick and in local thermal equilibrium (within the pellet, the solids and gases have the same temperature locally).
3. The biomass pellet is placed into a quasi–steady state environment.
4. The gas species obey the ideal gas law.
5. No external forces or fragmentation is considered in this model.

Table 2
Kinetic data used in this model.

Reaction index	Pre-exponential factor (s^{-1})	Activation energy (J/kmol)	Heat of reaction (kJ/kg)
1	3.4×10^4	6.9×10^7	− 1376.09
2	−	−	−
3	5.13×10^{10}	8.8×10^7	− 2440
4	3.42[a]	1.297×10^8	− 3919.436
5	3.42[a]	1.297×10^8	− 7294.38
6	3.42×10^{-3}	1.297×10^5	18723.8
7	3.0×10^8	1.26×10^8	− 11314.88
8	2.75×10^9	8.4×10^7	1469.82

[a] Those units are$\boldsymbol{m}/(\boldsymbol{s}\bullet\boldsymbol{K})$.

2.1. Key reactions

The particle size studied in the literature can be as small as a pulverized particle (around 1 mm), as well as a large piece of wood (around 10 mm) [39]. Whatever the size is, the key reactions that occur inside the pellet are similar, and, as introduced above, these are drying, devolatilization and gasification. All the reactions used in this model are listed in Table 1 and their kinetic data are listed in Table 2.

Much research has been done on a single biomass pellet drying process. In fact, as long as moisture still exists in the pellet; drying has to be considered in all the models for biomass pyrolysis or gasification. Haberle et al. [18] summarizes three kinds of evaporation that are published by other researchers. In this paper, the equilibrium model for water evaporation is used for the free water evaporation under 100°C, the thermal model is used for free water evaporation over 100°C, and the kinetic model is used for bound water evaporation [40].

For wood pyrolysis, there are many kinetic models, such as a one-step global devolatilization mechanism [22–25], a semi-global devolatilization mechanism [41,42], the one-step multi-reaction model [22,43–45], and so on. The devolatilization model affects the devolatilization rate, as discussed by Yang et al. [46]. In this simulation, a 'fast' one-step devolatilization rate by Nunn [47], and defined by Yang et al. [46], is used in the model, because it shows a better simulation agreement for poplar wood with experimental data from Lu et al. [20] and Mehrabian et al. [32].

The main properties used in this model are presented in Table 3.

2.2. Governing equations

The energy equation is expressed as eqn. (1), whilst the source term is given in eqn. (2).

$$\frac{\partial(\varepsilon C_{pg}\rho_g T) + \partial(\rho_s C_{ps} T)}{\partial t} + div(\varepsilon\rho_g u C_{pg} T_g) = div(k_{eff}\nabla T) + S_T \quad (1)$$

Table 1
Chemical reactions and reaction rate.

Reaction	Chemical reactions	Reaction rate	Ref
1	Biomass → Volatile + Char	$r_1 = \partial\rho_{Vol}/\partial t = k_1\rho_{vol}$	[46]
2	H_2O(free) → H_2O(g)	$r_2 = \frac{F_{heat}}{\Delta h_{evap}} = \frac{S_a(h_T(T_l - 373.15) + \varepsilon\sigma(T_l^4 - 373.15^4))}{\Delta h_{evap}}$	
3	H_2O(bound) → H_2O(g)	$r_3 = A_3 exp\left(-\frac{E_3}{RT}\right)\rho_{H_2O}$	[20,48]
4	C + CO_2 → 2CO	$r_4 = \partial C_{CO_2}/\partial t = s_{a,char}[\rho_C/(\rho_C + \rho_B + \rho_A)]k_4 C_{CO_2}$	[20]
5	C + H_2O → H_2 + CO	$r_5 = \partial C_{H_2O}/\partial t = s_{a,char}[\rho_C/(\rho_C + \rho_B + \rho_A)]k_5 C_{H_2O}$	[20]
6	C + 2H_2 → CH_4	$r_6 = \partial C_{H_2}/\partial t = s_{a,char}[\rho_C/(\rho_C + \rho_B + \rho_A)]k_6 C_{H_2}$	[28]
7	C_3H_8 + 3H_2O → 7H_2 + 3CO	$r_7 = \partial C_{C_3H_8}/\partial t = k_7 C_{C_3H_8}^{1.0} C_{H_2O}^{1.0}$	[49]
8	CO + H_2O → H_2 + CO_2	$r_8 = \partial C_{CO}/\partial t = k_8 C_{CO}^{1} C_{H_2O}^{1}$	[49]

Table 3
The main properties used in this model.

Properties	Expression	Reference
Permeability K	$K = \frac{\varepsilon^3 d_P^2}{150\times(1-\varepsilon)^2}$	[50]
Tortuosity τ	1.5	[51]
Effective diffusivity D_{eff}	$D_{eff} = \frac{\varepsilon}{\tau}(\frac{1}{D_{AB}} + \frac{1}{D_k})^{-1}$	[51]
Diffusivity D_{AB}	$D_{AB} = 2.0\times10^{-5}\left(\frac{T}{T_{ini}}\right)^{1.75}\frac{P}{P_0}$	[52]
Knudsen diffusivity D_k	$D_k = 48.5 d_{pore}\sqrt{T/MW_g}$	[51]
Pore diameter d_{pore}	3.2×10^{-6}	This work
Effective conductivity K_{eff}	$K_{eff} = \varepsilon K_{gas} + (1-\varepsilon)K_{solid} + \frac{\varepsilon\sigma T^3 d_{pore}}{\omega}$	[20,51]
Specific surface area $S_{a,Char}$	1.0×10^6	[20]
Porosity ε	0.6	[20]
Emissivity ω	0.8	This work
Heat capacity C_P	$1500 + T$	[53]

$$S_T = -\sum_{j=1}^{N} h_{f,j}^0 \dot{w}_j - \sum_{i=1}^{N} h_{f,j}^s \dot{w}_j \tag{2}$$

S_T is the source term of energy equation and consists of a sum of the formation enthalpy for each species and a sum of the sensible enthalpy of each species. For the boundary condition of temperature, the gradient is treated as zero at the center point. For the surface, due to the existence of radiation and convection, the boundary conditions for energy equation are as shown in Eqs. (3) and (4).

$$\frac{\partial T}{\partial x} = 0 \tag{3}$$

$$k_B A\frac{T_B - T_P}{\Delta x/2} = Ah_T(T_\infty - T_B) + A\varepsilon\sigma(T_\infty^4 - T_B^4) \tag{4}$$

To calculate the heat transfer coefficient, a gas film surrounding the particle is assumed. The temperature used for gas properties in the gas film is treated as reference temperature, as defined by the one-third law [54].

$$T_{ref} = T_s + 1/3(T_\infty - T_s) \tag{5}$$

$$h_T = \frac{Nu\lambda}{d_p} \tag{6}$$

Nu denote Nusselt number, here it uses the Nusselt number from Lu et al. [20] for a spherical particle, with the expression as

$$Nu \equiv \frac{h_T L_c}{\lambda} = 1.05 + 0.6Re^{0.65}Pr^{0.33} \tag{7}$$

The true velocity within the pellet is solved by Darcy's law, together with continuity equation as follows, whilst the pressure is calculated based on the ideal gas law.

$$\vec{u} = -\frac{\eta}{\mu}\nabla P \tag{8}$$

$$\frac{\partial(\varepsilon\rho_g)}{\partial t} + div(\varepsilon\rho_g\vec{u}) = S_g \tag{9}$$

The boundary conditions for the pressure in the center point is treated with a zero-gradient, and mass flow conservation is used for the surface boundary condition.

For the gaseous species, a transport equation is expressed as Eq. (10).

$$\frac{\partial(\varepsilon\rho_g Y_{ig})}{\partial t} + div(\varepsilon\rho_g u Y_{ig}) = div(\varepsilon\rho_g D_{ig}\nabla Y_{ig}) + S_{Y_{ig}} \tag{10}$$

Similar to the energy equation, the boundary condition of the gaseous species at the center point is set to a zero gradient. For the surface, the reference species of the gas film is calculated by using the one-third law.

$$\frac{\partial Y_j}{\partial x} = 0 \tag{11}$$

$$Y_{j,ref} = Y_{j,s} + 1/3(Y_{j,\infty} - Y_{j,s}) \tag{12}$$

$S_{Y_{ig}}$ denotes the source term of each gas species.

$$DA\frac{Y_B - Y_P}{\Delta x/2} = Ah_M(Y_\infty - Y_B) \tag{13}$$

h_M denotes the mass transfer coefficient, and can be calculated by the following correlation [54].

$$Sh \equiv \frac{h_M L_c}{D_g} = 2.0 + 0.6Re^{1/2}Sc^{1/3} \tag{14}$$

The solid terms have the simple expression given in Eq. (15).

$$\frac{\partial(\rho_i)}{\partial t} = s_i \tag{15}$$

ρ_i denotes the density of water and remaining volatile in solid and ash and carbon, and s_i denotes their source terms.

Since the porosity is assumed to be constant in this model, the size change of the biomass pellet is calculated based on the mass loss of the biomass pellet. According to Eq. (16), the volume change of the biomass pellet is only related to the mass change of the pellet. Therefore, the calculation of the volumetric change does not affect the size of the grid cells.

$$V = (1.0 - X_M * (1.0 - \beta_M) * M - X_B * (1.0 - \beta_B) * vol - X_C * (1.0 - \beta_C) * C) * V_0 \tag{16}$$

2.3. Numerical solutions

A CFD code, in C++, has been written for this model, based on the finite volume method [55] to numerically solve the transport equations. The convective terms are discretized by a central differencing scheme, the time step is set to 0.01 s, and the temporal scheme used is an implicit scheme. The biomass pellet is divided into 60 spherical shells based on the spherical particle. The meshing is along the radial direction, from the center of the spherical pellet to the surface of the pellet, in which there are 60 cells. During the simulation process, the cell size does not change, neither does the porosity.

3. Model validation and discussion

3.1. Validation

In order to validate the CFD model, two sets of experimental data are collected from the literature. Case 1: for the pyrolysis case where water evaporation is considered, an experiment using a poplar wood particle is chosen from the literature [32,20]. Case 2: for the pyrolysis case without water evaporation, a beech wood pellet is chosen from Rath et al. [56]. The wood properties and experimental conditions for both wood pellets are given in Table 4.

A grid independence study was carried out based on Case 1, as shown in Fig. 2a). Three different grid numbers were used for the grid independence check; they were 60, 80 and 100, respectively. As shown in Fig. 2a), both temperature curves on the pellet surface and in the pellet center show identical results for three different meshing numbers. Therefore, this model is considered as independent of the number of the cells meshed. To save computing resources, a grid number of 60 is used for both cases. Fig. 2b) shows the temperature profile using different time steps, 0.01 s and 0.001 s. Little discrepancy can be observed on the temperature profile from the two different time steps. To save the computer memory, a time step of 0.01 s is used in this work.

Table 4
Proximate and ultimate analysis of poplar wood.

	Case1 [20]	Case 2 [56]
Proximate analysis		
Fixed carbon (d.a.)	9.5%	11.46%
Moisture	6% and 40%	0
Ash (d.a.)	0.5%	0.39%
Volatile (d.a.)	90%	88.15%
Ultimate analysis		
C(d.a.)	47.4%	49.59%
H(d.a.)	8.8%	6.06%
O(d.a.)	43.7%	44.08%
Others		0.27%
LHV(6% moisture)	17.05 MJ/kg	19.89 MJ/kg
Density	545 kg/m^3	550 kg/m^3
Pellet size(diameter [mm])	9.5	20
Ambient temperature [K]	1275 (Wall) 1050 (Fluid)	1123
Primary air flow rate [m/s]	0.5	0.01587
Inert gas	N_2	N_2

Validation for both cases were also made upon the pellet temperature on the surface and in the center, as shown in Figs. 3 and 5.

In Fig. 3, the simulation results are compared with the experimental data of Lu et al. [20], together with their simulation results. Fig. 3 shows three obvious stages during pyrolysis at the pellet center by arrows. Together with Fig. 7, it is seen that, the water on the surface completely vanishes at 0.5 s, and the water in the center vanishes at about 20 s. When looking of the center temperature from this model, the temperature increases immediately after the water is evaporated. At this stage, the temperature profile from this model shows reasonable agreement with the results from Lu et al. As for the discrepancy from the experimental data at the pellet center at the evaporation stage, the thermal conduction from the thermal couple wire might be a contributing factor, as stated by Lu et al. [20]. The devolatilization starts immediately after the evaporation and stops at around 31 s. The pre-pyrolysis takes place from 400 K to 900 K, with the release of light gases. More than 80% of the mass of the biomass pellet is lost in this stage (as shown in Fig. 5). It is observed, during the devolatilization stage, that the temperature at the pellet center rises faster than the result from Lu et al, and fits better to the experimental data. The possible reason, in this model, is that it is assumed that there is no energy loss from the devolatilization stage, whilst in the model of Lu et al, the

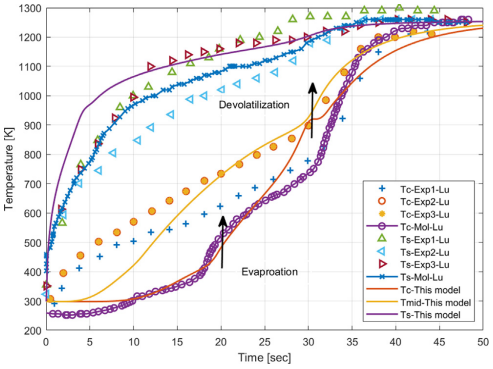

Fig. 3. Temperature profile from this model and lu et al's results.

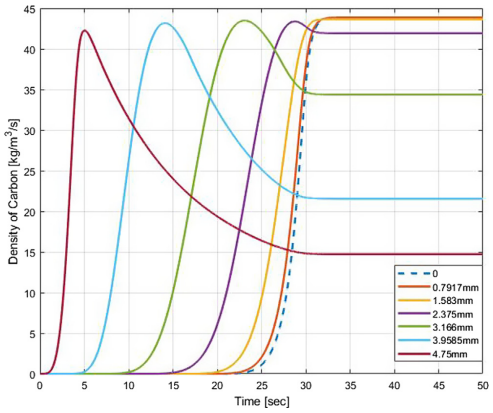

Fig. 4. Profile of carbon density within the pellet.

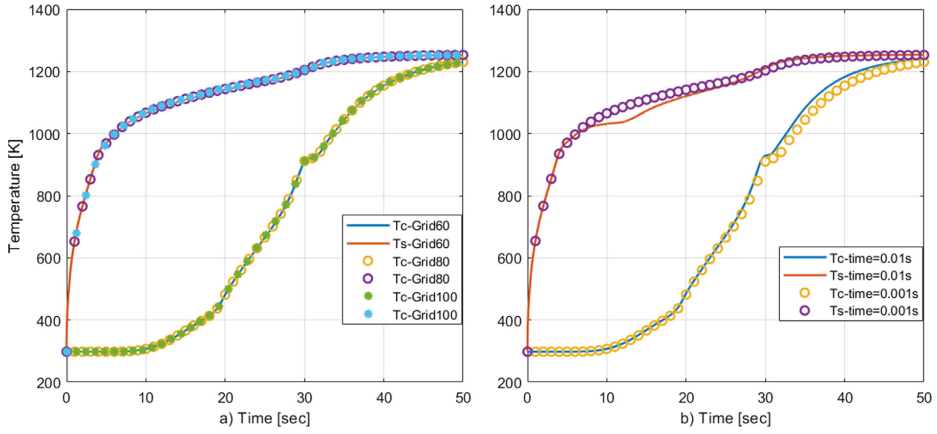

Fig. 2. Grid independence check and time sensitivity check (Fig. 2a) shows the center temperature and surface temperature based on 60, 80, 100 cells, Fig. 2b) shows the center temperature and surface temperature based on two different time steps).

devolatilization process is made up of five different endothermic and exothermic reactions, with the standard enthalpy of reactions from experiments or assumed by others [10,20,23]. In the last period of the devolatilization stage, the pellet temperature increases to around 900 K, where, due to the high temperature, the char reacts with carbon dioxide and water vapor. Carbon reaction with hydrogen is also considered in this model. However, the effects of reaction (6) on the temperature is nearly negligible due to the low reaction rate, as shown in Fig. 10. After the devolatilization stage, the heating rate at the pellet center is smaller compared to the heating rate in the devolatilization stage. The same tendency is also visible for the surface temperature. The most plausible reason could be, during this stage, that the heat endothermic reactions prevails, considering the reactions in Table 1. One can also deduce that the starting point for the endothermic reactions is around 900 K. When all the gases leave the pellet (at around 34 s as shown in Fig. 7), there is only a heating-up stage due to the radiation from the wall and the fluid convection. To verify this assumption, the density of char from six different locations of the pellet is shown in Fig. 4. In this figure, the carbon density at different locations increases to 42.2 $\frac{kg}{m^3}$ at a certain time, then decreases to different densities and remains stabilized. This means, that the carbon is released from the devolatilization stage following the passage from the pellet surface to the pellet center, as described in the layer model. Due to the high temperature at the pellet surface, the heterogeneous reactions at the pellet surface occurs immediately after the moisture and volatile is released and the reactions continues until all the gases have left the pellet. Therefore, the carbon at the pellet surface is consumed at a higher rate than the carbon within the particle. It can also be observed, near the pellet center, that the carbon is hardly consumed at all, even though the temperature is sufficient. This is because the reactants in reaction (4) and (5) (CO_2 and H_2O) are no longer present (seen in Fig. 7). Therefore, the stage after devolatilization at the pellet center is more or less only a heating-up stage. There is almost no heat convection after 31 s at the pellet center, because there is no velocity after all the gas species have left the pellet (see in Fig. 9).

Fig. 5 shows the simulation results from this model using the experimental data for beech wood from Rath et al. [57]. The solid lines show the temperature profiles at the center point and on the surface from the model presented in this paper. Fig. 5 also shows the experimental data and simulation data from Rath et al. It can be seen that the simulation results from this model agree well both with the experimental results, as well as the simulation results. The experimental condition of Rath et al's work was to place a cube of birch wood with an equivalent spherical diameter of 20 mm into a muffle furnace. The nitrogen gas flow blowing into the furnace was 800 l/h. The muffle furnace was preheated up to 1123 K and kept stabilized during the whole pyrolysis process. More information about this experiment can be found in the work by Rath et al. [56–58]. In Fig. 5, both this work and Rath et al. predict a good agreement with the experimental data on the surface temperature. Whilst Rath et al. predict a higher temperature at the beginning of the pyrolysis, and this work predict a slightly higher temperature at the end of the pyrolysis. At the pellet center, both the simulation from this work and from Rath et al. predict a higher temperature than the experimental data. This is because the expression for the heat capacity of the solid biomass is different at low temperature and high temperature. The heat capacity used in the simulation is shown in Table 3, which is taken for softwood [53], because the original beech wood properties are no longer available in the literature. In the range of higher temperature at the pellet center in Fig. 5, both models produce good results that fits the experimental data.

3.2. Detailed temporal modelling results from case 1

Since Case 1 represents a single spherical biomass pellet with moisture inside, the detailed results from this case can be more representative than case 2.

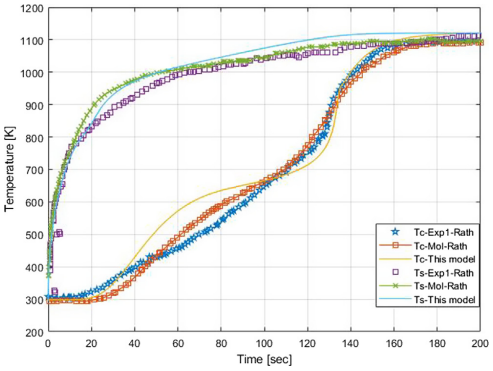

Fig. 5. Temperature profile from this model and Rath et al's results.

In case 1, the molecular formula of the volatile is summed up as $\mathbf{CH_xO_y}$ with a molecular mass of 28.0**kg/kmol** and a formation enthalpy of − 157767**kJ/kmol**. Assuming that the volatile will decompose into real species without energy or mass loss, that would be the composition of $\mathbf{C_3H_8}$, $\mathbf{H_2}$, **CO** and $\mathbf{CO_2}$. Considering the mass and energy balance, the light gases given by the artificial volatile is:

$$CH_xO_y = \alpha C_3H_8 + \beta H_2 + \gamma CO + \vartheta CO_2$$

And the heating value conservation shows:

$$LHV\_volatile = \alpha \Delta HC_3H_8 + \beta \Delta HH_2 + \gamma \Delta HCO + \theta \Delta HCO_2$$

By balancing the mass and energy conservation, the composition of volatile CH_xO_y can be solved.

Fig. 6 shows the mass loss profile from Case1. The (red) solid line shows the result from this model. The dashed line shows the prediction from Lu et al. [20], and exp1 to exp3 refers to the three parallel experiments that were done by Lu et al. [20]. As is shown in the figure, the curve follows the experimental data quite well, as well as model results from Lu et al. At the end, the mass reaches the same mass fraction as the experiment showed.

Fig. 7 shows the gas species distribution versus time at the surface of the biomass pellet. Since it is nitrogen pyrolysis, the oxygen mass fraction is set to zero. Seven other species are shown on the figure. A large amount of water vapor is observed in the beginning due to the high heat and mass transfer at the surface. The light gases, for example, the mass fractions of C_3H_8, CH_4, CO_2, CO and H_2 increase rapidly after the water vapor at the surface layers has been evaporated. CH_4 is barely observed in Fig. 7, which means reaction (6) barely occurs even at the highest temperature in this experimental condition. No other gases,

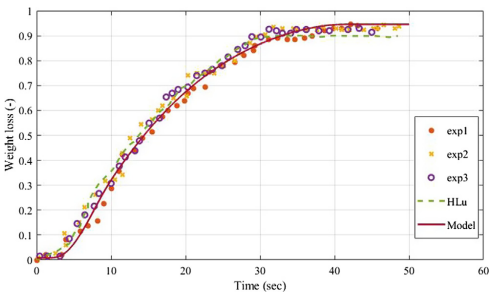

Fig. 6. Mass loss profile from model and experiment.

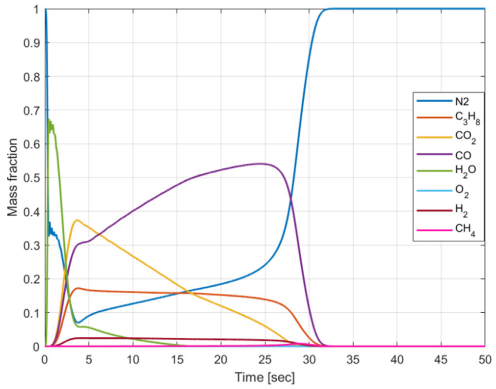

Fig. 7. Gas species released with respect to time at the surface of a biomass pellet.

except nitrogen, are observed after 32 s and this implies that the pellet is mainly heated up by external heat and no other reactions take place.

The distribution of moisture within the pellet is shown in Fig. 8. The drying stage ceases when the moisture evaporates totally, whilst the devolatilization stage finishes when the biomass is totally decomposed. Within the spherical pellet, the moisture disappears at around 18 s. At around the 10th or 11th second, no moisture exists at the middle of the radius, which means that most of the moisture has been evaporated, and only 1/8 of the moisture still exists.

The next section treats the behavior of the water within the pellet. Fig. 9 shows the water vapor fraction at different locations along the radius at two typical time points; the beginning of the evaporation and the end of the evaporation. There are 60 cells along the radius, and the X-axis is the normalized radius of the pellet. Fig. 9 shows, at 0.5 s, that there is significant water vapor at the outer part of the spherical pellet. Small amounts of water vapor are also observed in the inner locations due to diffusion of the gas species. No water vapor is observed after moisture is fully evaporated. There is a sudden decrease at the pellet surface in Fig. 2, and this is because the density at the pellet surface is much smaller than the density in the inner cells. As shown in Fig. 8, there is a sudden decrease near the pellet surface. That is because the evaporation layer moves from the pellet surface to the third grid from the surface, which is approximately 1.271×10^{-4} m from the surface. Fig. 10 shows the water reaction rate at 0.5 s. A large amount of water vapor is spotted in Fig. 10 in the location where the turning point is spotted in Fig. 9.

Fig. 11 shows the velocity changes with respect to time at five different locations within the biomass pellet in Case 1. Due to the symmetry structure of the spherical pellet, the velocity at the center of the pellet is set to zero. The location just close to the center is shown in Fig. 11 as Velocity-2, which has the peak velocity at 29 s, when devolatilization starts near the pellet center. The evaporation at the pellet center has a slight effect on the velocity. As shown in Fig. 11, the velocity is slightly higher than zero at 15 to 16 s. The velocity at the pellet surface has two significant points. On the pellet surface, the velocity quickly reaches 0.05 m/s as a result of the rapid water evaporation on the pellet surface. After that, the velocity keeps going up to 0.32 m/s due to the joint effects of reaction (1), (4), (5) and (6). The velocity at the 59th cell is smaller than the velocity at the pellet surface, as a result of mass conservation.

Figs. 12 and 13 illustrates the influence of the reactions with temperature and the distribution of gases. Fig. 12 plots the heterogeneous reaction rate at the pellet center and pellet surface. Fig. 13 shows the homogeneous reaction rate on both the center and surface locations. It can be seen that most of the visible mass flux is at the surface of the pellet. Reaction (4) and reaction (5) are endothermic reactions, reaction (6) is an exothermic reaction that does not easily occur (Fig. 12). It shows there is a quite big reaction rate at the center for reaction (4), where the vapor reaches the highest value in the simulation. After 31 s, the temperature, as shown in Fig. 3, is around 880 K, and this is sufficient for reaction (4) to take place. The reader may experience doubt because the reaction rate of reaction (5) is much higher than reaction (4) at the beginning of the whole process, since the evaporation is quite intense. A simple calculation is made at 5 s in the following expressions:

$$r_4 = \partial C_{CO_2}/\partial t = s_{a,char}\varepsilon[\rho_C/(\rho_C + \rho_B + \rho_A)]k_4 C_{CO_2}$$
$$= 10^6 * 0.60 * \frac{42.257}{42.257 + 13.985 + 8.175} * 3.42 * 970.27 * e^{-\frac{1.297\times10^8}{8315\times970.27}} * \frac{0.34103 * 0.31029}{44} = 14.3971\frac{\text{kg}}{\text{m}^3\bullet\text{s}}$$

$$r_5 = \partial C_{H_2O}/\partial t = s_{a,char}\varepsilon[\rho_C/(\rho_C + \rho_B + \rho_A)]k_5 C_{H_2O}$$
$$= 10^6 * 0.6 * \frac{41.529}{41.529 + 21.485 + 8.175} * 3.42 * 943.43 * e^{-\frac{1.297\times10^8}{8315\times943.43}} * \frac{0.033615 * 0.31029}{18} = 1.4191\frac{\text{kg}}{\text{m}^3\bullet\text{s}}$$

r_4 and r_5 shows the reaction rate when the concentration of all the reactants are sufficient within the pellet pores. However, the large evaporation and devolatilization rate leads to the rapid escape of the CO_2 andH_2O. Therefore, the gas concentration must be not sufficient at certain point in the pyrolysis process. In that case, the reaction rate is limited by the mass concentration of the reactant gases. For example, r_4 is calculated as $14.3971\frac{\text{kg}}{\text{m}^3\bullet\text{s}}$, r_5 is calculated as $1.4191\frac{kg}{m^3\bullet s}$ when there is sufficient water vapor in the pores (as shown above). When the water vapor is not sufficient, the real reaction rate is calculated as (also shown in Fig. 12):

$$r_4 = C_{CO_2}/\partial t = 0.34103 * \frac{0.31029}{0.01} = 10.582\frac{kg}{m^3\bullet s}$$

$$r_5 = C_{H_2O}/\partial t * \frac{r_5}{r_5 + r_7 + r_8}$$
$$= 0.033615 * \frac{0.31029}{0.01} * \frac{1.419}{1.419 + 3.4910 \times 10^{-4} + 1.0584}$$
$$= 0.35168\frac{kg}{m^3\bullet s}$$

Fig. 14 show the pressure changes at the pellet center and on the pellet surface during the pyrolysis process. The pressure at the pellet surface remains identical to the environmental pressure, which is

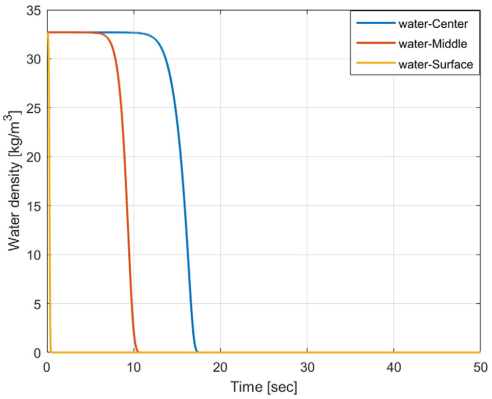

Fig. 8. Mass distribution of moisture with in the pellet.

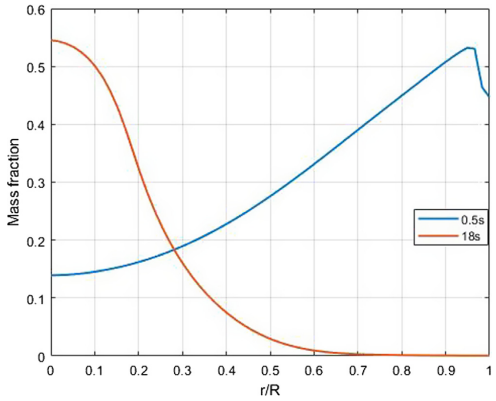

Fig. 9. Water vapor distribution at the beginning and in the end of evaporation.

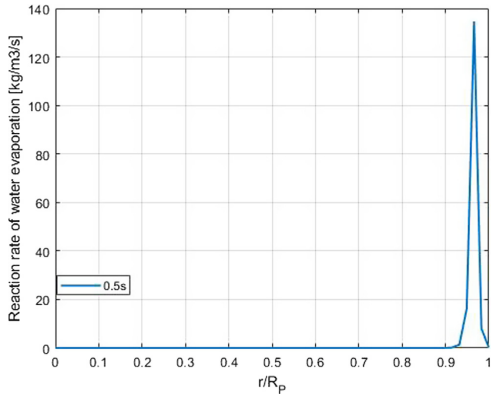

Fig. 10. Reaction rate of water evaporation at 0.5 s.

identical to the boundary condition assumed in the model. The pressure at the pellet center keeps going up until the devolatilization ends. After that, the pressure remains stabilized.

Fig. 15 shows the size change in terms of radius according to Eq. (16). The radius shrinks with the water and light gas release and then remains stabilized after devolatilization ends. The porosity is constant in this model, therefore, the control volumes remain constant during the simulation. Thus, the particle radius and mesh size stays constant during the model simulation.

3.3. Detailed spatial modelling results from Case 1

To better illustrate the heat transfer and reaction inside the pellet during the pyrolysis process, figures of spatial analysis are also presented. Temperature and gas species mass fraction at 15 s were chosen for the spatial analysis, because, at this moment, the moisture at the pellet center has not fully evaporated, whereas the temperature at the pellet surface is already close to the ambient temperature. Therefore, data from 15 s can reflect the diversity of temperature and gas species. Fig. 16 shows the temperature along the radius at 15 s. The temperature at both ends of Fig. 16 agree well with the temperature shown in Fig. 3 at 15 s. Between these two points, the temperature trend along the radius at 15 s is shown. It clearly shows that the closer to the pellet

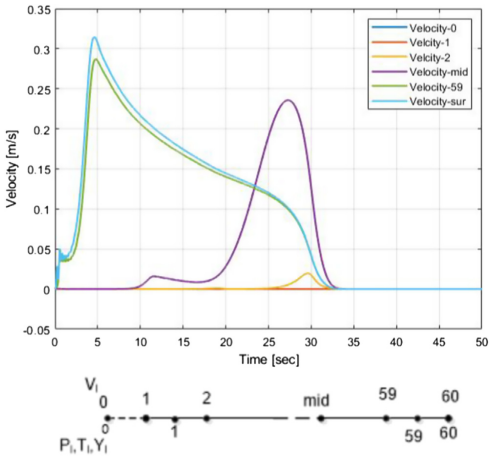

Fig. 11. Velocity distribution along the time at different radius locations (Velcotity-0 denotes velocity at pellet center, Velocity-1 denotes 8.4713*mm* from the pellet center, velocity-mid denotes the half way of the radius to the pellet center, which is 3.5414*mm* away from the pellet center, Velocity-59 denotes 4.95557*mm* away from the pellet center, Velocity–sur denotes the velocity at the pellet surface, which is 4.9981*mm* away from the pellet center).

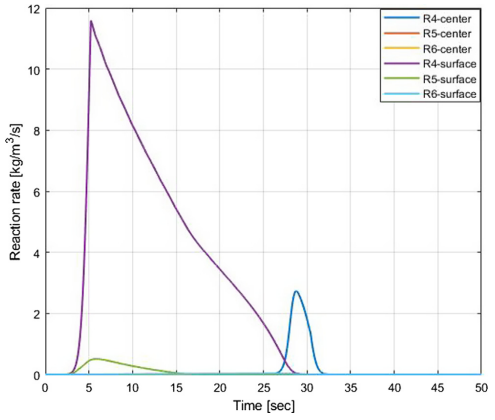

Fig. 12. Heterogeneous reaction rate.

surface, the higher is the temperature. Apparently, the heat exchange near the pellet surface is much stronger than the heat exchange near the pellet center.

Fig. 17 shows the distribution of different gas species along the pellet radius at 15 s. It shows the water mass fraction is much higher near the pellet center compared to the locations near the pellet surface. Whereas, the values of the other gases peaks much closer to the pellet surface. This means, at 15 s, that the moisture near the pellet center starts to evaporate and the decomposition of light gases already begins to be released near the pellet surface. Moreover, the value of CO peaks much closer to the pellet surface compared to the other species. This means there are reactions that happen at in higher temperature range that produce CO, which can backtracked to Fig. 12 where the reaction rate of reaction (4) is quite high at the pellet surface.

Fig. 18 shows the mass ratio at different locations along the pellet

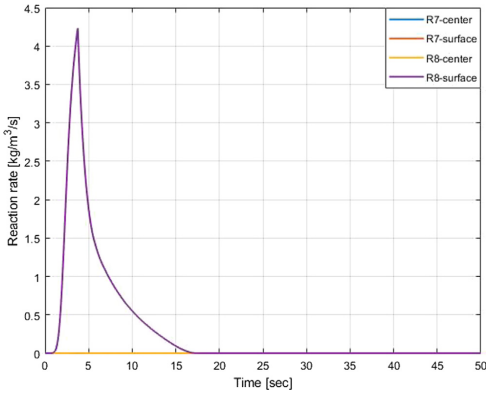

Fig. 13. Homogeneous reaction rate.

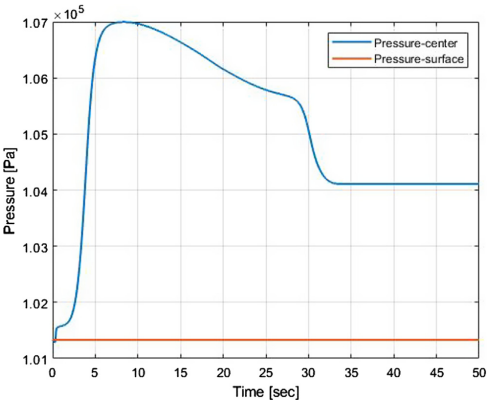

Fig. 14. Pressure distribution at the pellet center and on the pellet surface.

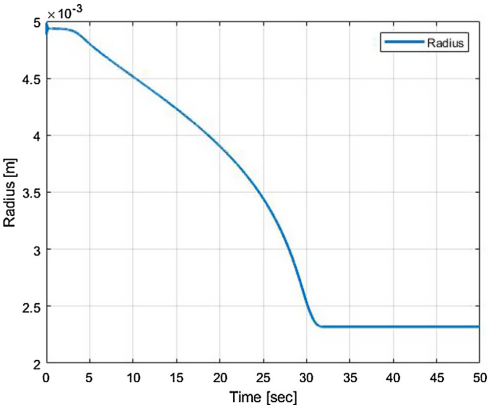

Fig. 15. Size changing during the pyrolysis process.

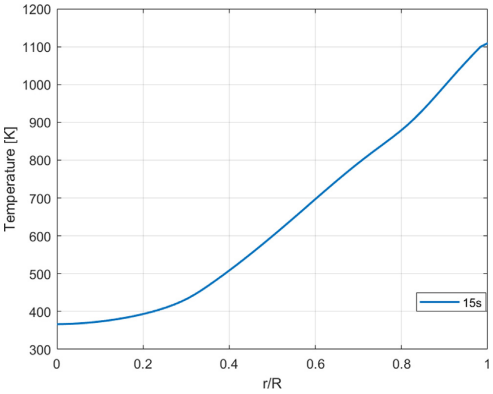

Fig. 16. Temperature along the pellet radius at 15 s.

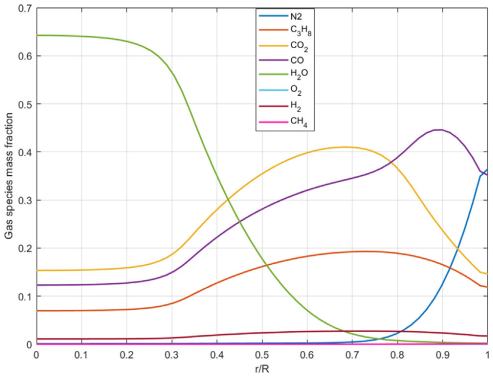

Fig. 17. Gas species along the pellet radius at 15 s.

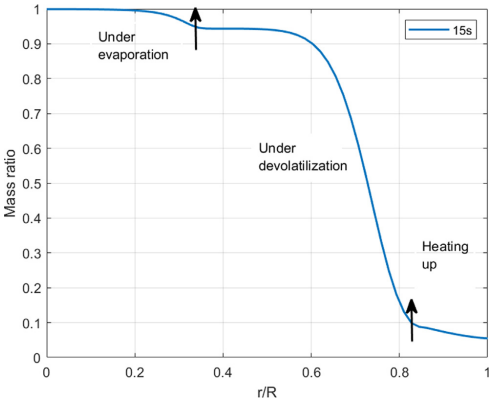

Fig. 18. Mass ratio along the pellet radius at 15 s.

radius at 15 s. Three different zones are found in the figure, the evaporation zone, the devolatilization zone and the heating-up zone. Under the evaporation zone, the main reaction is bound water evaporation, where the mass loss is quite low and the vapor fraction is quite high (see Fig. 17). The devolatilization zone is where the devolatilization reaction takes place. Since there is temperature gradient within the pellet, the mass loss is much greater near the pellet surface compared with the mass loss near the pellet center. In the heating-up zone, most of the mass in the pellet has been consumed; heterogeneous reactions might take place due to the high temperature close to the surface and the local temperature keeps rises until it reaches the environmental temperature.

4. Conclusion

In this paper, a detailed CFD model is formulated for a single biomass pellet under nitrogen pyrolysis. The model is written in C++, and a layer model assumption is used. In particular, a one-step devolatilization scheme is used; therefore, this model does not require much thermodynamic parameters during the decomposition, which reduces the errors from the input parameters from this model.

The model is validated on two sets of experimental data from the literature. The modelling results shows good agreement with the experimental data in both cases. Based on Case 1, both the temporal and the spatial results are presented and further discussed in this paper, such as temperature distribution, gas species distribution, pressure distribution, velocity distribution, reaction rate and pellet size changes.

The simulation results show that the temperature distribution, gas species distribution, pressure distribution and velocity distribution are greatly affected by the reactions that are selected. The pellet size shrinks with the evaporation and devolatilization. In conclusion, this paper presents a genetic CFD model that can predict the temporal and special results of the pyrolysis of a single biomass pellet.

CRediT authorship contribution statement

Xiyan Li: Conceptualization, Methodology, Validation, Data curation, Writing - original draft. **Chungen Yin:** Conceptualization, Methodology, Supervision, Writing - review & editing. **Søren Knudsen Kær:** Supervision, Writing - review & editing. **Thomas Condra:** Supervision, Writing - review & editing.

Declaration of Competing Interest

The authors declare that they have no known competing financial interests or personal relationships that could have appeared to influence the work reported in this paper.

Acknowledgments

The Authors are grateful to the help from Department of Energy Technology of Aalborg University and support from the Chinese scholarship council.

References

[1] Bridgwater AV. Review of fast pyrolysis of biomass and product upgrading. Biomass Bioenergy 2012;38:68–94. https://doi.org/10.1016/j.biombioe.2011.01.048.
[2] Heuer S, Senneca O, Wütscher A, Düdder H, Schiemann M, Muhler M, et al. Effects of oxy-fuel conditions on the products of pyrolysis in a drop tube reactor. Fuel Process Technol 2016;150:41–9. https://doi.org/10.1016/j.fuproc.2016.04.034.
[3] Antal MJ. Cellulose pyrolysis kinetics : the current state of knowledge. Ind Eng Chem Res 1995;34:703–17. https://doi.org/10.1021/ie00042a001.
[4] Antal MJ, Várhegyi G, Jakab E. Cellulose pyrolysis kinetics: revisited. Ind Eng Chem Res 1998;37:1267–75. https://doi.org/10.1021/ie970144v.
[5] Brown AL, Dayton DC, Daily JW. A study of cellulose pyrolysis chemistry and global kinetics at high heating rates. Energy Fuels 2001;15:1286–94. https://doi.org/10.1021/ef010084c.
[6] Miller RS, Bellan J. A generalized biomass pyrolysis model based on superimposed cellulose Hemicelluloseand Liqnin Kinetics. Combust Sci Technol 1997;126:97–137. https://doi.org/10.1080/00102209708935670.
[7] Kovfopanos CA, Maschio G, Lucchesi A. Kinetic modelling of the pyroysis of biomass and biomass components. Can J Chem Eng 1989;67:75–84. https://doi.org/10.1002/cjce.5450670111.
[8] Di Blasi C. Comparison of semi-global mechanisms for primary pyrolysis of lignocellulosic fuels. J Anal Appl Pyrolysis 1998;47:43–64. https://doi.org/10.1016/S0165-2370(98)00079-5.
[9] Gronli MG, Melaaen MC, Grønli M, Melaaen MC. Mathematical model for wood pyrolysis – Comparison of experimental measurements with model predictions. Energy Fuels 2000;14:791–800. https://doi.org/10.1021/ef990176q.
[10] Chan WCR, Kelbon M, Krieger BB. Modelling and experimental verification of physical and chemical processes during pyrolysis of a large biomass particle. Fuel 1985;64:1505–13. https://doi.org/10.1016/0016-2361(85)90364-3.
[11] Di Blasi C. Numerical simulation of cellulose pyrolysis. Biomass Bioenergy 1994;7:87–98. https://doi.org/10.1016/0961-9534(94)00040-Z.
[12] Battin-Leclerc F, Simmie JM, Blurock E. Cleaner Combustion: develop detailed chemical kinetic models. 1st ed. Springer; 2013.
[13] Niksa S. Predicting the rapid devolatilization of diverse forms of biomass with bio-FLASHCHAIN. Proc Combust Inst 2000;28:2727–33.
[14] Cuoci A, Faravelli T, Frassoldati A, Grana R, Pierucci S, Ranzi E, et al. Mathematical modelling of gasification and combustion of solid fuels and waste. Chem Eng Tansaction 2009;18:989–94. https://doi.org/10.3303/CET0918162.
[15] Thurner F, Mann U. Kinetic investigation of wood pyrolysis. Ind Eng Chem Process Des Dev 1981;20:482–8. https://doi.org/10.1021/i200014a015.
[16] Messai S, Sghaier J, Lecomte D, Belghith A. Drying kinetics of a porous spherical particle and the inversion temperature. Dry Technol 2008;26:157–67. https://doi.org/10.1080/07373930701831127.
[17] Mezhericher M, Levy A, Borde I. The influence of thermal radiation on drying of single droplet/wet particle. Dry Technol 2008;26:78–89. https://doi.org/10.1080/07373930701781686.
[18] Haberle I, Haugen NEL, Skreiberg Ø. Drying of thermally thick wood particles: a study of the numerical efficiency, accuracy, and stability of common drying models. Energy Fuels 2017;31:13743–60. https://doi.org/10.1021/acs.energyfuels.7b02771.
[19] Rezaei H, Lim CJ, Lau A, Bi X, Sokhansanj S. Development of empirical drying correlations for ground wood chip and ground wood pellet particles. Dry Technol 2017;35:1423–32. https://doi.org/10.1080/07373937.2016.1198912.
[20] Lu H, Robert W, Peirce G, Ripa B, Baxter LL. Comprehensive study of biomass particle combustion. Energy Fuels 2008;22:2826–39. https://doi.org/10.1021/ef800006z.
[21] Xue AJ, Pan JH, Tian MC, Zhang GM, Leng XL. Pyrolysis model of single biomass particle in stratified downdraft gasifier. Trans Tianjing Univ 2016;22:174–81. https://doi.org/10.3969/j.issn.0253-2417.2016.01.002.
[22] Branca C, Albano A, Di Blasi C. Critical evaluation of global mechanisms of wood devolatilization. Thermochim Acta 2005;429:133–41. https://doi.org/10.1016/j.tca.2005.02.030.
[23] Di Blasi C, Branca C. Kinetics of primary product formation from wood pyrolysis. Ind Eng Chem Res 2001;40:5547–56. https://doi.org/10.1021/ie000997e.
[24] Dryer FL, Westbrook CK. Simplified reaction mechanisms for the oxidation of hydrocarbon fuels in flames. Combust Sci Technol 1981;27:31–43. https://doi.org/10.1080/00102208108946970.
[25] Yu X, Hassan M, Ocone R, Makkawi Y. A CFD study of biomass pyrolysis in a downer reactor equipped with a novel gas-solid separator-II thermochemical performance and products. Fuel Process Technol 2015;133. https://doi.org/10.1016/j.fuproc.2015.01.002.
[26] Momeni M, Yin C, Kær SK, Hvid SL. Comprehensive study of ignition and combustion of single wooden particles. Energy Fuels 2013;27:1061–72.
[27] Jalan RK, Srivastava VK. Studies on pyrolysis of a single biomass cylindrical pellet—kinetic and heat transfer effects. Energy Convers Manag 1999;40:467–94. https://doi.org/10.1016/S0196-8904(98)00099-5.
[28] Thunman H, Leckner B, Niklasson F, Johnsson F. Combustion of wood particles - A particle model for Eulerian calculations. Combust Flame 2002;129:30–46. doi:10.1016/S0010-2180(01)00371-6.
[29] Li X, Yin C. Description of a comprehensive mathematical model Towards a comprehensive biomass particle gasification model.pdf, Stockholm: 2016. doi:10.5071/25thEUBCE2017-2CV.3.49.
[30] Babu BV, Chaurasia AS. Heat transfer and kinetics in the pyrolysis of shrinking biomass particle. Chem Eng Sci 2004;59:1999–2012. https://doi.org/10.1016/j.ces.2004.01.050.
[31] Biswas AK, Umeki K. Simplification of devolatilization models for thermally-thick particles: differences between wood logs and pellets. Chem Eng J 2015;274:181–91. https://doi.org/10.1016/j.cej.2015.03.131.
[32] Mehrabian R, Zahirovic S, Scharler R, Obernberger I, Kleditzsch S, Wirtz S, et al. A CFD model for thermal conversion of thermally thick biomass particles. Fuel Process Technol 2012;95:96–108. https://doi.org/10.1016/j.fuproc.2011.11.021.
[33] Okekunle PO, Pattanotai T, Watanabe H, Okazaki K. Numerical and experimental investigation of intra-Particle heat transfer and tar decomposition during pyrolysis of wood biomass. J Therm Sci Technol 2011;6:360–75. https://doi.org/10.1299/jtst.6.360.
[34] Gentile G, Debiagi PEA, Cuoci A, Frassoldati A, Ranzi E, Faravelli T. A computational framework for the pyrolysis of anisotropic biomass particles. Chem Eng J 2017;321. https://doi.org/10.1016/j.cej.2017.03.113.
[35] Di Blasi C. Heat, momentum and mass transport through a shrinking biomass particle exposed to thermal radiation. Chem Eng Sci 1996;51:1121–32. https://doi.org/10.1016/S0009-2509(96)80011-X.

[36] Kansa EJ, Perlee HE, Chaiken RF. Mathematical model of wood pyrolysis including internal forced convection. Combust Flame 1977;29:311–24. https://doi.org/10.1016/0010-2180(77)90121-3.
[37] La Villetta M, Costa M, Massarotti N. Modelling approaches to biomass gasification: a review with emphasis on the stoichiometric method. Renew Sustain Energy Rev 2017;74:71–88. https://doi.org/10.1016/j.rser.2017.02.027.
[38] Basu P. Biomass Gasification and Pyrolysis: Practical Design. First edii. Elsevier; 2010. doi:10.1017/CBO9781107415324.004.
[39] Yang YB, Sharifi VN, Swithenbank J. Effect of air flow rate and fuel moisture on the burning behaviours of biomass and simulated municipal solid wastes in packed beds. Fuel 2004;83:1553–62. https://doi.org/10.1016/j.fuel.2004.01.016.
[40] Li X, Yin C. A drying model for thermally large biomass particle pyrolysis. Energy Procedia 2019;158:1294–302. https://doi.org/10.1016/J.EGYPRO.2019.01.322.
[41] Anca-Couce A. Reaction mechanisms and multi-scale modelling of lignocellulosic biomass pyrolysis. Prog Energy Combust Sci 2016;53. https://doi.org/10.1016/j.pecs.2015.10.002.
[42] Li J, Paul MC, Younger PL, Watson I, Hossain M, Welch S. Characterization of biomass combustion at high temperatures based on an upgraded single particle model. Appl Energy 2015;156. https://doi.org/10.1016/j.apenergy.2015.04.027.
[43] Kan T, Strezov V, Evans TJ. Lignocellulosic biomass pyrolysis: A review of product properties and effects of pyrolysis parameters. Renew Sustain Energy Rev 2016;57. https://doi.org/10.1016/j.rser.2015.12.185.
[44] Branca C, Di Blasi C. A summative model for the pyrolysis reaction heats of beech wood. Thermochim Acta 2016;638:10–6. https://doi.org/10.1016/j.tca.2016.06.006.
[45] Huang X, Rein G. Thermochemical conversion of biomass in smouldering combustion across scales: the roles of heterogeneous kinetics, oxygen and transport phenomena. Bioresour Technol 2016;207:409–21. https://doi.org/10.1016/j.biortech.2016.01.027.
[46] Yang YB, Yamauchi H, Nasserzadeh V, Swithenbank J. Effects of fuel devolatilisation on the combustion of wood chips and incineration of simulated municipal solid wastes in a packed bed. Fuel 2003;82:2205–21. https://doi.org/10.1016/S0016-2361(03)00145-5.
[47] Nunn TR, Howard JB, Longwell JP, Peters WA. Product compositions and kinetics in the rapid pyrolysis of milled wood lignin. Ind Eng Chem Process Des Dev 1985;24:844–52. https://doi.org/10.1021/i200030a054.
[48] Bryden KM, Hagge MJ. Modeling the combined impact of moisture and char shrinkage on the pyrolysis of a biomass particle. Fuel 2003;82:1633–44. https://doi.org/10.1016/S0016-2361(03)00108-X.
[49] Yin C, Kær SK, Rosendahl L, Hvid SL. Co-firing straw with coal in a swirl-stabilized dual-feed burner: Modelling and experimental validation. Bioresour Technol 2010;101:4169–78. https://doi.org/10.1016/j.biortech.2010.01.018.
[50] Civan F. Porous media transport phenomena. John Wiley & Sons. Inc.; 2011.
[51] Teklay A, Yin C, Rosendahl L, Bøjer M. Cement and concrete research calcination of kaolinite clay particles for cement production: a modeling study. Cem Concr Res 2014;61–62:11–9. https://doi.org/10.1016/j.cemconres.2014.04.002.
[52] Haberle I, Haugen NEL, Skreiberg Ø. Combustion of thermally thick wood particles: a study on the influence of wood particle size on the combustion behavior. Energy Fuels 2018;32:6847–62. https://doi.org/10.1021/acs.energyfuels.8b00777.
[53] Stoppiello G, Claudio C. A Biomass Gasification – Process analysis and dimensioning aspects for downdraft units and gas cleaning lines Supervisors 2010:1–167.
[54] Yin C. Modelling of heating and evaporation of n-Heptane droplets: towards a generic model for fuel droplet/particle conversion. Fuel 2015;141:64–73. https://doi.org/10.1016/j.fuel.2014.10.031.
[55] H.K.Versteeg WM, Beutner T. An introduction to: Computational Fluid Dynamics The finite volume method. Second edi. Pearson Education; 2007. doi:10.2514/1.22547.
[56] Rath J, Steiner G, Wolfinger MG, Staudinger G. Tar cracking from fast pyrolysis of large beech wood particles. J Anal Appl Pyrolysis 2002;62:83–92. https://doi.org/10.1016/S0165-2370(00)00215-1.
[57] Rath J, Staudinger G. Vapour phase cracking of tar from pyrolysis of birch wood. Therm Sci 2001;5:83–94.
[58] Steiner G, Rath J, Wolfinger MG, Staudinger G. A method to determine the course of heating value and heat production rate of volatiles during the pyrolysis of a solid fuel particle. Thermochim Acta 2003;398:59–71. https://doi.org/10.1016/S0040-6031(02)00396-9.

Paper C

A detailed computational fluid dynamics model on biomass pellet smoldering combustion and its parametric study

Xiyan Li, Søren Knudsen Kær, Thomas Condra, Chungen Yin

The paper has been submitted to the
Biomass & Bioenergy, 2020.

The layout has been revised.

A detailed computational fluid dynamics model on biomass pellet smoldering combustion and its parametric study

Xiyan Li [a*], Søren Knudsen Kær[a], Thomas Condra [a], Chungen Yin [a]

a. Department of Energy Technology, Aalborg University, Aalborg, Denmark

Abstract

The aim of this article is to present a complete and detailed gasification/smoldering model for a single biomass pellet. The four main objectives were: to write a modified one-dimensional numerical model using C++, to validate the results using experimental data from the literature, to present an overview of the one-dimensional model results, and to investigate the effects of main parameters used in the model. This model used includes all the necessary partial differential equations describing continuity, species, energy and pressure. All the equations are highly coupled and are solved using a finite volume, central difference scheme. A time-marching procedure is based on a fully implicit scheme. Validation, with air smoldering combustion, are presented. The validation results show good agreement with the experimental data. The detailed results from this model show, for example, the temperature profile, the gas species distribution, the carbon content and the reaction rate. A discussion about the important parameters and their effects on this model is also presented at the end of the paper. The parametric study shows that the devolatilization rate can prolong or shorten the time of finishing devolatilization stage but it cannot affect the highest temperature that the combustion can reach. A two-step and four-step hydrocarbon combustion scheme is implemented in this one-dimensional CFD model. The results show that, both schemes can predict the temperature quite well compared to the experimental data, with an error of up to 5% in the temperature simulation.

Keywords

Single particle; Biomass gasification; Combustion; Computational fluid dynamics (CFD); Finite volume method (FVM); Porous media

Word count: 7039

Highlights

- A detailed description of a numerical smoldering combustion model.
- Validation shows good agreement with experimental data.
- Detailed results of smoldering combustion are given.
- Parametric study on devolatilization rate and hydrocarbon combustion scheme.

Nomenclature

Letters

A_s	Surface area [m^2]

* Corresponding author. Tel.: +45 20703591
E-mail address: xli@et.aau.dk (X. Li).

A	Pre-exponential factor [s^{-1}]
E_a	Activation energy of water evaporation, [J/kmol].
C_P	Specific heat [J/(kg·K)]
CFD	Computational Fluid Dynamics
C_{mix}	Mixing coefficient for gas phase combustion, C_{mix}=0.5
C_{fuel}	Mole concentration of fuel [kmol/m^3]
$D_{eff,fw}$	Free water effective mass diffusivity [m^2/s]
d_p	Diameter of the pellet [mm]
DTG	Differential Thermogravimetry
FSP	Fiber saturation point, %
Δh_{evap}	Latent heat of evaporation [J/kg]
h_f^0	Enthalpy of formation [J/kg]
ΔH	Heat of reaction [J/kg]
h_T	Heat transfer coefficient [W/(m^2·K)]
h_M	Mass transfer coefficient [m/s]
K_{eff}	The thermal conductivity [W/(m·K)]
k_{H_2O}	Reaction rate constant [s^{-1}]
M	Number of species
MW_i	Molecular weight of species i [kg/kmol]
N	Number of reactions
Nu	Nusselt number
Pr	Prandtl number
R_g	Universal gas constant [J/(mol·K)]
r_i	Reaction rate [J/(mol·K)]
r_{H_2O}	The volumetric vaporization rate [kg/(m^3·s)]
SBC	Sub Bituminous Coal
Sc	Schmidt number
S_{fuel}	Stoichiometric coefficient for homogeneous reactions
Sh	Sherwood number
S_T	Source term in energy equation [W/m^3]
S_a	Specific area of the wood particle, 1.0×10^6 [m^2/m^3]
T_{ini}	Initial temperature [K]
T_P	Local temperature of the current control volume[K]
T_∞	Ambient gas temperature [K]
T_S	Particle surface temperature [K]
$T_{j,S}$	Particle surface temperature for species j [K]
T_C	Particle center temperature [K]
T_{evap}	Water evaporation temperature [K]
u	Velocity [m/s]
Y_{vap}	The percentage of vapor within all the species,
$Y_{j,ref}$	Reference mass fraction of species *j* in the gas film around the particle
$Y_{j,s}$	Mass fraction of species *j* at particle surface
$Y_{j,\infty}$	Mass fraction of species *j* in the ambient gas
ρ_g	Gas density [kg/m^3]
ρ_{vol}	Remaining volatile in solid [kg/m^3]

$\rho_{vol,\infty}$	Ultimate yield of volatile [kg/m^3]
ρ_{fw}	The free water density at the present time [kg/m^3]
$\dot{w}_k$	Reaction rate [kg/(m^3·s)]

Greek symbols

λ	The average conductivity of all the gases in the film [W/(m·K)]
ε	Porosity
μ	Dynamic viscosity [kg/(m·s)]
σ	Boltzmann radiation constant, 5.86×10^{-8} (W/m^2K^4)

Subscripts

i	Reaction index/Species index
g	Gas
k	Number of species
l	Liquid
P	The center point the current control volume
rad	Radiation
s	Solid
∞	Ambient

Superscripts

*	Results from last iteration step

1. Introduction

As the current main energy source of the world, fossil fuels are an object of controversy. Due to the declining supply of fossil fuels and the issues related to greenhouse gas emissions, there is an urgent need for alternative energy sources. According to a report from United Nations Environment Programme (UNEP), the global CO_2 content at sea level has increased from 315.71 ppm in 1980 to 410.26 ppm in 2018 [1]. Biomass is an environmentally friendly source of energy if it is sustainably cultivated, as the CO_2 released during its use is offset by the CO_2 captured from the atmosphere during its growth. Biomass gasification uses gases, such as steam, air, nitrogen, carbon dioxide, hydrogen or a mixture of these as a medium to react with biomass to produce syngas.

In order to make full use of the biomass, research has been done on pyrolysis, gasification and combustion, based on both experimental methods and simulation methods. Experimental methods can give a way of describing real reaction phenomena and gaining a set of practical data; for example, the temperature profile, kinetic parameters, reaction order etc.; whilst simulation gives a rapid way of looking into the results before experiments or before scaling-up is considered.

The thermal treatment for biomass, especially in CFD modelling, are normally classified in three ways, based on the conversion technology: a) a fixed biomass pellet or a fixed bed as porous media, b) free-moving particle in a reactor as multi-fluid model and c) free-moving discrete particle[2]. This paper focus on the first type of model, because of its potential of operational stability and convenience of scaling-up from a particle scale to a reactor scale.

Biomass, as the only renewable sustainable resource in the natural carbon cycle, attracts interest for industrial use as the substitute for fossil fuels. Therefore, biomass has been used for many processes that normally used fossil fuels, such as coal. Consequently, both experimental methods and theories used in fossil fuels pyrolysis, gasification and combustion can also be used in biomass studies.

A detailed research on biomass thermal treatment began in the 1970's. Kansa et al. [3] developed a one-dimensional mathematical model considering a porous structure and internal forced convection.

In their model, analytical fluid mechanics methods were used. In addition, the experimental results and simulation results were compared. Due to the use of less sophisticated computational methods, or due to the incomplete measuring technology or possibly due to the immature chemical reaction mechanics, etc., the discrepancies in some results between the simulation and measurement was quite considerable. In conclusion, Kansa et al. [3] used a two-step pyrolysis reaction scheme, which can be traced back to the research done by Bamford et al. [4] who also numerically investigated the temperature distribution during wood combustion, which is one of the earliest article that can be found on the numerical simulation of biomass thermal treatment.

The development of a reaction scheme in biomass pyrolysis has been a critical issue since then. Over the past few decades, three main schemes were used for numerical simulations. Figure 1 shows an overview of these three schemes.

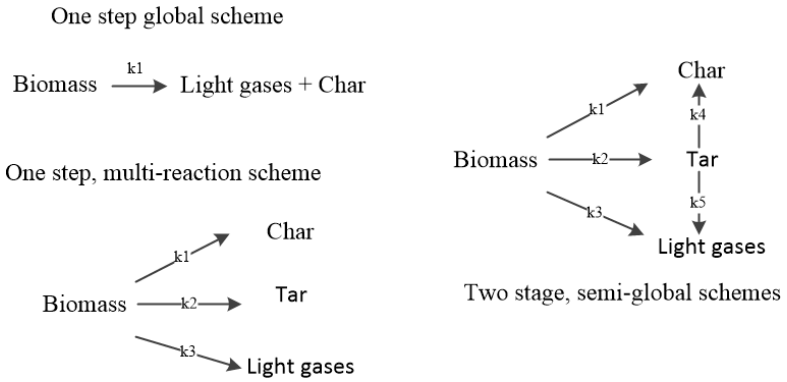

Fig.1 Pyrolysis reaction schemes

For a number of years, the numerical research in biomass thermal treatment has had two main issues. The first one was to choose the suitable pyrolysis scheme; the second is to find the correct combustion mechanism. Both of them are still not quite resolved even today. In practice, this encouraged scientists to develop precision instruments for kinetic data and to use the latest data for simulation. The two-step pyrolysis schemes was quite popular during the last decades of the last century. Thurner and Mann [5] calculated the kinetic data by measuring the pyrolysis of oak sawdust in a given temperature range. By assuming all the reactions are first-order reactions, they produced the kinetic data parameters for the first step of a two-step pyrolysis scheme.

Pyle and Zaror [6] investigated the one step three parallel reactions for cellulose low temperature pyrolysis. They compared three models for cellulose pyrolysis by comparing the temperature distribution. They found that pure kinetic control is acceptable for small particle pyrolysis, whilst the particle with a diameter of 5-10 cm will be controlled by heat transfer.

Chan et al. [7] performed numerical simulation on large biomass particle pyrolysis, by using a two-stage multi-reaction pyrolysis scheme. The model predicted the temperature distribution and the devolatilization rate. The experiments show different tar distributions during different heat flux and particle geometric scale. Nunn et al [8] investigated the product compositions during the rapid pyrolysis of sweet gum hardwood. The results show that a one-step first-order general decomposition model describes the global rates evolution of most products, except tar, quite well.

With the maturity of DTG technology since 1980's, a sequence of kinetic data based on the three models mentioned was published [9][10][11][12][13]. By using a modified one-step pyrolysis model, Koufopanos et al [11] found that it is possible to predict the pyrolysis rate with a wide range of temperatures and particle dimensions.

All the three devolatilization scheme were mentioned and summarized by Di Blasi [14], shown in Fig. 1. Even though in the paper she argued about the inapplicability of the one-step multi-reaction scheme and the one step global scheme, these two schemes are still in used [15][16][17]. The instability of tar, brings along the uncertainties to the simulation, therefore, the prediction of secondary gases produced by tar is not reliable in general. In the studies where tar is treated as an intermediate product, the relative data has to be tuned in order to fit the experimental data. For example, Gronli [18] found that the heat of reaction of tar cracking has to be modified in order to use it in modelling. For this reason, the one-step global reaction scheme is used in this paper.

For gasification or smoldering combustion, the reactions are usually more complicated. For example, the chemical mechanisms of homogeneous reactions and heterogeneous reactions have to be taken into account. In particular, the homogeneous reaction can be quite complex, when considering complex intermediate products. To minimize the side-effects from the intermediate products, much work has been done. To start with, the easiest way is to ignore the intermediate products at all. In this case, there is only CO_2 and H_2O after the fuel combusts with oxygen. However, this situation is very idealized, since intermediate products from incomplete combustion are quite important for biomass gasification. Dryer and Westbrook [19] published a two-step combustion scheme for hydrocarbons. This scheme requires only one intermediate product, which is CO. In the two-step combustion scheme, the fuel will react with oxygen to produce CO and H_2O. The two-step combustion scheme in their work can be used to predict flame propagation in a laminar flow.

Jones and Lindstedt [20] published a four-step global reaction schemes for hydrocarbon combustion. In this global reaction scheme, there are two intermediate products, CO and H_2. Their scheme shows good agreement with the species chosen, with respect to concentration, temperature, velocity and pressure in the flame, and for this reason, this derived hydrocarbon combustion scheme is also used in this paper.

Heterogeneous reactions during biomass gasification and combustion are mainly about how char reacts with oxygen, steam, carbon dioxide and hydrogen [21]. Laurendeau [21] summarized these four reaction rates and gave experimental kinetic results. Similar work has also been done by Vaclav et al. [22], Yoon et al. [23], Evans and Emmons [24].

Many researchers have worked on the thermal processing of biomass. Apart from Di Blasi [25][26], Lu et al. [27][28] also studied the flame combustion of a single biomass pellet. Mehrabian [29] has also done similar work by using the same biomass material as Lu et al. [24] and Momeni [31]. Detailed results about packed bed combustion/gasification have been published just recently [32][33]. However, there is still room to improve the simulation of biomass smoldering or gasification.

In this paper, a model aimed at presenting a complete set of results from biomass air smoldering combustion has been developed. Considering the unstable states of tar and its complexity during simulation, a one-step global pyrolysis scheme is used. Water evaporation, pyrolysis, homogeneous reactions and heterogeneous reactions are considered with a one-dimensional CFD model. The results of the temperature distribution, gas species distribution, pressure and velocity distributions are given and the concentrations of char and carbon reaction rate are also plotted. Moreover, a parametric study of the key parameters has been performed.

2. Material and methods

The pellet in this model is considered as a one-dimensional spherical solid fuel pellet, whose properties are isotropic. The fuel pellet is under local thermal equilibrium during the entire conversion process, which means, at any point with in the pellet, the local gas and the solid stay the same temperature. The CFD model uses a central difference scheme with a staggered grid for the velocity calculation. The number of grid points used in the grid independency study, was 120, 160 and 200.

A fully implicit scheme is used for temporal discretization. More details about the partial differential equations are presented below.

The validation experiment for gasification is based upon two data sets, for both a sub-bituminous coal (SBC) and a poplar wood pellet. These are classified as Case 1 and Case 2 in the results and discussion section. Table 1 shows the composition of these two fuels.

The heat source for the biomass pellet in this model includes two terms: the external heat from radiation and convection from the environment and the internal heat (endothermic or endothermic reactions). The external heat largely affects the surface temperature, whilst the internal heat affects the internal temperature.

For the internal heat, the source term can be written as:

$$S_T = -\sum_{k=1}^{M} h_{f,k}^0 \dot{w}_k - \sum_{k=1}^{M} h_{f,k} \dot{w}_k = \sum_{k=1}^{N} \Delta H_i \dot{w}_i - \sum_{k=1}^{M} h_{f,k} \dot{w}_k \quad (1)$$

Table 1: Proximate analysis, ultimate analysis and heating value [34][35]

Fuel	Moisture[%, a.d]	Volatile[%, d.b]	FC[%,.d.b]	Ash[%, d.b]	HHV[kJ/kg, a.d]
Poplar pellet	6	90	9.5	0.5	18871
	C[%, d.b]	H[%, d.b]	O[%, d.b]	N[%, d.b]	S[%, d.b]
	48.1	5.77	45.53		
	Moisture[%, a.d]	Volatile[%, d.b]	FC[%, d.b]	Ash[%, d.b]	HHV[kJ/kg, a.d]
Sub-bituminous coal	5.07	21.08	49.93	23.90	31490
	C[%, d.b]	H[%, d.b]	O[%, d.b]	N[%, d.b]	S[%, d.b]
	83.58	4.68	9.2	1.74	0.8

* [d.b]: dry base. [a.d]: as received base

Except for the beginning and end of the combustion, when the source term is large enough, the temperature inside the pellet is mainly controlled by three parameters: the enthalpy of formation, sensible enthalpy and the reaction rate. This implies that, the internal heat transfer is dominated by the local temperature and the properties of the biomass pellet. The enthalpy of formation can be calculated from the heating value of the solid fuel.

The gas species composition during pyrolysis or gasification can be quite diverse. For the sake of model simplification, the volatiles are treated as one solid species before the decomposition. Moreover, it breaks down into light gases during decomposition based on the mass conservation and heat conservation. There were also some other researchers who used a composition of light gases directly derived from strict experimental conditions [36][37][27].

For example, the volatile from SBC can be expressed as $CH_{4.2197}O_{0.5226}$ after considering mass conservation and ignoring N and S. This molecular formula, with a molecular weight of $26.9343\ \mathrm{kg/kmol}$ and the enthalpy of formation of $-34527\ \mathrm{kJ/kg}$, is used as input for the simulation. Similarly, according to the proximate analysis and ultimate analysis of the poplar wood, the composition of volatile from polar wood can be calculated as $CH_{1.7812525}O_{0.8855055}$, with a molecular weight of $28.005272\mathrm{kg/kmol}$. The formation enthalpy of this volatile is $-157767\mathrm{kJ/kmol}$. By considering the heat and mass conservation, the breakdown of the volatile from poplar wood can be written as the following equation:

$$CH_{1.7812525}O_{0.8855055} = 0.1265471C_3H_8 + 0.3813275H_2 + 0.12921CO + 0.3439CO_2 \quad (2)$$

It needs to be emphasized that the HHV in Table1 is not from the experiment, since the original heating value was not specified. So the HHV is calculated by a unified correlation from Channiwala and Parikh[40].

For the simplicity of calculation, an artificial component is used to represent volatile in the model, as shown in Table 2.

Table 2 shows all the reactions used for gasification with oxygen participation. The first is the devolatilization reaction as mentioned previously. The second and the third are the mechanisms for free water and bound water. It should be noticed that the free water is only considered when the FSP is above

30% [41]. Reactions 4 to 6 are heterogeneous reactions. It is worth mentioning that the last heterogeneous reaction (reaction 6) does not occur under atmospheric pressure [22] at the gasification temperature, and it is included for reference, but it is not considered in the model. Reaction 7 to reaction 11are the homogeneous reactions. The light hydrocarbon reactions used here obeys the two-step combustion scheme for hydrocarbons proposed by Westbrook and Dryer [19], which are shown in Table 2. In the two-step mechanism, the main aim is to oxidize volatile and produce CO and H_2O, and this is the first step. The second step is to burn CO into CO_2, as shown in reaction 8.

Table 2: Chemical reactions and reaction rate

index	Chemical reactions	Rate expression	Ref
1	Biomass → Volatile + Char	$r_1 = \partial\rho_{vol}/\partial t = k_1(\rho_{vol,\infty} - \rho_{vol})$	[33]
2	H_2O (free) → H_2O (g)	$r_2 = S_a \frac{h_T(T_j - T_{ini}) + \varepsilon\sigma(T_j^4 - T_{ini}^4)}{\Delta h_{evap}}$	
3	H_2O (bound) → H_2O (g)	$r_3 = A_{evp} exp\left(-\frac{E_{evp}}{RT}\right)$	
4	$C + \alpha O_2 \rightarrow 2(1-\alpha)CO + (2\alpha - 1)CO_2$	$r_4 = \partial C_{O_2}/\partial t = \frac{s_{a,char}[\rho_C/(\rho_C+\rho_B+\rho_A)]k_4 P_{O_2}}{1/K_r + 1/k_d}$	[27]
5	$C + H_2O \rightarrow H_2 + CO$	$r_5 = \partial C_{H_2O}/\partial t = \frac{s_{a,char}[\rho_C/(\rho_C+\rho_B+\rho_A)]k_4 P_{H_2O}}{1/K_r + 1/k_d}$	[27]
6	$C + CO_2 \rightarrow 2CO$	$r_6 = \partial C_{CO_2}/\partial t = \frac{s_{a,char}[\rho_C/(\rho_C+\rho_B+\rho_A)]k_4 P_{CO_2}}{1/K_r + 1/k_d}$	[27]
7	$H_2 + 1/2O_2 \rightarrow H_2O$	$r_7 = \partial H_2/\partial t = k_7 {C_{H_2}}^{0.25} C_{O_2}^{1.5}$	[38]
Two-step global combustion mechanism for hydrocarbon			[19]
8	$CO + 1/2O_2 \rightarrow CO_2$	$r_8 = \partial C_{CO}/\partial t = k_8 C_{CO} C_{O_2}^{0.25} C_{H_2O}^{0.5}$	[38]
10[a]	$CH_{4.2197}O_{0.5226} + 1.293625O_2 \rightarrow CO + 2.10985H_2O$	$r_{10} = \partial C_{CH_{4.2197}O_{0.5226}}/\partial t = k_{10} C_{CH_{4.2197}O_{0.5226}}^{0.5} C_{O_2}^{1.25}$	[19]
10[b]	$CH_{1.7812}O_{0.8855} + 0.4991O_2 \rightarrow CO + 0.8756H_2O$	$r_{10} = \partial C_{CH_{1.7812}O_{0.8855}}/\partial t = k_{10} C_{CH_{1.7812}O_{0.8855}}^{0.5} C_{O_2}^{1.25}$	[19] [30]
Four-step global combustion mechanism for alkane hydrocarbons up to butane			[39]
8	$CO + 1/2O_2 \rightarrow CO_2$	$r_8 = \partial C_{CO}/\partial t = k_8 C_{CO} C_{O_2}^{0.25} C_{H_2O}^{0.5}$	[38]
9	$C_3H_8 + 3H_2O \rightarrow 3CO + 7H_2$	$r_9 = \partial C_{C_3H_8}/\partial t = k_9 C_{C_3H_8} C_{H_2O}$	[39]
10[c]	$C_3H_8 + 1.5O_2 \rightarrow 3CO + 4H_2$	$r_8 = \partial C_{C_3H_8}/\partial t = k_{10} {C_{C_3H_8}}^{0.5} C_{O_2}^{1.25}$	[39]
11	$CO + H_2O \rightarrow CO_2 + H_2$	$r_{11} = \partial C_{CO}/\partial t = k_{11} C_{CO}^1 C_{H_2O}^1$	[38]

10[a] represents the volatile derived from SBC. 10[b] represents the volatile derived from poplar wood pellet.

Table 3: Kinetic data used in this model

Reaction index	Pre-exponential factor (A) $[s^{-1}]$	Activation energy (E_a) [J/kmol]	Heat of reactions (ΔH) [kJ/kg]
1	3.12×10^5	7.4×10^7	-1376.09
2	$-$	$-$	-2440
3	5.13×10^{10}	8.8×10^7	-2440
4	0.658[a]	7.4831×10^7	$(9992.068\alpha - 1048.159)$
5	3.42[a]	1.297×10^5	-9738.98
6	3.42[a]	1.297×10^5	-3919.39
7	6.8×10^{15}	1.67×10^8	13435.94
8	2.39×10^{12}	1.702×10^8	10114.28
9	3.0×10^8	1.26×10^8	-14313.75
10^a	2.119×10^{11}	2.027×10^8	30420.72[a]
10^b	2.119×10^{11}	2.027×10^8	1685.643[b]
10^c	4.1×10^{11}	1.26×10^8	5175.43
11	2.75×10^9	8.4×10^7	-101.73

[a] Units are $m/s^{-1}K^{-1}$

Table 3 shows the data for the kinetic parameters used in most of the reactions in Table 2, calculated from the Arrhenius equation shown in equation (3). The reaction rate of reactions 4-7 use the

expression in equation (4). For reaction 7, the value of n is assigned to -1, whilst for the rest, the value of n is 1.

$$k_i = Ae^{-\frac{E_a}{RT}} \quad (3)$$

$$k_i = AT^n e^{-\frac{E_a}{RT}} \quad (4)$$

The fuel pellet here is considered as a spherical pellet. The mesh is done by dividing the radius into many shells. Then the control volume can be seen as an approximate cuboid wrapped by two surfaces within the pellet surface, as shown in Fig.2.

The reaction rate of combustion is not only dominated by the kinetic rate, but also by the partial pressure of oxygen, which is also called the mixing rate in the work of Yang et al [42].In this work, the mixing rate of combustion is applied to all the combustion reactions, such as reaction 4, 7, 8, 10. The mixing rate is based on the expression in eqn. (5).

$$R_{mix} = C_{mix}\rho_g\{150\, D_g(1-\varepsilon)^{2/3}/(d_p^2\varepsilon) + 1.75|u_g|(1-\varepsilon)^{1/3}\}min\{C_{fuel}/S_{fuel}, C_{O_2}/S_{O_2}\} \quad (5)$$

In this work, the reaction rate is taken as the minimum value between the kinetic reaction rate and the mixing rate.

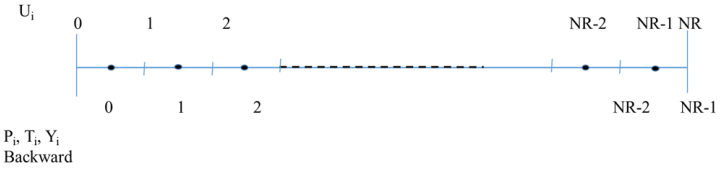

Fig.2 staggered grid of velocity and other parameters

3. Model description

The theory of the numerical model is based on a sequence of partial differential equations. A fully implicit scheme is used for the time integration. A tri-diagonal matrix algorithm (TDMA) is applied to solve the linear equations. The finite volume method guarantees the mass and energy conservation in and out the control volume.

For solid species, such as biomass, char, volatile before release from the solid face, only a transient term is considered, as shown in Eqn. (6). The diffusion and convection of liquid water are also neglected:

Table 4: Governing equations

Iterm	Transport equations	
Solid species	$\frac{\partial(\rho_i)}{\partial t} = s_i$	(6)
Gas species	$\frac{\partial \varepsilon\rho_g(Y_{ig})}{\partial t} + \frac{\partial \varepsilon\rho_g u Y_{ig}()}{\partial r} = \frac{\rho_g D_{ig}\partial}{\partial r}\left(\frac{\partial(Y_{ig})}{\partial r}\right) + S_{Y_{ig}}$	(7)
Continuity	$\frac{\partial(\varepsilon\rho_g)}{\partial t} + \frac{\partial(\varepsilon\rho_g u)}{\partial r} = S_g$	(8)
Pressure	$\vec{u} = -\frac{\eta}{\mu}\nabla P$	(9)
Energy equation	$\frac{\partial \varepsilon\rho_g C_{pg}(T)+\rho_s C_{ps}\partial(T)+\rho_l C_{pl}\partial(T)}{\partial t} + \frac{\varepsilon\rho_g u C_{pg} T_g \partial()}{\partial r} = k_{eff}\frac{\partial}{\partial r}\left(\frac{\partial T}{\partial r}\right) + S_T$	(10)

$$Y_{j,ref} = Y_{j,s} + 1/3\left(Y_{j,\infty} - Y_{j,s}\right) \quad (11)$$

$$T_{ref} = T_s + 1/3\,(T_\infty - T_s) \quad (12)$$

$Y_{j,ref}$ and T_{ref} here are used for calculating the gas properties in the gas film. Once the dimensionless parameters, such as, Re, Nu, Sh, Pr are determined, h_M and h_T can be calculated using the following equations.

$$Sh \equiv \frac{h_M L_c}{D_g} = 2.0 + 0.6 Re^{\frac{1}{2}} Sc^{\frac{1}{3}} \quad (13)$$

$$Nu \equiv \frac{h_T L_c}{k_g} = 1.05 + 0.6 Re^{0.65} Pr^{0.33} \quad (14)$$

The boundary condition at surface of the pellet for mass transfer can be expressed as:

$$DAs \frac{Y_{j,s} - Y_{j,p}}{\Delta r/2} = A_s h_M \left(Y_{j,\infty} - Y_{j,s}\right) \quad (15)$$

The outer boundary condition for temperature is shown as:

$$k_{eff} A_s \frac{T_S - T_P}{\Delta r/2} = A_s h_T (T_\infty - T_S) + A_s \varepsilon \sigma (T_{rad}^4 - T_S^4) \quad (16)$$

The source term can be linearized by a Taylor expansion:

$$\left(\frac{k_{eff} A_s}{\frac{\Delta r}{2}} + A_s h_T + 4 A_s \varepsilon \sigma (T_s^*)^3\right) T_S = \frac{k_{eff} A_s}{\frac{\Delta r}{2}} T_P + A_s h_T T_\infty + A_s \varepsilon \sigma (T_{rad}^4 - 3(T_s^*)^4) \quad (17)$$

4. Results and discussion

Using the model described above, two validation cases were made. For each of the validation cases, a grid independent validation is made. The two cases are: Case 1: a gasification case of the experiments taken from Bu et al [34][35]. This experiment is based on a 10mm spherical sub-bituminous coal pellet in a fluidized bed on a temperature of 850 ℃. The ambient gas is 30% oxygen and 70% carbon dioxide. Case 2: an air smoldering combustion case of a poplar pellet. The poplar pellet is spherical in shape with a diameter of 9.5mm and water content of 40%. The experiment is operated under a radiation temperature of 1273K and an ambient temperature of 1080K. The ambient gas is air. Table 5 and Table 6 show some properties used in both cases.

Table 5: Properties for SBC pellet[34]

Properties	Units	Values	Ref.
Apparent density, ρ_{SBC}	kg/m^3	1662	[35]
Specific heat capacity, $C_{P_{SBC}}$	J/(kg·K)	1049	[35]
Heat transfer coefficient, h_T	W/(m^2·K)	200	[34]
Fluid temperature, T_f	K	1088	[35]
Effective conductivity, K_{eff}	W/(m^2·K)	0.6	[35]
Wall temperature, T_{wall}	K	1123	[35]
Velocity at pellet surface, u_g	m/s	0.28	[43]
Pellet diameter, d_p	mm	10	[34]

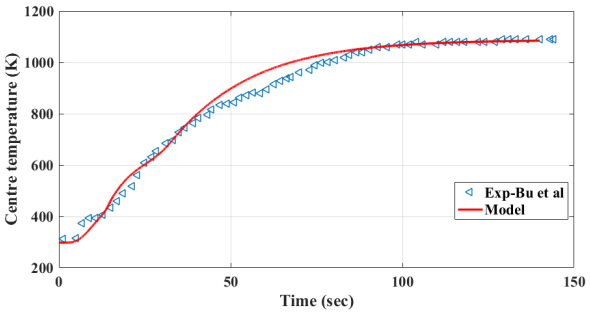

Fig. 3 Simulation results compared with an experiment of a SBC pellet during gasification(30% $O_2$and 70% CO_2)

Figure 3 shows the temperature at the SBC pellet center during smodering gasification under 30% $O_2$and 70% CO_2, which is Case 1. Fig.3 shows that the simulation results agree with the experimental data very well. The temperature increases after a short stationary period, which is due to the evaporation of water. After 100 seconds, the temperature at the pellet center is stable again, which means that the pellet has completely reached the environment temperature. It needs to be emphasied that this does not mean that all the reactions have finished at that time, considering large amount of carbon in the SBC pellet. It only means that the homogeneous reaction has finished, but the oxygen at the pellet center is still low enough to cause a high combustion rate.

Table 6: Properties for a poplar pellet

Properties	Units	Values	Ref.
Apparent density, ρ_B	kg/m^3	545	[27]
Thermal conductivity	W/(m²·K)		
K_B		$0.056 + 2.6 \times 10^{-4}T$	[30]
K_{Char}		0.071	[30]
K_{Ash}		1.2	[30]
Specific heat capacity	J/(kg·K)		
$C_{p,wood}$		1500+T	[30]
$C_{p,char}$		$420 + 2.09T + 6.8510^{-4}T^2$	[30]
Diffsivity			
Molecular diffusivity, D_{AB}		$-2.775 \times 10^{-6} + 4.479 \times 10^{-8}T + 1.656 \times 10^{-10}T^2$	[44]
Knudsen diffusivity, D_k		$2/3 \times d_{pore} \times \sqrt{2RT/\pi MW_i}$	[30]
Effective diffusivity, D_{eff}		$\frac{\varepsilon}{\tau}\left(\frac{1}{D_{AB}} + \frac{1}{D_k}\right)^{-1}$	
Pore size, d_{pore}	m	2.6×10^{-6}	
Tutorisity, τ		1.5	[45]
Effective conductivity, K_{eff}	W/(m²·K)	$\varepsilon K_{gas} + (1-\varepsilon)K_{solid} + \varepsilon\sigma T^3 d_{pore}/\epsilon$	
Permeability, K	m^2	1.5×10^{-11}	This work
Emissivity, ϵ		0.8	This work
Porosity, ε		0.65	[27]

Figure 4 shows the weight loss of Case 2 with respect to time. The solid line is the simulation results from this model, and the other two lines are the experimental results from Lu et al [27]. There is a quite close agreement to the experimental results.

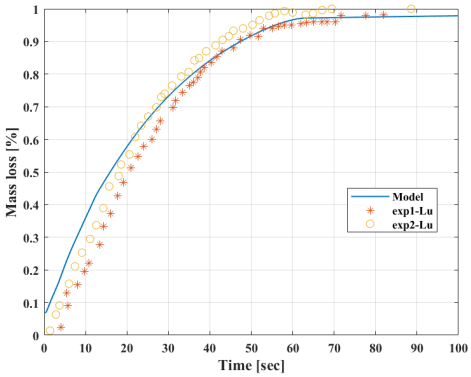

Fig.4 Mass loss of the biomass pellet with 40% water with an atmosphere of air

Since the drying model has already been discussed in another paper [46], therefore a water content of 6% is used here [27]. Considering the experiment that was done in Lu et al's [27] work was referred

to flame combustion, therefore the temperature at the pellet surface from the experiment is not directly applicable for the model simulation here.
The temperature of radiation used in this model is the same as the original measured temperature, which is 1273K, and the preheated gas temperature is 1080K. The results are produced with an assumed slip gas velocity of 0.5m/s. The gas atmosphere is assumed as air. A grid independence study using poplar biomass from Lu et al [27] is shown in Fig.5, where the simulation results of temperature at the pellet center were plotted on 120, 160, and 200 grid points, respectively. The independence check shows that the meshing numbers have little effect on the final temperature results. In this work, 200 grid points were used.

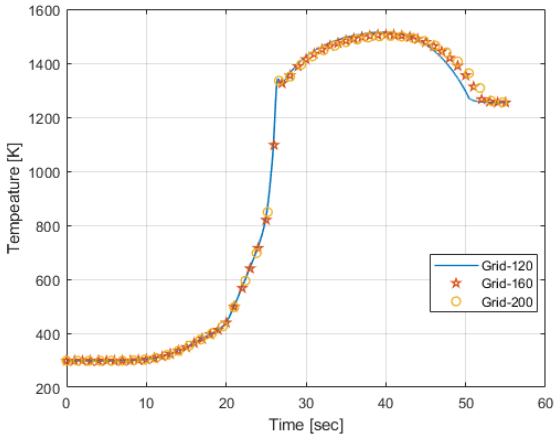

Fig.5 Temperature at the center of the biomass pellet with three different grid numbers

Figure 6 shows the temperature validation against modelling and experimental data from Lu et al [27] under the condition of air combustion. Probably because a flame layer is assumed out of the pellet surface, the surface temperature from Lu et al's simulation is higher than the results from this model. Both this model and the model from Lu et al predict the correct starting time of pyrolysis, which is the point, shown by arrow on the center temperature, when two simulation results start to cross each other, at around 25 seconds. The stage before pyrolysis is drying stage. At this stage, both the simulation result and the experimental result from Lu et al at the pellet center is higher than the temperature from this model. However, it is quite unlikely to have the pellet temperature to exceed 300 ℃ before the water fully evaporated. Therefore, even though the simulation result for the temperature at the pellet center is not close to the experimental data, the simulation results from this model might reflect the true situation inside the pellet. At the same time, the thermo-couple for the measurement, especially for the measurement of the center temperature shows quite an error. The small error might come from the random error, but the large error might come from the method error. In this case, the thermo-couple is placed at the pellet center for the temperature measurement; therefore, the heat from the pellet surface is conducted through the thermo-couple to the pellet center. Another obvious feature in Fig. 6 is that, after devolatilization, the temperature at the pellet center is higher than the temperature at the pellet surface. This phenomenon is similar to the simulation result from Haberle et al [47]. This is because the char combustion releases massive heat at the pellet center, while the heat exchange at the pellet surface keeps the pellet surface temperature identical to the environment temperature. The energy from the char combustion contributes to the temperature rise at the pellet surface at the very beginning. After that, the main heating source for the pellet surface is the radiation from the chamber and the convection from the hot air, both of them are below 1273 K.

While at the surface, the carbon oxidation reaction helps the temperature to increase rapidly at the beginning. More details of the char reaction rate can be found in Fig. 7.

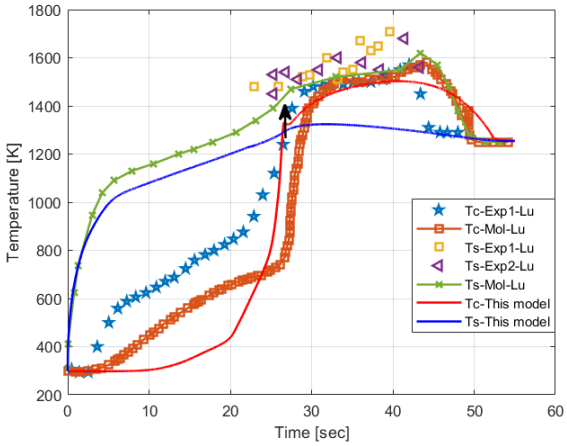

Fig. 6 Temperature validation with modelling and experimental results from Lu et al [27]

Figture 7 shows the detailed results from this model. Fig. 7 a) shows the gas species distribution at the pellet surface. At the pellet surface, the water evaporation starts immediately, whilst the oxygen and nitrogen mass fraction decrease. The moisture content vanishes at around 5 seconds. The concentration of other species, such as CO_2, CO, C_3H_8 and H_2 increases with the decrease in water vapor. The concentration of CO_2 starts to drop at around 3 seconds at the pellet surface, which is recognised as the point where heterogeneous reactions occur at the pellet surface. This finding is identical to that shown in Fig. 7 g) and h) : the reaction rate of carbon oxidation and the content of carbon reaches a peak after 3 seconds. Fig. 7 a) also shows that the concentration of CO drops at 26 seconds, whereas the concentration of CO_2 and O_2 increases. This means the carbon oxiation gets more intense with the increase in O_2 .

Fig. 7 g) shows the density of carbon during the smodering combustion at different locations in the pellet. The carbon density near the surface is less than the carbon density at the pellet center, which means that the carbon generation and carbon consumption happen simultaneously near the surface, which is mostly due to the higher temperature at the pellet surface. Fig. 7 c) and h) shows that the carbon reacts with CO_2, H_2O and O_2, respectively. The carbon oxidation reactions take place earlier than the other two heterogeneous reactions, which contributes to the temperature increase on the surface at the beginning. Since the reaction rate of carbon with CO_2 and H_2O is higher than the carbon oxidation rate, the temperature growth slows down after 3 seconds, where the carbon oxidation rate is lower than the reaction rate of the other two heterogeneous reactions. Fig. 7 h) shows the reaction rate of carbon oxidation. It reveals that the carbon oxidation happens layer by layer with the oxygen diffusion.

Fig 7 c) and d) shows the homogeneous reaction rate, which shows that most of the homogeneous reactions finish at around 26 seonds. This is the time where the biomass decomposition finishes and only carbon is left in the pellet. R8 denotes the reaction of CO oxidation, which is shown in Table 2. The CO in this reaction is from carbon oxidation, which is also shown in Table 2.

Fig. 7 e) and f) shows the pressure and velocity distribution. The pressure at the pellet surface remains identical to the environment pressure. The pressure at the pellet center is higher than the environment pressure due to the huge gas release from the devolitilization, after which, the pressure goes negative so that oxygen can penetrate into the pellet to oxidise with carbon. Similarly, the velocity is higher at the devolitilization stage and lower after that. The peaks of the velocities show up at different times for each

location. The tendency of the peak velocity happens where the sum of the reaction rate reaches the highest value.

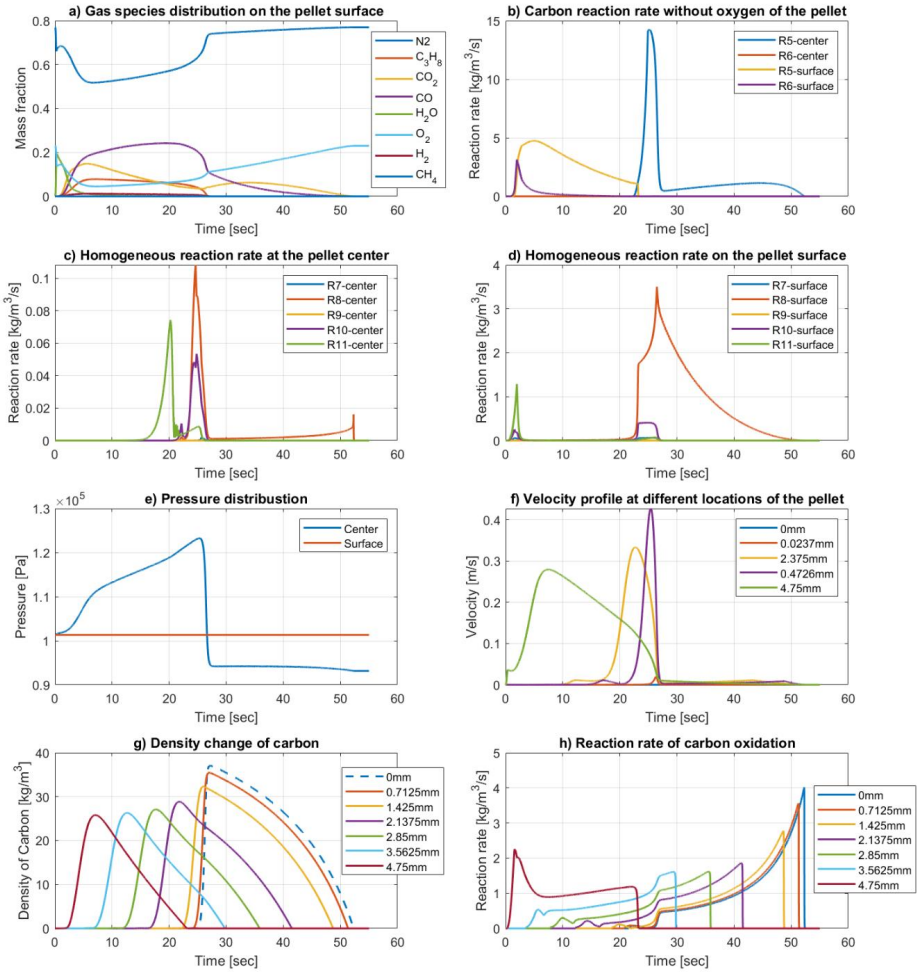

Fig.7 Result predicted from the simulation of this model

5. Parametric study

Many impact factor can influence the results of the simulation. Some of those can lead to wrong results. This paper focuses on the impact factor that can increase or moderate the whole smodering combustion process. In this paper, two most important factors are studied, the devolatilization rate and the genreal combuston mechanism for light hydrocarbons.

5.1 Impact of devolatilization rate

Yang et al [33] mentioned five devolatilization rates, from very slow to very fast. In this paper, three of them are studied, and the temperature at the pellet center is plotted in Fig. 8. The devolatilization rates are listed in Table 7.

Table 7 Devolatilization rate used in the parametric study

Kinetic data	Pyle and Zaror [33]	Alves and Figueiredo [33]	Nunn et al [33]
A (s^{-1})	3.0×10^3	7.0×10^4	3.4×10^4
E (kJ/mol)	69	83	69
Rating	Slow	Medium	Fast

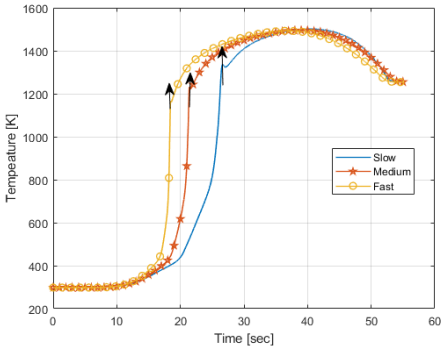

Fig. 8 Temperature profile at the pellet center with different devolatilization rate

Figure 8 shows the temperature at the pellet center after the devolitilizaion rates in Table 7 have been applied. It shows that the faster devolatilization rate leads to a shorter devolatilization time (the arrow marks where the devolitilization stage stops). However, the kinetic data used in the simulation does not affect the highest temperature in the simulation. The highest temperature that the smodering combustion can reach is still determined by carbon oxidation.

5.2 Impact from global hydrocarbon reaction schemes

The schemes of light hydrocarbon combustion are studied here. The reactions and kinetic data that are used in this model are shown in Table 2 and Table 3. The two-step mechanism only considers CO as the intermediate product, and the four-step mechanism considers CO and H_2 as intermediate products.

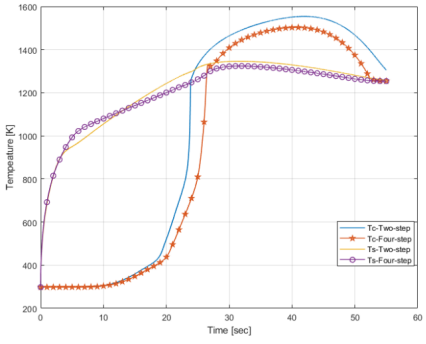

Fig. 9 Temperature profile by using two different hydrobarbon combustion mechanisms

Figure 9 shows the temperature profile after applying these two mechanisms to hydrocarbon combustion. There is little difference on the surface temperature from using two different hydrocarbon combustion mechanisms. For the center temperature, there is up to a 5% error between these two mechanisms. The possible reason is that the gas properties used in these two simulations are different. By using a two-step combustion mechanism, an assumed artifical hydrocarbon is used. The properties of the artifical hydrocarbon, such as the heat capacity, the conductivity and the viscosity are all represented by using data from a molecule of a similar structure and molecular mass. Whilst in the four-step mechanism simulation, all the gases are real, and the gas properties all exist. However, a 5% error is relatively low for a single biomass smodering combustion. Therefore, both the two-step combustion mechanism and the four-step combustion for the hydrocarbon combustion are reasonable.

6. Conclusion

This paper describes a detailed gasification model for a spherical solid fuel. The kinetic mechanism, the transport equations, the chemical reactions are considered in the model. A four-step reaction mechanism for volatile gasification is used in this model. Two validation results on gasification and smoldering combustion shows good agreement with the experimental data. Detailed results about smoldering combustion under air atmosphere are also presented. The results show that the model is reasonable for predicting the gas and temperature distribution. The right reaction rate, pressure distribution and velocity within the pellet can also be predicted. The results from the carbon combustion shows that the carbon is burnt layer by layer, and combustion rate is affected by both the existence of oxygen and carbon. The carbon reaction rate changes considerably at ignition and at the end of the combustion. The gas distribution is not only affected by temperature but also affected by diffusion and convection. The model also shows that the pressure is higher than the atmospheric pressure whenever there is a water vapor and volatile release, and the pressure is lower than the atmospheric pressure after the devolatilization. The sum of the reaction rates has a great impact with regard to the velocity changes.

Two parametric studies are presented in this paper. The impact of different devolatilization rate is studied. It shows that the higher devolatilization rate leads to an earlier end of the devolatilization process. In addition, the devolatilization rate has little impact on the temperature during char combustion.

The impact of the global hydrocarbon reaction schemes is also studied in this paper. Two global reaction schemes for hydrocarbon are studied, the two-step reaction mechanism from Dryer and Westbrook [19] and the four-step reaction mechanism from Jones and Lindstedt [20].

The impact of the hydrocarbon combustion mechanism scheme is shown at the end of the paper. The simulation result shows both schemes are effective in the simulation of a single biomass smoldering combustion. A maximum error of 5% is found between these two combustion schemes.

Acknowledgements

Xiyan Li are grateful to the help from department of energy technology of Aalborg University and support from Chinese scholarship council.

References

[1] EDE / UNEPlive n.d. http://geodata.grid.unep.ch/extras/graph_co2_concentration.php (accessed May 28, 2018).

[2] Xiong Q, Yang Y, Xu F, Pan Y, Zhang J, Hong K, et al. Overview of computational fluid dynamics simulation of reactor-scale biomass pyrolysis. ACS Sustain Chem Eng 2017;5:2783–98. doi:10.1021/acssuschemeng.6b02634.

[3] Kansa EJ., Perlee HE., Chaiken RF. Mathematical model of wood pyrolysis including internal forced convection. Combust Flame 1977;29:311–24. doi:10.1016/0010-2180(77)90121-3.

[4] Bamford CH, Crank J, Malan DH, Wilson AH. The combustion of wood. Part I. Math Proc Cambridge Philos Soc 1946;42:166. doi:10.1017/S030500410002288X.

[5] Thurner F, Mann U. Kinetic investigation of wood pyrolysis. Ind Eng Chem Process Des Dev 1981;20:482–8.

doi:10.1021/i200014a015.
[6] Pyle DL, Zaror CA. Heat transfer and kinetics in the low temperature pyrolysis of solids. Chem Eng Sci 1984;39:147–58. doi:10.1016/0009-2509(84)80140-2.
[7] Chan WCR, Kelbon M, Krieger BB. Modelling and experimental verification of physical and chemical processes during pyrolysis of a large biomass particle. Fuel 1985;64:1505–13. doi:10.1016/0016-2361(85)90364-3.
[8] Nunn TR., Howard JB., Longwell JP., Peters WA. Product compositions and kinetics in the rapid pyrolysis of sweet gum hardwood. Ind Eng Chem Process Des Dev 1985;24:836–44. doi:10.1021/i200030a053.
[9] Varhegyi G, Antal MJ, Szekely T, Szabo P. Kinetics of the thermal decomposition of cellulose, hemicellulose, and sugarcane bagasse. Energy & Fuels 1989;3:329–35. doi:10.1021/ef00015a012.
[10] Kovfopanos CA, Maschio G, Lucchesi A. Kinetic modelling of the pyroysis of biomass and biomass components. Can J Chem Eng 1989;67:75–84. doi:10.1002/cjce.5450670111.
[11] Font R, Marcilla A, Verdu E, Devesa J. Kinetics of the pyrolysis of almond shells and almond shells impregnated with cobalt dichloride in a fluidized bed reactor and in a pyroprobe 100. Ind Eng Chem Res 1990;29:1846–55. doi:10.1021/ie00105a016.
[12] Wagenaar BM, Prins W, van Swaaij WPM. Flash pyrolysis kinetics of pine wood. Fuel Process Technol 1993;36:291–8. doi:10.1016/0378-3820(93)90039-7.
[13] Font R, Marcilla A, Devesa J, Verdu E. Kinetic study of the flash pyrolysis of almond shells in a fluidized bed reactor at high temperatures. J Anal Appl Pyrolysis 1993;27:245–73. doi:10.1016/0165-2370(93)80012-O.
[14] Di Blasi C. Heat, momentum and mass transport through a shrinking biomass particle exposed to thermal radiation. Chem Eng Sci 1996;51:1121–32. doi:10.1016/S0009-2509(96)80011-X.
[15] Branca C, Albano A, Di Blasi C. Critical evaluation of global mechanisms of wood devolatilization. Thermochim Acta 2005;429:133–41. doi:10.1016/j.tca.2005.02.030.
[16] Mahmoudi AH, Hoffmann F, Peters B. Detailed numerical modeling of pyrolysis in a heterogeneous packed bed using XDEM. J Anal Appl Pyrolysis 2014;106:9–20. doi:10.1016/j.jaap.2013.12.001.
[17] Haseli Y, van Oijen JA, de Goey LPH. A detailed one-dimensional model of combustion of a woody biomass particle. Bioresour Technol 2011;102:9772–82. doi:10.1016/j.biortech.2011.07.075.
[18] Gronli MG, Melaaen MC, Grønli M, Melaaen MC. Mathematical model for wood pyrolysis - Comparison of experimental measurements with model predictions. Energy & Fuels 2000;14:791–800. doi:10.1021/ef990176q.
[19] Dryer FL, Westbrook CK. Simplified reaction mechanisms for the oxidation of hydrocarbon fuels in flames. Combust Sci Technol 1981;27:31–43. doi:10.1080/00102208108946970.
[20] Jones WP, Lindstedt RP. Global reaction schemes for hydrocarbon combustion. Combust Flame 1988;73:233–49. doi:10.1016/0010-2180(88)90021-1.
[21] Laurendeau NM. Heterogeneous kinetics of coal char gasification and combustion. Proc. energy Combust. Sci., vol. 7, 1978, p. 2447–50. doi:doi.org/10.1016/0360-1285(78)90008-4.
[22] Vaclav B, Macak J, Klose E, Jirl M. Mathematical model for the gasification of coal under pressure. Ind Eng Chem Process Des Dev 1978;17:92–8. doi:10.1016/0016-2361(93)90662-L.
[23] Yoon H, Wei J, Denn M. A model for moving bed coal gasification reactors. AIChE J 1978;24:885–903. doi:10.1002/aic.690240515.
[24] Evans DD, Emmons HW. Combustion of wood charcoal. Fire Saf J 1977;1:57–66. doi:10.1016/0379-7112(77)90008-X.
[25] Di Blasi C. Modeling and simulation of combustion processes of charring and non-charring solid fuels. Prog Energy Combust Sci 1993;19:71–104. doi:10.1016/0360-1285(93)90022-7.
[26] Di Blasi C. Combustion and gasification rates of lignocellulosic chars. Prog Energy Combust Sci 2009;35:121–40. doi:10.1016/j.pecs.2008.08.001.
[27] Lu H, Robert W, Peirce G, Ripa B, Baxter LL. Comprehensive study of biomass particle combustion. Energy and Fuels 2008;22:2826–39. doi:10.1021/ef800006z.
[28] Lee YR, Choi HS, Park HC, Lee JE. A numerical study on biomass fast pyrolysis process: A comparison between full lumped modeling and hybrid modeling combined with CFD. Comput Chem Eng 2015;82. doi:10.1016/j.compchemeng.2015.07.007.
[29] Mehrabian R, Zahirovic S, Scharler R, Obernberger I, Kleditzsch S, Wirtz S, et al. A CFD model for thermal conversion of thermally thick biomass particles. Fuel Process Technol 2012;95:96–108. doi:10.1016/j.fuproc.2011.11.021.
[30] Mehrabian R, Zahirovic S, Scharler R, Obernberger I, Kleditzsch S, Wirtz S, et al. A CFD model for thermal conversion of thermally thick biomass particles. Fuel Process Technol 2012;95:96–108. doi:10.1016/j.fuproc.2011.11.021.
[31] Momeni M, Yin C, Kær SK, Hvid SL. Comprehensive study of ignition and combustion of single wooden particles. Energy & Fuels 2013;27:1061–72.
[32] Mehrabian R, Shiehnejadhesar A, Scharler R, Obernberger I. Multi-physics modelling of packed bed biomass

combustion. Fuel 2014;122:164–78. doi:10.1016/j.fuel.2014.01.027.
[33] Yang YB, Yamauchi H, Nasserzadeh V, Swithenbank J. Effects of fuel devolatilisation on the combustion of wood chips and incineration of simulated municipal solid wastes in a packed bed. Fuel 2003;82:2205–21. doi:10.1016/S0016-2361(03)00145-5.
[34] Bu C, Liu D, Chen X, Pallarès D, Gómez-Barea A. Ignition behavior of single coal particle in a fluidized bed under O2/CO2and O2/N2 atmospheres: A combination of visual image and particle temperature. Appl Energy 2014;115:301–8. doi:10.1016/j.apenergy.2013.10.040.
[35] Bu C, Leckner B, Chen X, Pallarès D, Liu D, Gómez-Barea A. Devolatilization of a single fuel particle in a fluidized bed under oxy-combustion conditions. Part B: Modeling and comparison with measurements. Combust Flame 2015;162:797–808. doi:10.1016/j.combustflame.2014.08.015.
[36] Blasi C Di. Dynamic behaviour of stratied downdraft gasifiers. Chem Eng Sci 2000;55:2931–44. doi:doi.org/10.1016/S0009-2509(99)00562-X.
[37] Di Blasi C. Modeling wood gasification in a countercurrent fixed-bed reactor. AIChE J 2004;50:2306–19. doi:10.1002/aic.10189.
[38] Yin C, Kær SK, Rosendahl L, Hvid SL. Co-firing straw with coal in a swirl-stabilized dual-feed burner: Modelling and experimental validation. Bioresour Technol 2010;101:4169–78. doi:10.1016/j.biortech.2010.01.018.
[39] Jones WP, Lindstedt RP. Global reaction schemes for hydrocarbon combustion. Combust Flame 1988;73:233–49. doi:10.1016/0010-2180(88)90021-1.
[40] Channiwala S. A., Parikh P. P. A unified correlation for estimating HHV of solid, liquid and gaseous fuels. Fuel 2002;81:1051–63. doi:10.1016/S0016-2361(01)00131-4.
[41] Sharma A, Pareek V, Zhang D. Biomass pyrolysis - A review of modelling, process parameters and catalytic studies. Renew Sustain Energy Rev 2015;50. doi:10.1016/j.rser.2015.04.193.
[42] Yang Y Bin, Ryu CK, Sharifi VN, Swithenbank J. Effect of model and operating parameters on air gasification of char. Energy and Fuels 2006;20:1698–708. doi:10.1021/ef060036y.
[43] Bu C, Leckner B, Chen X, Pallarès D, Liu D, Gómez-barea A. Devolatilization of a single fuel particle in a fluidized bed under oxy-combustion conditions . Part A : Experimental results. Combust Flame 2015;162:797–808. doi:10.1016/j.combustflame.2014.08.015.
[44] Teklay A. Aalborg Universitet CFD Modelling and Experimental Testing of Thermal Calcination of Kaolinite Rich Clay Particles - An Effort towards Green Concrete Abraham Teklay Gebremariam Dissertation submitted to the faculty of Engineering and Science Department of. Aalborg university, 2015.
[45] Teklay A, Yin C, Rosendahl L, Bøjer M. Cement and Concrete Research Calcination of kaolinite clay particles for cement production : A modeling study. Cem Concr Res 2014;61–62:11–9. doi:10.1016/j.cemconres.2014.04.002.
[46] Li X, Yin C. A drying model for thermally large biomass particle pyrolysis. Energy Procedia, vol. 158, Elsevier Ltd; 2019, p. 1294–302. doi:10.1016/j.egypro.2019.01.322.
[47] Haberle I, Haugen NEL, Skreiberg Ø. Combustion of Thermally Thick Wood Particles: A Study on the Influence of Wood Particle Size on the Combustion Behavior. Energy and Fuels 2018;32:6847–62. doi:10.1021/acs.energyfuels.8b00777.

Paper D

Description of a comprehensive mathematical model: towards a comprehensive biomass particle gasification model

Xiyan Li, Chungen Yin

The paper has been published in the
Proceedings of the 25th European Biomass Conference & Exhibition, EUBCE2017
pp.853-859, 2017.

The layout has been revised.

DESCRIPTION OF A COMPREHENSIVE MATHEMATICAL MODEL: TOWARDS A COMPREHENSIVE BIOMASS PARTICLE GASIFICATION MODEL

Xiyan Li, Chungen Yin
Department of Energy Technology, Aalborg University, Pontoppidanstraede 111, 9220 Aalborg East, Denmark
Email: xli@et.aau.dk

ABSTRACT: Biomass gasification is still a promising technology after over 30 years' research and development and has success only in a few niche markets. In this paper, a comprehensive mathematical model for biomass particle gasification is developed within a generic particle framework, assuming the feed is a woody biomass pellet. The particle is discretized into a number of cells along radical direction, on each of which the gas governing equations are numerically solved by using the finite volume method (FVM). FVM is used to solve transport equations of each process. All the key processes, e.g., moisture evaporation, pyrolysis, heterogeneous char reactions, intra-particle heat and mass transfer, and changes in thermos-physical properties and so on, are properly taken into account to update the densities of various solid/liquid components in each cell as well as to provide source terms to the relevant gas-phase governing equations. For the source term, different chemical reactions are assumed, the density, the species, the velocity, the temperature changes, the size of pellet, et al. will be studied and calculated in the end of the project.
Keywords: Biomass, Gasification, modelling.

1 INTRODUCTION

Biomass gasification has received unprecedented attention, as a renewable source of energy and chemicals. In biomass gasification, biomass pyrolysis is a key, inseparable initial sub-process, resulting in a complex system of intermediate products (or product groups: gases, tars and char). Then the gases and tar vapors undergo further gas-phase reactions (e.g., cracking, reforming, shift) whilst the char takes part in heterogeneous reactions, yielding the final gasification products. Partly due to government regulation and partly due to unsolved technological hurdles (e.g., lack of reliable modelling tool for biomass pyrolysis/gasification, lack of dominant design, fuel flexibility, efficiency, tar reduction, gas cleaning, scaling up), biomass gasification is still a promising technology after over 30 years' research and development (R&D) and has success only in a few niche markets [1].

On the other hand, with the fast consumption of fossil fuels, appealing from the public for looking for renewable resources is stronger and stronger. Biomass, as one of the readily available renewable resources, come to public view.

According to Danish Energy Agency (DEA) [2], the use of wood pellets and wood chips increase significantly this century. In Fig. I and Fig. II, we can see that solid biomass consumption is not only increase in Denmark, but also increase in the whole west Europe. In Fig. II, a prediction of the next ten years was given, we can see in 10 years, demand for wood pellets will be more than doubled, but demand for straw and biodegradable waste will keep almost the as the same stage as now.

Biomass has many benefits. Firstly, biomass is flexibly in technology [3], for biomass gasification on syngas generation, it has a wide option of choosing biomass species. Secondly, Biomass is clean renewable energy [4]. During the gasification, the CO_2, SO_2 and other harmful gas emissions are less compared to fossil fuel, the emissions are less even compared with the emission from producing photovoltaic cell materials [5]. Lastly but not least, the temperature for gasification is relative low, which is around 700℃- 900℃ [6]. Around that temperature, NO_x generation can be ignored.

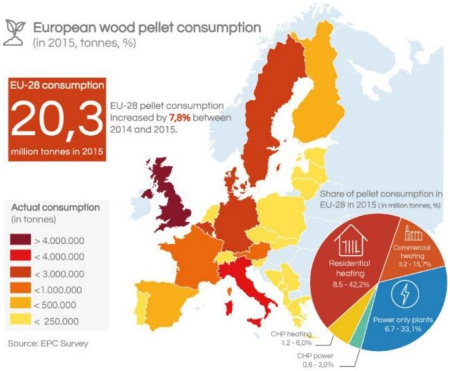

Figure I Use of solid biomass in Europe in 2015 [7]

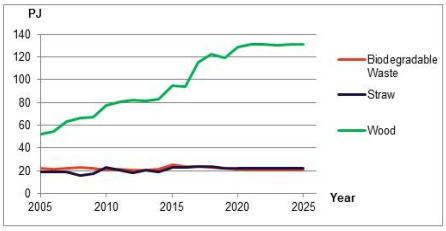

Figure II Use of solid biomass in electricity and heat production 2005-2015, and projection to 2025 [3]

There are also some defects using biomass transformation technology. The first and foremost is biomass syngas is a low value fuel (aroud 6～10 MJ/Nm^3) [8]. For syngas, the tar and alkali inside the gas may ruin the device if it goes into gas turbine directly after gasification [9].

As a result of these reasons, there has been a compelling need for reliable, cost-effective modelling tools for the design of biomass pyrolysis/gasification processes and components. Using CFD simulation is one of the most popular methods.

Many scholars worked on this field and gain remarkable achievements. Bamford [10] started to use mathematic method for solving a single sheet of wood combustion problem at an early stage. After that, around eighties and nineties of last century and the beginning of this century, there is a great heat for kinetics study. Font[11][12], Di Blasi [13][14][15][16], Babu [17][18] are all active at working on that. Kinetic equations for mechanism were discussed, experimental data from different scholars using different technologies were compared. Until recently, most kinetic parameters used are from that time [19][20][21]. After the kinetic mechanism study, next step is to build a reliable mathematical model for the whole reaction process. As a young pioneer, Di Blasi started the exploration with using mathematical model [3], actually she stated this based on cellulose pyrolysis [16] and combustion of conceptual solid fuels [15]. She kept modifying this model and use it at different reactors [22]. Other researchers contribute to fertilize biomass gasification, combustion and pyrolysis under different assumptions. Bernhard [23] and Wu[24] studied their objects with solid phase and gas phase separated. An imaginary heat and mass transfer between phases were assumed. Haseli [25] compared his simulation results with former researchers according to different size. H.Fatehi [26] built his model based on one dimentional single large biomass particle combustion without particle size changes. Lu [21] [27][28] did a systematic study based one biomass pellet combustion with a fixed mass and heat transfer coefficient in ambient flow.

In order to make use of these advantages of biomass, as well as to decrease the defects as much as possible, a reliable mathematical model is still in need. This project try to combine the work of predecessors together, at the same time, to remove the defects and to consummate mathematical model. In this article, it mainly focus on consummating source term of reaction and revising transport equations. A brief case of using FVM to solve PDE is given in the end.

2 MODEL DESCRIPTION

2.1 Assumptions:

In order to make the best use of the theories and correlations, as well as to make the simulation results more credible, assumptions are necessary. In this paper, a one-dimensional mathematics model based on a single biomass pellet under gasification is assumed.

(1) Assuming the biomass pellet shape is nearly sphere.
(2) Assuming the biomass particle is in local thermal equilibrium.
(3) During the reaction, the biomass particle is considered as a porous structure media, and the gases generated inside the particle obey ideal gas law.
(4) The specific surface area changes during the whole gasification, thus shrinkage or swelling is also considered.
(5) The airflow inside the particle obeys Darcy law.
(6) Boundary layer thickness exist. And its outer surface properties equal to those in outer spaces, inner surface properties equal to those in the surface of particle.
(7) External forces are not considered.
(8) There is no fragmentation of the particle during the whole gasification.

Fig. III gives out the key issue to be solved in this project. There three key issues, which is very important during the calculation: the heat and mass transfer of boundary between gas phase and solid phase, the conversion process inside the particle itself, and the particle size changes during the whole reaction process.

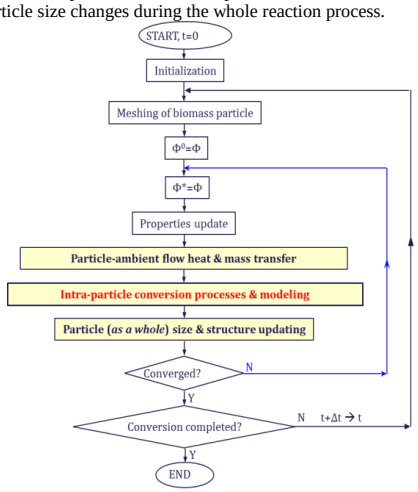

Figure III Key issue to be solved

It is also necessary to assume the right reaction during the gasification process. Thirteen chemical reactions happened inside the pellets are considered, as showing in table I. In table I, the reaction rate is also given. It is worth noting that:

$$K_i = A_i \exp(-E/RT)$$

K_i is the kinetic rate coefficients for all the reactions in table I. A is pre-exponential factor and E is activation energy. It is only dependent on temperature. The whole expression is called as Arrhenius expression.

Table I: Reactions

Reaction index	Chemical reactions	Rate expression	Ref.
1	biomass→gases	$r_1 = \partial\rho_B/\partial t = k_1\rho_B$	[28]
2	biomass→tar	$r_2 = \partial\rho_B/\partial t = k_2\rho_B$	[28]
3	biomass→char	$r_3 = \partial\rho_B/\partial t = k_3\rho_B$	[28]
4	tar→gases	$r_4 = \partial\rho_g/\partial t = k_4\rho_g Y_T$	
5	tar→char	$r_5 = \partial\rho_c/\partial t = k_5\rho_g Y_T$	
6	H_2O (free)→ H_2O (g)	$r_6 = \partial\rho_{fw}/\partial t = s_a(\rho_{fw}/\rho_{fw}^0)h_{m,pore}(\rho_\vartheta^{sat} - Y_{V\rho g})$	[28]
7	H_2O(bound)→H_2O (g)	$r_7 = \partial\rho_{bw}/\partial t = k_7\rho_{bw}$	[29]

8	$C+1/2O_2 \rightarrow CO$	$r_8 = \partial C_{O_2}/\partial t = s_{a,char}[\rho_C/(\rho_C+\rho_B+\rho_A)]k_8 C_{O_2}$	[30]
9	$C+O_2 \rightarrow CO_2$	$r_9 = \partial C_{O_2}/\partial t = s_{a,char}[\rho_C/(\rho_C+\rho_B+\rho_A)]k_9 C_{O_2}$	
10	$C+CO_2 \rightarrow 2CO$	$r_{10} = \partial C_{CO_2}/\partial t = s_{a,char}[\rho_C/(\rho_C+\rho_B+\rho_A)]k_{10} C_{CO_2}$	
11	$C+H_2O \rightarrow CO+H_2$	$r_{11} = \partial C_{H_2O}/\partial t = s_{a,char}[\rho_C/(\rho_C+\rho_B+\rho_A)]k_{11} C_{H_2O}$	[28]
12	$C+2H_2 \rightarrow CH_4$	$r_{12} = \partial C_{H_2}/\partial t = s_{a,char}[\rho_C/(\rho_C+\rho_B+\rho_A)]k_{12} C_{H_2}$	
13	$CO+1/2O_2 \rightarrow CO_2$	$r_{13} = -\partial C_{CO}/\partial t = -k_{13} C_{CO} C_{O_2}^{0.25} C_{H_2O}^{0.5}$	
14	$H_2+1/2O_2 \rightarrow H_2O$	$r_{14} = -\partial H_2/\partial t = -k_{14} C_{H_2} C_{O_2}^{0.5}$	
15	$CH_4+2O_2 \leftrightarrow CO_2+2H_2O$	$r_{15} = -\partial CH_4/\partial t = -(k_{15} C_{CH_4} C_{O_2}^2 - \overleftarrow{K_{15}} C_{CO_2} C_{H_2O}^2)$	
16	$CO+H_2O \leftrightarrow CO_2+H_2$	$r_{16} = -\partial CO/\partial t = -(k_{16} C_{CO} C_{H_2O} - \overleftarrow{K_{16}} C_{CO_2} C_{H_2})$	
17	$CO+H_2 \rightarrow 1/2CO_4+1/2CO_2$	$r_{17} = -\partial CO/\partial t = -k_{17} C_{H_2} C_{CO}$	
18	$CO+3H_2 \leftrightarrow CH_4+H_2O$	$r_{18} = -\partial CO/\partial t = -(k_{18} C_{CO} C_{H_2}^3 - \overleftarrow{K_{18}} C_{CH_4} C_{H_2O})$	
19	$CO+4H_2 \rightarrow CH_4+2H_2O$	$r_{19} = -\partial CO/\partial t = -(k_{19} C_{H_2}{}^4 C_{CO} - \overleftarrow{K_{19}} C_{CH_4} C_{H_2O}^2)$	
20	$CH_4+H_2O \leftrightarrow CO+3H_2$	$r_{20} = -\partial CH_4/\partial t = -(k_{20} C_{CH_4} C_{H_2O} - \overleftarrow{K_{20}} C_{CO} C_{H_2}{}^3)$	
21	$CH_4+0.5O_2 \rightarrow CO+2H_2$	$r_{21} = -\partial CH_4/\partial t = -k_{21} C_{CH_4} C_{O_2}^{0.5}$	

2.2 Biomass gasification process and meshing

Flow chart of biomass gasification is given in Fig. IV. The virgin biomass is put into the reactor, with the temperature growing up, different reactions happens. As we see from Fig. III, at low temperature, it is mainly vaporization happening, during which process, free water coming out first, when the temperature is higher than 100℃, hydrate water comes out. With temperature increasing, pyrolysis happens, during which process, biomass cracking into different species. These species keep cracking, finally small molecule gases and tar generate. During gasification process, which happens at much higher temperature, tar keep cracking into gases, and vapor may combine with these gas phase and solid phase to generate new species. Mainly the homogeneous and heterogeneous reactions happen in this stage.

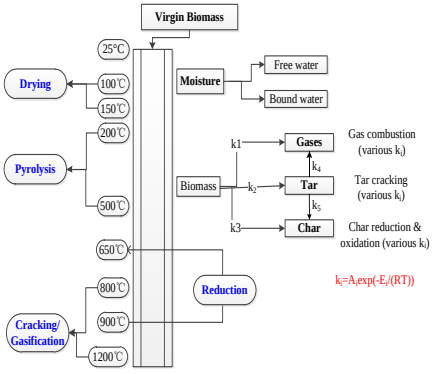

Figure IV Flow chart of biomass gasification

2.2 For boundary conditions

For all the N nodes we set in the control volume, there should be (N-1) partial differential equations for solving all the transport equations. Apparently, there is one equation missing for mass and energy equilibrium. Therefore the imaginary gas film Fig. V in between the solid and outside condition is crucial for deciding the heat and mass transport. Within each time step, the boundary conditions for mass and energy equation are shown in Table II.

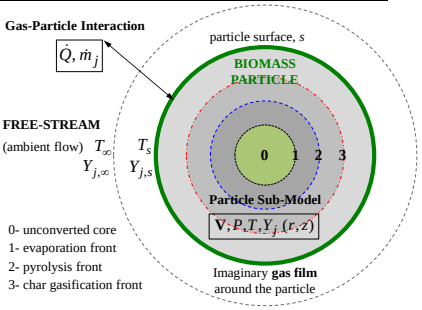

Figure V A conceptual view of the interaction of a large biomass particle with ambient flow and its conversion.

The h_T and h_M in the boundary condition is solved by Ranz-Marshall [31] model, with the following expression:

$$Nu \equiv \frac{h_T L_c}{k_g} = 2.0 + 0.6 Re^{1/2} Pr^{1/3}$$

$$Sh \equiv \frac{h_M L_c}{D_g} = 2.0 + 0.6 Re^{1/2} Sc^{1/3}$$

The reference temperature and species used in the boundary obey the one – third law [32]:

$$T_{ref} = T_s + 1/3\,(T_\infty - T_s)$$

$$Y_{j,ref} = T_{j,s} + 1/3\,(T_{j,\infty} - T_{j,s})$$

3 TRANSPORT EQUATIONS

3.1 Description of all transport equations

Partial differential equations (PDE) are used here to calculate all the result derived in the model. The general transport equations of different species are described as below:

$$\frac{\partial}{\partial t}(\varepsilon\rho\phi) + div(\rho\vec{u}\phi) = div(\rho\Gamma\nabla\phi) + S$$

ϕ can be any term we want to solve, for example temperature, pressure, density, species etc.

The first term is transient term, which represent the changing rate for unsteady flow, the second term is convection term, the third one is diffusion term and the last one is source term.

Table II: Transport equations

Density	
Biomasss	$\partial\rho_B/\partial t = S_B$ $S_B = -(r_1 + r_2 + r_3)$
Char	$\partial\rho_C/\partial t = S_C$ $S_C = r_3 + r_5 - r_8\frac{2M_C}{M_{O_2}} - r_9\frac{M_C}{M_{O_2}} - r_{10}\frac{M_C}{M_{CO_2}} - r_{11}\frac{M_C}{M_{H_2O}} - r_{12}\frac{M_C}{2M_{H_2}}$
Moisture	$\partial\rho_w/\partial t = \frac{\partial}{\partial r}\left(D_{eff,water}\frac{\partial\rho_{water}}{\partial r}\right) + S_{water}$ $S_{water} = -r_6 - r_7$
Ash	$\partial\rho_A/\partial t = 0$
Continuity equations	$\frac{\partial}{\partial t}(\varepsilon\rho_g) + div(\rho_g\vec{u}) = s_g$ $s_g = r_1 + r_2 - r_5 + r_6 + r_7 + r_8\frac{2M_C}{M_{O_2}} + r_9\frac{M_C}{M_{O_2}} + r_{10}\frac{M_C}{M_{CO_2}} + r_{11}\frac{M_C}{M_{H_2O}} + r_{12}\frac{M_C}{2M_{H_2}}$
Species transfer equations	$\frac{\partial}{\partial t}(\epsilon\rho_g Y_j) + div(\rho_g\vec{u}Y_j) = div(\rho_g D_{j,m}\nabla Y_j) + S_{Y,j}$ Source terms for gas species: $S_{co_2} = r_9\frac{M_{CO_2}}{M_{O_2}} - r_{10} + r_{13}\frac{M_{CO_2}}{M_{CO}} + r_{15}\frac{M_{CO_2}}{M_{CH_4}} + r_{16}\frac{M_{CO_2}}{M_{CO}} + r_{17}\frac{M_{CO_2}}{2M_{CO}} + (r_1 + r_4)\alpha_{CO_2}$ $S_{CO} = r_8\frac{2M_{CO}}{M_{O_2}} + r_{10}\frac{2M_{CO}}{M_{CO_2}} + r_{11}\frac{M_{CO}}{M_{H_2O}} - r_{13} - r_{16} - r_{17} - r_{18} - r_{19} + r_{20}\frac{M_{CO}}{M_{CH_4}} +$ $r_{21}\frac{M_{CO}}{M_{CH_4}} + (r_1 + r_4)\alpha_{CO}$ $S_{O_2} = -r_8 - r_9 - r_{14}\frac{M_{O_2}}{2M_{H_2}} - r_{15}\frac{2M_{O_2}}{M_{CH_4}} - r_{21}\frac{M_{O_2}}{M_{CH_4}}$ $S_{H_2} = (r_1 + r_4)\alpha_{H_2} + r_{11}\frac{M_{H_2}}{M_{H_2O}} - r_{12} - r_{14}\frac{M_{O_2}}{2M_{H_2}} + r_{16}\frac{M_{H_2}}{M_{CO}} - r_{17}\frac{M_{H_2}}{M_{CO}} - r_{18}\frac{3M_{H_2}}{M_{CO}} -$ $r_{19}\frac{4M_{H_2}}{M_{CO}} + r_{20}\frac{3M_{H_2}}{M_{CO}} + r_{21}\frac{2M_{H_2}}{M_{CO}}$ $S_{H_2O} = (r_1 + r_4)\alpha_{H_2O} + r_6 + r_7 - r_{11} + r_{14}\frac{M_{H_2O}}{M_{H_2}} + r_{15}\frac{2M_{H_2O}}{M_{CH_4}} - r_{16}\frac{M_{H_2O}}{M_{CO}} +$ $r_{18}\frac{M_{H_2O}}{M_{CO}} + r_{19}\frac{2M_{H_2O}}{M_{CO}} - r_{20}\frac{M_{H_2O}}{M_{CH_4}}$ $S_{CH_4} = r_2 + (r_1 + r_4)\alpha_{CH_4} + r_{12}\frac{M_{CH_4}}{2M_{H_2}} - r_{15}\frac{M_{CH_4}}{2M_{O_2}} + r_{17}\frac{M_{CH_4}}{2M_{CO}} + r_{18}\frac{M_{CH_4}}{M_{CO}} + r_{19}\frac{M_{CH_4}}{M_{CO}} -$ $r_{20}\frac{M_{CH_4}}{M_{H_2O}} - r_{21}\frac{2M_{CH_4}}{M_{O_2}}$ $S_{N_2} = 0$
Energy equations	$\frac{\partial}{\partial t}\left(\sum_{s,i}\rho_i h_i + \sum_{l,k}\rho_k h_k + \rho_g h_{mix}\right) + div(\rho_g\vec{u}h) = div(k_{eff}\nabla T) +$ $div\left(\sum_j h_j\rho_g D_{j,m}\nabla Y_j\right) + S_h$ $h \triangleq \sum_j h_j Y_j$ $h_j = \int_{T_{ref}}^{T} C_{p,j}(T)dT$ $S_h = -\sum_{k=1}^{N}\Delta h_{f,k}^0\dot{w}_k = \sum_{k=1}^{N}\Delta h_{R,k}\dot{w}_k$
Darcy law Ideal gas law	$u = -\frac{k}{\mu}\frac{\partial p}{\partial x}$ $p = \frac{\rho_g RT}{W_g}$
Boundary conditions	Outer face: $D_{j,m}A_s\frac{\partial Y_{i(j,k)}}{\partial r}\Big\vert_{r=r_p} = h_m A_s\left(Y_{i(j,k),\infty} - Y_{i(j,k),s}\right)$ $k_{eff}A_s\frac{\partial T}{\partial r}\Big\vert_{r=r_p} = h_T A_s\left(T_f - T\right) + A_s\omega\sigma(T_w^4 - T^4)$ Inner face: $\frac{\partial\phi}{\partial r}\Big\vert_{r=0} = 0\,, u = 0, P = P_{atm,}\, T = 298K, Y_j = 0$
Initial conditions	Outer face: $T_\infty = T_f, u_\infty = u_f, Y_{O_2,\infty} = 0.23, Y_{N_2,\infty} = 0.77, P_\infty = P_{atm}$

3.2 Discretized form of PDEs

Integrate all these partial differential equations and then discrete it into discretized equations which can be easily solved by Tri-diagonal matrix algorithm (TDMA). Geometry of a simple case using central differential method for discretion is shown in Fig. VI. P is the central

point of each node, while W and E represent the west face and east face. w and e represent the centers of west and east face. W and E are located in the center of previous point and the next point separately. In central differential method, the distance between each point is the same. For the transient term, a weighting parameter θ is chosen as zero during the integration, as a typical form of fully implicit scheme.

A typical discretized form PDEs using central differential method and fully implicit scheme is as shown below.

$$a_p \emptyset_p = a_w \emptyset_w + a_e \emptyset_e + a_P^0 \emptyset_P^0 + b$$

4. UPDATING STRUCTURE

Shrinking or swelling happens during gasification process. In this project, empirical parameters were used to calculate the size change. The shrinking factor θ has following expression:

$$\theta = V_P/V_{p,0} = (d_p)^3/(d_{p,0})^3 = 1 + (1-\theta_m)\left(\frac{\rho_m}{\rho_{m,0}} - 1\right) + \theta_m(1-\theta_v)\left(\frac{\rho_m}{\rho_{m,0}} - 1\right) + \theta_m\theta_v(1-\theta_c)\left(\frac{\rho_c}{\rho_{c,0}} - 1\right)$$

θ_m, θ_v, θ_c represent three empirical shrinking factors of moisture, volatile and char.

Particle porosity ε is connected to size change as below:

$$\frac{\partial \varepsilon}{\partial t} = \frac{1}{\rho_{true}} \sum_k \vartheta_{c,k} \omega_k - \frac{\varepsilon}{\theta}\frac{\partial \theta}{\partial t}$$

ω_k is reaction rate of char reaction k,

$\vartheta_{c,k}$ is the stoichiometric coefficient of char in reaction k,

ρ_{true} is solid density without porous.

5. A SIMPLE CASE OF USING FVM

Given the complexity of solving such a highly coupled mathematical equations in this model. At this stage, a simple example is stated here about how to use central differential scheme to solve a transient convection diffusion equation with a source term.

The followings are the main descriptions of this problem.

$t > 0;\ a = -200, b = 100;\ x_1 = 0.6, x_2 = 0.2;$

$T = 0, x = 0;\ \frac{\partial T}{\partial x} = 0, x = L;$

$L = 1.5, u = 2.0, \rho = 1.0, \Gamma = 0.03$

Following are the numerical description:

$$\frac{\partial(\rho T)}{\partial t} + \frac{\partial(\rho u T)}{\partial x} = \frac{\partial}{\partial x}\left(\Gamma \frac{\partial T}{\partial x}\right) + S$$

For S, there are:

$0 < x \le 0.6, S = 100 - 200x;$

$0.6 < x \le 0.8, S = 100x - 80;$

$0.8 < x \le 1.5, S = 0$

The discretized form of transport equations are:

$AE[i] = D - F/2$

$AW[i] = D + \frac{F}{2}$

$AP[i] = AW[i] + AE[i] + ap\_0$

$dx = \frac{Lmax - Lmin}{NR}$

$D = (\Gamma)/dx$

$F = \rho * U$

$ap\_0 = \rho * dx/dt$

At boundary nodes, the coefficients of equations are:

At the first node:

$AW[0] = 0$

Here are all the PDEs, and there discretized form:

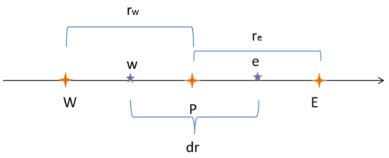

Figure. VI Geometry of a simple example

$AP[0] = AW[0] + AE[0] + ap\_0 + F + 2 * D$

At the last node:

$AE[NR-1] = 0$

$AP[NR-1] = AW[NR-1] + AE[NR-1] + ap_0$

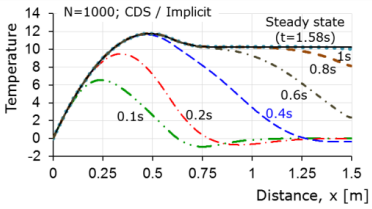

Figure VI Comparison of analytical solution and numerical solution based on a simple case

Fig. VI shows the final results from analytical and numerical calculation. A discretized grids N=1000 is taken. The solid black line is the result from analytical solution. The different dash lines show the result calculated from numerical solution with time from t=0.1s, 0.2s, 0.4s, 0.6s, 0.8s, 1s and 1.58s. Compared the blue dash line with the solid line, it is easy to find that the results from using FVM is almost the same with using analytical solution.

In another way, since using FVM can solve a fully general transport equation. It should be capable of solving a sequence of highly coupled similar transport equations. And with the best expectation, a similar overlap should be found between numerical calculation and experimental results.

6. CONCLUSIONS

Biomass gasification is processing technology in the future. Although a lot of work both in simulation and in experiments has been done in this area. There are still many issues waiting ahead. The key conclusions from this project are summarized below:

(1) Briefly summarizing the development of modelling of biomass gasification in state of arts.

(2) A relatively integral mathematical model is given in this paper. All the twenty one chemical reactions and their reaction rates are given. The key transport equations of a single biomass pellet during gasification is presented.

(3) Analytical solution and numerical solutions from a fully general transport equations are compared. Highly overlapping between an analytical solution and a stable state of numerical solution certify the

possibility of using central differential scheme to solve complete mathematical questions.

7. REFERENCES

[1] Kirkels AF, Verbong GPJ. Biomass gasification: Still promising? A 30-year global overview. Renew Sustain Energy Rev 2011;15:471–81.

[2] Danish Energy Agency. Biomass. Danish Energy Agency (DEA) 2017. https://ens.dk/en/our-responsibilities/bioenergy/solid-biomass (accessed April 13, 2017).

[3] Di Blasi C. Influences of physical properties on biomass devolatilization characteristics. Fuel 1997;76:957–64.

[4] Sadhukhan AK, Gupta P, Saha RK. Modelling and experimental studies on pyrolysis of biomass particles. J Anal Appl Pyrolysis 2008;81:183–92.

[5] EPC - Engineering Procurement Construction News. Are Solar PV Farms Polluting? - Electronics For You n.d. http://aworldgate.over-blog.com/2016/04/are-solar-pv-farms-polluting-electronics-for-you.html (accessed April 13, 2017).

[6] Kuo PC, Wu W, Chen WH. Gasification performances of raw and torrefied biomass in a downdraft fixed bed gasifier using thermodynamic analysis. Fuel 2014.

[7] Katie Fletcher. European Biomass Association releases 2016 bioenergy outlook | Biomassmagazine.com n.d. http://biomassmagazine.com/articles/13837/european-biomass-association-releases-2016-bioenergy-outlook (accessed April 17, 2017).

[8] Tasma D, Panait T, Jos D, St D. the Quality of Syngas Produced By Fluidised Bed Gasification Using Sunflower Husk 2012:33–6.

[9] Bridgwater AV. The technical and economic feasibility of biomass gasification for power generation 1995;14:631–53.

[10] Bamford CH, Crank J, Malan DH, Wilson AH. The combustion of wood. Part I. Math Proc Cambridge Philos Soc 2008;42:166.

[11] Font R, Marcilla A, Verdii E, Devesa J. Kinetics of the Pyrolysis of Almond Shells and Almond Shells Impregnated with CoC12 in a Fluidized Bed Reactor and in a Pyroprobe 100. Ind Eng Chem Res 1990:1846–55.

[12] Font R, Marcilla A, Devesa J, Verdú E. Kinetic study of the flash pyrolysis of almond shells in a fluidized bed reactor at high temperatures. J Anal Appl Pyrolysis 1993;27:245–73.

[13] Di Blasi C. Kinetic and Heat Transfer Control in the Slow and Flash Pyrolysis of Solids. Ind Eng Chem Res 1996;35:37–46.

[14] Di Blasi C, Branca C. Kinetics of Primary Product Formation from Wood Pyrolysis. Ind Eng Chem Res 2001;40:5547–56.

[15] Blasi C Di. Modeling and Simulation of Combustion Processes of Charring and Non-Charring Solid Fuels. Prog Energy Combust Sci 1993;19:71–104.

[16] Di Blasi C. Numerical simulation of cellulose pyrolysis. Biomass and Bioenergy 1994;7:87–98.

[17] Babu B V., Chaurasia AS. Modeling, simulation and estimation of optimum parameters in pyrolysis of biomass. Energy Convers Manag 2003;44:2135–58.

[18] Babu B V., Chaurasia AS. Heat transfer and kinetics in the pyrolysis of shrinking biomass particle. Chem Eng Sci 2004;59:1999–2012.

[19] Jin G. Multiscale coupling framework for modeling of large-size biomass particle gasification in fluidized beds. Ind Eng Chem Res 2013;52:11344–53.

[20] Di Blasi C. Combustion and gasification rates of lignocellulosic chars. Prog Energy Combust Sci 2009;35:121–40.

[21] Lu H, Ip E, Scott J, Foster P, Vickers M, Baxter LL. Effects of particle shape and size on devolatilization of biomass particle. Fuel 2010;89:1156–68.

[22] Blasi C Di. Dynamic behaviour of stratified downdraft gasifiers 2000;55.

[23] Peters B. Validation of a numerical approach to model pyrolysis of biomass and assessment of kinetic data. Fuel 2011;90:2301–14.

[24] Wu Y, Zhang Q, Yang W, Blasiak W, Y. Wu, Q. Zhang, W. Yang and WB. Two-Dimensional Computational Fluid Dynamics Simulation of Biomass Gasification in a Downdraft Fixed-Bed Gasifier with Highly Preheated Air and Steam Preheated Air and Steam. Energy Fuels 2013;27:3274–3282.

[25] Haseli Y, Van Oijen JA, De Goey LPH. Modeling biomass particle pyrolysis with temperature-dependent heat of reactions. J Anal Appl Pyrolysis 2011;90:140–54.

[26] Fatehi H, Bai XS. A Comprehensive Mathematical Model for Biomass Combustion. Combust Sci Technol 2014;186:574–93.

[27] Lu H. Experimental and Modeling Investigations of Biomass Particle Combustion. Dep Chem Eng 2006;PhD Thesis.

[28] Lu H, Robert W, Peirce G, Ripa B, Baxter LL. Comprehensive study of biomass particle combustion. Energy and Fuels 2008;22:2826–39.

[29] Chan WCR, Kelbon M, Krieger BB. Modelling and experimental verification of physical and chemical processes during pyrolysis of a large biomass particle. Fuel 1985;64:1505–13.

[30] Evans DD, Emmons HW. Combustion of wood charcoal. Fire Saf J 1977;1:57–66.

[31] Ranz WE, Marshall WR. Evaporation from drops - Part 1. Chem Eng Prog 1952;48:141–8.

[32] Yin C. Modelling of heating and evaporation of n-Heptane droplets: Towards a generic model for fuel droplet/particle conversion. Fuel 2015;141:64–73.

8. ACKNOWLEDGEMENTS

The Authors are grateful to the help from department of energy technology of Aalborg University and support from Chinese scholarship council.

Paper E

Importance of the sub-processes in solid fuel particle gasification: heat conservation and reaction mechanism

Xiyan Li, Chungen Yin

The paper has been published in the
Proceedings of the 13th Conference on Sustainable Development of Energy, Water, and Environment Systems, pp.1–10, 2018.

The layout has been revised.

Proceedings of the 13th Conference on Sustainable Development of Energy, Water, and Environment Systems, SDEWES2018. SDEWES2018.0489, 1-10

Importance of the sub-processes in solid fuel particle gasification: heat conservation and reaction mechanism

Xiyan Li*,
Department of Energy Technology
Aalborg University, Aalborg, Denmark
e–mail: xli@et.aau.dk

Chungen Yin, Thomas Condra
Department of Energy Technology
Aalborg University, Aalborg, Denmark
e–mail: chy@et.aau.dk, tc@et.aau.dk

ABSTRACT

The aim of this article is to develop a complete and detailed gasification model for a single solid fuel pellet. Three main objectives are achieved: a modified one-dimensional model using C++ code, a reliable results validation using experimental data from literature and an overview of the detailed one-dimensional model results. This model is based upon the partial differential equations (PDEs) describing continuity, species transport, energy and pressure equations. All the equations are highly coupled and are solved using a central-differential scheme (CDS). A time-marching procedure is based on a fully implicit scheme. Both a grid independent validation and a validation against experimental data are given in the paper. The validation results show good agreement with the experimental data. The temperature profile, the definition of the end of each pyrolysis/gasification stages and the effects of sensible enthalpy are presented. Based on this work, an engineering model can be generated in the future, which will be a novelty in biomass (coal) gasification/pyrolysis/combustion, and will do a great use to industry.

KEYWORDS

Single particle, Gasification, Pyrolysis, Computational fluid dynamics (CFD), Finite volume method (FVM)

INTRODUCTION

As the main energy source of the world, fossil fuels are persistently at the focus of controversy. Due to the declining supply of fossil fuels and the issues related to greenhouse gas emissions, there is an urgent need for alternative energy sources. Biomass is in the public focus, not only because it is sustainable but also because of its environmentally friendly characteristics. According to data report from United Nations Environment Programme, the global CO_2 content at the sea level has increased from 315.71 ppm in 1980 to 410.26 ppm in 2018 [1]. Biomass gasification uses gases such as, steam, air, nitrogen, carbon dioxide, methane or a mixture of these gases as gaseous medium to react with biomass. In this way, the greenhouse gases are recycled and syngas is produced.
In order to make full use of the biomass, research has been done on pyrolysis, gasification and combustion, based on both experimental methods and simulation methods. The experimental methods give a way of describing real reaction phenomenon and gaining a set of practical data, for example,

* Corresponding author

temperature profile, kinetic parameters, reaction order etc., whilst simulation gives a rapid way of looking into the results before experiments or before scale- up is considered. The early research started with crudely measuring the gas components and unreacted carbon and predicting the weight loss value [2]. Laurendeau [3] in 1977 already found out the complete heterogeneous reaction mechanism for coal char and constructed a complete particle reaction model. Limited by the computational capacity at the time, there are not many simulation results, but it still gave a good point for the research that followed. Thurner and Mann [4] put more efforts on the kinetic mechanism of a so-called two-step devolatilization mechanism. Using this mechanism, they compared the composition of gases, tar and residues between experimental data and simulated data. However, no further information about the real gasification results were given. Through the years, the debate about one-step devolatilizaion mechanism and two-step devolatilization mechanism has continued.
One-step global devolatilization mechanism can be described as:

$$Biomass \rightarrow Char + Volatile/Light\ gas(CO, CH_4, CO_2, H_2 \cdots)$$

The advantage of one-step global devolatilization mechanism is that the reaction heat is easy to obtain from the measurement of heating value and the composition of the light gas can be easily calculated from the proximate and ultimate analyses. Therefore, the predicted results are reasonably transparent. The difficulty lies in finding a global reaction mechanism data for this reaction. As is known, biomass has complex components and each component has its own reaction mechanism. Perhaps for this reason, some researchers go for the three-parallel devolatilization mechanism or the two-step devolatilization mechanism.
The three parallel devolatilization mechanism is shown simply as:

$$\begin{cases} Cellulose & \\ & \dfrac{Volatile}{Light} gas(CO, CH_4, CO_2, H_2 \cdots) + char \\ Semi - cellulose \xrightarrow{produce} & \dfrac{Volatile}{Light} gas(CO, CH_4, CO_2, H_2 \cdots) + char \\ & \dfrac{Volatile}{Light} gas(CO, CH_4, CO_2, H_2 \cdots) + char \\ Lignin & \end{cases}$$

The three-parallel mechanism can be seen as three one-global devolatilization mechanisms combined together, but with a much simpler composition of reactants. It makes it easier to finding out the mechanism of devolatilization of every single component. The defect is three reactions need to be considered in the model, which may lead to the experimental error accumulating.
A two-step devolatilization mechanism is based on the three parallel devolatilization mechanism. The idea is also to make the reaction mechanism data easier to measure and calculated. The difference is that the classification starts from the products. A medium product, tar is considered. Tar is generated from the primary decomposition, and then further cracking into gas and char. This mechanism describes better the phenomena that occur during pyrolysis, combustion or gasification. However, tar is an unstable matter. The percentage of tar in the products relies on the experimental conditions. Because of that, it is also not easy to find out the reaction heat of producing tar. There are five reactions that need to be considered in the two-step devolatilization model. If the reaction heat is not properly addressed, the simulation error can be much bigger than using the other two devolatilization mechanisms. This will be discussed later in this paper.
The two-step mechanism model is shown as:

$$Biomass \xrightarrow{produces} \begin{cases} Gas \\ \uparrow \\ Tar \\ \downarrow \\ Char \end{cases}$$

This work is based on a one-dimensional numerical model for the pyrolysis of a single spherical biomass particle. The model is further extended for gasification and combustion. The one-step global devolatilization model is used in this model for its simplicity and accuracy.

METHODOLOGY

The pellet in this model is considered as a one-dimensional spherical fuel pellet, whose properties are isotropic and is under local thermal equilibrium during the heating up process. The CFD model uses central differential scheme with staggered grid for the pressure calculation. The grid number is set to 80. A fully implicit scheme is used a fully implicit scheme for solving the transient term. More details about the partial differential equations are presented below.
The validation experiment is based on data from a sub-bituminous coal (SBC) in a fluidized bed at 850℃ [5][6]. The diameter of the fuel pellet was 10 mm.

Reaction mechanism

Within all the three devolatilization models discussed above, there is one issue has to be considered, and that is to solve the enthalpy of formation of volatile for one-step global devolatilization model and two-step devolatilization model. For the three-parallel devolatilization model, it can be seen as three one-step global devolatilizaiton models combined.
Solid fuel can usually be seen as a combination of moisture, volatile, fixed carbon and ash, as shown in proximate analysis in Table 1. The heating value in the proximate analysis can be treated as the sum of the heating values of the carbon and the volatile. Depending on the form of water when the heating value is measured, the heating value can be classified as lower heating value (LHV) or higher heating value (HHV). In the model that is discussed in this paper, the moisture is treated separately. Therefore, the heating value of volatile is calculated as:

$$HHV_{Volatile} \times \%_{Volatile} + HHV_{Char}\%_{Char} = HHV_{Proximate} \quad (1)$$

$$Volatile \ + \ O_2 \ \rightarrow \ CO_2 \ + \ H_2O + N_2 + SO_2 + \cdots + HHV_{Volatile} \quad (2)$$

$$h^0{}_{Volatile} = h^0{}_{CO_2} + h^0{}_{H_2O} + h^0{}_{N_2} + h^0{}_{SO_2} + \cdots + HHV_{Volatile} - h^0{}_{O_2} \quad (3)$$

$HHV_{Volatile}$ represents the heat that released when the volatile is oxidized completely, and water vapor is still in gaseous state. Equation (3) shows the calculation of enthalpy of formation of the volatile.

Table 1: Proximate analysis, ultimate analysis and heating value [5][6]

Fuel	Moisture[%, a.d]	Volatile[%, a.d]	FC[%, a.d]	Ash[%, a.d]	HHV[kJ/kg, a.d]
Sub-bituminous coal	5.07	21.08	49.93	23.90	31490
	C[%, d.b]	H[%, d.b]	O[%, d.b]	N[%, d.b]	S[%, d.b]
	83.58	4.68	9.2	1.74	0.8

The composition of the volatile can be calculated through the proximate analysis and the ultimate analysis. Table 1 shows an example of these values, including heating values of a sub-bituminous coal particle. Referring to the reference cited in this table [5][6], it is also easy to see that these values can be different depending on the sample even though using the same fuel type.
The calculation of volatile is therefore straightforward, since carbon only exist in the volatile and in the fixed carbon according to the proximate analysis in Table 1. So for a formula of a volatile molecular, $C_xH_yO_zN_wS_v$, the stoichiometry of carbon can be calculated as:

$$x = \frac{C-FC}{Volatile}/M_C \tag{4}$$

H, O, N, S only exist in volatile. Similarly, y, z, w, v can be calculated. Taking the example from Table 1, the volatile can be expressed as: $CH_{4.2197}O_{0.5226}$ after normalization and ignoring N and S. This molecular with a molecular weight of 26.9343 kg/kmol and the enthalpy of formation of -34527 kJ/kg, will be used as input for the validation.
Volatile can be treated as artificial components in the numerical model or can be broken down into real species (such as CO, CO_2, CH_4, C_2H_6, . . .). In the case we study here, it is not easy to break down the volatile into real species, therefore, an artificial component is used to represent volatile in the model, as shown in Table 2.

Table 2: Chemical reactions and reaction rate

index	Chemical reactions	Rate expression	Ref
1	Biomass $\rightarrow$ Volatile + Char	$r_1 = \partial\rho_{vol}/\partial t = k_1(\rho_{vol,\infty} - \rho_{vol})$	[7]
2	H_2O (free) $\rightarrow$ H_2O (g)	$r_2 = S_a \frac{h_T(T_j - T_{ini}) + \varepsilon\sigma(T_j{}^4 - T_{ini}^4)}{\Delta h_{evap}}$	
3	H_2O (bound) $\rightarrow$ H_2O (g)	$r_3 = A_{evp} exp\left(-\frac{E_{evp}}{RT}\right)$	
4	$C + \alpha O_2 \rightarrow 2(1-\alpha)CO + (2\alpha - 1)CO_2$	$r_4 = \partial C_{O_2}/\partial t = s_{a,char}[\rho_C/(\rho_C + \rho_B + \rho_A)]k_4 C_{O_2}$	[8]
5	$C + H_2O \rightarrow H_2 + CO$	$r_5 = \partial C_{H_2O}/\partial t = s_{a,char}[\rho_C/(\rho_C + \rho_B + \rho_A)]k_5 C_{H_2O}$	[8]
6	$C + 2H_2 \rightarrow CH_4$	$r_6 = \partial C_{H_2}/\partial t = s_{a,char}[\rho_C/(\rho_C + \rho_B + \rho_A)]k_6 C_{H_2}$	[8]
7	$H_2 + 1/2O_2 \rightarrow H_2O$	$r_7 = \partial H_2/\partial t = k_7 C_{H_2} C_{O_2}^{0.5}$	[9]
8	$CO + 1/2O_2 \rightarrow CO_2$	$r_8 = \partial C_{CO}/\partial t = k_8 C_{CO} C_{O_2}^{0.25} C_{H_2O}^{0.5}$	[9]
9	$CO + H_2O \rightarrow CO_2 + H_2$	$r_9 = \partial C_{CO}/\partial t = k_9 C_{CO}^1 C_{H_2O}^1$	[9]
10	$CH_{4.2197}O_{0.5226} + 1.29365O_2 \rightarrow CO + 2.10985H_2$	$r_{10} = \partial C_{CH_{4.2197}O_{0.5226}}/\partial t = k_{10} C_{CH_{4.2197}O_{0.5226}}^{0.2} C_{O_2}^{1.3}$	[10]

Table 2 shows all the reactions used in this model. The first is the devolatilization mechanism as mentioned previously. The second and the third are the mechanisms for free water and bound water. It should be notice that the free water is only considered when the FSP is over 30% [11]. Reactions 4 to 6, are heterogeneous reactions. It is worth mentioning that the last heterogeneous reaction (reaction 6) does not occur under atmospheric pressure [12] during the gasification temperature. It is presented for reference but not considered in the model because of the relatively low pressure. Reaction 8 to reaction 12 are the homogeneous reactions. The light hydrocarbon here obey the two-step combustion scheme for hydrocarbons proposed by Westbrook and Dryer [13], which are shown as reactions 7, 8,

9, 10 in Table 2. In the two-step mechanism, the main aim is to oxidize volatile and produce CO and H_2, this is the first step. The second step is to gasify CO and H_2, as shown in reactions 7-9.
Table 3 shows the data for the kinetic parameters used in Table 2, calculated from Arrhenius equations with the following expression:

$$k = Ae^{\frac{E_a}{RT}} \tag{5}$$

Table 3: Kinetic data used in this model

Reaction index	Pre-exponential factor (A) $[s^{-1}]$	Activation energy (E_a) [J/kmol]	Heat of reactions (ΔH) [kJ/kg]
1	3.12×10^5	7.4×10^7	-1376.09
2	-	-	-
3	5.13×10^{10}	8.8×10^7	-2440
4	0.658[a]	7.4831×10^7	3950
5	3.42[a]	1.297×10^5	-14383.33
6	2083[a]	115137	1701.59
7	$10^{12.71}$	1.71×10^5	13435.94
8	2.39×10^{12}	1.702×10^8	10114.28
9	2.75×10^9	8.4×10^7	-12879,38
10	2.119×10^{11}	2.027×10^8	-30420.72

[a] Units are $m/s^{-1}K^{-1}$

Transport equations

For solid species, there is only transient term considered, as show below:

$$\frac{\partial(\rho_i)}{\partial t} = s_i \tag{6}$$

For the gas species, transient term, diffusion term and convective terms are considered, so we have:

$$\frac{\partial(\varepsilon\rho_g Y_{ig})}{\partial t} + \frac{\partial(\varepsilon\rho_g u Y_{ig})}{\partial r} = \frac{\partial}{\partial r}\left(D_{ig}\frac{\partial(\varepsilon\rho_g Y_{ig})}{\partial r}\right) + S_{Y_{ig}} \tag{7}$$

At the inner boundary for solid species, the gradient is set to zero. For the outer boundary, a mass transfer coefficient is used. Therefore a gas film around the pellet is assumed. A reference species and reference temperature are calculated as follows [14].

$$Y_{j,ref} = Y_{j,s} + 1/3\left(Y_{j,\infty} - Y_{j,s}\right) \tag{8}$$

$$T_{ref} = T_s + 1/3\left(T_\infty - T_s\right) \tag{9}$$

$Y_{j,ref}$ and T_{ref} here are used for calculating the gas properties in the gas film. Once the dimensionless parameters, such as, Re, Nu, Sh, Pr are determined, h_M and h_T can be calculated using the following equations.

$$Sh \equiv \frac{h_M L_c}{D_g} = 2.0 + 0.6Re^{\frac{1}{2}}Sc^{\frac{1}{3}} \tag{10}$$

$$Nu \equiv \frac{h_T L_c}{k_g} = 1.05 + 0.6Re^{0.65}Pr^{0.33} \tag{11}$$

The outer boundary for mass transfer can be expressed as:

$$DA\frac{Y_B-Y_P}{\frac{\Delta x}{2}} = A_s h_M(Y_\infty - Y_B) \tag{12}$$

For pressure calculations, considering that the pressure inside the pores of coal/biomass will not change dramatically, the Darcy Law is applied here:

$$\vec{u} = -\frac{\eta}{\mu}\nabla P \tag{13}$$

Continuity equations are combined to solve both velocity and pressure:

$$\frac{\partial(\varepsilon\rho_g)}{\partial t} + \frac{\partial(\varepsilon\rho_g u)}{\partial r} = S_g \tag{14}$$

The most commonly used energy equations are written in terms of temperature, as shown in equation (15). The use of this form of transport equation is advantageous because it not only takes into account the heat of reactions, but also a sum of sensible enthalpy caused by temperature increase within the fuel pellet. By using one-step global devolatilization model, the only uncertainty in equation (15) is the enthalpy of formation of volatile, which can be calculated by knowing the heating value of the solid fuel pellet.

$$\frac{\partial(\varepsilon\rho_g C_{pg}T+\rho_s C_{ps}T)}{\partial t} + \frac{\partial(\varepsilon\rho_g u C_{pg}T_g)}{\partial r} = \frac{\partial}{\partial r}\left(k_{eff}\frac{\partial T}{\partial r}\right) + S_T \tag{15}$$

$$S_T = -\sum_{k=1}^{N} h_{f,k}^0 \dot{w}_k - \sum_{k=1}^{N} h_{f,k}\dot{w}_k = \sum_{k=i}^{N} \Delta H_i \dot{w}_i - \sum_{k=1}^{N} h_{f,k}\dot{w}_k \tag{16}$$

The outer boundary condition for temperature is shown as:

$$k_B A\frac{T_B-T_P}{\Delta r/2} = A_s h_T\,(T_\infty - T_B) + A_s\varepsilon\sigma(T_\infty^4 - T_B^4) \tag{17}$$

Besides, for the two-step decomposition model, it was found that the heat of reaction of biomass decomposing into gas, tar and char can be very different, varying from -150kJ/kg [15] to -418kJ/kg [16]. The heat of reaction of intermediate product (tar) cracking and reforming is also not easy to determine, shown in literature from around 42kJ/kg [17] to 50kJ/kg [18] by somehow modified. In the case of three-step parallel model for biomass, the enthalpy of formation of lignin, cellulose, semi-cellulose should be calculated separately, which means the error is accumulated three times by measuring the heating values of these three species separately.

VALIDATION AND RESULTS

Using the model developed above, two validations were made. Both of the experiments are taken from Bu et al [5][6]. The first experiment is based on a 10mm sub-bituminous coal pellet in a fluidized bed with a temperature of 850 ℃. The second experiment uses the same pellet with the same bed temperature, but the atmosphere is changed to 30% oxygen and 70% carbon dioxide. Table 3 shows some properties taken from that experiment.

Table 3: Properties taken from Bu. et al

ρ_{SBC}	$C_{P_{SBC}}$	h_T	T_f
1662	1049	200	1088
K_B	T_{wall}	u_g	D_P
0.6	1123	0.28	10

Figure 1 shows the results of sub-bituminous coal under pyrolysis with nitrogen. The solid line represents the simulated temperature profile at the centre of the SBC pellet. The triangles represent the measured centre temperature results from the experiment. It can be seen that the simulation results follow the experimental investigation. A further determination of pyrolysis stages are shown in Fig. 2.

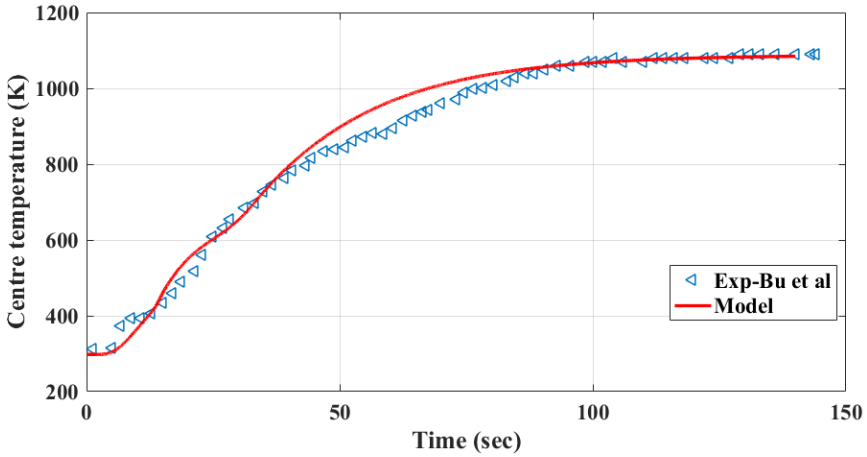

Figure 1 Centre temperature during N_2 pyrolysis calculated by model and measured by Bu et al

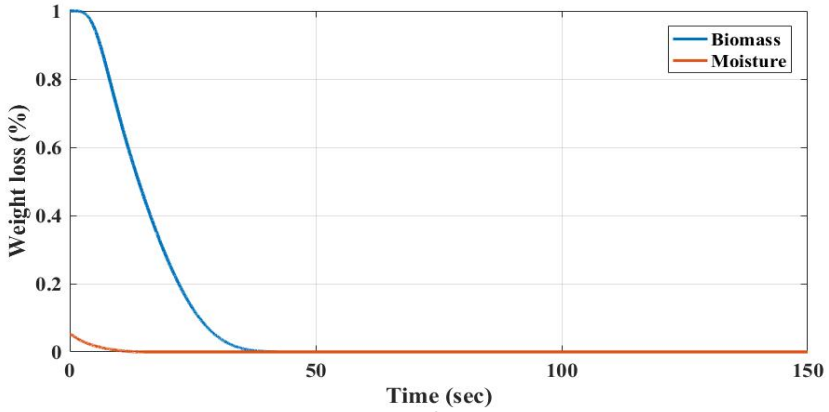

Figure 2 Weight loss profile during pyrolysis

Figure 2 shows the weight loss profile during pyrolysis. Ash is not counted during the calculation, since the mass of ash doesn't change during the pyrolysis process. Water dispears after 14 seconds of reaction. The devolatilization stage is finished after 40 seconds of pyrolysis. In Fig.3, these two stages are shown by arrows.

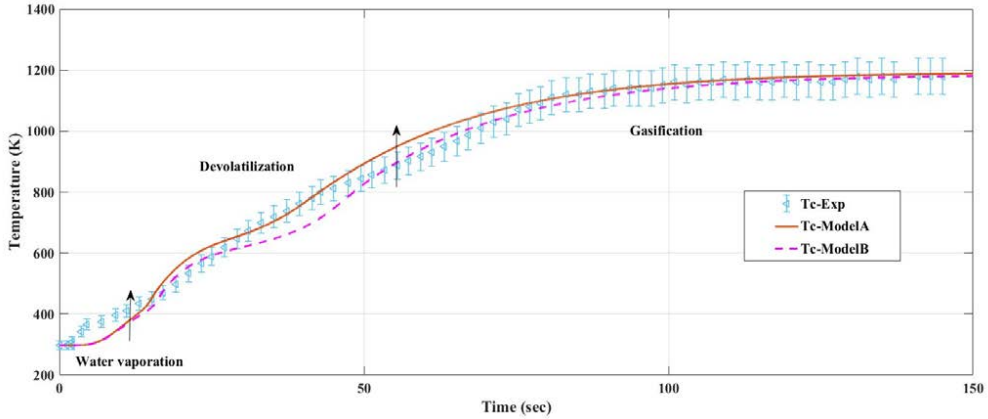

Figure 3 Centre temperature (30% O_2 & 70% CO_2) calculated by model and measured by Bu et al

Figure 3 shows the results of another gasification case, in which the atmosphere of the fluidized bed is changed to 30%$_{vol}$ oxygen and 70%$_{vol}$ carbon dioxide. The solid line shows the simulation result from the model presented in this paper, whereas the dashed line shows the simulation results without considering the sensible enthalpy in the energy equation. The triangles with error bar represents the experimental results from Bu et al [5]. The three stages of the SBC gasification process are marked by arrows. It can be seen that both simulation results agree well with the experimental data. However, considering sensible enthalpy in the energy equation gives a better fit for the temperature at the pellet centre, especially during the devolatilization stage. Sensible enthalpy has negligible effects during the water vaporation stage. In other word, enthalpy of formation is more important than sensible enthalpy during solid fuel pyrolysis, gasification and combustion.

CONCLUSION

This paper describes a detailed gasification model for a sphere solid fuel. Kinetic mechanism, the transport equations, the chemical reactions are considered in the model. A two-step reaction mechanism for volatile gasification is used in this model. A way of calculating the composition of volatile is outlined. Moreover, the mass and heat conservation of a one-step global devolatilization reaction are presented. In the end, two validation results are given. The validation results show the model agrees well with experimental data for both pyrolysis and combustion/gasification processes for a single spherical solid fuel. The gasification validation also shows that energy equation with sensible enthalpy considered agrees better to the experimental results. This work gives a starting point to further investigate a single biomass particle gasification in 2D or 3D, and can serve as a basis for extending the single solid fuel particle to an industrial packed bed gasification/pyrolysis research.

NOMENCLATURE

A_s	The surface area [m^2]
A	Pre-exponential factor [s^{-1}]
E_a	Activation energy of water evaporation, [J/Kmol].
C_P	Specific heat [J/(kg·K)]
$D_{eff,fw}$	Free water effective mass diffusivity [m^2/s]
FSP	Fiber saturation point, %
Δh_{evap}	Latent heat of vaporation [J/kg]
h_f^0	Enthalpy of formation [J/kg]
ΔH	Heat of reactions [J/kg]
h_T	Heat transfer coefficient [W/(m^2·K)]
h_M	Mass transfer coefficient [m/s]
K_B	The thermal conductivity [W/(m·K)]
k_{H_2O}	Reaction rate constant [s^{-1}]
Nu	Nusselt number
Pr	Prandtl number
R_g	Universal gas constant [J/(mol·K)]
r_i	Reaction rate [J/(mol·K)]
r_{H_2O}	The volumetric vaporization rate [kg/(m^3·K)]
SBC	Sub bituminous coal
Sc	Schmidt number
Sh	Sherwood number
S_T	Source term in energy equation [W/m^3]
S_a	The specific area of the wood particle, 2.26×10^4 [m^2/m^3]
T_{ini}	Initial temperature [K]
T_∞	Ambient gas temperature [K]
T_S	Particle surface temperature [K]
$T_{j,S}$	Particle surface temperature for species j [K]
T_C	Particle centre temperature [K]
T_{evap}	Defined as evaporation point of liquid water [K]
u	Velocity [m/s]
Y_{vap}	The percentage of vapor within all the species,
$Y_{j,ref}$	Reference mass fraction of species *j* in the gas film around the particle
$Y_{j,s}$	Mass fraction of species *j* at particle surface
$Y_{j,\infty}$	Mass fraction of species *j* in the ambient gas
ρ_g	Gas density [kg/m^3]
ρ_{vol}	Remaining volatile in solid [kg/m^3]
$\rho_{vol,\infty}$	Ultimate yield of volatile [kg/m^3]
ρ_{fw}	The free water density at the present time [kg/m^3]
$\dot{w}_k$	Reaction rate
λ	The average conductivity of all the gases in the film [W/(m·K)]
ε	Porosity
μ	Dynamic viscosity [kg/(m·s)]
σ	Boltzmann radiation constant, 5.86×10^{-8} (W/m^2K^4)

i	Number of reactions
g	Gas
k	Number of species
l	Liquid
s	Solid

REFERENCES

1. EDE / UNEPlive n.d. http://geodata.grid.unep.ch/extras/graph_co2_concentration.php (accessed May 28, 2018).
2 Arthur JR. Reactions between carbon and oxygen. *Trans Faraday Soc* 1951;47:164.
3 Laurendeac NM. Heterogeneous Kinetics of Coal Char Gasification and Combustion. *Progress in Energy and Combustion Science* 1978;7:2447–50.
4 Thurner F, Mann U. Kinetic investigation of wood pyrolysis. *Ind Eng Chem Process Des Dev* 1981;20:482–8.
5 Bu C, Liu D, Chen X, Pallarès D, Gómez-Barea A. Ignition behavior of single coal particle in a fluidized bed under O2/CO2and O2/N2atmospheres: A combination of visual image and particle temperature. *Appl Energy* 2014;115:301–8.
6 Bu C, Leckner B, Chen X, Pallarès D, Liu D, Gómez-Barea A. Devolatilization of a single fuel particle in a fluidized bed under oxy-combustion conditions. Part B: Modeling and comparison with measurements. *Combust Flame* 2015;162:797–808.
7 Yang YB, Yamauchi H, Nasserzadeh V, Swithenbank J. Effects of fuel devolatilisation on the combustion of wood chips and incineration of simulated municipal solid wastes in a packed bed. *Fuel* 2003;82:2205–21.
8 Lu H, Robert W, Peirce G, Ripa B, Baxter LL. Comprehensive study of biomass particle combustion. *Energy and Fuels* 2008;22:2826–39.
9 Yin C, Kær SK, Rosendahl L, Hvid SL. Co-firing straw with coal in a swirl-stabilized dual-feed burner: Modelling and experimental validation. *Bioresour Technol* 2010;101:4169–78.
10 Jones WP, Lindstedt RP. Global reaction schemes for hydrocarbon combustion. *Combust Flame* 1988;73:233–49.
11 Sharma A, Pareek V, Zhang D. Biomass pyrolysis - A review of modelling, process parameters and catalytic studies. *Renew Sustain Energy Rev* 2015;50.
12 Klose E, Köpsel R. Mathematical model for the gasification of coal under pressure. *Fuel* 1978;72:714.
13 Dryer FL, Westbrook CK. Simplified Reaction Mechanisms for the Oxidation of Hydrocarbon Fuels in Flames. *Combust Sci Technol* 1981;27:31–43.
14 Yin C. Modelling of heating and evaporation of n-Heptane droplets: Towards a generic model for fuel droplet/particle conversion. *Fuel* 2015;141:64–73.
15 Branca C, Albano A, Di Blasi C. Critical evaluation of global mechanisms of wood devolatilization. *Thermochim Acta* 2005;429:133–41.
16 Chan WCR, Kelbon M, Krieger BB. Modelling and experimental verification of physical and chemical processes during pyrolysis of a large biomass particle. *Fuel* 1985;64:1505–13.
17 Haberle I, Haugen NEL, Skreiberg Ø. Drying of thermally thick wood particles: A study of the numerical efficiency, accuracy, and stability of common drying models. *Energy & Fuels* 2017
18 MG Grønli. A theoretical and experimental study of the thermal degradation of biomass.pdf 1996:339.

ISSN (online): 2446-1636
ISBN (online): 978-87-7210-676-2 AALBORG UNIVERSITY PRESS